

Auditory learning
in the Mongolian gerbil
(*Meriones unguiculatus*)
investigated with auditory functional
magnetic resonance imaging

Thesis

for the degree of

doctor rerum naturalium (Dr. rer. nat.)

approved by the Faculty of Natural Sciences of
Otto von Guericke University Magdeburg

by M.Sc. Annika Michalek
born on 03.03.1993 in Herrenberg

examiners: Prof. Dr. Eike Budinger
Prof. Dr. Andreas Hess
Prof. Dr. Susann Boretius

submitted on 20.03.2024

defended on 08.04.2025

Abstract

Learning auditory cues and distinguishing between them is imperative for our daily social interactions and essential for our perception of the external world. Disorders in the hearing system and in auditory learning can lead to social isolation and create a wide variety of health risks. Auditory research aims to understand mechanisms of auditory learning, e.g. learning-induced brain plasticity changes to enable treatment of such disorders. In humans, the extent of this research is limited in its invasiveness due to ethical restrictions. Mongolian gerbils (*Meriones unguiculatus*) are rodents with hearing thresholds similar to humans. Their ability to perform complex auditory tasks makes gerbils a popular animal model for invasive auditory learning experiments that cannot be performed on human participants. Auditory functional magnetic resonance imaging (fMRI) would be a suitable non-invasive method to improve translatability from auditory research implemented in gerbils to ongoing human research. But so far this method has not been implemented in gerbils.

To facilitate direct comparison of gerbil and human auditory research, I established auditory fMRI in Mongolian gerbils. While doing so, an appropriate anaesthesia protocol was found, fMRI sequences optimized for the rodent model, and an auditory stimulation setup, intended for human auditory fMRI, refined for usage in small animals. With optimization of the auditory fMRI measurement setup, acquired auditory activation patterns feature bilateral activation in auditory cortex, auditory thalamus and auditory midbrain.

In a second project, the newly established auditory fMRI was evaluated with cerebral blood flow SPECT imaging. More precisely, the effects of medetomidine anaesthesia and the substantial fMRI background noise on auditory activation patterns were investigated. In this study, only minor effects of medetomidine anaesthesia were found. The fMRI background noise showed more impact on the obtained auditory activation patterns, in the form of lowered subcortical activation to auditory stimulation and increased activation in higher order auditory cortex areas.

Finally, auditory fMRI was utilized to investigate auditory learning in Mongolian gerbils in a standard tone discrimination task in a shuttle box. The task was implemented in two alternative designs, one adding punishment for “False Alarms” to the aversive avoidance paradigm. With repeated application of auditory fMRI, we were able to distinguish activation changes and consolidation processes in various brain structures with a clear and significant performance dependency. The addition of punishment in the training led to higher correlation of the animals’ learning score to the activation levels of multiple neuromodulatory and associative brain regions.

These observed activation changes attest to the usefulness of auditory fMRI in Mongolian gerbils for auditory research and its potential in bridging the gap to human research.

Content

Abstract	i
Content	v
Abbreviations.....	ix
General introduction.....	1
Auditory learning research	1
The auditory pathway of humans and rodents.....	1
Auditory learning research in the Mongolian gerbil.....	3
Aim of this thesis	4
1. Establishment of auditory fMRI in the Mongolian gerbil.....	5
1.1. Introduction	5
1.1.1. Magnetic resonance imaging.....	5
1.1.2. Functional magnetic resonance imaging.....	7
1.1.3. Functional magnetic resonance imaging in rodents.....	9
1.2. Method establishment	12
1.2.1. Experimental animals.....	12
1.2.2. Measurement setup.....	12
1.2.3. Anaesthesia protocol	12
1.2.4. Optimization of different fMRI sequence types	13
1.2.5. Auditory stimulation.....	14
1.2.6. fMRI data analysis.....	15
1.3. Results	17
1.3.1. Interim results throughout the establishment process of auditory fMRI.....	17
1.3.2. Optimized auditory fMRI in the Mongolian gerbil.....	23
1.4. Discussion	27
1.4.1. Effectiveness of fMRI anaesthesia protocol.....	27
1.4.2. Image quality of functional MRI	28
1.4.3. Quality of auditory evoked activation patterns	29
2. Evaluation of auditory fMRI in the Mongolian gerbil with CBF SPECT	33
2.1. Introduction	33
2.1.1. Anaesthesia effect on brain activation	33
2.1.2. Effect of MRI background noise on auditory processing.....	34
2.1.3. CBF SPECT imaging	36

2.2.	Methods	38
2.2.1.	Experimental design	38
2.2.2.	Experimental animals.....	38
2.2.3.	Injection of CBF SPECT tracer.....	39
2.2.4.	Auditory stimulation.....	40
2.2.5.	CBF tracer injection in the awake gerbils	40
2.2.6.	CBF tracer injection under Medetomidine anaesthesia	40
2.2.7.	CBF tracer injection during fMRI measurements	41
2.2.8.	SPECT/CT readout.....	42
2.2.9.	Data analysis	43
2.3.	Results	45
2.3.1.	Effect of medetomidine anaesthesia	45
2.3.2.	Effect of GRE-EPI background noise.....	47
2.4.	Discussion	54
2.4.1.	Effect of medetomidine anaesthesia	54
2.4.2.	Effect of GRE-EPI background noise.....	55
2.4.3.	Comparison of fMRI and SPECT data	57
3.	Effects of auditory learning revealed by auditory fMRI in the Mongolian gerbil.....	59
3.1.	Introduction	59
3.1.1.	Investigation of learning processes via conditioning.....	59
3.1.2.	Discrimination learning.....	61
3.1.3.	Changes in brain plasticity through auditory discrimination learning	62
3.2.	Methods	64
3.2.1.	Experimental animals.....	64
3.2.2.	Experimental design	64
3.2.3.	FM direction discrimination training.....	65
3.2.4.	Auditory fMRI measurements.....	65
3.2.5.	Data analysis	67
3.3.	Results	70
3.3.1.	Auditory-evoked brain activation patterns.....	70
3.3.2.	Changes in activation patterns induced by discrimination learning without aP.....	72
3.3.3.	Differences in performance are reflected in the brain activation patterns.....	74
3.3.4.	Discrimination learning and brain activation patterns with aP	83
3.3.5.	Comparison of gerbils trained with and without aP.....	90

3.4.	Discussion	94
3.4.1.	Auditory-evoked brain activation patterns.....	94
3.4.2.	Brain areas involved in auditory discrimination learning.....	94
3.4.3.	Performance dependent activation changes.....	100
3.4.4.	Effect of additional punishment.....	103
3.4.5.	Summary of auditory learning-induced effects observed with auditory fMRI.	105
	General discussion	107
	Challenges and Limitations	107
	Outlook and implications for future research	109
	Citations	111
	Appendix.....	A
	List of Figures.....	A
	Supplements	C
	(i) Information on the additional surgical interventions	Q

Abbreviations

2D	two-dimensional	mm	millimetre(s)
3D	three-dimensional	ms	millisecond(s)
^{99m} Tc	radioactive technetium-99m	MR	magnetic resonance
^{99m} Tc-O ₄ ⁻	^{99m} -technetium pertechnetate	MRI	magnetic resonance imaging
<i>A1</i>	<i>primary auditory cortex</i>	NaCl	sodium chloride, saline
<i>AC</i>	<i>auditory cortex</i>	NIfTI	Neuroimaging Informatics Technology Initiative (standard image format)
<i>AuD</i>	<i>secondary auditory cortex, dorsal area</i>	nl	nanolitre(s)
<i>AuV</i>	<i>secondary auditory cortex, ventral area</i>	<i>NLL</i>	<i>nuclei of the lateral lemniscus</i>
avg	average(s)	No.	number
BOLD	blood oxygen level dependent	pb	phosphate buffer
BOLD%	BOLD percent signal change	PET	positron emission tomography
Bruker	Bruker BioSpin GmbH & Co. KG, Germany	PFA	paraformaldehyde
CBF	cerebral blood flow	<i>mPFC</i>	<i>medial prefrontal cortex</i>
<i>CNu</i>	<i>cerebral nuclei</i>	<i>rAC</i>	<i>right auditory cortex</i>
CS	conditioned stimulus	RARE	rapid acquisition with relaxation enhancement
CS+	GO tone	reps	repetitions
CS-	noGo tone	RF	radiofrequency
CR	conditioned response(s)	ROI	region(s) of interest
CR+	“Hit”, correct response to GO tone	rpm	revolutions per minute
CR-	“False Alarm”, incorrect response to noGo tone	<i>RSC</i>	<i>retrosplenial cortex</i>
CT	computed tomography	s	second(s)
dB	decibel	SAI	small animal imaging
degs	degrees	s.c.	subcutaneous
DICOM	Digital Imaging and Communications in Medicine (standard image format)	SE	spin echo
EPI	echo-planar imaging	SEM	standard error of the mean
ERA	event related average	SPECT	single photon emission computed tomography
FDG	fluorodeoxyglucose, (glucose analogue labelled with radioactive ¹⁸ F)	SPL	sound pressure level
FDR	false discovery rate	STC	signal time course
FID	free induction decay	stim	stimulation
FLASH	fast low-angle shot	T1	time constant for longitudinal relaxation
FoV	field of view	T2	time constant for transversal relaxation
FM	frequency modulation/modulated	T2*	effective T2 due to field homogeneity effects
fMRI	functional magnetic resonance imaging	TE	echo time
FWHM	full width at half maximum	<i>Th</i>	<i>thalamus dorsalis</i>
g	gram(s)	TR	repetition time
GLM	general linear model	TTL trigger	transistor-transistor logic trigger
GRE	gradient echo	UCS	unconditioned stimulus
GRE-EPI	gradient echo with echo-planar imaging	USA	United States of America
h	hour(s)	VOI	volume(s) of interest
<i>HF</i>	<i>hippocampal formation</i>	VTC	volume time course
HMPAO	hexamethylene propyleneamine oxime	WN	white noise
HRF	hemodynamic response function	ZTE	zero echo time
<i>IC</i>	<i>inferior colliculus</i>	μ	CBF normalized to the global mean (brain)
i.m.	intramuscular	μl	microliter(s)
i.p.	intraperitoneal	μm	micrometre(s)
i.v.	intravenous	μA	microampere(s)
kg	kilogram(s)		<i>directions within the brain</i>
kHz	kilohertz, unit for frequency	A	anterior
kVp	peak kilovoltage	L	left
<i>lAC</i>	<i>left auditory cortex</i>	D	dorsal
<i>LL</i>	<i>lateral lemniscus</i>	P	posterior
MBq	mega Becquerel(s)	R	right
mg	milligram(s)	V	ventral
<i>MGB</i>	<i>medial geniculate body</i>		
ml	millilitre(s)		

General introduction

Auditory learning research

Behavioural adaptation, learning and memory are important survival mechanisms of all species that possess a nervous system (Nairne et al., 2012; Papini, 2012). In particular, auditory cues are often imperative for early detection of danger. Distinguishing between such cues and remembering them is essential for survival (Concina et al., 2018; Oertel, 1999; Pereira et al., 2020). The ability to learn underlies malleability and adaptation of the brain. The brain, its networks and neurons are not rigid after maturation, but have the ability to change their activity in response to internal and external stimulation by adaptation of their structure, functionality and connections, which is known as neuroplasticity or brain plasticity (Mateos-Aparicio & Rodríguez-Moreno, 2019; Puderbaugh & Emmady, 2023). Despite extensive research on neuroplasticity, learning and memory, the precise mechanisms governing these adaptive changes are not fully understood.

In the last decades, functional magnetic resonance imaging (fMRI) has evolved into the brain imaging technique at the forefront of modern cognitive neuroscience research (Kennerley et al., 2010; Larsen et al., 2023; Peelle, 2014; Ritvo et al., 2019). fMRI is a non-invasive monitoring tool, that offers valuable insights into motor, sensory and cognitive brain processing and shows which structures are involved and active during the performance of particular tasks (Kosslyn, 1999). Due to its non-invasiveness, auditory-stimulated fMRI is frequently implemented to investigate processing of auditory cues and particular sound features in auditory research on humans (Angenstein & Brechmann, 2013a, 2013b, 2015, 2017; Behler & Uppenkamp, 2016; Brechmann & Angenstein, 2019; Brechmann et al., 2002; Czoschke et al., 2021; Danielsen et al., 2014; Schulze et al., 2013). The functional imaging technique is also implemented in human subjects to observe changes in neuroplasticity that are induced by auditory learning mechanisms (Bonnici et al., 2016; Brown & Penhune, 2018; Jiang et al., 2018; Wolff & Brechmann, 2023).

However, fMRI does not directly record neuronal cell firing. It indirectly reports on neuronal activation via neurovascular coupling, a comparatively slow response of the local cerebral blood flow that regulates the adequate supply of nutrients and oxygen to the active cells in the brain (Cauli & Hamel, 2010; Hillman, 2014; Kleinfeld et al., 2011; Phillips et al., 2016). To understand the biological background of activation patterns and learning-induced activity changes acquired with fMRI, controlled experimental conditions and interventional experiments are required that are only achievable in experimental animals (Markicevic et al., 2021).

The auditory pathway of humans and rodents

Rodents are currently the most prominent experimental mammals in neurobiological research, as the research on vertebrates is highly regulated under the European law: researchers must use the least “highly-developed” organism that allows the conformation of a hypothesis (Brown et al.,

2023]). In rodents, available methods for investigation of stimulus processing and neuroplasticity range from *ex vivo* studies like immunohistochemistry, and histological tracing studies, over highly invasive *in vivo* approaches such as lesioning of structures, electrophysiology, functional ultrasound, calcium imaging and fibre photometry to the non-invasive, directly translatable methods of SPECT, PET and fMRI.

The central auditory pathway of rodents is similar to the human pathway in its functionality and anatomical substructures (Malmierca, 2013), presented in a schematic overview in Figure 1, which makes them viable for the field of auditory research.

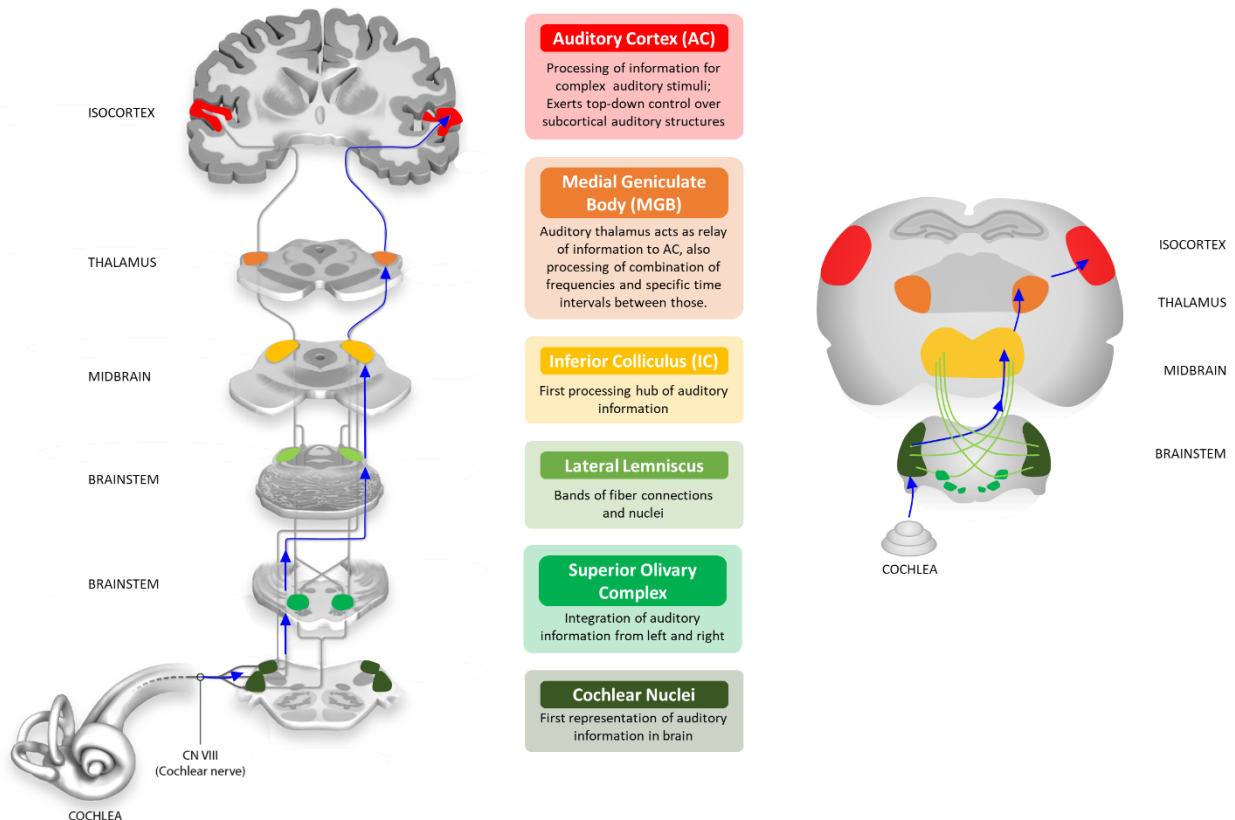


Figure 1: Structures of the auditory pathway in human and rodent brain

Common structures found in the central auditory pathway in humans and rodents. Those structures include auditory cortex (AC), medial geniculate body (MGB) and inferior colliculus (IC), which have shown changes in neuronal plasticity and activation induced by auditory learning in both, humans and rodents.

*Figure of human auditory pathway adapted from Emily Cooper (Cooper, 2016), made available by Creative Common Attribution 4.0 International

In ascending order, electrical transmission of the auditory pathway starts out with the mechano-sensitive hair cells of the cochlea, which transform mechanical energy of motion caused by sound waves into an electrical signal that is sent to the brain via the cochlear nerve (Moore, 2012). Through gradual decrease of stiffness and resulting varying resonance frequencies along the cochlea partition, the sound waves are transduced frequency-specifically and organized into tonotopic projections that remain coherent throughout the entire auditory pathway (Robles & Ruggero, 2001). The cochlear nerve projects into the first instance of the auditory brain structures, the cochlear nuclear complex, which may in turn project their information to the

superior olivary complex (some auditory information bypasses this structure), where information from left and right ear are integrated (Yost, 2002). Through the fibers and nuclei of the lateral lemniscus, the auditory information is passed mainly to the contralateral inferior colliculus (IC), which serves as a first processing hub of auditory information (Oliver & Huerta, 1992). The medial geniculate body (MGB) is the ensuing auditory processing structure of the thalamus. MGB acts as relay for the auditory information and selectivity shows for frequency combinations as well as specific time intervals between those (Purves et al., 2004). From there, the auditory information is primarily projected into the auditory cortex (AC), in which stimuli characteristics are proposedly combined into auditory objects more suitable for further processing (King & Nelken, 2009; Nelken & Ahissar, 2006). From AC (i) top-down modulation is exerted on the subcortical structures (Nuñez & Malmierca, 2007), and (ii) auditory information is fed bottom-up to higher cortical areas, for e.g. cognitive processes (Budinger et al., 2008; Pandya & Seltzer, 1982).

Auditory learning research in the Mongolian gerbil

The Mongolian gerbil (*Meriones unguiculatus*) is rodent with a pronounced hearing sensitivity to lower frequencies similar to humans (Ryan, 1976), its range is visualized in Figure 2.

Multiple studies have shown gerbils' ability to learn complex auditory tasks such as categorization of frequency modulation (FM) direction (Ohl et al., 2001; Wetzel, Wagner, et al., 1998) or even perception and discrimination of human speech (Juchter et al., 2022). Beyond that, studies have shown lateralization of certain features of acoustic stimuli in the Mongolian gerbil (Scheich et al., 2007; Wetzel et al., 2008). Lateralization refers to specialization of neuronal networks that are responsible for processing specific information that is organized exclusively or dominantly in either the left or the right hemisphere (Herve et al., 2013). Lateralization is also found in humans in the AC for the processing of different parameters of acoustic stimuli such as intensity, duration and frequency. Here, studies suggest that the left AC has a higher temporal resolution and is more involved in sequential processing while the right AC has a higher spectral resolution and is predominantly responsible for global processing (Angenstein & Brechmann, 2013a; Zatorre et al., 2002). The Mongolian gerbil shows a very similar lateralization in the ACs (Wetzel et al., 2008) easily demonstrated through unilateral lesions of this area. While lesions of the left AC lead to an impairment in the discrimination of gaps in auditory stimuli, which are translationally comparable to discrimination of speech segmentation, gerbils with a lesioned right AC were unable to discriminate direction of FM (Wetzel et al., 2008; Wetzel, Ohl, et al., 1998), which corresponds to speech prosody or slow harmonic changes in music. Altogether, these research findings suggest the suitability of Mongolian gerbils for auditory research. This also shows in the continued presence of the animal model in auditory research, especially in more challenging behavioural studies that involve auditory learning, since its emergence in this research field in 1972 (Finck et al., 1972).

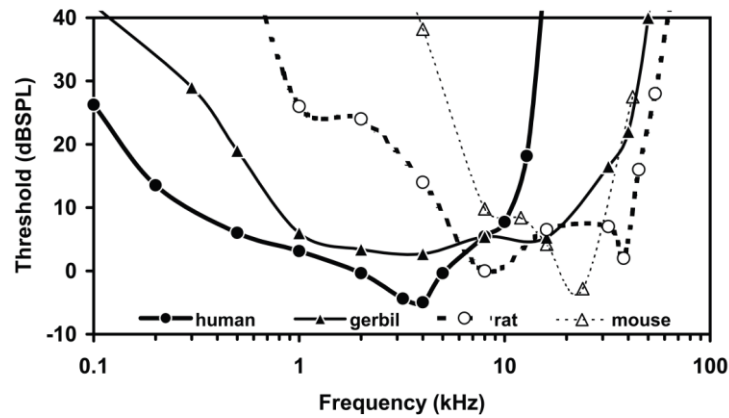


Figure 2: Hearing range of humans, rats, mice and gerbils

*Figure published by Gleich & Strutz (Gleich & Strutz, 2012), distributed under the terms of the Creative Commons Attribution 3.0 License

While invasive preclinical studies show great insight into brain functions during learning, an improved translation to human brain function is necessary. In neuroscience, one way to translate neuronal activity directly from animal to human research is possible with fMRI (Barron et al., 2021; Markicevic et al., 2021). Its non-invasiveness does not only ethically warrant research in humans, in addition it enables repeated measurements in the same subject, which lends itself perfectly to studies concerning learning processes. In animal research, this method can be combined with other, more invasive procedures. Despite its potential of direct transferability of preclinical auditory research in gerbils to ongoing human studies, auditory fMRI in the Mongolian gerbil has not been presented in literature yet.

Aim of this thesis

The overall aim of the hereby-presented thesis was to enable and to study auditory learning processes *in vivo* on whole-brain level with auditory fMRI in Mongolian gerbils. In the scope of this dissertation thesis, I therefore describe the following projects:

- (1) Establishment of auditory fMRI in the Mongolian gerbil;
 - (2) Evaluation of auditory fMRI in the Mongolian gerbil and possible confounds caused by the MR background noise and the animal anaesthesia with an additional imaging technique, the cerebral blood flow (CBF) SPECT;
- and in particular,
- (3) Auditory learning-induced changes in brain activation patterns acquired with auditory fMRI in the Mongolian gerbil.

These three aims of the thesis will be introduced, presented and discussed in separate chapters, followed by a general discussion.

1. Establishment of auditory fMRI in the Mongolian gerbil

1.1. Introduction

As elaborated in the general introduction, the Mongolian gerbil is a highly valuable model for auditory learning research. However, this model does not yet have a foothold in auditory fMRI, which would offer straightforward transferability to ongoing human research.

Performing fMRI in rodents is challenging, not just because of their small brain size. It requires either sophisticated anaesthesia regimes that prevent stress and motion of the animals but allow stimulus perception and preservation of normal brain function, or extensive behavioural training for animals to endure the scanning procedure in an awake state. Auditory-stimulated fMRI in rodents becomes even more demanding as functional MR scanning always produces non-negligible background noise by the fast switching of the magnetic gradients necessary for spatial resolution.

Another more specific difficulty of performing auditory fMRI, and fMRI in general, on Mongolian gerbils in comparison to other rodents arises from one key feature that makes them a popular choice for auditory research: their extended hearing range caused by extensive middle ear cavity expansions or *bullae*. These cavities are filled with air and are located in close proximity to the brain. In MRI, air-tissue interfaces cause distortions of the magnetic field and hence distortion of the MR images, commonly referred to as susceptibility artefacts. These occur particularly in prone imaging sequences like the gold standard of fMRI, gradient-echo echo-planar imaging (GRE-EPI).

Nevertheless, in the scope of this thesis, I established a protocol for auditory fMRI in the Mongolian gerbil, allowing for the observation of the functionality of its complete central auditory pathway *in vivo*. For a better understanding of the establishment process, the basic principle of MRI, fMRI and specifics in fMRI application in rodents is shortly explained in the following sections.

1.1.1. Magnetic resonance imaging

Nuclear magnetic resonance (NMR) is a physical phenomenon that relies on the properties of protons, which have an intrinsic momentum, a spin. These spins are aligned according to the Pauli Exclusion Principle whereas they are inversely arranged within an atom, cancelling each other out in atoms with even numbers of protons. Atoms with an odd number of protons have a nuclear spin that carries a magnetic moment and, therefore, can be aligned through a static magnetic field B_0 . In medical applications, the most commonly observed isotope is hydrogen (^1H). Proton spins rotate in precession along their own rotation axis parallel to B_0 in their resonance frequency, the Larmor frequency, which depends on the involved chemical isotope and the strength of the applied B_0 field. The proton spins can be perturbed out of their alignment and equilibrium by a radiofrequency (RF) pulse, a weak oscillating magnetic field of this resonance frequency applied

in a defined flip angle. A big proportion of the spins are tilted and transversal magnetization M_{xy} occurs. After the pulse, the proton spins return to their equilibrium state in the B_0 field, producing an electromagnetic RF signal in their precession movement (Figure 3) that induces voltage in the receiving coil. This voltage is the measured signal, the free induction decay (FID). (Plewes & Kucharczyk, 2012)

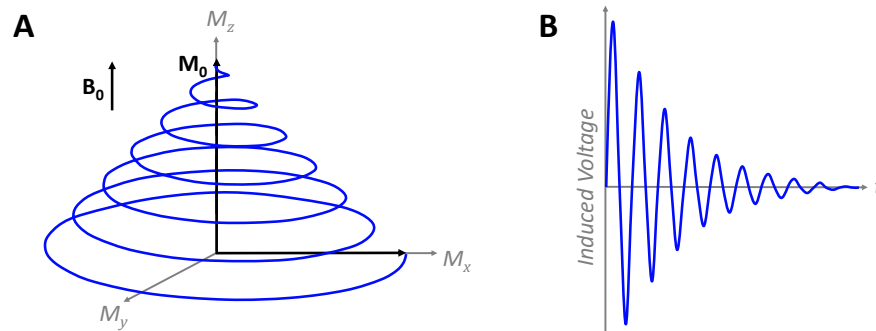


Figure 3: Radiofrequency signal after excitation with an RF pulse with 90° flip angle

A. Precession movement (blue) of a proton spin returning to equilibrium state M_0 in B_0 and **(B)** resulting measurable signal, the FID.

After proton spin excitation, the deterioration of the NMR signal proceeds in two independent relaxation processes. The process of the proton spins returning to the equilibrium M_0 in B_0 is termed longitudinal relaxation or spin-lattice relaxation, referring to the necessary energy transfer of the spins to its surroundings, and is described by the time constant T_1 . Transverse relaxation described with the relaxation time constant T_2 is the decrease of the M_{xy} magnetization perpendicular to B_0 through dephasing of the precessing protons after excitation, which leads to a gradual decrease of the signal. It is also referred to as spin-spin relaxation as the dephasing is caused by energy transfer between neighboring spins. Inhomogeneities in the B_0 field can accelerate the dephasing process and therefore change the time of signal decay from T_2 into a shorter time T_2^* . As both relaxation times, T_1 and T_2 , are dependent on the chemical surroundings of the protons, they are individual for each tissue type due to its composition. The contrast of an MR image is dependent on three major parameters of the tissue: the T_1 , the T_2 and the overall proton density within the tissue which determines the overall maximal signal intensity available in a tissue. As in most cases multiple excitation pulses are required for the acquisition of an MR image, it can be weighted according to one parameter or another by adjusting the time of re-excitement of the protons with another RF pulse referred to as the repetition time (TR), and the time of recording the RF signal emitted by the protons, the echo time (TE). For T_1 -weighted images, longitudinal relaxation is only partially allowed with a short TR and the effect of proton dephasing minimized by a short TE. Tissues with short T_1 show a brighter signal than tissues with a long T_1 , since more longitudinal magnetization is recovered and can be excited with the next RF pulse. To gain T_2 -weighted images, the longitudinal relaxation in between RF pulses is mostly

achieved by long TRs and the dephasing effect maximized with a long TE. (Plewes & Kucharczyk, 2012; Weishaupt et al., 2009)

For actual magnetic resonance imaging (MRI) an MR scanner is setup with three major components: (i) the main magnet producing the stationary magnetic field B_0 , (ii) RF coils for generation of RF pulses and RF signal detection, which can be achieved by one or two separate coils, and (iii) a gradient coil system that forms field gradients in B_0 in x, y and z direction to enable spatial encoding of the RF signal. This spatial encoding can be achieved, for example, by one gradient coil forming a gradient in the main magnetic field. As a consequence, protons in different slices experience a slightly different magnetic field which also changes the local resonance frequency. Through different excitation pulses, the different layers can be selected section wise in slices. The other two gradients are applied for phase and frequency encoding of the signal. This allows processing of the acquired raw RF signals from the k-space, a graphic matrix containing frequency information on the x-axis and phase information on the y-axis, into spatially resolved images through Fourier transformation. (Plewes & Kucharczyk, 2012)

In MRI acquisition, the FID is usually not measured directly. Usually an echo after an additional reverse pulse is applied to enhance the signal by reversion of the dephasing of the spins caused by B_0 inhomogeneities. In this regard MR sequences can be separated by reversion method in two main classes: the spin echo (SE) and the gradient echo (GRE). For the SE a 180° RF pulse is generated following the primary excitation pulse after half of the TE is elapsed. For GRE, a gradient field is applied for directed dephasing of the spins followed by an inverse gradient reversed by 180° for rephasing (Bjørnerud, 2008b). In a practical application, rapid acquisition of data can be obtained with less time consuming sequences. For instance with the fast low angle shot (FLASH) sequence, an incoherent GRE (Haase et al., 1986), or the rapid acquisition with relaxation enhancement (RARE), a spoiled fast SE (Hennig et al., 1986).

1.1.2. Functional magnetic resonance imaging

In fMRI, the activation of large populations of neurons is monitored by the principle of neurovascular coupling. This term describes the relationship of neuronal activation and a subsequent change in local cerebral blood flow (CBF) that regulates the adequate supply of nutrients and oxygen to the active cells in the brain (Cauli & Hamel, 2010; Hillman, 2014; Kleinfeld et al., 2011; Phillips et al., 2016). Increase of perfusion in the active regions through micro vasodilation additionally elevates the local amount of cerebral blood volume (CBV) (Hillman, 2014). Both, CBF and CBV can be recorded with appropriate fMRI sequences. CBF can be observed through the injection of contrast agents in combination with perfusion-weighted fMRI (Belliveau et al., 1991), or by arterial spin labelling (Detre et al., 1992). Increase in CBV can be recorded with MRI with application of superparamagnetic iron oxide (SPIO) contrast agents (Kim et al., 2013; Mandeville et al., 1998). SPIOs are based on iron oxide crystals, each containing iron ions (Fe^{2+}

and Fe^{3+}) in a large quantity. When iron ions are aligned in a magnetic field they induce net magnetic moment, which considerably surpasses that of typical paramagnetic ions, hence the name superparamagnetism. The enhancement mainly affects the T2 relaxation or rather T2* but can also affect T1, depending on size and composition of the nanoparticles. (Bjørnerud, 2008a; Lin & Brown, 2007)

On top of these measurable changes in CBF and CBV caused by neurovascular coupling, the magnetic properties of the haemoglobin in the blood itself change with its oxygenation status. Whereas fully oxygenated haemoglobin is diamagnetic and has no different impact on the magnetic field than normal brain tissue, fully deoxygenated haemoglobin is highly paramagnetic (Glover, 2011; Kennerley et al., 2010) and hence shortens the T2* time. This effect is termed blood oxygenation level dependent (BOLD) contrast (Ogawa et al., 1990) and currently the most commonly recorded signal change in fMRI. The most frequently used sequence for imaging of the BOLD contrast is the gradient-echo echo-planar imaging (GRE-EPI) sequence, as it is very sensitive to T2* effects. The term EPI refers to the mode of signal readout, where the data of an entire 2D plane can be collected with one single RF-excitation pulse through multiple fast switches in gradients. Because of these fast switches in gradient fields, EPI sequences produce extremely high noise due to Lorentz forces acting on the gradient coils (Hall et al., 1999).

During neuronal activation, CBF increase outweighs increased oxygen consumption by 2:1 (Buxton & Frank, 1997), which leads to a washout of deoxygenated haemoglobin and local surplus of oxygenated haemoglobin (Kennerley et al., 2010). This generates the typical measurable signal curve for stimulated neurological activation upon presentation of stimuli in fMRI, mathematically described by the hemodynamic response function (HRF), as illustrated in Figure 4.

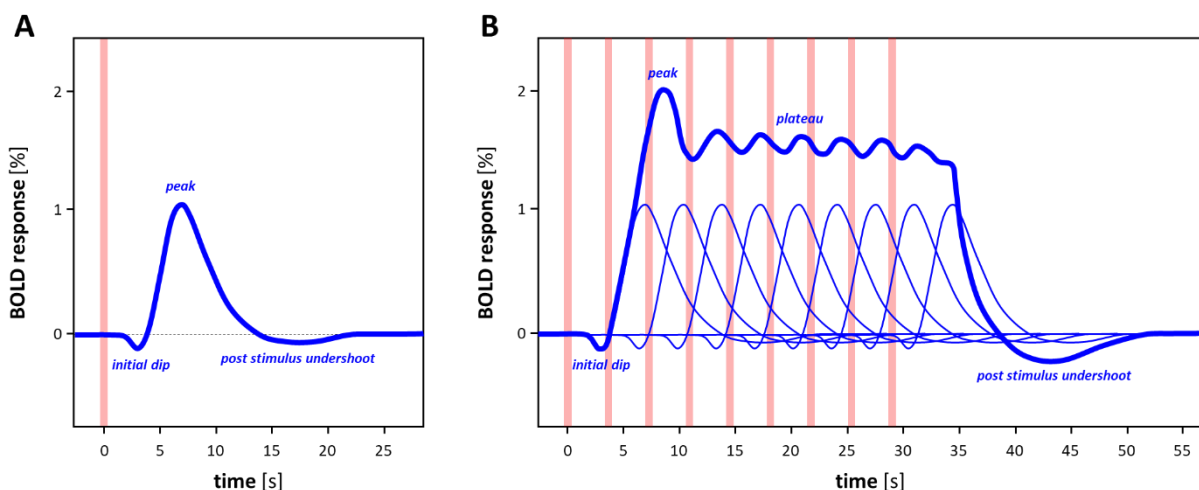


Figure 4: Hemodynamic response function to sensory stimulation

A. Signal curve of the BOLD response measurable with short stimulus (marked in light red), also referred to as haemodynamic response function. **B.** Add-up of multiple short stimuli leads to an increase in BOLD-response with an initial overshoot peak and a plateau of increased BOLD throughout the repetition of the stimulus, dropping off after the stimulus ends. Both curves show the typical time span for the HRF measured in cortical areas of human subjects.

*Images were adapted from MRIquestions.com by courtesy of Allen D. Elster (Elster, 2023)

The curve starts with an initial dip in signal intensity after stimulus onset, thought to be caused by increased oxygen consumption with slow vascular response (Hu & Yacoub, 2012). This dip is followed by a steep increase to positive peak signal intensity through CBF increase and washout of the deoxygenated haemoglobin, which is upheld throughout the stimulus duration in a plateau, especially if it is a pulsed stimulus (Blamire et al., 1992); and finally a post-stimulus undershoot due to the drastic drop of CBF (Chen & Pike, 2009).

The expected HRF following a stimulus presentation is the basis for the standard analysis of sensory-evoked fMRI. In a preprocessing step the measured data is corrected amongst others for head motion, signal drifts, slice-timing discrepancies occurring during the acquisition time. Afterwards, statistical analysis is performed to obtain maps that show where the signal changes correlate best with a convolution of the hemodynamic response function and the stimulation paradigm (Chen & Glover, 2015; Friston et al., 1998). For stimulus-evoked fMRI, statistical analysis with the general linear model (GLM) is the most commonly used approach, relying on single voxel-based matrix algebra (Monti, 2011).

Through stimulus-evoked fMRI, two essential classes of neuroscientific questions can be addressed: (i) from which location in the brain does the processing of information give rise to a specific ability, and (ii) when this processing is evoked (Kosslyn, 1999).

Auditory fMRI poses additional challenges, as it requires the perception of the auditory stimulus over the inevitable background noise generated by the scanning procedure itself, which in turn can affect the sound processing in the auditory brain structures and the measured BOLD signal (Hall et al., 1999; Moelker & Pattynama, 2003; Peelle, 2014). The search for quieter fMRI acquisition methods and reduction of the scanning background noise through masking with passive or active noise cancellation is an ongoing endeavour (Damestani et al., 2021; Heismann et al., 2015; Ljungberg et al., 2021).

1.1.3. Functional magnetic resonance imaging in rodents

While fMRI is one of the leading techniques in investigation of whole-brain function in humans, only a limited number of research centres have access to small animal MR scanners with the field strengths required for functional imaging of the much smaller brains of rodents. Consequently, other than in most areas in modern neuroscience, fMRI in rodents followed and still follows to this day findings and advances achieved in the human research field. However, to truly understand the implication of the large-scale network activations acquired with fMRI and their biological origin, controlled experimental conditions and invasive interventional experiments are needed that are only attainable in experimental animals (Markicevic et al., 2021).

fMRI in rodents poses additional challenges to the acquisition protocol used in human research. For one, as mentioned before, the relatively smaller size of the rodent brains (e.g. weight difference factor of 3000:1 between human brain and mouse brain, see Table 1) necessitates

higher field strength and better gradient systems for spatial encoding (Xu et al., 2022), or alternatively, exceedingly longer acquisition times for comparable spatial resolution of the brain structures.

Table 1: Average brain weight of rodents and humans

Average brain weight of humans (Azevedo et al., 2009), exemplary laboratory rats and mice (Herculano-Houzel et al., 2006) and Mongolian gerbil (Wilkinson, 1986) and a comparison of human brain weight factor vs. those of rodents.

		brain weight [g]	weight difference compared to human brain
human	<i>homo sapiens</i>	1,200 -1,300	1:1
rat	<i>wistar rats</i>	1.80	1:700
gerbil	<i>mongolian gerbil</i>	1.06	1:1200
mouse	<i>swiss mice</i>	0.42	1:3000

Longer acquisition times are not feasible for rodent fMRI. The acquisition in rodents requires an increase in time resolution instead, as the time window of the hemodynamic response is shortened compared to humans' (Lambers et al., 2020). In studies investigating rodent HRF values under standard anaesthesia settings, discovered time to maximum peak and time to undershoot occur already after 2.8 ± 0.8 s and 6.1 ± 3.7 s in rat cortex (Lambers et al., 2020) and 3.32 ± 0.10 s and 9.12 ± 0.10 s throughout the mouse brain (Chen et al., 2023). Comparative HRF values used for standard human fMRI analysis are 5 s and 15 s (Friston & Ashburner, 2020).

Higher field strength, however, comes with increases in image distortions through susceptibility artefacts (Farahani et al., 1990; Yang et al., 2006). Unfortunately, increase in field strength does not lead to higher BOLD contrast (Seehafer et al., 2010), so apart from higher spatial resolution it does not offer advantages over functional imaging acquired in lower fields.

Furthermore, fMRI acquisition requires either sophisticated anaesthesia protocols or extensive behavioural training for rodents to lay still and lower their stress levels during the scanning procedure. Anaesthesia protocols have to be carefully adjusted to the individual fMRI setup and research purpose, since anaesthetics tend to alter measured BOLD signal. For example medetomidine, a frequently used sedative in rodent fMRI (Cabral et al., 2023; Pawela et al., 2009; Zerbi et al., 2015), acts on the α_2 -adrenoceptor and induces sedation, but also respiratory depression, bradycardia, hypertension, diuresis, muscle relaxation and analgesia in higher dosages (Bol et al., 1997; Correa-Sales et al., 1992; Savola, 1989). Additionally, it affects the BOLD signal through vasoconstriction (Kint et al., 2020). Isoflurane, an inhalation anaesthetic often used for anatomical MRI and sometimes also for fMRI purposes (Huang et al., 2022; Masamoto et al., 2006), on the other hand, lowers the measurable BOLD signal through systemic vasodilation (Sullender et al., 2022). As a result, many fMRI studies in rodents revolve around anaesthesia effects (Paasonen et al., 2016; Paasonen et al., 2018; Schlegel et al., 2015; Schroeter et al., 2014), the optimization of protocols for better perception of stimuli (Pawela et al., 2009; Petrinovic et al., 2016; Shim et al., 2018) and prolonged stability of the sedation (Simpilatzte et al., 2019). fMRI

measurements of awake rodents should only be conducted with thorough acclimatization training to the acquisition procedure to reduce the experienced stress of the animals (King et al., 2005; Russo et al., 2021). Such acclimatization protocols for awake mouse fMRI range from 3 to 28 days, according to a recently published review addressing this topic (Mandino et al., 2023). In this review, Mandino et al. also comment on poorly characterized stress levels of the animals with wide ranges of reported stress hormones such as corticosterone during acclimation training and actual awake fMRI acquisition even within the same strain of mice (Dinh et al., 2021; Gutierrez-Barragan et al., 2022; Harris et al., 2015). Additionally, fMRI performed with awake rodents usually requires a surgical installation of a head holder that keeps the animals head fixated in the same position during the acquisition (Mandino et al., 2023; Tsurugizawa et al., 2021).

Lastly, space in small animal MR scanners is extremely limited and not all sophisticated stimulation equipment used in human fMRI studies can be accommodated for.

1.2. Method establishment

1.2.1. Experimental animals

All experiments were performed on adult male Mongolian gerbils (*Meriones unguiculatus*, bred in-house, or purchased from Charles River, Italy). The gerbils were housed in groups of up to 5 animals in a temperature-controlled room with 12h/12h dark light cycle (6:00/18:00) with food in form of rodent pellets and sunflower seeds, and water *ad libitum*. All animal experiments performed in pursuit of this dissertation thesis were approved by the ethics committee of Saxony-Anhalt (No. 42502-2-1489 and No. 42502-2-1591, LIN).

1.2.2. Measurement setup

A 9.4 T horizontal small animal scanner (*BioSpec® 94/20 USR*, Bruker BioSpin GmbH & Co. KG, Germany (Bruker)) equipped with a gradient system producing up to 660 mT/m and enabling shimming with up to 2700 Hz/cm in all directions (*B-GA12S HP*, Bruker) was implemented with the accompanying acquisition software *ParaVision Acquisition Workplace* (version 6 and 7, Bruker) for all MRI measurements.

For setup improvement, a variation of sequence types in combination with different RF coils were tested to optimize the overall image quality and BOLD signal.

The coils used during the establishment phase were: a ¹H-transmit-receive volume coil with inner diameter of 40 mm (*MT0205*, Bruker) by itself, or a ¹H-transmit-receive volume coil with inner diameter of 86 mm (*MT0381*, Bruker) combined with ¹H planar receive-only surface coils of diameters: 20 mm, 10 mm and later 15 mm (*MT0105-20/MT0105-10/MT0105-15*, Bruker) connected to a RF coil preamplifier (*MT0105*, Bruker).

With an automated positioning system (*AutoPac™*, Bruker) the animals' position was adjusted so that the laser crosshairs were situated slightly anterior to the pinnae or alternatively on the indicated center of the volume coil.

Measurement setup improvement was not limited to MR technical components and sequences. At the same time, changes in mode of anaesthesia and temperature control of the animals, improvements on the auditory stimulation setup and fMRI data analysis were made.

1.2.3. Anaesthesia protocol

All Mongolian gerbils underwent the MRI measurements in an anaesthetised state to prevent motion and stress of the animals. For the initial establishment of the setup and the prior sequence optimization in regard to image quality, the animals were measured under 1.5 % isoflurane (*Vetflurane*, Virbac Arzneimittel GmbH, Germany) in a mixture of equal amounts of oxygen and nitrogen (evaporator: *UniVet Porta*, GROPLER medizintechnik, Germany). To investigate functional measurements, different regimes of medetomidine were investigated; originally starting with s.c. injection of an initial bolus through 0.1 mg/kg medetomidine (*Domitor*, Orion

Pharma GmbH, Germany) followed by continuous *s.c.* injection of 1.0 mg/kg/h after 20 min with a peristaltic pump (*Peristaltic Pump P-1*, GE Healthcare Bio-Sciences AB, Sweden).

Throughout the establishment phase, a wide variety of appropriate dosages and dilutions of medetomidine, as well as combinations with low dosages of isoflurane (0.2-0.5 %) were systematically tried out and adapted from commonly used mouse and rat anaesthesia protocols (Paasonen et al., 2018; Schlegel et al., 2015). This included a change in administration route from *s.c.* to *i.v.* with an infusion pump (*Pump 11 Elite Infusion Only Single Syringe*, Harvard Apparatus, USA). To find the lowest possible medetomidine *i.v.* dosage, medetomidine standards applied in rats with 0.1 mg/kg/h (Paasonen et al., 2018) were administered to the gerbil combined with isoflurane. The dosage of medetomidine was incrementally elevated with reduction of the concurring isoflurane administration until isoflurane anaesthesia could be stopped completely without awakening of the animal.

Additionally, the clinical standard of light anaesthesia with propofol (*PropoVet Multidose*, Abbot Logistics B.V., Netherlands), also known as 2,6-Diisopropylphenol, was established for the Mongolian gerbil. For propofol anaesthesia, the protocol of 20 mg/kg initial bolus followed by 75 mg/kg/h continuous *i.v.* injection was adapted from comparable fMRI anaesthesia protocols for mice and rats (Paasonen et al., 2018; Schroeter et al., 2014). Throughout those measurements, we closely observed the animals breathing rate and body temperatures. Initially the temperature control ensued with a heating mat positioned underneath the animals combined with measurement of body temperature and manual adjustment of the connected heated water bath. Later on, a body temperature controlled air warming system (*MR-compatible Small Rodent Air Heater System*, Small Animals Instruments Inc., USA) was implemented instead.

1.2.4. Optimization of different fMRI sequence types

To achieve fMRI of the Mongolian gerbil in a reasonable time resolution, multiple imaging sequences were implemented and optimized from the standard settings supplied by Bruker. Image sequences optimized and tested for potential in recording BOLD signal changes included: a T2* sensitive GRE-EPI, a T2-weighted SE-EPI, a T2-weighted segmented SE-EPI, a T1-weighted FLASH sequence, a dynamic contrast enhancement (DCE) FLASH sequence, and a zero echo time (ZTE) sequence with and without application of a superparamagnetic iron oxide (SPIO) contrast agent. The contrast agent application was adapted from a similar CBV-ZTE method established in rats (Shih & MacKinnon, 2020; Shih et al., 2011). It was implemented by *i.v.* injection of 3 mgFe/kg Molday ION™ (30 nm SPIO with 10 mgFe/ml, BioPAL, Inc., USA), or alternatively 0.6 mgFe/kg BW FeraSpin™ XS, (10-20 nm USPIO, Viscover – nanoPET pharma GmbH, Germany) in the scanner directly prior to fMRI acquisition.

For each sequence, the field of view (FoV) was first adjusted to encompass the entire gerbil brain. Under observation of acquired SNR and increase in measurement time, the sequences were

further refined in spatial resolution and slice thickness. Flip angle, TR and TE were adjusted mostly with respect to recorded BOLD signal changes. For FLASH and ZTE sequences, a trigger-module had to be coded into the sequence program, to enable a time coupling of fMRI measurement and auditory stimulation protocol.

Other factors that were adjusted and tested included changes of the read-out direction, measured bandwidth of the signal readout, and even changes of the overall shape of the gradient ramps in pursuit of higher image quality and reduction of scanner noise.

1.2.5. Auditory stimulation

Auditory stimulation delivery into the scanner was achieved via air transmission through hollow silicone tubes with pliable earplug tips (*Pillow Soft Silicone Putty Earplugs*, Mack's, USA) that were pushed in the outer ears of the animals and fixated by a variation of means; tape (*3M Transpore Tape*, Minnesota Mining and Manufacturing Company, USA) proving to be the most reliable method. For sound delivery the air tubes were connected to speakers (manufactured in-house by Andreas Fügner, additional information in the supplements in Figure S 1) fixated to the outer wall of the MR scanner and via an amplifier (*901 Personal Stereo Amplifier*, Kramer Tools GmbH, Switzerland) connected to a stimulation computer, where the sounds were generated. This computer also received the TTL trigger signal from the MR scanner via a terminal block (*BNC-2110*, National Instruments, USA). The stimulation tones and block protocols were programmed and computed in LabView (version 2016, National Instruments, USA). The stimulation design included coupling of sound transmission to the TTL trigger signal to ensure precise stimulation onsets. For the fMRI scans, the LabView stimulation protocols were manually started after the sequence pre-adjustments ran through. The stimulation protocol was presented either binaurally or monaurally in a block design with a 120 s baseline and 10 repetitions of a stimulation blocks (8 to 20 s) alternating with rest blocks (20 to 60 s), length varying for both in different setup tests and for sequence types. Different stimulation tones included pulsed pure and frequency modulated (FM) tones in a range of frequencies within the optimal hearing range of the Mongolian gerbil (e.g. 1-2 kHz sweeps), and pulsed Gaussian white noise (WN). All tones were generated with amplitude envelopes with linear 10 ms rise and decay ramps to prevent unwanted noise artefacts like clicks.

A standard auditory stimulation protocol implemented during the establishment process went as follows. Pulsed 1-2 kHz sweeps of 200 ms length with 300 ms inter-stimulus intervals (ISI) were presented binaurally in a block design at a sound level of 95 dB. This design was often set up with a 120 s baseline, followed by ten stimulation blocks of 10 s length interleaved by 50 s breaks, as schematically visualized in Figure 5.

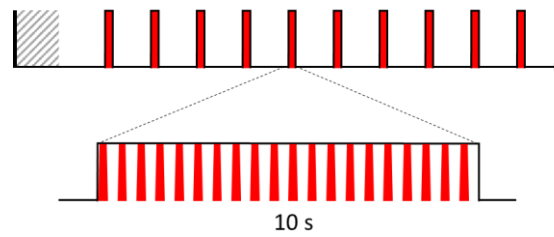


Figure 5: Protocol for auditory stimulations with pulsed presentation of the stimulation tone

After an initial baseline without any stimulation, stimulation blocks (red) are alternated with rest blocks. For pulsed stimulation, repeating tones of 200 ms were interleaved by 300 ms inter-stimulus intervals (ISI).

The sound profiles of the stimulation tones and additionally of the finally selected fMRI sequence were recorded with an MR-compatible optical microphone (MO 2000 Set, Sennheiser Electronic GmbH & Co. KG, Germany). The sound pressure levels (SPL) of pulsed stimulation tones were recorded over the ambient noise level in the MR scanner room outside of the MR scanner with a frequency bandwidth reaching from 0.67 Hz to 22.05 kHz (each recording 30 s). The sound profile of the optimized GRE-EPI sequence was recorded likewise inside the bore of the 9.4 T scanner for the most accurate representation of to the background noise experienced by the animals. The ambient background noise was recorded in addition and subtracted from the sound profiles. Non-frequency specific measurements of the SPL level of the stimulation tones on left and right speaker were regularly tested for the fMRI experiments with a handheld sound level meter (Sauter SU 130, Sauter GmbH, Germany).

1.2.6. fMRI data analysis

Preprocessing and analysis of the fMRI data was performed mainly with BrainVoyager (version 20.6, Brain Innovation, Maastricht, Netherlands). The exported DICOM images were loaded into the imaging analysis program and the applied stimulation protocol attached to the file, taking possible delays due to dummy scans occurring at the beginning of some sequence types into account.

For preprocessing of the imaging data, a slice time correction with a cubic spline interpolation was performed, 3D motion correction trilinear/sinc interpolation to the first functional image, smoothing by a FWHM of 2 x the inplane voxel resolution in space domain and temporal filtering with a Gaussian high pass filter (2 cos/sin of data points). Any spontaneous voxel displacement bigger than the recorded voxel size was considered movement and the scan was excluded from analysis. For functional ZTE images, a mean intensity adjustment was performed in addition.

Each scan was evaluated with an individual GLM, the two-gamma HRF applied to the stimulation protocol of each run adjusted with time to response peak of 3 s and time to undershoot peak of 10 s, to accommodate for the shortened hemodynamic response in rodents in comparison to humans. First comparisons between different setups, anaesthesia protocols and sequence types were achieved by visual inspection of the activation patterns with thresholds set to similar values with false discovery rate (FDR) correction. The signal time course (STC) and event related

averages (ERA) were extracted from activation clusters located in the auditory structures and their progression profile and peak values set side by side.

To enable comparisons for the higher quality data sampled towards the end of the establishment process, the high quality anatomy of each scan was manually coregistered to a high definition 3D-anatomical MRI template of a gerbil brain (*in vivo* measurement of 4 h performed by Patricia Wenk, 48 h after injection of a manganese-chloride contrast agent). The coregistration parameters were applied to the associated functional scans, converting them to 3D volume time course (VTC) data in the same native space. The threshold for FDR correction with $q < 0.001$ was noted and the statistical maps were exported to NIfTI-format. The images shown in chapter 1.3.2 were obtained with MRICroGL (version 20, ([MRICroGL, 2019](#))).

Region of interest analysis was implemented on basis of the gerbil brain atlas (alpha version, hitherto unpublished by Gottschall, Budinger *et al.*), the atlas structures originally intended for lightsheet images were grouped into anatomically correct larger regions. These regions were then manually adjusted to the 3D-anatomical MRI template in BrainVoyager (version 22.4, Brain Innovation, Maastricht, Netherlands) under observation of the “Brain atlas of the Mongolian gerbil (*Meriones unguiculatus*) in CT/MRI-aided stereotaxic coordinates” ([Radtke-Schuller et al., 2016](#)). Final terminology of these atlas regions, their grouping and hierarchical order are listed in the supplements in Table 4. %-transformed BETA values¹ and ERAs of each measurement were extracted within volumes of interest (VOI) allocating the auditory structures.

¹ %-transformed BETA values give quantitative information on stimulus-evoked activation changes and correspond to the BOLD signal change (BOLD%) when the GLM-model fits the measured STC.

1.3. Results

1.3.1. Interim results throughout the establishment process of auditory fMRI

Initial fMRI scans with available standard sequences and coil configurations showed no BOLD contrast and strong susceptibility artefacts.

Anaesthesia protocol optimization

Significant BOLD contrast was not acquired until after the anaesthesia protocol for Mongolian gerbils was refined. The impact of anaesthesia protocols on breathing rates and measured raw fMRI signal is presented in Figure 6. Throughout the first fMRI attempts, it became apparent that an infrequent breathing rate had a direct impact on the measured STC: abrupt changes in breathing translated directly into simultaneously occurring signal jumps in fMRI, which was most striking in experiments with propofol anaesthesia (Figure 6E). These signal jumps were not removable from the STC through the described preprocessing steps or any kind of additional temporal filtering and consequently may have masked BOLD contrast induced by the auditory stimulation.

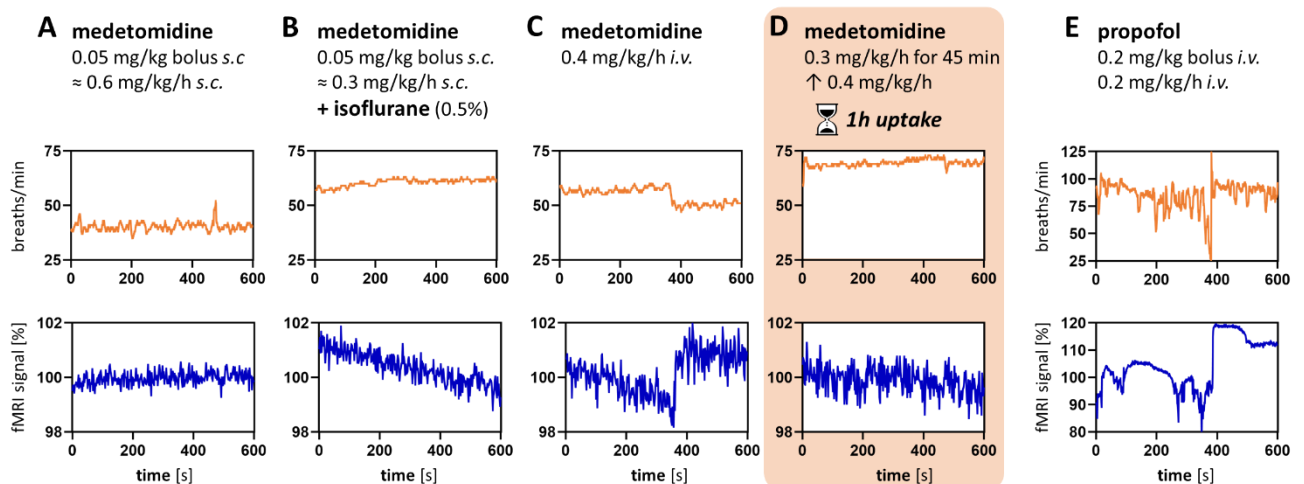


Figure 6: Stability of different anaesthesia regimes during fMRI acquisition

Breathing rate of representative gerbils (top, orange) during the fMRI scan and its influence on the uncorrected fMRI signal (bottom, blue) measured with a standard GRE-EPI sequence. A-D. Different protocols of medetomidine anaesthesia resulted in relatively stable breathing rates. Any abrupt changes in breathing rates, even small ones, resulted in simultaneous fMRI signal jumps (C). E. Under propofol anaesthesia, breathing rate and measured fMRI signal were highly irregular.

The initial subcutaneous administration of medetomidine worked well to immobilize the gerbils and practically guaranteed movement-free fMRI recordings, but resulted in low breathing rates under 40 breath/min. fMRI images acquired under these low and stable respiratory rates were absent of abrupt signal jumps (Figure 6A), but also did not show any auditory-evoked BOLD contrast (not shown). Continuous intravenous administration of a lower dosage of medetomidine (0.4 mg/kg/h) through the tail vein rendered first BOLD responses to auditory stimulation with respiratory rates in ranges between 50 and 60 breath/min. Further decrease in dosage of

medetomidine led to movement and spontaneous awakening of the gerbils, when MR sequences were started. Whereas higher dosages led to lower respiratory rates and decreased BOLD responses. Throughout the ensuing sequence optimization process, higher BOLD responses were found in later fMRI runs within the same session. The anaesthesia regime was therefore further refined to contain an initial uptake phase of medetomidine, where the animals received 0.3 mg/kg/h *i.v.* for 45 min, after which the dosage was increased to 0.4 mg/kg/h. The MRI measurements were started after an overall medetomidine uptake phase of 1 h. As visible in Figure 6D, this protocol allows for relatively high breathing rates (60 – 85 breaths/min) without abrupt fMRI signal changes.

Coil and sequence selection

Since the signal to noise ratio (SNR) for surface coils in combination with the 86 mm volume coil turned out higher within the region of the brain, than the 40 mm volume coil by itself (by at least 10% and up to 100%, depending on the surface coil), this setup was implemented for most of the establishment phase. While the 10 mm surface coil had the highest SNR with normalized value of 13,000 /mm³, it did not cover the whole gerbil brain and caused signal loss towards the anterior, posterior and dorsal regions of the brain. The 20 mm loop covered all of the gerbil brain and even some extra areas but had a substantially worse SNR of 7,300 /mm³. Consequently, a custom coil of 15 mm diameter was commissioned from Bruker, to maximize on both, coverage and SNR for the gerbil brain. This 15 mm surface coil acquires average normalized SNR values of 11,500 /mm³ in the regular MRI quality measurements.

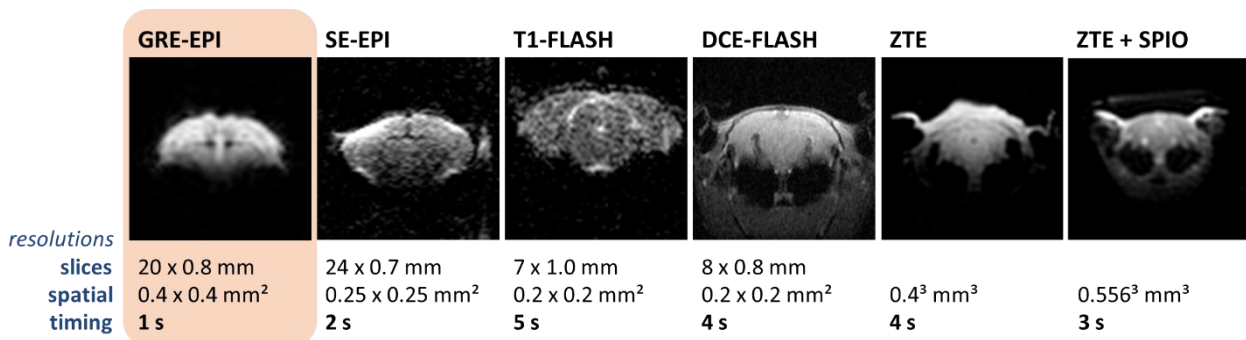


Figure 7: fMRI image quality of different optimized sequence types acquired with a 20 mm surface coil
Example images of different sequence types tested and optimized for auditory fMRI in the Mongolian gerbil. Note that only the GRE-EPI sequence resulted in stable BOLD activation upon auditory stimulation.

Highest image qualities were achieved with the optimized DCE-FLASH sequence, as can be seen in representative coronal images in the areas most affected by the middle ear cavities in Figure 7. Unfortunately, this measurement sequence yielded no significant signal change through auditory stimulation (FDR $q < 0.05$), even though the sequence itself was audibly quieter than the EPI alternatives. The optimized SE-EPI, T1-FLASH and ZTE without contrast enhancement did not acquire any significant BOLD contrast either.

In terms of BOLD sensitivity, the GRE-EPI method recorded the highest and most consistent auditory-evoked signal changes, even without particular adjustments. The downsides of this sequence type were the actual image quality, with strong distortion artefacts towards the posterior parts of the gerbil brains, and its enormous noise production (> 120 dB).

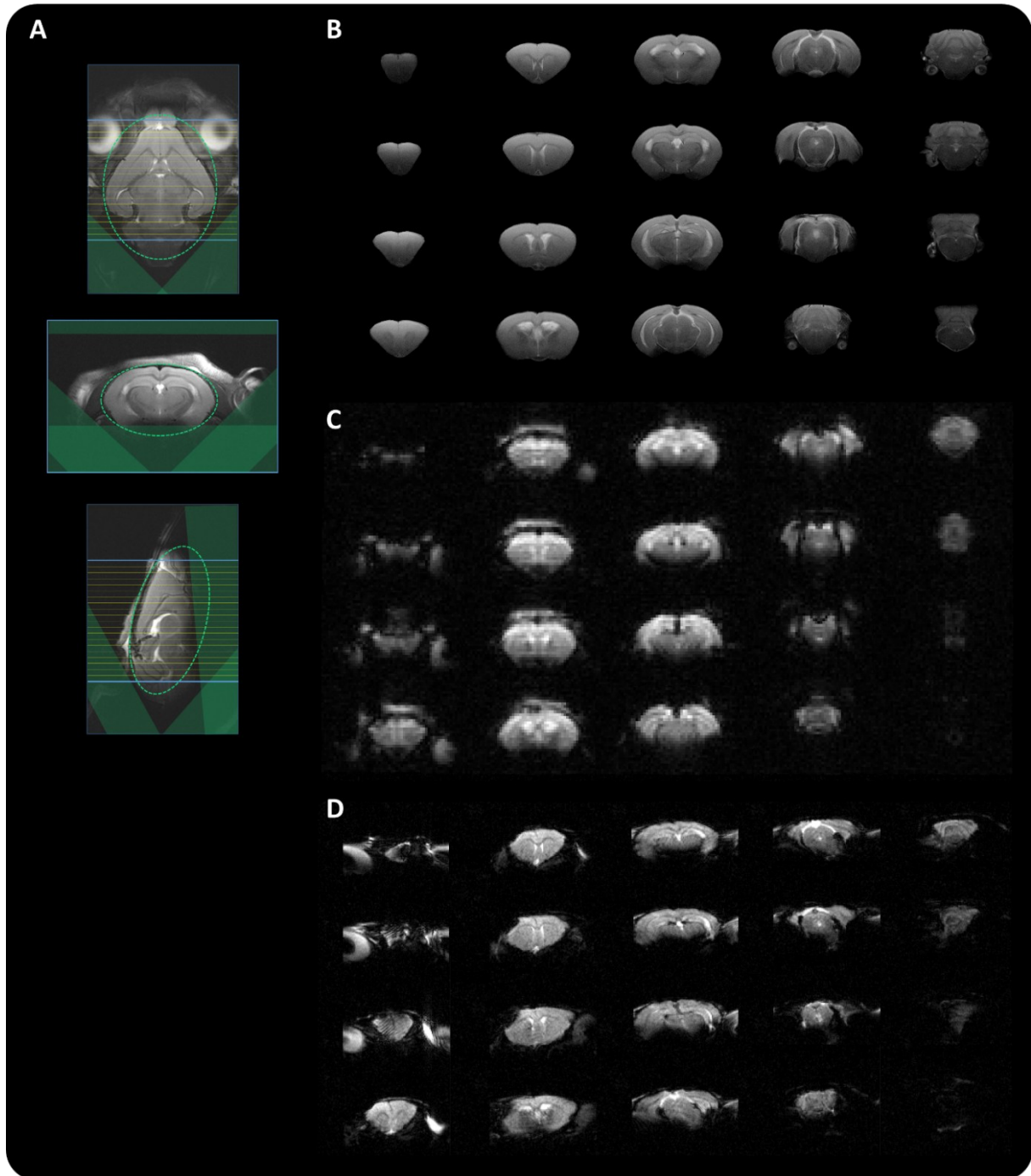


Figure 8: Functional images acquired with optimized mode of GRE-EPI acquisition

A. Position of the 20 coronal image slices (blue outline), FoV saturation slices (green semi-transparent areas) and shim volume (serrated green oval) for the optimal acquisition of **(B)** T2-weighted anatomical images and **(C)** GRE-EPI optimized for functional imaging of the Mongolian gerbil, acquired with a single repetition in 1 s time resolution. Representative anatomical and functional images were consecutively recorded with the 15 mm surface coil. **D.** Comparative GRE-EPI images from earlier fMRI attempts prior to effective optimization show huge distortions artefacts throughout the entire brain; acquired with the 20 mm surface coil.

The GRE-EPI image quality was improved and image distortion effects diminished by strategic placement of FoV saturation slices over the air-filled *bullae*, shimming throughout the brain tissue and adjustment of various sequence parameters. Representative resulting GRE-EPI images are presented in Figure 8C, remaining image artefact was signal bleed-out towards more anterior, posterior, and ventral parts of the gerbil brain. In comparison, earlier attempts resulted in strongly distorted images even with application of some FoV saturation slices in the region of the bullae, shown in Figure 8D.

An example of BOLD activation measured with the optimized GRE-EPI is shown in Figure 9. The activation was induced by stimulation with pulsed 1-2 kHz FM tones presented in a block design with 10 s stimulation blocks alternating with 50 s breaks.

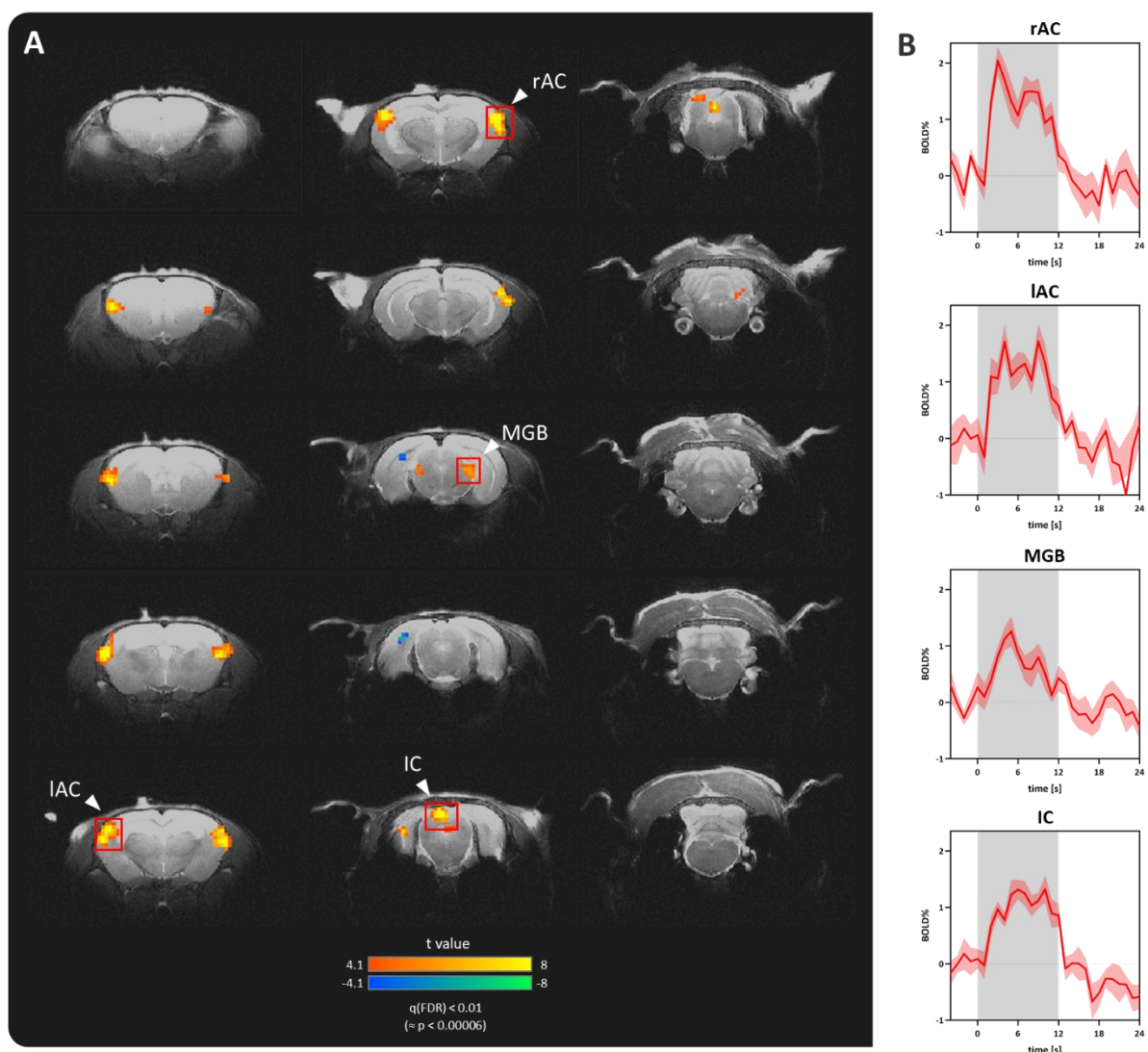


Figure 9: Auditory activation patterns acquired with GRE-EPI after sequence optimization

A. T2-weighted anatomy overlaid with activation patterns (FDR corrected to $q < 0.01$) induced by auditory stimulation, implemented bilaterally with 1-2 kHz sweeps (repeated 200 ms with 300 ms ISI) and presented in a block design with 10 x 10 s stimulation blocks alternating with 50 s breaks at 95 dB SPL. Maximal signal changes in the activation clusters framed in red amounted up to **(B)** 2 % in rAC, 1.8 % in IAC, and 1.25 % in MGB and IC region. (Acquired following the protocol for “Optimized auditory fMRI in the Mongolian gerbil” in chapter 1.3.2)

Another sequence type that showed at least some potential in detection of auditory-evoked brain activation was an optimized ZTE with contrast enhancement through *i.v.* injection of the SPIO Molday ION™. Advantages of this sequence were the extremely low background noise (MR scanner noise of 55 dB measured directly next to the scanner during acquisition, compared to 51 dB without scanning), and relatively few imaging artefacts caused by the *bullae*, as is already visible in Figure 7. However, signal intensity changes acquired with the same measurement setup and auditory stimulation through repeated 1-2 kHz FM tones were much lower than changes detected with the GRE-EPI sequence, despite contrast enhancement (Figure 10 vs. Figure 9). BOLD contrast acquired with the ZTE + SPIO peaked at a maximum of 0.5 % signal change in the very small activation clusters in AC (Figure 10B); whereas peak values of clusters measured with GRE-EPI in AC reached 2 % (Figure 9B). Additionally, with ZTE + SPIO the region of the eyes of the gerbil showed huge BOLD contrast that superimposed into the brain tissue (Figure 10A).

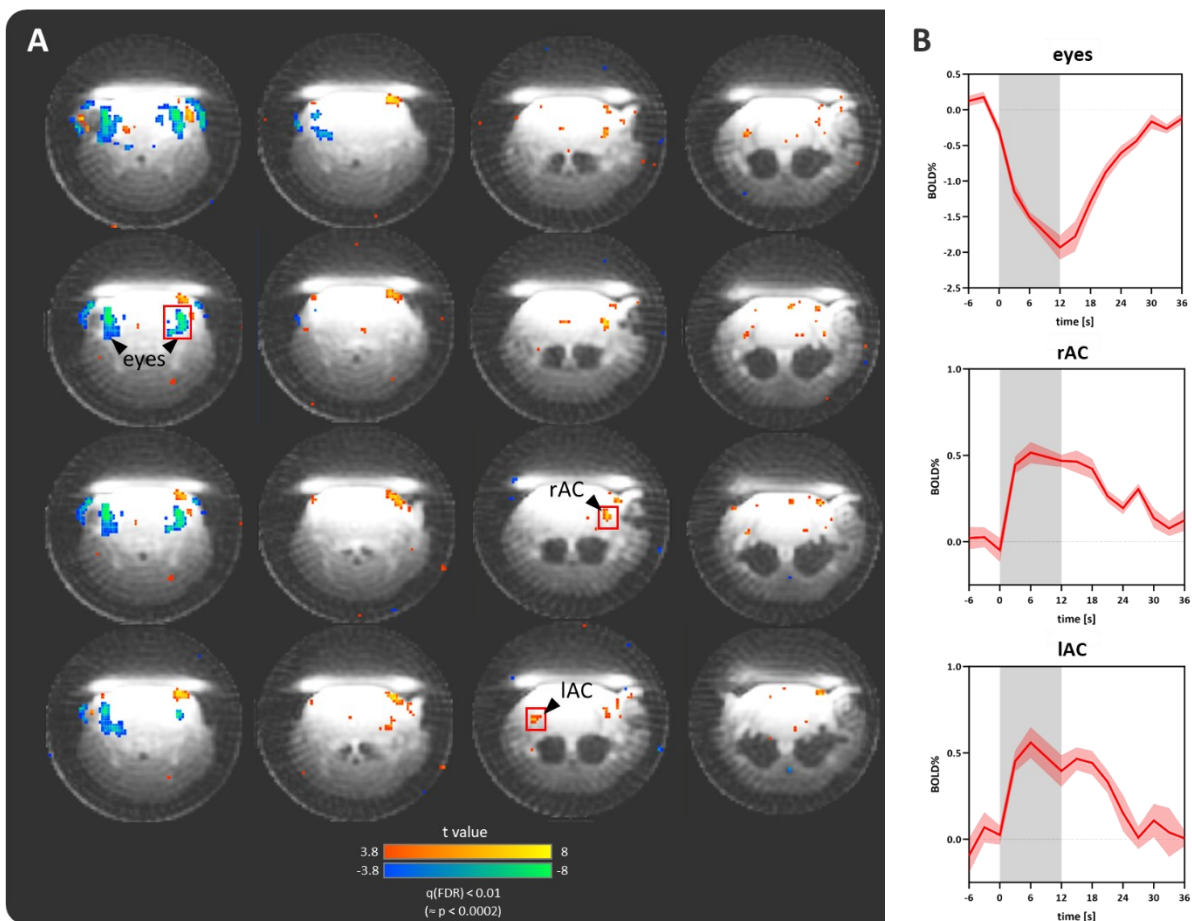


Figure 10: Auditory activation patterns acquired with ZTE sequence after SPIO injection

A. 16 of the 72 reconstructed slices ranging from the posterior end of the olfactory bulb to the maximum of the middle ear extensions show the image quality of the optimized ZTE-fMRI sequence with activation patterns overlay (FDR corrected to $q < 0.01$). Distinction of brain tissue from signals originating from other tissue types or even the coil itself was challenging; maximal signal changes in the activation clusters framed in red amounted to (B) 0.5 % in IAC and rAC, and -3 % in the eye region. Images were acquired following the optimized protocol presented in chapter 1.3.2, with additional contrast agent injection and diverging fMRI sequence. Auditory stimulation was presented bilaterally with 1-2 kHz (200 ms sweeps, 300 ms ISI) in a block design with 10 x 12 s stimulation blocks alternating with 36 s breaks, SPL was adjusted to 75 dB as louder stimulation led to movement of the animals.

Optimization of auditory stimulation

The auditory stimulation tones were transduced with relatively low SPL over the ambient noise level in the scanner room in comparison to the noise generated by the GRE-EPI. Sound profiles of both are presented in Figure 11. Pulsed FM tones rising from 1 to 2 kHz (200 ms sweep, 300 ms ISI) resulted in the most distinct frequency band in the expected frequency range between 1 and 2 kHz in these recordings. Stimulation with higher frequencies, for example pulsed 15 kHz pure tones, primarily resulted into an SPL peak at 5 kHz and additional lower peaks at 10 kHz and 15 kHz, possibly caused by refraction and/or absorption of the sound wave at the plastic tube walls leading the air transmission into the animals' outer ear. Non-frequency specific SPL measurements of this 1-2 kHz stimulation with the handheld sound level meter amounted to overall SPL of 95 dB on both speakers' ends.

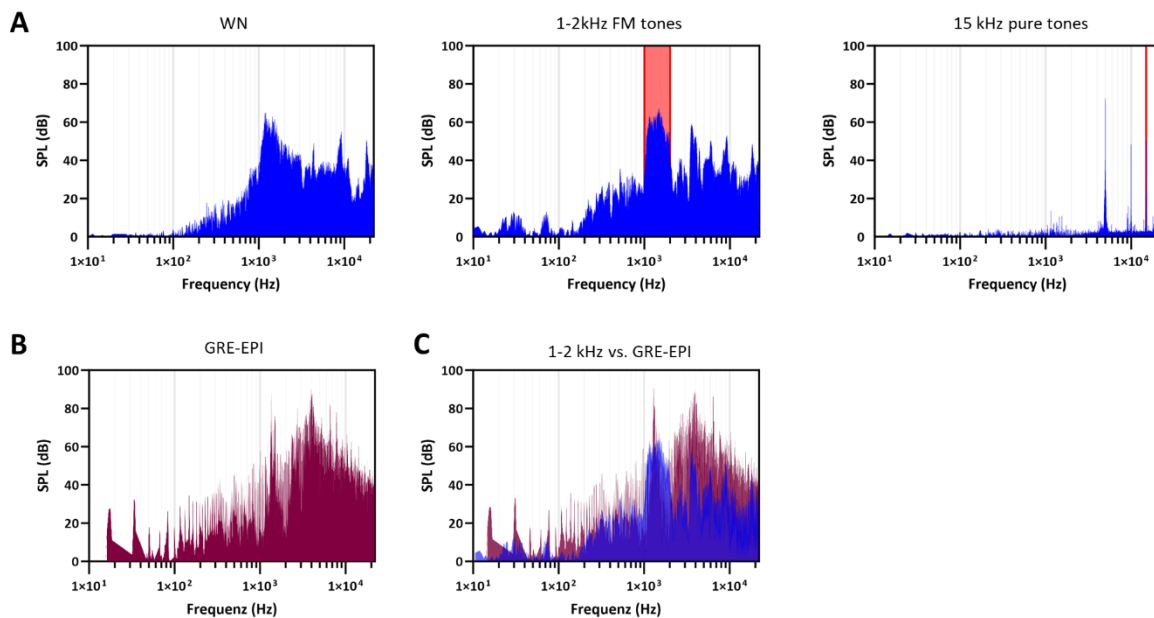


Figure 11: Sound profiles of different stimulation tones vs. GRE-EPI noise

Frequency-dependent sound pressure levels with background of ambient noise level of MR scanner room subtracted. A. Stimulation tones were measured from the tips of the earphones; sound profiles of presented Gaussian white noise (WN), 1-2 kHz sweeps and 15 kHz pure tones are illustrated in blue, the stimulation frequencies of 1-2 kHz FM tone and 15 kHz pure tone and are displayed in red. B. GRE-EPI noise level was measured directly in the bore of the 9.4 T scanner. C. Sound profile of 1-2 kHz FM tone laid over GRE-EPI noise.

1.3.2. Optimized auditory fMRI in the Mongolian gerbil

Overall, the highest quality of auditory-evoked BOLD activation patterns, shown for an exemplary scan with 1-2 kHz sweep stimulation in Figure 9 and Figure 13, were achieved with the following protocol.

Protocol for optimized measurement setup

The 9.4 T horizontal small animal scanner (*BioSpec® 94/20 USR*, Bruker) is equipped with a ^1H -transmit-receive volume coil with inner diameter of 86 mm (*MT0381*, Bruker) combined with the ^1H planar receive-only surface coil with 20 mm diameter (*MT0105-20*, Bruker).

The gerbils are anaesthetized with 1.5% isoflurane (*Vetflurane*, Virbac Arzneimittel GmbH, Germany) in oxygen and nitrogen (50:50; evaporator: *UniVet Porta*, GROPPER medizintechnik, Germany), the hair removed from the top of their head and their tails with hair removal cream (*Veet sensitive*, Veet, Germany), and an *i.v.* catheter is laid into the tail vein of the animals for the duration of the MRI scan. Subsequently, the animal is placed on the MRI bed, head positioned in a custom-made gerbil headpiece (designed and built in-House) for isoflurane application and head fixation with an adjustable bite bar, schematically visualized in Figure 12.

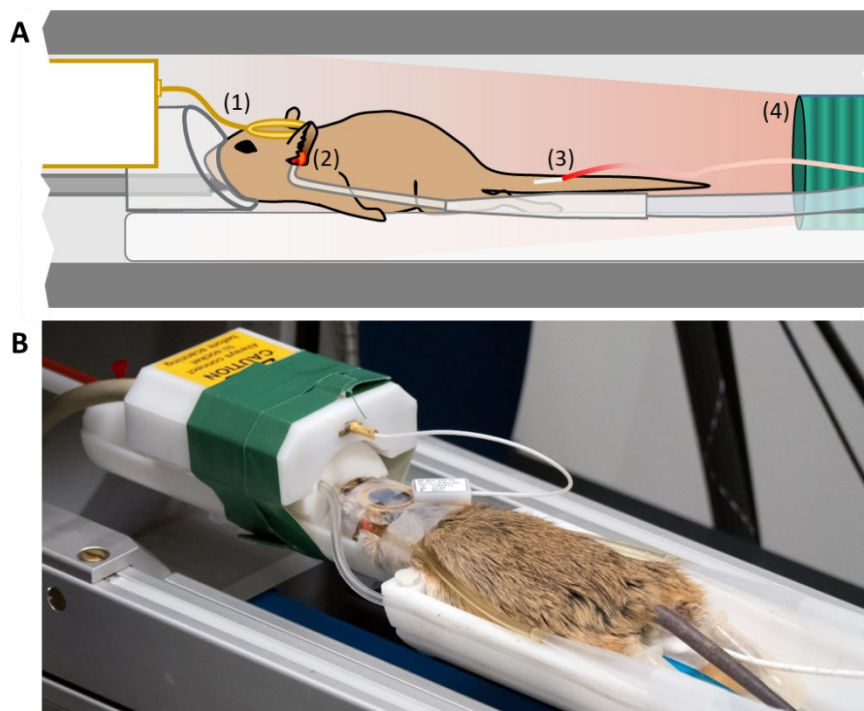


Figure 12: Overview of final auditory fMRI measurement setup

A. Schematic representation of the optimized measurement setup for auditory fMRI in the Mongolian gerbil. Featured setup adjustments: (1) placement of planar surface coil, (2) ear phones for auditory stimulation presentation, (3) tail vein catheter for administration of medetomidine anaesthesia, and (4) feedback-controlled air heater system. **B.** Photography of gerbil placed in optimized setup for an auditory fMRI measurement.

The breathing rate of the animals is observed with an MR-compatible animal monitoring unit (*ERT Control/Gating Module Model 1030*; Small Animals Instruments Inc., USA) and the body

temperature of the animals maintained at 37°C with a feedback-controlled air warming system (*MR-compatible Small Animal Air Heater System*; Small Animals Instruments Inc., USA).

Hollow air tubes with pliable earplug tips are placed in the outer ears of the animals and immediately fixated with tape. The planar surface coil is placed between the ears directly on the skin of the animals to prevent signal loss due to air interference. Earplugs and surface coil are fixated to the animal bed with multiple carefully applied strands of tape (*3M Transpore Tape*, Minnesota Mining and Manufacturing Company, USA) to ensure a tight fit and enable less movement during the fMRI scans. The gerbils are additionally secured to the MR bed around their body and their feet are placed in silicone pistons to prevent possible injuries in case the animals awake during the scanning process. Then the animal is positioned in the centre field of view inside the core of the scanner using an automatic animal positioning system.

After full preparation of the animals, the anaesthesia is switched from isoflurane inhalation to continuous intravenous injection of medetomidine (1:10 in sodium solution, initially 0.3 mg/kg/h, after 45 min increased to 0.4 mg/kg/h; *Domitor*, Orion Pharma GmbH, Germany) applied with a high precision syringe pump (*Pump 11 Elite Infusion Only Single Syringe*, Harvard Apparatus, USA). During medetomidine uptake and MRI scanning, the animals are constantly monitored; in case of consistent movement, indicating an awake state of the animal, isoflurane is turned back on and the measurement cancelled or repeated on another occasion if possible.

Protocol for optimized fMRI measurements

The MRI measurements start after 1 h of medetomidine uptake. From there, scout scans are run with a low-resolution FLASH sequence imaging all 3 dimensions in 3 exploratory slices to assess the animal position and adjust if necessary. The volume resonator is manually matched and tuned to correct for field inhomogeneities caused by the animal and measurement setup itself. The scout scans further serve as orientation for the positioning of the slices, FoV saturation slices and shim volume of the anatomical and functional images.

For high resolution anatomical images, a TurboRARE sequence with TR/TE 2200/8 ms in 15 contiguous frontal slices of 0.8 mm thickness and 85 µm in-plane resolution (image matrix 355 x 234, FoV 30 x 20 mm²; RARE-factor 8; 1 avg) is run. As correction for susceptibility artefacts caused by air/tissue interfaces, especially in the region of the bullae, shimming is performed on basis of a previously run B0-map (TR 15 ms, 4 avg; image matrix 64³, FoV 30 mm³). Three FoV saturation slices are strategically placed around the brain to block out most of the signal originating from the bullae.

For functional imaging, an optimized gradient echo EPI sequence is run within the same FoV/slices position with an in-plane resolution 400 µm and TR/TE of 1000/16 ms (image matrix 75 x 50, FoV 30x20 mm²). Again, for better image quality, shimming and the same saturation slices are implemented. After an initial run of this EPI-sequence with 10 repetitions

(reps) to check for image quality and possible artefacts, the sequence is run with 300 reps as warm-up of the gradient system.

Then the functional scans are to be recorded with an appropriate auditory stimulation protocol, optimally containing 120 s of baseline followed by binaural auditory stimulation in a block design; repeated FM tones in ranges of 1-2 kHz ideally serve as stimulation for this auditory fMRI approach in Mongolian gerbils.

After the acquisition of all functional scans, medetomidine infusion is stopped and the inhalation anaesthesia with isoflurane resumed for a second anatomical MRI scan. This additional scan is run (i) for assurance that no movement occurred in between previous scans and (ii) with 6 avg for higher image quality.

After conclusion of the MRI measurement, the animal is extracted from the MR setup, injected s.c. with 0.4 mg/kg atipamezole hydrochloride (1:10 in NaCl; *Antisedan*, Orion Pharma, Finland) and returned to its home cage.

Exemplary auditory activation patterns acquired with the optimized protocol for auditory fMRI

With the described optimized protocol for auditory fMRI, significant bilateral auditory activation in the central auditory pathway of Mongolian gerbils was acquired. Exemplary activation patterns are visualized in Figure 13 together with ERAs and BETA values extracted via the more advanced analysis pipeline that enables direct comparison of measured activation (described in chapter 1.2.6.). For comparative purposes, results of the same scan obtained with the basic analysis pipeline were already presented in Figure 9.

Induced by auditory stimulation with 1-2 kHz FM tones in the standardly used block design (see description in chapter 1.2.5), atlas-based BETA values were highest in AC, amounting to 1.13 ± 0.07 % in left AC and 0.93 ± 0.05 % in right AC, followed by MGB (left: 0.38 ± 0.05 %, right: 0.39 ± 0.06 %), and IC (left: 0.35 ± 0.04 % and right 0.21 ± 0.03 %).

It must be generally acknowledged, that these atlas-based BETA values and ERA peaks are considerably lower than values extracted from smaller, local activation clusters as presented in Figure 9. Nevertheless, this more objective, atlas-based analysis facilitates statistical comparison of different measurement time points and experimental groups, which is desirable for the investigation of learning induced changes in activation.

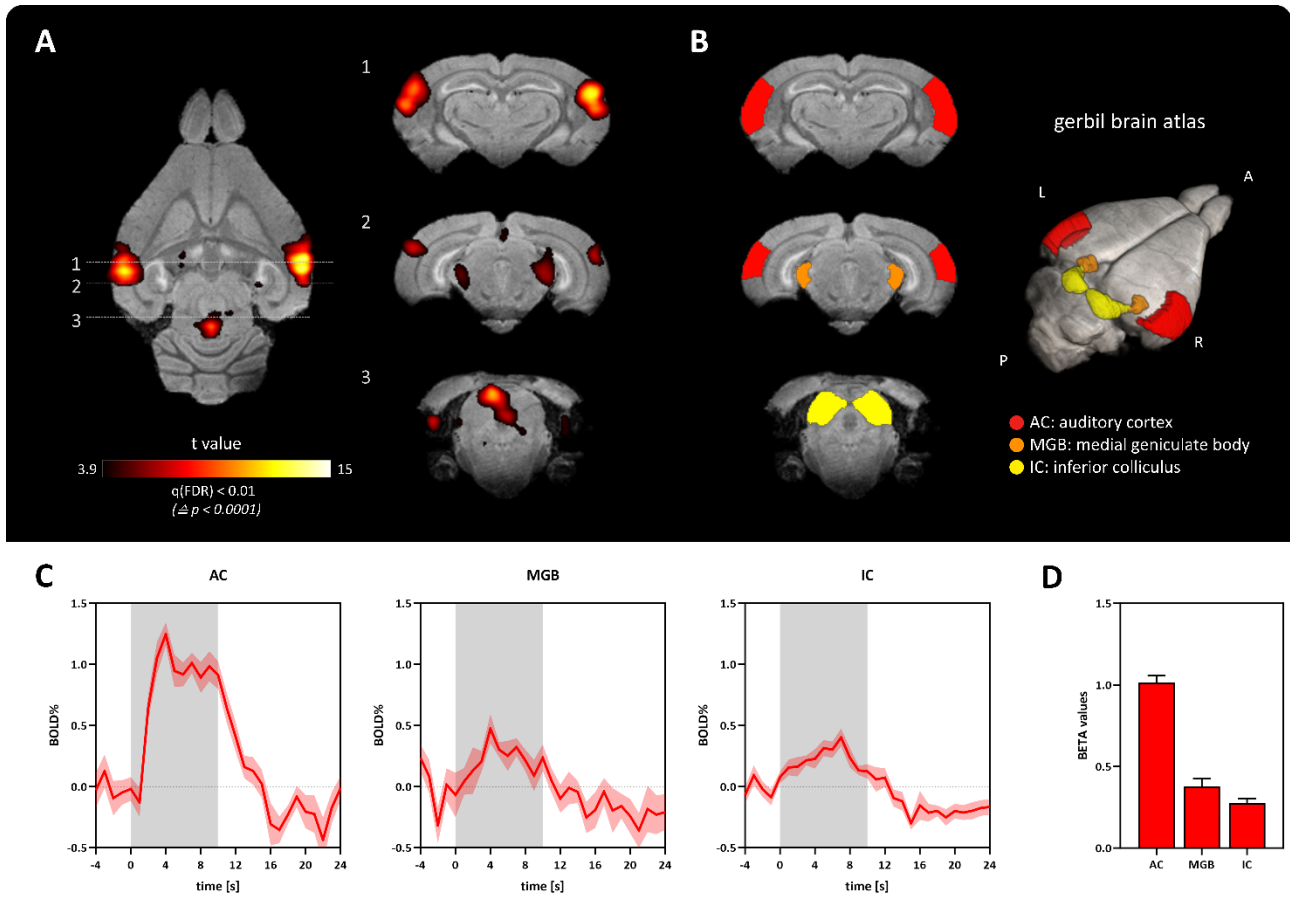


Figure 13: Auditory-evoked brain activation in the Mongolian gerbil with optimized auditory fMRI

A. Horizontal overview of brain activation patterns with coronal slices in region of AC (1), MGB (2) and (3) IC. **B.** Corresponding coronal slices of the gerbil brain atlas, showing additionally a 3D-rendered overview of the central auditory pathway. **C.** Extracted event-related averages of the auditory atlas regions, grey area depicting the auditory stimulation and **(D)** extracted BETA values of the same regions. (Acquired following the optimized protocol)

1.4. Discussion

fMRI of auditory-evoked brain activity in the Mongolian gerbil proved itself challenging. So far, fMRI in gerbils has only been presented in one scientific publication by Hess et al. (Hess et al., 2000), reporting somatosensory-stimulated BOLD responses in the barrel field of somatosensory cortex and auditory cortex under halothane anaesthesia. Difficulties arose from a lack in standard fMRI anaesthesia protocols for Mongolian gerbils, image distortion through their extended middle ear cavities, and immense background noise caused by the GRE-EPI, that coincidentally showed highest BOLD responses upon auditory stimulation.

1.4.1. Effectiveness of fMRI anaesthesia protocol

Anaesthesia protocols for other, more commonly applied anaesthetics in rodent fMRI such as medetomidine, isoflurane or propofol (Paasonen et al., 2016; Paasonen et al., 2018; Schlegel et al., 2015; Schroeter et al., 2014), have not been established or at least not been published for the Mongolian gerbil to this point. Even with consideration of standard protocols used in fMRI with mice and rats, finding a proper functioning mode of application in the Mongolian gerbil took many trials and an extensive amount of time. For mild or moderate sedation with medetomidine in gerbils, manufacturer information recommends doses of 0.1-0.2 mg/kg through *i.m.* or *i.p.* injection, for deeper anaesthesia in combination with Ketamine for surgery up to 0.5 mg/kg (Ko, 2004). However, there was no information available on how to sustain a sedative state of gerbils with medetomidine over longer periods. In first fMRI attempts, a bolus injection of the minimum recommended dosage with 0.1 mg/kg via *s.c.* injection, followed by an hourly rate of additional 1.0 mg/kg induced sedation depths that met the criteria for successful immobilization of the animals but not for measurable BOLD responses. Breathing rates, while very constant, were rather low, averaging below 40 breath/min in comparison to the natural range of 70-120 breath/min (Batchelder et al., 2012). Following standard medetomidine fMRI protocols used in rats and mice, the mode of application was switched to *i.v.* medetomidine injection into the lateral tail vein. This proved difficult due to coarse hair coating the gerbils' tails and dark pigmentation of subjacent skin; additionally, gerbils are known to be highly susceptible to tail slipping and accordingly have to be handled with caution (Batchelder et al., 2012). Nevertheless, through application of hair removal cream the implantation of temporary tail vein catheters was possible. Our optimal medetomidine protocol for fMRI in Mongolian gerbils ended up with an initial dosage of 0.3 mg/kg/h, raised to 0.4 mg/kg/h after 45 min, and an overall uptake period of 1 h before MR acquisition start. The observed effect of medetomidine anaesthesia stabilizing only after some uptake time has been described and discussed in multiple studies and reviews before (Magnuson et al., 2014; Pan et al., 2015; Sirmipilatze et al., 2019).

On the other hand it is worth noting, that our determined dose is considerably higher than standard dosages applied in rat fMRI with 0.1 mg/kg/h (Paasonen et al., 2018; Sirmipilatze et al.,

2019) and mouse fMRI with 0.2 mg/kg/h after an initial 0.1 mg/kg bolus (Bukhari et al., 2017; Schlegel et al., 2015; Schroeter et al., 2014). Since many studies already showed brain activation altering effects caused by relatively mild anaesthesia protocols including decrease in functional connectivity (Magnuson et al., 2014) and delays in the HRF (Paasonen et al., 2017; Schlegel et al., 2015), our high dosage raised the question, whether we can realistically acquire meaningful brain activation patterns with this protocol. Consequently, we addressed these concerns in a subsequent study with CBF SPECT, described in chapter 2 of this thesis.

1.4.2. Image quality of functional MRI

As to be expected, fMRI acquired with the standard GRE-EPI acquisition produced highest BOLD responses of the applied sequences, but also considerable image distortions. It is well established in MRI, that tissue bordering on different tissue types of deviating susceptibility or air can cause severe susceptibility artefacts (Stadler et al., 2007). Gerbils have an extended hearing range, overlapping with large parts of natural hearing ranges found in humans and other rodent species such as rats, due to extended middle ear cavities named *bullae* (Gleich & Strutz, 2012; Mason, 2016; Rosowski et al., 1999; Teoh et al., 1997). These air-filled structures are situated directly ventral to the gerbil's brain (Mason, 2016) and caused major distortion artefacts in our first GRE-EPI attempts. Even though the overall image resolution and visible contrast between different tissue types was higher in these initial adjustments, huge distortion artefacts make the images useless for spatial localization of functional activation. Through optimization of GRE-EPI sequence parameters, shimming on basis of measured B₀-maps and placement of FoV saturation slices over the area of the air-filled *bullae*, the distortion effects were reduced and an acceptable functional image quality achieved (Figure 8C). This image quality is comparable to published fMRI study results acquired with GRE-EPI in mice (Jonckers et al., 2015; Schlegel et al., 2015). Despite our sequence optimization efforts, anterior and posterior regions of the gerbil brain as well as some ventral parts suffered from signal loss, affecting especially the hypothalamus, olfactory areas, and cerebellum. Lowered signal intensity was also measured in most anterior and posterior brain regions in the anatomical images acquired with a TurboRARE (Figure 8B); hence, the signal loss effects are most likely caused by coverage limitations of the surface coil. An advantage of covering only part of the gerbil head with a surface signal readout is, that noise by electromagnetic interference, in our case especially caused by the *bullae*, do not affect the images as much (Ferris & Tenney, 2014; Hayes & Axel, 1985). A negative consequence of surface coils can be underrepresentation of signals originating from lower areas, such as the amygdala or the ventral hippocampus compared to areas closer to the surface of the brain (Ferris & Tenney, 2014). Therefore, interpretation of data collected from peripheral regions of the gerbil brain in further ventral, posterior and anterior locations with our optimized setup should be done with caution.

Comparably less distortion and signal loss artefacts were recorded with the optimized ZTE applied with contrast enhancement through the SPIO Molday ION™, roughly following a method protocol that was introduced by Shih and MacKinnon in a Bruker online seminar (Shih & MacKinnon, 2020). The low differences in soft tissue contrasts, made identification of brain structures or even the overall brain shape a tedious task. Additional images with better contrast distinction and longer acquisition time could potentially be recorded to guide the coregistration process (Ljungberg et al., 2021).

1.4.3. Quality of auditory evoked activation patterns

Measured CBV changes in AC with ZTE and SPIO application were much lower than BOLD signal changes detected with the GRE-EPI. Since the GLM-analysis of fMRI data relies on statistical correlation of the measured signal to an expected STC, the lower time resolution of the ZTE sequence could have resulted in a lowered sensitivity to brain activation changes (Constable & Spencer, 2001; Yoo et al., 2018), especially considering the predictably faster HRF of rodents (Chen et al., 2023; Lambers et al., 2020).

Additionally, in fMRI measurement with CBV-ZTE, functional artefacts appeared around the eye region, probably caused by eye movement of the animal upon hearing the stimulation tone (Schaefer et al., 1981). Movement of the eye can cause ghosting, blurring or local signal variations in reconstructed images (Chen & Zhu, 1997; Godenschweger et al., 2016), which complicates the interpretation of activation patterns. Since the ZTE is read out radially, the readout-direction cannot be adjusted to avoid these artefacts. Nevertheless this issue could potentially be resolved by placement of FoV saturation slices over the eye region (Chen & Zhu, 1997). Although this adjustment would come at cost of additional MR scanner noise during acquisition. Another drawback of the CBV-ZTE approach is the requirement of high volumes of contrast agent, which necessitates the placement of a second *i.v.* catheter in the tail vein. This was a challenging task and on multiple occasions extravasation of the contrast agent occurred. Moreover, small SPIOs have a relatively long clearance; Molday ION™ according to the manufacturer with a half-life of “several hours” (BioPAL, 2013). In a study on long-term retention of SPIOs, including the contrast agent Molday ION™, GRE MRI showed obvious contrast enhancement even 7 days after the last contrast agent injection (Gorman et al., 2018). Since the measurable CBV signal change depends on the concentration of the SPIO in the blood (Mandeville & Marota, 1999; Zhao et al., 2006), repeated fMRI measurements within a short interval will most probably be affected in intensity of brain activation induced signal changes. Consequently, the method is impracticable for observation of short-term changes in brain activation patterns throughout a learning process.

Acquisition with GRE-EPI showed much higher signal changes and bigger areas of elicited activation increase than the CBV-ZTE imaging. Highest signal activation was generally evoked by stimulation with a pulsed 1-2 kHz FM tones in comparison to other stimulation tones. FM tones

by definition have a wider spectral range than pure tones, and therefore can activate a higher number of frequency specific neurons (Ohl et al., 2000). Additionally, frequency modulated sweeps add a temporal complexity to pure tones that leads to increased recruitment of higher order auditory areas, such as the auditory cortex, which makes them preferable to pure tones for auditory stimulation in auditory research (Ohl et al., 1999; Rauschecker & Tian, 2000). Likewise, lower auditory structures are also more strongly activated when stimulated with FM tones (Sinex & Geisler, 1981). The frequency range between 1 and 2 kHz lies in the optimal hearing range of Mongolian gerbils (Gleich & Strutz, 2012); in addition, upward FM sweeps themselves are an important part of gerbils' communication calls (Nishiyama et al., 2009). A technical advantage of these lower frequencies lead to less artefacts in the auditory stimulation setup also applied in human studies with high-field fMRI (Figure 11A). Altogether, this makes the 1-2 kHz FM tones an excellent auditory stimulation for fMRI in the Mongolian gerbil.

With this auditory stimulation, highest signal change within auditory structures was recorded in both cases, GRE-EPI and CBV-ZTE acquisition, in region of the AC. The overly strong BOLD increase in AC can possibly be traced back to its superficial position and acquisition with surface coils, as discussed in the previous section. Comparably lower signal change recorded in the subcortical structures MGB and IC, could conceivably be explained by concurring signal loss effects. Upon stimulation with 1-2 kHz FM tones, peak activation of AC would be expected in frequency-specific dorsoventral bands within primary AC (A1) according to both, electrophysiological tonotopy maps of AC (Thomas et al., 1993) and comparative tonotopy maps of glucose metabolism acquired with 2DG (Scheich et al., 1993). Clearly visible in the coronal slices of Figure 13, GRE-EPI measured activation within AC did not show throughout the entire depth of AC and peak activation was not situated in the centre of AC, where the primary AC is located, but in a more dorsally located region. In worst-case scenario, the high AC activation measured with GRE-EPI might be an overestimation caused by image distortion of the AC areas and compression of the signal into a smaller region (Hutton et al., 2002). This could have occurred due to susceptibility artefacts caused by the *bullae* of the Mongolian gerbils. On the other hand, it has been reported in human studies that high background noise as is occurring with GRE-EPI acquisition can necessitate more information processing within AC and as a result lead to higher BOLD increases in this area (Hall et al., 1999; Moelker & Pattynama, 2003; Peelle, 2014). This would likely be an explanation for our AC activation, as the recorded SPL for the generated EPI noise was only slightly lower in the frequency range of 1 to 2 kHz than the measured SPL for the 1-2 kHz FM stimulation tones themselves (Figure 11C). Of course, the placement of the headphones used for auditory stimulation should optimally reduce the concurring EPI background noise, but to which extend cannot be estimated without further investigation.

To understand this effect and the actual quality of our acquired auditory activation patterns, the individual composition of our recorded auditory-evoked brain activation patterns needs to be

resolved with further experiments with another methodology. Therefore, we performed a study with CBF SPECT to evaluate our newly established auditory fMRI in the Mongolian gerbils, presented in chapter 2. There we investigated possible side effects through medetomidine anaesthesia and GRE-EPI background noise, and did a side-by-side comparison of the auditory-evoked patterns measured under same conditions in fMRI and SPECT.

2. Evaluation of auditory fMRI in the Mongolian gerbil with CBF SPECT

2.1. Introduction

Even though echo-planar imaging (EPI) under medetomidine anaesthesia is one of the most widely used approaches for BOLD fMRI in rodents, the effects of this anaesthesia and the EPI-noise on brain activation patterns, particularly on auditory-evoked patterns, is largely unknown. While some research groups actively compared fMRI activation patterns and connectivity of brain regions in rodents under different anaesthetic agents and awake animals, the comparison to a more natural awake, unrestricted state is not possible with fMRI by itself. Since MRI scanning always produces some kind of background noise, the effect of this noise needs to be investigated with another imaging method. Furthermore, this second method is necessary for validation of our auditory-evoked activation patterns acquired with the optimized GRE-EPI.

To ensure that the auditory-evoked activation patterns we derive from our Mongolian gerbils with the newly established auditory fMRI measurement protocol are not largely influenced by the above mentioned confounds, we used CBF SPECT as a comparative imaging approach. By this means, we were not only able to obtain auditory evoked activation patterns with and without concurring background noise generated by GRE-EPI inside the MR scanner, but also in an awake unrestrained condition, outside of the MR scanner.

2.1.1. Anaesthesia effect on brain activation

Within the last decade, standardly used anaesthesia paradigms in rodent fMRI, implemented to facilitate motion-free measurements and reduction of stress for the animals, have been called into question. Setups allowing for awake rodent measurements are becoming increasingly prevalent in neurobiological research ([Mandino et al., 2023](#)).

As mentioned in the introduction to fMRI in rodents in chapter 1.1.3, a variety of anaesthetics are commonly applied for rodent fMRI, including amongst others, medetomidine, isoflurane, propofol, α -chloralose and urethane ([Paasonen et al., 2016](#); [Schlegel et al., 2015](#)) each presenting individual advantages and challenges due to unintended side effects off the neuroimaging approach.

Medetomidine anaesthesia, despite having shown to cause decrease in functional connectivity ([Magnuson et al., 2014](#); [Nasrallah et al., 2012](#)) and delays in the HRF ([Paasonen et al., 2017](#); [Schlegel et al., 2015](#)), remains one of the most commonly used anaesthetic agents in rodent fMRI ([Cabral et al., 2023](#); [Kalthoff et al., 2011](#); [Pawela et al., 2009](#); [Weber et al., 2006](#); [Zerbi et al., 2015](#)). It allows for repeated measurements in the same animal without the high effort of habitational training that awake rodent measurements usually require ([Mandino et al., 2023](#)). Additionally, it does not necessitate intubation of the animals and its effects can be easily reversed with

atipamezole to initiate rapid awakening after conclusion of the fMRI measurements (Baker et al., 2011; Pan et al., 2015).

Medetomidine acts as α 2-adrenergic agonist and induces anaesthesia, or rather a form of sedation, mainly through its action on the locus coeruleus (Correa-Sales et al., 1992; Nelson et al., 2003). This structure has the highest presynaptic α 2-adrenergic receptor concentration in the brain (Chamba et al., 1991; Pan et al., 2015). Locus coeruleus is a key structure for regulation of sleep and wakefulness (Hayat et al., 2020; Swift et al., 2018; Van Egroo et al., 2022). Through medetomidine administration, its endogenous sleep pathways decrease afferent input to the thalamus and thereby overall thalamus activity (Nelson et al., 2003). Additionally, medetomidine induces global CBF decrease, which was reported in studies on humans and animals (Drummond et al., 2008; Fukuda et al., 2013; McPherson et al., 1997; Prielipp et al., 2002), presumably via its vasoconstrictive effects (Ishiyama et al., 1995; Kint et al., 2020; Prielipp et al., 2002).

Through the combination of these effects, resting-state fMRI connectivity under medetomidine sedation is clearly altered (Magnuson et al., 2014; Nasrallah et al., 2012; Paasonen et al., 2018; Yoshida et al., 2016). It can cause disconnection of different brain regions, dependent on the applied dosage (Nasrallah et al., 2012). In humans, infusion with another comparable α 2-adrenergic agonist type, clonidine, has additionally shown concentration dependent decrease in spindle activity in thalamus and neuromodulatory isocortex structures (Bonhomme et al., 2008). In stimulus-evoked fMRI in rats, sedation with medetomidine has led to a moderate deceleration of the HRF, but similar spatial distribution of activation patterns (Paasonen et al., 2016).

While the neurological side effects clearly suggest that awake fMRI measurements are preferential to measurements under medetomidine anaesthesia, this is not always the case. Rodents measured with fMRI in an awake state have shown signs of stress, in both acute form despite the acclimatization training to the acquisition procedure and chronically caused by the training itself, which ultimately alters their response to fear (Han et al., 2019; López-Moraga et al., 2022; Low et al., 2016; Mandino et al., 2023). Therefore, awake measurements should also be implemented and interpreted with caution when investigating fear-related behaviours and a well-adjusted sedation with medetomidine might be preferential.

2.1.2. Effect of MRI background noise on auditory processing

To obtain spatially resolved images with MRI, multiple switches of gradient coils are required, ergo changing electrical currents in a magnetic field. These are inevitably concomitant with Lorentz force: mechanical forces that act on the gradient coils and their connecting wires. The induced vibrations in the MR hardware lead to the typical audible noise during MRI measurements (Amaro Jr. et al., 2002; Edelstein et al., 2002; Hall et al., 1999; Hedeem & Edelstein, 1997; Katsunuma et al., 2002; Moelker & Pattynama, 2003). The most frequently used sequence for imaging of the BOLD contrast in fMRI, the GRE-EPI sequence, has a signal readout, in which the

data of an entire 2D plane can be collected with one single RF-excitation pulse through multiple very fast switches in gradients (Cohen & Schmitt, 2012; Mansfield, 1977), and consequently produce a loud scanning noise. The RF-excitation pulse and eddy currents occurring throughout the MR hardware also contribute to heightened noise levels during fMRI acquisitions (Edelstein et al., 2002; Katsunuma et al., 2002; Moelker & Pattynama, 2003). In addition, the helium cooling system of the MR scanner produces a pumping noise and the ventilation system a constant humming within the MR scanner room, which together create an ambient background noise independent from the MRI acquisition (Cho et al., 1997; Counter et al., 1997; Moelker & Pattynama, 2003; Ravicz et al., 2000).

All these sources of noise during an fMRI acquisition combined can induce intense acoustic noise with peak SPL above 130 dB (Ravicz et al., 2000), which makes fMRI, and particularly auditory fMRI, susceptible to confounds (Moelker & Pattynama, 2003; Peelle, 2014).

The acoustic noise generated by the fMRI acquisition has shown to induce activation in the auditory pathway, including the AC, in humans and rodents (Bandettini et al., 1998; Di Salle et al., 2001; Hall et al., 2000; Hikishima et al., 2023; Scarff et al., 2004; Talavage et al., 1998). Therefore, it has the potential to mask and reduce the detectable signal induced by the intended auditory stimulation (Gaab et al., 2007; Hall et al., 1999; Hikishima et al., 2023; Langers et al., 2005; Peelle, 2014; Shah et al., 1999; Talavage & Edmister, 2004).

Through the length of the HRF in comparison to the time resolution of fMRI, the auditory masking effect on the measurable auditory activation via neurovascular coupling proceeds on two instances: (i) through concurrent scanner noise during auditory stimulus presentation and resulting stimulus-masking, and (ii) through heightened baseline activation within the auditory system caused by the scanner noise prior to auditory stimulus presentation (Moelker & Pattynama, 2003; Talavage et al., 1998). Accordingly, multiple auditory fMRI studies on humans reported decreased activation in the frequency specific regions in primary AC (A1) (Gaab et al., 2007; Hall et al., 1999; Langers et al., 2005; Talavage & Edmister, 2004).

On the other hand, the perception of specific sounds is more difficult with concurring background noise. For some experimental paradigms, which depend on discrimination of different sounds, this can lead to additional activation for the processing of the auditory stimulus and overestimation of the auditory stimulation effect (Hall et al., 1999; Robson et al., 1998). Through concurring MRI background noise, stronger activation in A1 and higher order auditory areas has been observed in humans (Bandettini et al., 1998; Robson et al., 1998; Talavage et al., 1999) as well as in awake mice (Chen et al., 2020).

Another effect occurring throughout the auditory system is adaptation to noise (Willmore & King, 2023). Protective mechanisms of loud noise include the stapedius muscle reflex in the middle ear that changes the impedance of the tympanic membrane and therefore the sound wave transmission (Cheng et al., 2021; Trevino et al., 2023) and threshold shifts of the hair cells of the

cochlea in the inner ear (Vetter, 2015; Yoshida & Liberman, 2000). Exposure to continuous noise also leads to firing rate adaptation of the auditory nerve (Costalupes et al., 1984; Harris & Dallos, 1979; Smith, 1979; Westerman & Smith, 1984) and in the central auditory pathway (Angeloni et al., 2023; Gibson et al., 1985; Malmierca et al., 2009; Phillips, 1985; Rees & Palmer, 1988; Siveke et al., 2021). This occurs for example via feedback mechanisms such as the olivocochlear reflex (Kawase & Liberman, 1993) and corticofugal modulation (Nuñez & Malmierca, 2007). Activation through auditory stimulus and concurring MR scanner noise do not add up linearly in AC (Cheng et al., 2021; Talavage & Edmister, 2004), possibly due to noise adaptation effects. This non-linearity makes a simple subtraction of scanner noise from the auditory activation patterns unfeasible. The extent of MR scanner noise effects on auditory activation patterns depends on the individual MR sequence noise and its similarity to the auditory stimulus, as well as duration and intensity of both (Brechmann et al., 2002; Hall et al., 2001; Jäncke et al., 1998; Robson et al., 1998).

Additionally to effects within the auditory system, GRE-EPI scanner noise has shown to cause discomfort and anxiety in human subjects (Meléndez & McCrank, 1993; Quirk et al., 1989), which can lead to distraction from the auditory stimulus (Peelle, 2014). This circumstance likely extends to experimental animals, especially rodents, since they startle easily and experience anxiety upon exposure to acoustic noise (Davis et al., 1993; Peng et al., 2023). Attention modulating brain areas have shown higher activation for memory-tasks through the increase of fMRI noise levels (Tomasini et al., 2005). Generally, the background noise generated by fMRI does not only alter the activation to auditory stimuli, but also stimulation with other modalities (Cho et al., 1998; Elliott et al., 1999; Loenneker et al., 2001; Nuernberger et al., 2022) and resting-state networks (Hikishima et al., 2023; Pellegrino et al., 2022; Pinardi et al., 2023). Therefore, MR scanner noise is of concern in every fMRI study.

The effects of MRI background noise on auditory stimulation are diverse and depend strongly on the individual fMRI sequence, auditory stimulus and participation of the measured individual in a task. The effects of such MRI background noise in rodents under mild medetomidine anaesthesia on auditory stimulus perception has not been investigated so far.

2.1.3. CBF SPECT imaging

Single-photon emission computed tomography (SPECT) belongs to the family of nuclear imaging modalities. In contrast to MRI, it does not image naturally abundant molecules, but detects and allocates radiolabelled substrates administered to the subject, which are referred to as radiotracers (Webb, 2003). SPECT measures the gamma rays emitted during radioactive decay of the tracer's radionuclide. Localization of the decay is achieved with collimators, which only let gamma rays from limited angles pass to detector crystals (Van Audenhaege et al., 2015). In combination with rotation and translation of these detectors along the measured subject, three-

dimensional images of tracer distribution patterns are reconstructable from the measured gamma projections (Bruyant, 2002).

Functional brain imaging can be implemented with SPECT through the injection of radioactive technetium-99m-labelled hexamethylene propyleneamine oxime (^{99m}Tc -HMPAO), a lipophilic tracer that rapidly accumulates in the brain, presumably in astrocytes (Zerarka et al., 2001), in a CBF-dependent manner, where it is converted to a hydrophilic form and thereby trapped (Neirinckx et al., 1988; Zerarka et al., 2001). Implantation of a chronic jugular vein catheter enables administration of the radiotracer to awake, unrestrained rodents (Oelschlegel & Goldschmidt, 2020) and thus to rodents in practically any experimental setting. Afterwards, the distribution of the accumulated ^{99m}Tc -HMPAO is read out with SPECT/CT in static images depicting spatial patterns of average CBF throughout the tracer injection period. A disadvantage of this static readout is the lack of information on any temporal dynamics during the tracer accumulation period. To achieve images of effects of different stimulation conditions, separate measurements are required. However, the images of different experimental conditions can be subtracted to visualize brain activation changes due to differentiating parameters or presented stimuli (Oelschlegel & Goldschmidt, 2020; Raichle, 1998).

The prospect of being able to observe, compare and subtract brain activation patterns of different experimental states in a largely restriction-free manner makes the method of CBF SPECT highly convenient for the investigation of GRE-EPI noise and anaesthesia effects on auditory activation patterns. Apart from that, CBF SPECT and BOLD fMRI both rely on the principle of neurovascular coupling with indirect estimation of neuronal activation through the measurement of locally arising energy demands (Cauli & Hamel, 2010; Hillman, 2014; Kleinfeld et al., 2011; Phillips et al., 2016). Therefore, a direct comparison of images acquired with both modalities has the potential to validate the auditory-evoked activation patterns attained with the newly established auditory fMRI in the Mongolian gerbil.

2.2. Methods

2.2.1. Experimental design

Effects of medetomidine anaesthesia and GRE-EPI background noise on auditory-evoked brain activation patterns were investigated with static SPECT-imaging of CBF. To this purpose, Mongolian gerbils were injected with ^{99m}Tc -HMPAO under different conditions and afterwards the accumulated tracer distribution read out through SPECT/CT. The conditions compared in this chapter are (1) awake and unrestrained, (2) medetomidine-anaesthetized and positioned in the MR scanner setup without any scanner noise, (3) medetomidine-anaesthetized and positioned in the MR scanner setup while a GRE-EPI sequence runs simultaneously for fMRI. Each condition lasted 12 min, during which tracer was injected continuously through chronically implanted external jugular vein catheters. To obtain auditory-evoked brain activation patterns from these static CBF SPECT images, all three conditions were performed with and without auditory stimulation. For auditory stimulation, FM tones (1-2 kHz rising) were presented through in-ear headphones in the MR scanner, or via free-field loudspeakers in awake animals. An overview of the different groups investigated in this study is presented with Table 2.

Table 2: Overview of different conditions investigated with CBF SPECT

Each condition was performed at least in $N = 5$ Mongolian gerbils, resulting in overall 40 individual static CBF SPECT images.

condition	protocol	medetomidine anaesthesia	GRE-EPI noise	auditory stimulation	group size
(1)	A			+	$N = 5$
	B				$N = 5$
(2)	C	+		+	$N = 5$
	D	+			$N = 5$
(3)	E	+	+	+	$N^1 = 5 ; N^2 = 6$
	F	+	+		$N^1 = 5 ; N^2 = 4$

CBF SPECT measurements of condition (3) were repeated because the results indicated an issue with the transmission of the auditory stimulation ($N^2 = 6$ with protocol E, $N^2 = 4$ with protocol F). For this 2nd implementation, the headphone fixation was revised and the revision applied to following studies – including the discrimination learning experiments presented in chapter 3 of this dissertation.

2.2.2. Experimental animals

The CBF SPECT/fMRI experiments were performed on adult male Mongolian gerbils (*Meriones unguiculatus*, bred in-house) in the age range of 12-16 weeks. The animals were housed individually in a temperature-controlled room with a 12h/12h dark light cycle (6:00/18:00) and given food in the form of rodent pellets and sunflower seeds and water *ad libitum*. The ethics committee of Saxony-Anhalt approved all animal experiments (No. 42502- 2-1591 LIN).

Throughout the whole study, including preliminary pilot runs of the fMRI-SPECT experiments (data not shown), 23 individual gerbils were imaged repeatedly with CBF SPECT.

2.2.3. Injection of CBF SPECT tracer

Animal preparation – catheter surgeries

At least one day prior to their first CBF SPECT measurement, the gerbils underwent a surgical procedure for chronic implantation of an external jugular vein catheter. The procedure is described in detail by Oelschlegel and Goldschmidt (Oelschlegel & Goldschmidt, 2020) and was performed by Dr. Anja Oelschlegel and later by Lisa-Marie Goncalves. In short, the animals were anaesthetized with isoflurane (*Vetflurane*, Virbac Arzneimittel GmbH, Germany), the anaesthesia depth checked and adjusted by means of their pedal withdrawal reflexes throughout the surgery. The right external jugular vein was carefully exposed and ligated. Caudally of the ligation, the vein was opened and a catheter tube (*Mouse Jugular Catheter-AL*, Alzet osmotic pumps, USA) inserted, which was fixated with additional ligations caudal of this incision hole. To keep the catheter out of the animals' reach, it was subcutaneously tunnelled to an exit closely behind their shoulder blades. The catheter was filled with catheter locking solution (SAI infusion technologies, USA), the incisions closed up with surgical thread and the animals left on a heating mat during recovery from the anaesthesia. The entire surgery lasted approximately one hour.

The catheters were flushed daily with saline solution and backfilled with 20 μL of catheter locking solution to prevent clotting in the catheter tube, which ultimately renders the catheter useless. On average, the catheters stayed open and usable for two weeks.

Tracer preparation

Immediately before the planned injection, $^{99\text{m}}\text{Tc}$ -HMPAO was synthesised from $^{99\text{m}}\text{TcO}_4^-$ ($^{99\text{m}}\text{Tc}$ -technetium pertechnetate, OvGU radiology department, Magdeburg Germany) in saline solution and HMPAO in the presence of the reducing agent Sn(II)Cl_2 from an aliquoted kit (*CERETEC™*, GE Healthcare AS Nycveien, Norway). The tracer was set to a dilution containing roughly 300 MBq of $^{99\text{m}}\text{Tc}$ in 400 μL volume.

Tracer injection

The entire volume of the prepared SPECT tracer was drawn into a thin plastic tube of 150 cm length and was then attached to a syringe containing saline solution on one end and to the chronic jugular vein catheter of the experimental animal on the other. The subsequent continuous intravenous injection of the tracer was executed with a high precision syringe pump (*Pump 11 Elite Infusion Only Single Syringe*, Harvard Apparatus, USA) at 40 $\mu\text{L}/\text{min}$ for 12 min with a 1 min automatized delay, flushing out the tracer solution with saline in the process.

2.2.4. Auditory stimulation

FM tones rising from 1 to 2 kHz served as auditory stimulation throughout the entire CBF SPECT study. A scheme of the stimulation protocol is presented in Figure 14. The stimulation commenced in a block design starting out with an initial baseline of 90 s, followed by 15 blocks of auditory stimulation of 20 s length alternating with 20 s blocks of silence. Within the stimulation blocks, repeated 1-2 kHz tones of 200 ms, enveloped by 10 ms ramps to prevent sound artefacts, were interleaved by 300 ms inter-stimulus intervals. The injection of the CBF SPECT tracer started 30 s before first stimulation onset.

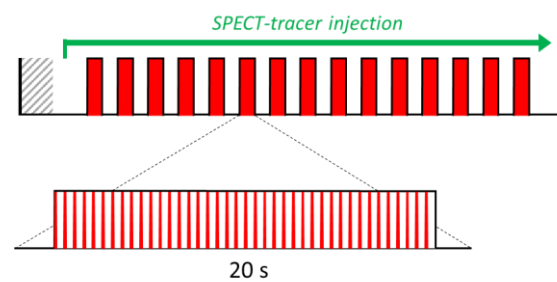


Figure 14: Auditory stimulation protocol for CBF SPECT study on medetomidine anaesthesia and GRE-EPI noise effects

Tracer injection was started 30 s before onset of the first stimulation block, consisting of 40 FM tones (200 ms each) rising from 1 to 2 kHz interleaved by 300 ms inter-stimulus intervals. Such stimulation blocks were presented 15 times alternating with 20 s breaks. Tracer injection concluded 50 s after the 15th presentation of the tone.

2.2.5. CBF tracer injection in the awake gerbils

For awake unrestrained measurements, the gerbils were habituated for 20 min in a standard two-compartment shuttle box (38 x 22.5 x 19 cm³, Hasomed GmbH, Germany) without hurdle. The box was situated in a sound chamber (250 series mini sound shelter, IAC GmbH, USA) to reduce background noise. After habituation, the tube with tracer solution was connected to the animal and the pump started. For condition (1) with auditory stimulation, thus protocol A, auditory stimulation in the form of pulsed 1-2 kHz FM tones was presented to the animal via loudspeakers suspended from above at 70 dB SPL. The protocol for auditory stimulation was programmed and compiled with the Graph State Suite (version 4, Coulbourn Instruments, USA) and designed to correspond to the auditory stimulation that was standardly used in the auditory fMRI in this thesis. Afterwards, the animals were taken to the SPECT/CT for readout of the tracer that accumulated in active brain areas during the injection period. For comparative CBF-images without the auditory stimulation (i.e. protocol B), the animals were treated exactly the same, but the protocol in Graph State Suite was not executed.

2.2.6. CBF tracer injection under Medetomidine anaesthesia

Tracer-injections for experimental conditions (2) and (3) were conducted with the animals inside the bore of the 9.4 T MRI scanner. The overall auditory fMRI measurement setup matches

chapter 1.3.2 on page 23. In the following, only alterations of this protocol that served to accommodate for the additional SPECT imaging are described in detail.

The standard ^1H -transmit-receive volume coil with inner diameter of 86 mm combined with a ^1H planar receive-only surface coil with 20 mm diameter was used for the initial run-throughs in this study, as the 15 mm custom coil had not arrived at this point. Later on, the custom 15 mm coil was used in the 2nd implementation of condition (3) combined with an improved placement of the headphones.

The animals were prepared for the scanning procedure as described in 1.3.2. After placement of the tail vein catheter for administration of medetomidine anaesthesia, the animals were positioned on the animal cradle, earphones positioned and fixated together with the surface coil to the animals head. The animals were then brought into the bore of the 9.4 T scanner with the automatic positioning system, AutoPac™. The isoflurane anaesthesia used for animal placement was exchanged for continuous i.v. injection of medetomidine (0.3 mg/kg/h), after 45 min the dosage was increased to 0.4 mg/kg/h.

After an overall 1 h of medetomidine uptake, the experimental animal was shortly driven out of the scanner with the AutoPac™ (Bruker, Germany) system to connect the tube containing the readily prepared CBF SPECT tracer to the chronic jugular vein catheter. The gerbil was then immediately returned to its previous position in the MRI core.

For condition (2), protocol C, the gerbils were injected with the CBF tracer while under anaesthesia inside the MR scanner. 15 min after the animal was repositioned in the scanner core, the continuous injection protocol of the SPECT-tracer pump was started simultaneously to the auditory stimulation protocol. Sound generation, stimulation programming and sound transmission was conducted as described in detail in chapter 1.2.5 on page 14 with Labview, but without MR-trigger coupling. The sound stimulation setup was tested prior to each measurement and calibrated to a SPL of 95 dB on both sides. For protocol D the tracer was injected in the exact same setting but without auditory stimulation.

2.2.7. CBF tracer injection during fMRI measurements

For condition (3), the gerbils were measured in the MR scanner according to the newly established auditory fMRI protocol for Mongolian gerbils. After attachment of the SPECT tracer tube and return of the animal to the bore of the MR scanner as described in chapter 2.2.6, scout scans were run and the volume resonator was manually matched and tuned.

In the 1st implementation of the experiments, we used the TurboRARE sequence with TR/TE 2200/8 ms in 15 contiguous frontal slices of 0.8 mm thickness and 85 μm in-plane resolution (image matrix 355 x 234, FoV 30 x 20 mm²; RARE-factor 8; 1 avg). Shimming was performed on basis of a previously run B0-map, the 3 FoV saturation slices positioned correctly.

The sequence was repeated at the very end of the MRI measurement with 6 avg under 1.5 % isoflurane anaesthesia for higher image quality and to check on possible movement of the animals.

For functional imaging, the optimized GRE-EPI sequence was run within the same FoV/slices position with an in-plane resolution 400 μm and TR/TE of 1000/16 ms (image matrix 75 x 50, FoV 30x20 mm^2). Later, the GRE-EPI sequence was slightly altered with a less steep gradient ramp and to a TR/TE of 1000/15 ms, to avoid hardware issues and imaging artefacts resurfacing randomly. Additionally the number of slices was increased to 20 slices of 0.8 mm; here, the anatomical scans' number of slices was also adjusted accordingly.

The GRE-EPI sequence was run with 300 reps as warm-up of the gradient system.

fMRI measurements with simultaneous CBF tracer injection

The SPECT-fMRI functional scan was recorded with 720 reps, during which the SPECT-tracer was injected simultaneously. Depending on the measurement paradigm, the fMRI was run as a resting-state measurement without any stimulation (protocol E), or with auditory stimulation (protocol F) according to the previously described protocol.

After the functional scans, medetomidine infusion was stopped and the inhalation anaesthesia with isoflurane resumed for the second longer anatomical MRI scan. Thereafter, the gerbils were removed from the fMRI setup and injected s.c. with 0.4 mg/kg atipamezole. The gerbils were then transferred to the SPECT/CT for readout of the tracer distribution in the gerbils' brain.

2.2.8. SPECT/CT readout

The $^{99\text{m}}\text{Tc}$ -distribution was statically read out after the stimulation period under conditions (1), (2) and (3) with a four-head NanoSPECT/CT (*NanoSPECT/CT™ InVivo Animal Imager*, Mediso GmbH, Germany) equipped with 4 apertures that were optimized for brain imaging in Mongolian gerbils (APT 13, 10 pinholes with [3-4-3] FoV, SciVis GmbH, Germany). For the measurement, the animals were (re-)anaesthetized with 1.5 % isoflurane and positioned on the tooth bar of a gerbil cradle, provided with air heating to 37 °C (URT Multipostes, Equipment Vétérinaire Minerve SA, France). A topogram, i.e. a planar X-ray image, showing the entire body of the animals in 2D was made for FoV selection. Then an initial CT was acquired with 45 kVp, 177 μA with a spatial resolution of 96 μm . The SPECT readout of the $^{99\text{m}}\text{Tc}$ -distribution was acquired in a 2 h measurement with 24 projections coregistered to the CT. In order to control for potential movement artefacts a second CT was acquired after the SPECT scan.

After the SPECT/CT measurement was completed, the animals were taken from their cradle and returned to their home cage. The cage was warmed with a heating mat until they woke up from anaesthesia.

2.2.9. Data analysis

Analysis of SPECT data

CT data was reconstructed in InVivoScope (version 1.43, Bioscan Inc., USA) with a filtered back projection at isotropic voxel-resolution of 100 μm . SPECT data reconstruction was carried out using the manufacturer's software (*HiSPECT™*, SciVis wissenschaftliche Bildverarbeitung GmbH, Germany) for iterative ordered subset reconstruction at a voxel-size of 167 x 167 x 167 μm^3 with 24-iterations and 150 % smoothing. All individual SPECT data sets were manually aligned to a MR gerbil reference template from the gerbil brain atlas ([Radtke-Schuller et al., 2016](#)) with the MPI-Tool software (version 6.36, Advanced Tomo Vision, Germany) on basis of skull-landmarks in the coregistered CTs. A brain mask was applied to the data, the images of each SPECT-scan were normalized to their global mean CBF. Mean images of each protocol were computed, and the auditory activation pattern of each condition generated by subtraction of the auditory-stimulated with the non-stimulated images. Additionally, images of p-values, t-values and variances of the mean CBF images and differential activation patterns were computed. All image operations beyond coregistration were compiled in Matlab (scripts written in-House, 2017 version with 'Statistics and Machine Learning Toolbox', The MathWorks Inc., USA). The CBF SPECT images shown in the results of this thesis were created with the OsiriX MD viewer (version 12.0.1, BioCom GbR, Germany). These images depict either mean CBF or CBF increase, as the main concern of this study was the effect size of auditory stimulation and GRE-EPI noise. Significance of CBF increase was ensured in all of the structures presented in the results with the corresponding p-maps, unless explicitly stated otherwise.

Analysis of the fMRI data

Preprocessing and analysis of the fMRI data was primarily performed with BrainVoyager (version 20.6, Brain Innovation, Maastricht, Netherlands). The exported DICOM images were loaded into the imaging analysis program with 45 volumes skipped in addition to a 5 s delay occurring due to the dummy scan duration at the start of each EPI-sequence, leaving a 40 s baseline for the analysis.

For preprocessing of the imaging data, a slice time correction with a cubic spline interpolation was performed, 3D motion correction trilinear/sinc interpolation to the first EPI-image, smoothing by a FWHM of 0.8 mm in space domain and temporal filtering with a Gaussian high pass filter (2 cos/sin of data points). Any spontaneous voxel displacement bigger than the recorded voxel size (0.4 mm) was considered as movement of the animals and the entire measurement discarded and repeated at a later time point, as the simultaneous CBF tracer uptake was likely corrupted.

Each measurement was evaluated with an individual GLM, the two-gamma HRF applied to the stimulation protocol of each run adjusted with time to response peak of 3 s and time to

undershoot peak of 10 s. To enable group analysis, the high quality anatomy of each scan was manually coregistrated to a high definition 3D-anatomical template of a gerbil brain (*in vivo* measurement of 4 h performed by Patricia Wenk, 48 h after injection of manganese chloride as contrast agent). The coregistration parameters were applied to the corresponding functional scans, converting them to 3D volume time course (VTC) data in the same native space.

A multi subject GLM, based on the single study GLMs design, was run on the VTC data of the 1st and 2nd implementation of condition (3) individually with correction for serial correlation, %-transformation and separate subject predictors. FDR-corrected thresholds were noted and images exported in NIfTI format for image presentation with MRICroGL (version 20, ([MRICroGL, 2019](#))).

Through region of interest analysis with a gerbil brain atlas (described in detail in chapter 1.2.6 on page 15), BETA values (single subject, %-transformed) of the statistical maps and ERAs were extracted for the auditory structures AC, MGB and IC.

Comparison of CBF SPECT and BOLD fMRI

A direct spatial comparison of the auditory-evoked activation patterns acquired with CBF SPECT and BOLD fMRI was facilitated through automatic coregistration of the high-resolution MRI template used for fMRI analysis to the MR gerbil reference template from the gerbil brain atlas with SPM 12 (*Statistical Parametric Mapping*, Functional Imaging Laboratory, Wellcome Trust Centre for Neuroimaging, UK). Auditory activation patterns obtained with the GRE-EPI sequence were repositioned into SPECT-space applying the same transformation matrix.

2.3. Results

2.3.1. Effect of medetomidine anaesthesia

With injection of ^{99m}Tc -HMPAO into awake, unrestrained gerbils, auditory stimulation with FM tones rising from 1-2 kHz resulted in significant, right lateralized CBF increase in AC. This increase in CBF is already easily distinguishable on individual and mean SPECT-images measured with protocol A; area of AC is marked with an arrowhead in Figure 15A. The performed coregistration and normalization processes allow us the calculation of the response magnitude to the auditory stimulus by a simple subtraction of the mean CBF SPECT images measured under the same condition without auditory stimulation (protocol B). This way the CBF increase due to auditory stimulation is clearly visible (Figure 15B), especially in the right AC (rAC). The response magnitude in this area reached up to 22 % of CBF increase for stimulation with 1-2 kHz FM tones compared to the non-stimulated measurements with an uncorrected p-value of 0.005.

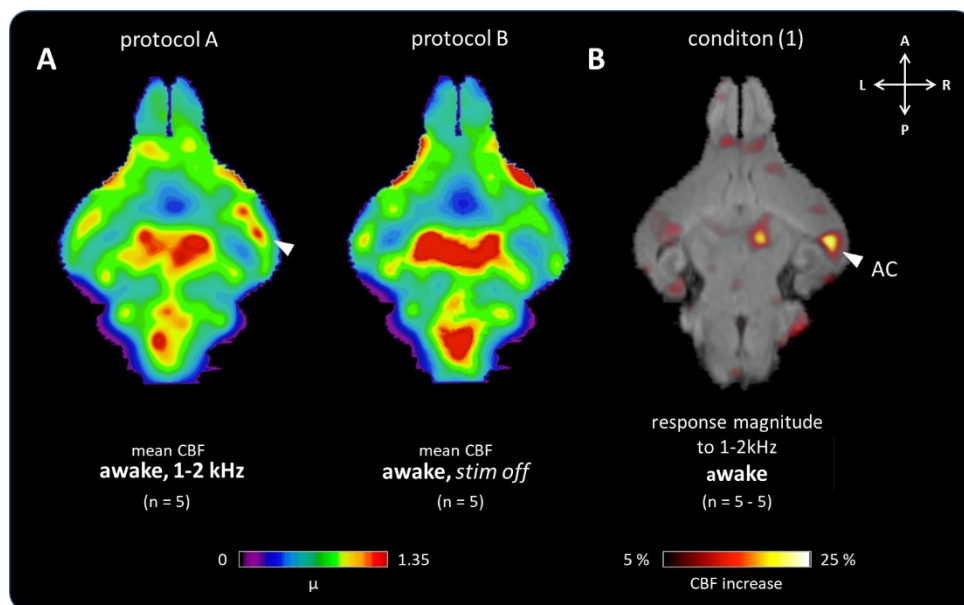


Figure 15: CBF distribution in the brain of awake gerbils with and without auditory stimulation

A. Transversal sections of mean CBF (μ) under the awake condition with auditory stimulation in form of 1-2 kHz FM tones (left) and without auditory stimulation (right) already show a distinct difference in the area of auditory cortex. **B.** Calculated response magnitude images directly show the CBF increase of up to 22 % in rAC.

CBF increase in AC upon FM tone stimulation are presented in a series of hemisections from awake and medetomidine anesthetized gerbils in Figure 16A&B. CBF response magnitudes to FM tones were remarkably similar in AC of awake and medetomidine-anesthetized gerbils. Peak activation in this area was approximately 22 % in awake and 21 % in medetomidine-anaesthetized condition, both with $p < 0.005$. 3D-rendered data show dorsoventral tonotopic bands in the AC that are typical for auditory stimulation within the frequency range of 1-2 kHz (Figure 16C). As comparison the 1 kHz band is marked in a tonotopic map of the gerbil AC (Thomas et al., 1993) in Figure 16D (adapted from left to right AC). Both, awake and medetomidine-anaesthetized gerbils show these typical tonotopic bands within A1. Gerbils

injected under awake conditions had an additional significant CBF increase in the anterior field of the AC (AFF) with a peak of approximately 21 % ($p < 0.02$), as indicated in Figure 16C. In medetomidine-anaesthetized gerbils, the CBF increase in AFF amounted to 16 % ($p < 0.02$). Interestingly, both conditions revealed an overall higher CBF increase in rAC than in left AC (lAC), possibly due to preferential processing of FM tones in rAC (Wetzel, Ohl, et al., 1998). lAC peak response magnitudes yielded up to 15 % in awake ($p < 0.05$) and 17 % in medetomidine-anaesthetized condition ($p < 0.005$).

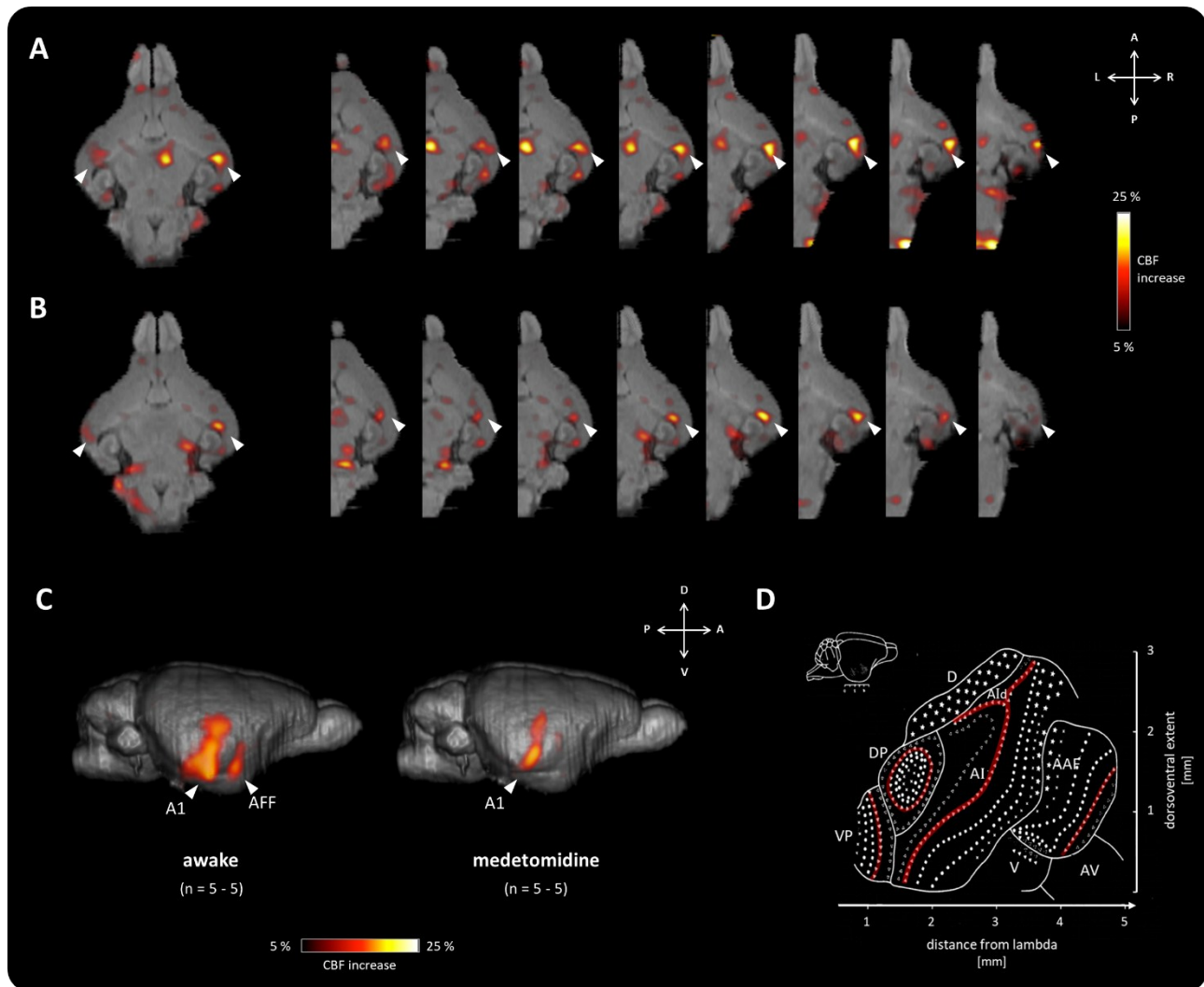


Figure 16: Comparison of AC activation to auditory stimulation with 1-2 kHz FM tones in awake and medetomidine-anaesthetized gerbils

A. Activation of AC in differential images of awake condition with auditory stimulation subtracted by awake condition without auditory stimulation show a clear right-lateralized activation throughout a series of hemisections in the entire region of A1. **B.** Comparative AC activation to 1-2 kHz FM tones. Note the similarity in auditory-evoked activation patterns throughout rAC for awake and medetomidine-anaesthetized gerbils. **C.** 3D-rendered response to 1-2 kHz FM tones within AC for awake and medetomidine-anaesthetized condition; **D.** Comparative tonotopic bands in different areas of AC measured with electrophysiology by Thomas et al., the 1 kHz specific bands marked in red*.

* Figure adapted from "Functional Organization of Auditory Cortex in the Mongolian Gerbil (*Meriones unguiculatus*). I. Electrophysiological Mapping of Frequency Representation and Distinction of Fields", Scheich, Heil, Tillein et al., *European Journal of Neuroscience* (Thomas et al., 1993); permission granted by John Wiley and Sons.

The subcortical auditory pathways were more clearly delineated for auditory stimulation with 1-2 kHz FM tones in the medetomidine-anesthetized gerbils in comparison to awake gerbils, which can be easily seen in Figure 17. Here, medetomidine-anaesthetized animals show distinct activation increase throughout the entire subcortical central auditory pathway: starting with left nuclei of the lateral lemniscus (NLL) with peak activation of up to 19 % CBF increase, followed by right IC with a response magnitude of up to 23 % and right MGB with up to 16 % of CBF increase, all at least at significance levels of $p < 0.005$. Comparatively, the animals measured under the awake condition showed little to no activation increase upon 1-2 kHz FM tone stimulation.

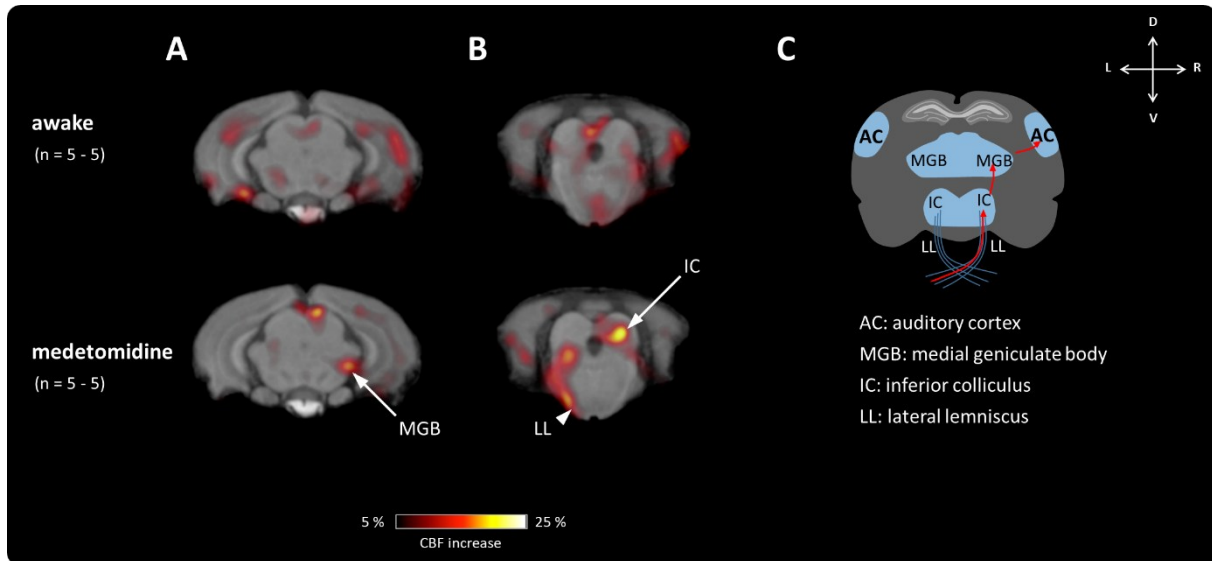


Figure 17: Subcortical activation to auditory stimulation with 1-2 kHz in awake and medetomidine-anaesthetized animals

A. Comparative activation patterns in the region of the MGB with visibly higher activation of the right MGB in medetomidine-anaesthetized animals (lower row). **B.** Prominent activation path from left lateral lemniscus to right IC in medetomidine-anaesthetized animals. Awake animals do not show distinct subcortical activation. **C.** Schematic overview of the central auditory pathway above level of the superior olivary complex.

2.3.2. Effect of GRE-EPI background noise

With auditory fMRI, significant 1-2 kHz FM tone-induced activation increases were acquired as well (Figure 18). Figure 18A&D show first fMRI results with low BOLD responses to the 1-2 kHz stimulation, and average extracted BETA values of 0.24 ± 0.02 % in AC, 0.21 ± 0.02 % in MGB, and -0.02 ± 0.06 % in IC (mean \pm SEM of N=5 animals). Activation patterns and BETA values had a clear lateralization to the right hemisphere in this 1st implementation of the measurements, with much less stimulus-dependent activation in the left AC and MGB; ANOVA testing proved this lateralization effect to be significant with a p-value of 0.02.

At a later time point, when the earphone positioning and fixation process had been revised, a repetition of these experimental conditions resulted in the auditory activation patterns presented in Figure 18C with strong bilateral activation of AC, MGB and IC. These findings were concomitant with much higher BETA values, averaging at 0.49 ± 0.05 % in AC, 0.34 ± 0.04 % in MGB and 0.15 ± 0.02 % in IC. Furthermore, the shape of the response signal curves (Figure 18E), especially

in AC, complied more to the theoretical response function of the auditory stimulation design than was the case in the 1st implementation. With improvement of the earphone position, the prominent lateralization effect to the right hemisphere disappeared altogether.

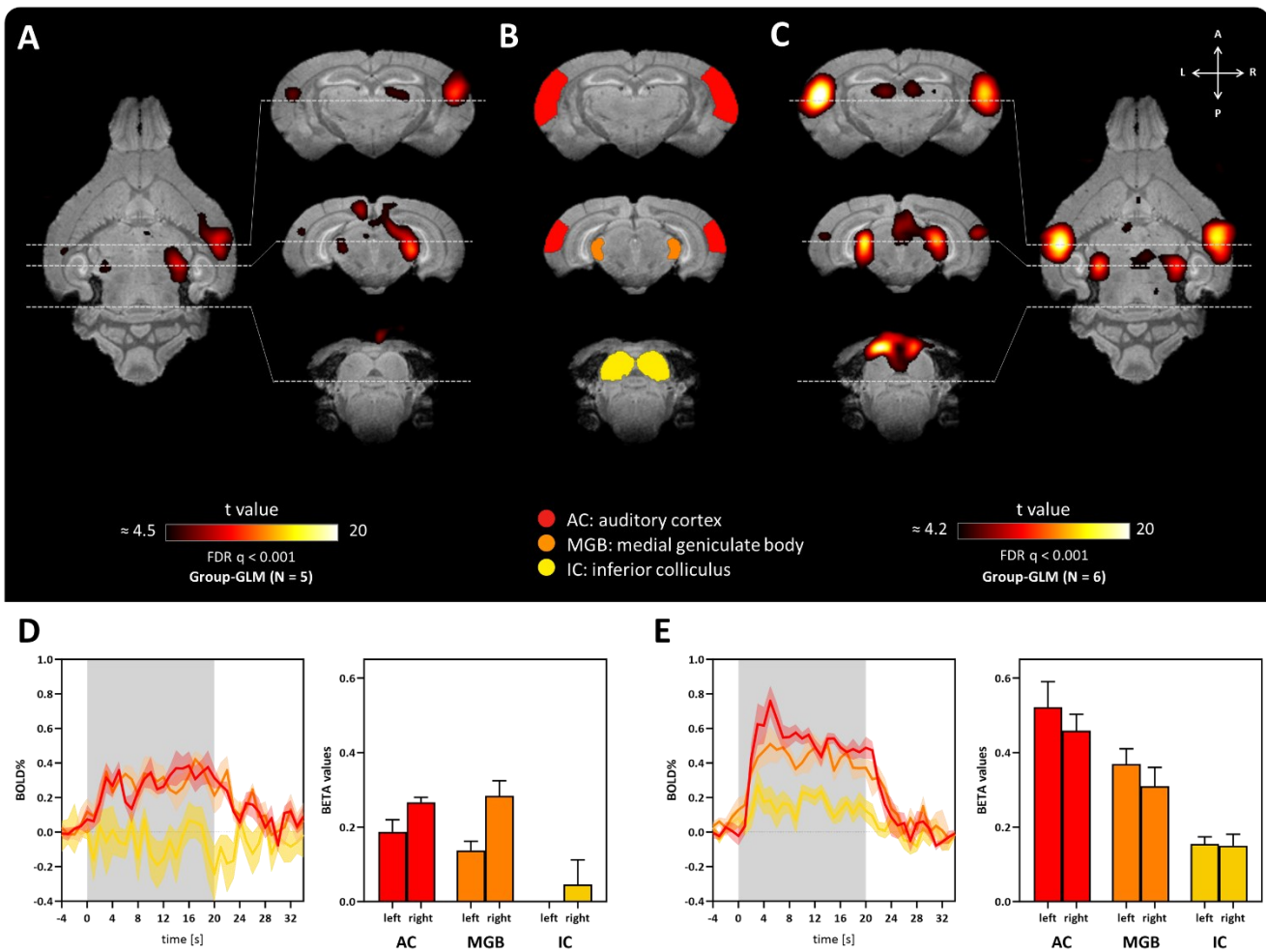


Figure 18: Auditory-evoked BOLD response measured with fMRI during simultaneous CBF-tracer injection
A. Results in first viable fMRI acquisition show strongly right-lateralized BOLD response in AC and MGB, and no activation in IC. **B.** Gerbil brain atlas indicating regions of AC, MGB and IC at identical coronal sections. **D.** Corresponding extracted ERA-curves have similar plateau heights for MGB and AC; again without considerable BOLD response for IC, extracted BETA values are higher in right AC and MGB than on the left. **C.** fMRI results acquired with improved earphone positioning show bilateral BOLD-response in AC, MGB and IC; extracted ERA-curves (**E**) exhibit the typical HRF for longer stimuli in AC, a slightly levelled response in MGB and a much weaker activation increase in IC region; BETA values of AC and MGB are comparable but slightly higher in left hemisphere. (Group-GLMs with FDR correction of 0.001)

An overview of the mean CBF patterns acquired through injection of ^{99m}Tc-HMPOA during the fMRI measurements is given in Figure 19. Unlike the mean CBF patterns measured in awake gerbils, a distinct surplus of CBF due to the 1-2 kHz stimulation is difficult to recognize in AC. Increased CBF values are visible in the IC (Figure 19B&D) of all images acquired with concurring fMRI in comparison to the medetomidine-anaesthetized condition attained without auditory stimulation or GRE-EPI background noise (protocol D).

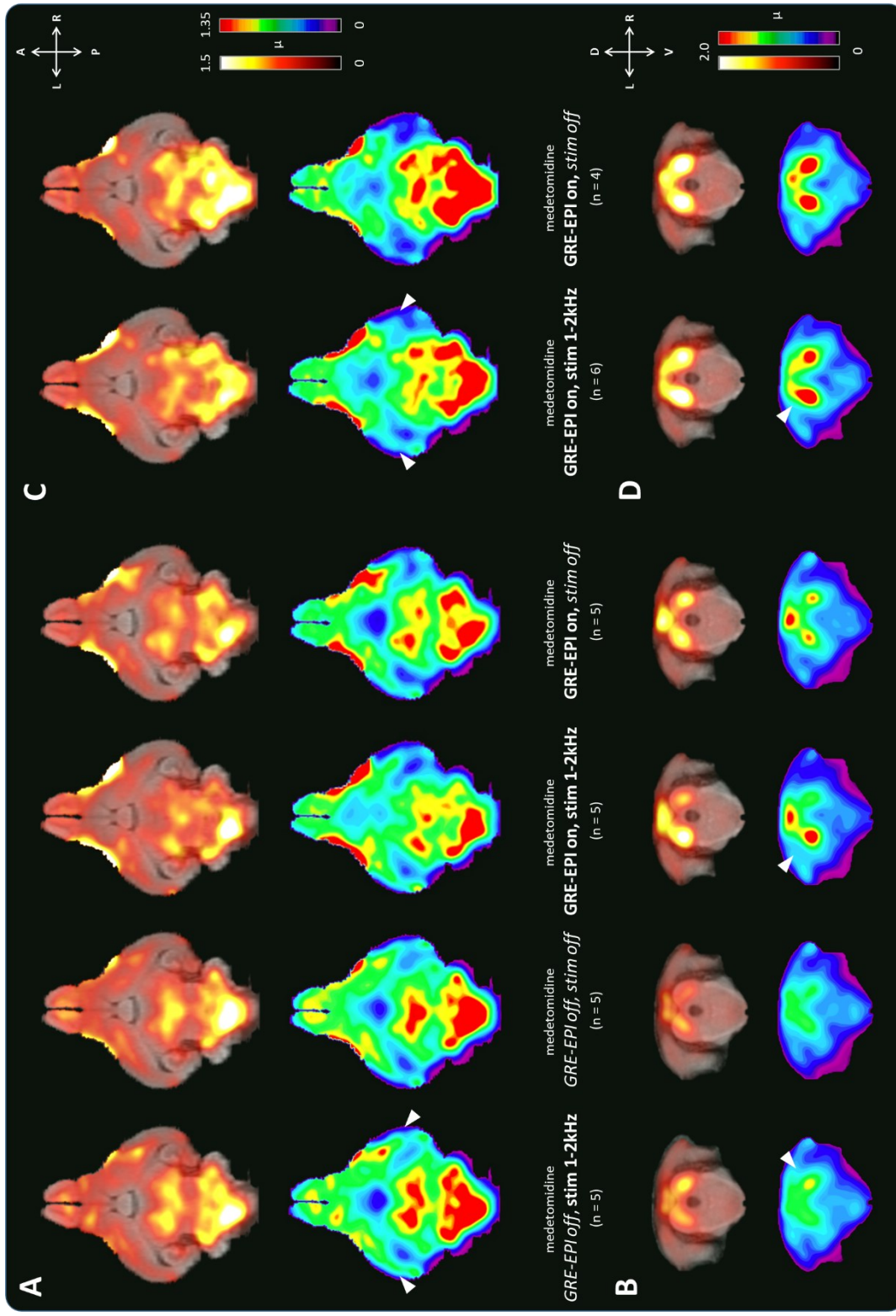


Figure 19: Mean CBF of medetomidine-anaesthetized animals under different conditions with and without 1-2 kHz stimulation

A. Transversal images of mean CBF (μ) at the level of auditory cortex. Auditory activation in AC through 1-2 kHz FM tone stimulation is marked by arrows. Upper rows show μ overlaid onto the gerbil brain anatomy to enable localisation of hotspots, the colour scale adjusted to show the range of μ through a wider colour palette. Here the thresholds are matching those in Figure 15 to enable direct comparison to the CBF patterns of awake animals. **B.** Coronal images in region of the IC depicting μ with increased thresholds to account for the higher CBF values. Visible auditory activation in IC through stimulation with 1-2 kHz is marked by arrows. **C&D.** Equivalent images of the repeated measurements for GRE-EPI noise with and without 1-2 kHz auditory stimulation (condition 3) after adjustment of the headphone placement.

The effect magnitude of GRE-EPI background-noise is visualized in Figure 20D. Overall, the GRE-EPI background-noise caused up to a 40 % CBF increase in left and right IC with a significance level of $p < 0.0001$, 20 % CBF increase in NLL ($p < 0.005$) and 15 % CBF increase in MGB ($p < 0.01$). In AC, the GRE-EPI noise showed little to no CBF increase; only a tiny cluster in rAC had increased CBF by 11 % ($p = 0.025$). In fact, the majority of the AC showed decreased CBF in this condition when contrasted against medetomidine-anaesthetized gerbils subjected only to the ambient background noise in the MR scanner room (peak CBF decrease of -14 % with $p < 0.02$; *not shown*).

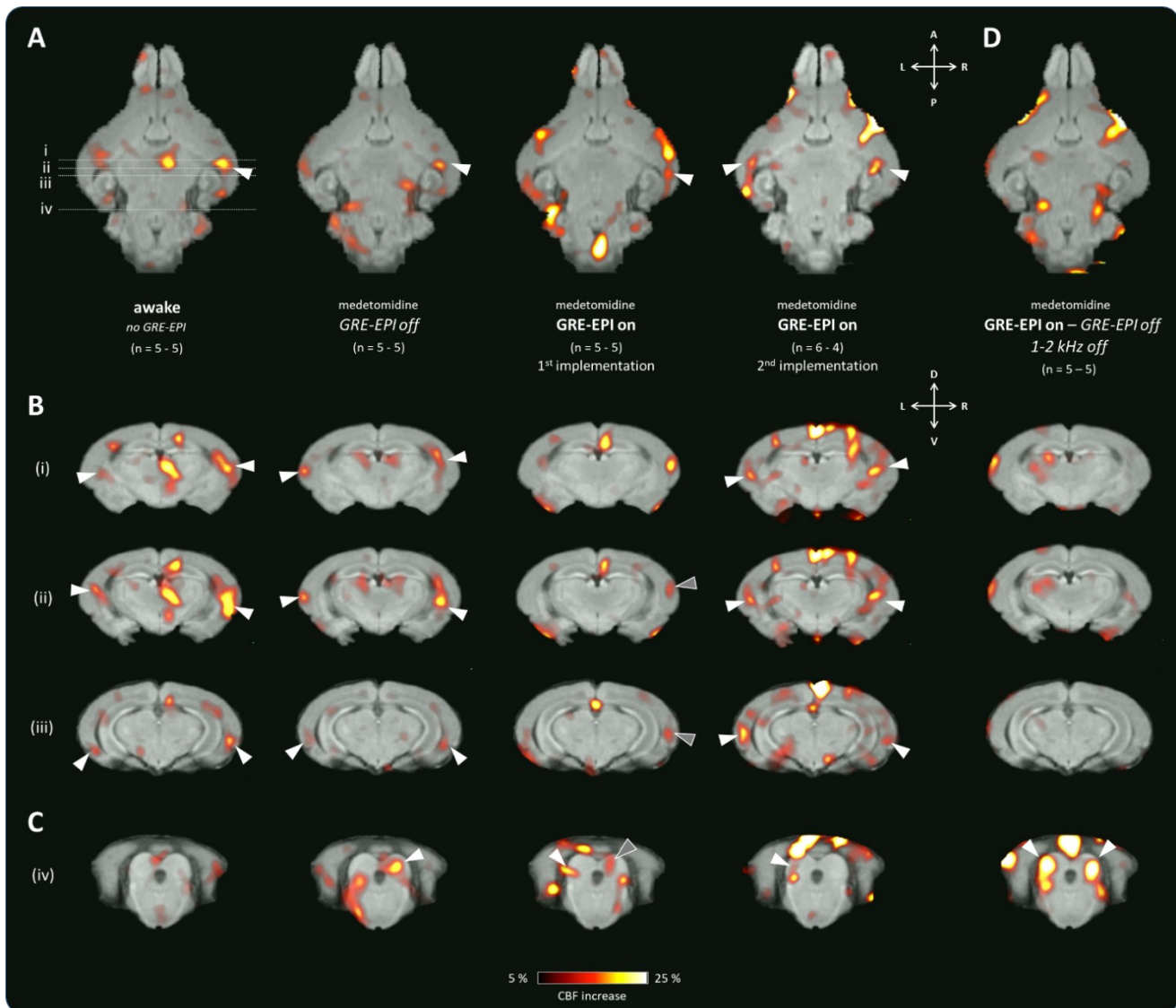


Figure 20: 1-2 kHz stimulation induced CBF increase under different conditions and GRE-EPI effect

A. Transversal sections of the MR template showing the CBF increase in AC due to 1-2 kHz stimulation from left to right in awake condition (1), medetomidine-anaesthetized condition (2) and for both implementations of GRE-EPI noise condition (3). **B.** Spatial activity patterns of CBF increase in serial coronal sections of AC with peak increase marked by arrows. Note the shift of activity from rostradorsal to caudoventral in condition (1) and (2). The 1st implementation of condition (3) only shows slight, non-significant activation of the right AC without activation shift. In the 2nd implementation, bilateral activation of AC is visible with a slight activation shift. **C.** CBF increase in region of IC shows prominently in right IC for condition (2). Condition (3) features small focal points of additional CBF over the GRE-EPI noise increase. **D.** Same sections for subtraction images of protocol F (GRE-EPI noise without 1-2 kHz stimulation, 1st implementation) and protocol D (no noise and no stimulation), which depict the effect magnitude of GRE-EPI noise with strong CBF increase in IC.

Compared to the auditory stimulation-dependent increase observable in awake and medetomidine-anaesthetized animals without GRE-EPI background noise (Figure 20B, 1st and 2nd from left), the 1st implementation of the simultaneous SPECT-fMRI condition showed only minor CBF increase in AC (Figure 20B ii&iii, 3rd from left). This CBF increase was strongly lateralized to the right side with peak values of up to 16 %, however, lacking significance. The only significant CBF increase of this condition occurred in small focal points in left IC with up to 26 % ($p < 0.005$). On top of the generally lower CBF increase in AC through concurring GRE-EPI noise, 3D-rendered images of this area show a shift of the peak increase from the frequency-specific dorsoventral bands observed in right A1 of both, awake and medetomidine-anaesthetized gerbils without GRE-EPI background noise, to a more dorsal region (Figure 21A).

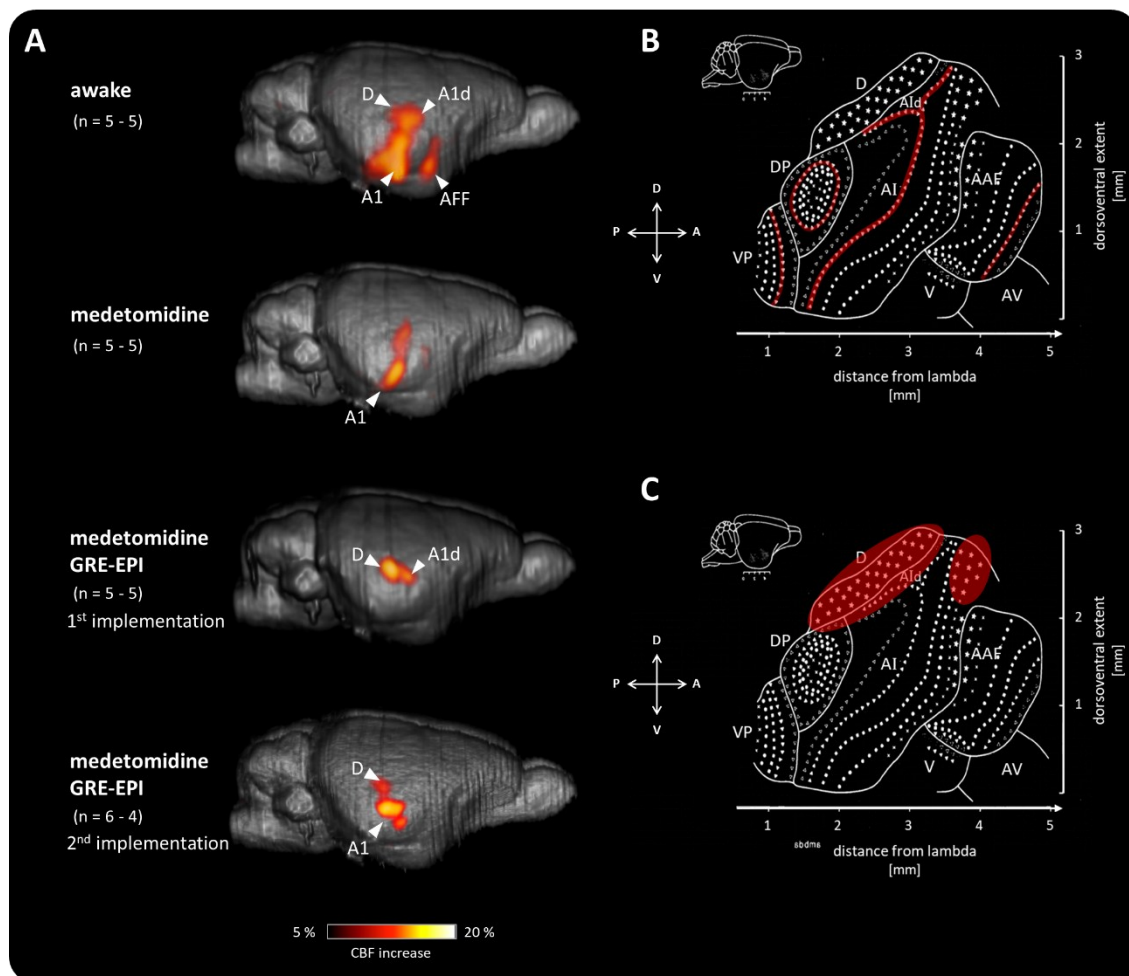


Figure 21: 3D-rendered auditory-evoked CBF increase due to 1-2 kHz stimulation shows a shift of peak activation with concurring GRE-EPI noise in rAC

A. 3D rendered images of awake and medetomidine-anaesthetized rAC shows peak CBF increase upon auditory stimulation delineating the typical tonotopic bands for frequencies of 1-2 Hz, when compared to **(B)** tonotopic map adapted from Thomas et al. (1 kHz Band marked in red)*. Same renders of condition with GRE-medetomidine shows no bands but peak activations in a more dorsal region, possibly in dorsal field of A1 and dorsal field, also marked in red **(C)***. In the repetition of the GRE-EPI condition with improved earphone placement, 1-2 kHz tone induced CBF increase is visible in the dorsal field again, but also in the frequency specific part of A1.

* Figure adapted from "Functional Organization of Auditory Cortex in the Mongolian Gerbil (*Meriones unguiculatus*). I. Electrophysiological Mapping of Frequency Representation and Distinction of Fields", Scheich, Heil, Tillein et al., *European Journal of Neuroscience* (Thomas et al., 1993); permission granted by John Wiley and Sons.

As indicated in Figure 21C, this dorsal region could possibly be the dorsal subfield of A1 (A1d) and the dorsal field of AC (AuD) according to the tonotopic map of the gerbil AC (Thomas et al., 1993).

With adjustment of the earphone position, significant CBF increase emerged in both AC (Figure 20B i-iii, 4th from left) under the same condition (3), with peak response magnitudes of 19 % in rAC ($p < 0.002$) and 17 % in lAC ($p < 0.02$). CBF increase in IC occurred only in small focal points with peaks of up to 32 % ($p < 0.01$) and in the upper layers in close proximity of the cerebellum with 30 % ($p < 0.002$). As visualized in Figure 21A, 3D-rendering of CBF increase in AC again showed a slight activation in the more dorsal region that probably matches the AuD, however, the highest response magnitude occurred in the frequency specific region of A1, matching the middle region of the tonotopic band measured in the awake condition.

Generally, the auditory-evoked CBF patterns of the 2nd implementation of condition (3) exhibit noticeably more background signal than the other conditions under medetomidine anaesthesia. This is possibly caused by the smaller sample size for the non-stimulated measurement ($n=4$) due to premature clotting of the chronic jugular vein catheters in this later repetition of the CBF SPECT experiments. This additional statistical noise could potentially have caused inaccuracies in the precise localization of the activation peaks within the AC.

The findings observed with CBF SPECT in condition (3) are highly similar to the BOLD responses measured in the concurring auditory fMRI, especially in AC. A direct comparison of the differently acquired auditory-evoked activation patterns is presented in Figure 22. For the 1st implementation of the experiments, lateralized activation of AC with a strong shift of peak activation from A1 to a more dorsally located region was observable with both imaging modalities (Figure 22B slice i & ii). In the 2nd implementation, bilateral activation of AC with the activation peak shifted to a lesser degree towards this dorsal region was recorded, again, with both modalities. Interestingly, fMRI activation patterns clearly show stimulus-induced activation in MGB, whereas SPECT imaging did not show significant CBF increase in this structure. For the 1st implementation of the measurements, both modalities lacked activation increase in IC, whereas in the 2nd implementation the upper layer of IC showed at least some activation increase. In comparison to CBF SPECT, activation patterns recorded with fMRI generally showed less activation in extra-auditory areas.

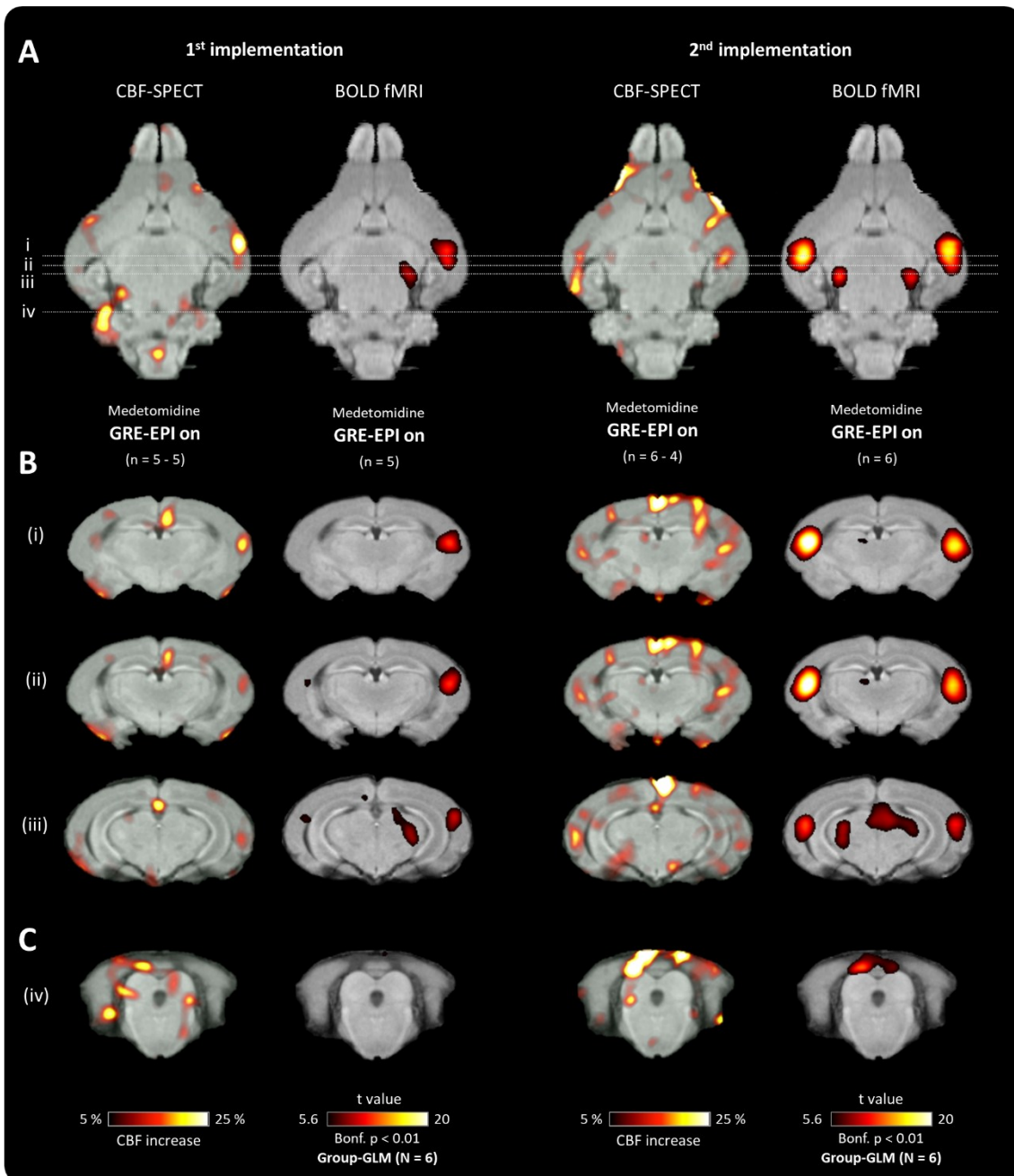


Figure 22: Direct comparison of patterns for auditory-evoked CBF and BOLD increase

A. Transversal overviews of auditory activation patterns to 1-2 kHz FM tones measured with CBF SPECT and BOLD fMRI. **B.** CBF and fMRI share similar activation patterns with a bigger impact of GRE-EPI noise in the 1st implementation (left) showing through low activation and shifted activation peak location to dorsal regions of AC. In comparison, after revision of the earphones (right) both modalities show higher activation in AC and less noise-induced activation shift. **C.** CBF increase and BOLD contrast in region of the IC present similarly little to none activation to the 1-2 kHz tone (left) and slight activation in the upper layers of IC in the 2nd implementation (right). BOLD fMRI results present additional activation in MGB and overall little to activation in extra-auditory regions. fMRI thresholds were increased to facilitate comparison of the activation patterns.

2.4. Discussion

2.4.1. Effect of medetomidine anaesthesia

Through our measurements of CBF with SPECT, we found that auditory cortical activation patterns during medetomidine anaesthesia closely mimic those of the awake states, especially in AC. Here, administration of low dosages of medetomidine led to only slightly weaker peak response magnitudes of CBF to the stimulation tone of 1-2 kHz in A1 and less pronounced activation in AFF, especially apparent in the 3D-rendered view of the data. On the contrary, differential CBF-images displayed much higher and more defined CBF increase in the subcortical brain structures including MGB, IC and LL under medetomidine anaesthesia.

Higher CBF increase in subcortical structures of medetomidine-anaesthetized animals as opposed to the awake condition could arise from different factors. First, the awake gerbils underwent the stimulation with 1-2 kHz FM tones unrestrained and were free to move around in the shuttle box. This movement could have caused irregular auditory noise in itself, despite the reduction of background noise by placement in a soundproof cabin. Additionally, within the thalamic nuclei many different stimuli types are integrated ([Sampathkumar et al., 2021](#)). The gerbils were able to perceive many other sensory impressions while freely moving around through e.g. visual, olfactory and sensory sensation. This could have caused highly variable CBF increase in these multisensory-integration areas throughout the trials of the individual animals, which in turn could have masked activation increase caused by the auditory stimulation.

Secondly, the SPL was set to 70 dB in the awake condition, to ensure that the animals were not startled or even frightened by the auditory stimulation onset, whereas in medetomidine anaesthesia, the measured SPL of the stimulation tones ranged from 90 - 95 dB, as to stay comparable to the presented sound levels required for auditory fMRI. However, this value is an approximation as there is always an inevitable ambient background noise level in the MR scanner room originating from the cooling pumps of the MR scanner setup. Cheung et al. investigated tonotopy in rats with sparse imaging fMRI and reported a linear proportional relationship of SPL to activation in IC and cochlear nuclei ([Cheung, Lau, Zhou, Chan, Zhang, et al., 2012](#)), matching our findings in IC. Their measurement setup and anaesthesia protocol, however, acquired only minimal activation in higher auditory structures, which makes further comparison difficult. Another study on auditory adaptation to sound intensity performed with FDG-PET imaging in awake rats by Jang et al. supports these findings with a glucose metabolism increase in lower subcortical structures for higher SPL. In addition, this study reports a concurring decrease in AC metabolism through louder auditory stimulation, which they studied and verified in further tests ([Jang et al., 2012](#)). Therein also lies one possible explanation to our measured CBF in the AC of awake compared to the lower CBF in AC of medetomidine-anaesthetized gerbils. Contradictorily, other studies describe activation increase in AC with incremental SPL in mice ([Hikishima et al., 2023](#)), as well as in humans ([Behler & Uppenkamp, 2016](#); [Wolak et al., 2017](#)).

Another more obvious interpretation of the lower AC activation in the anaesthetized gerbils is that the medetomidine anaesthesia itself could have had an effect on the cortical processing of the auditory stimulation, which overall suggests medetomidine anaesthesia leading to a slightly lessened connectivity within the auditory cortex. Medetomidine acts as an $\alpha 2$ -adrenergic agonist, which means in the CNS it has the potential to lower neuronal signal transduction (Khan et al., 1999). In anaesthesia studies performed with resting-state fMRI, medetomidine resulted in significant suppression of functional connectivity, especially in intra-cortical and thalamo-cortical connectivity (Magnuson et al., 2014; Paasonen et al., 2018). Many auditory studies conducted on anaesthetized rodents report little to no activation in AC, whether implemented with manganese-enhanced MRI (Yu et al., 2005), FDG-PET (Kessler et al., 2018), or BOLD fMRI with reduced-noise sequences (Blazquez Freches et al., 2018).

In a study with ablation of AC, higher subcortical activation was discovered with missing AC input (Gao et al., 2015), which could explain our heightened subcortical and lowered AC CBF measured in medetomidine-anaesthetized animals as a correlation of lowered AC activation through the anaesthesia and subsequent lower top-down modulation of MGB and IC.

Altogether, our observed effects of slightly lowered AC activation in the anaesthetized animals is most likely a direct effect of medetomidine. However, with our optimized anaesthesia protocol the effects were relatively small in comparison to other rodent auditory imaging studies that used anaesthesia (Blazquez Freches et al., 2018; Cheung, Lau, Zhou, Chan, Cheng, et al., 2012; Cheung, Lau, Zhou, Chan, Zhang, et al., 2012; Kessler et al., 2018; Yu et al., 2005). Apart from the activation patterns recorded with SPECT imaging without concurring GRE-EPI noise, comparison of the acquired auditory fMRI patterns of gerbils sedated with our optimized medetomidine anaesthesia protocol (and adjusted earphone placement) to a similarly-conducted auditory fMRI study on awake mice, our anaesthesia yielded surprisingly similar BOLD activation strength in AC, MGB and IC (Chen et al., 2020).

A good anaesthesia regime can uphold stable brain states and enable robust BOLD signal changes in stimulus-evoked fMRI (Pradier et al., 2021). Weighed against the anaesthesia benefits of preventing movement of the gerbils and reducing their stress during the fMRI acquisition, these minor changes in CBF in comparison to the awake state can be tolerated.

2.4.2. Effect of GRE-EPI background noise

GRE-EPI noise by itself showed the strongest effect in CBF SPECT patterns in IC with almost double peak CBF increases in comparison to stimulation with the 1-2 kHz FM tones. Interestingly, noise-induced CBF increase in AC and MGB was sparse. This could be a sign of ongoing adaptation in the auditory pathway to the GRE-EPI noise (Willmore & King, 2023), with filtering of the repetitive noise stimulus at the level of the IC, which was similarly observed in IC neuronal firing rates in macaques (Rocchi & Ramachandran, 2018, 2020), guinea pigs (Dean et al., 2005) and rats

(Malmierca et al., 2009). IC neurons are in particular characterized by temporal responses such as onset vs. sustained firing (Xie et al., 2008), and are suspected to facilitate detection of auditory stimulus changes like gaps by translation of time-course firing rates to a population code via neuronal adaptation (Yuan et al., 2014). The GRE-EPI noise was not newly introduced to the anaesthetized gerbils at the start of the CBF-tracer injection, but was presented during the warm-up of the gradient coils for 5 min and an additional 60 s of baseline in the GRE-EPI trial. This should have been more than sufficient time for the auditory system to adapt to the GRE-EPI background noise, which for instance occurs in the time span of 160 ms up to multiple seconds in different types of IC neurons of guinea pigs (Dean et al., 2008).

Contrary to our findings, studies on the processing of MR-acquisition related noise throughout the auditory pathway have found distinct activation in A1 and higher order AC to the pulsed noise generated by EPI sequences in humans (Bandettini et al., 1998; Di Salle et al., 2001; Hall et al., 2000; Scarff et al., 2004; Talavage et al., 1998) and in mice (Hikishima et al., 2023). However, these measured AC activations induced by EPI noise were often based on repeated block-like presentations of scanner noise (Bandettini et al., 1998; Hall et al., 2000; Hikishima et al., 2023; Talavage et al., 1998; Talavage et al., 1999). This way, the measured signal is largely influenced by the on and off-set of the EPI-noise (Harms et al., 2005; Harms & Melcher, 2002). Comparatively, with the injection start of the CBF-tracer after a baseline of GRE-EPI noise had passed, we observed the auditory system activation after adaptation effects to the EPI-noise should have taken place (Dean et al., 2008), not the effect of its acute onset. As most fMRI stimulation paradigms first present blocks of any stimulation after a baseline period, we propose this as a more accurate representation of continuous EPI-noise measured in fMRI activation patterns.

While the continuous GRE-EPI noise showed little CBF changes in MGB and AC in comparison to the measurement with ambient noise levels, its presence resulted in high changes of CBF levels induced by the 1-2 kHz stimulation throughout the entire auditory pathway. Medetomidine-anaesthetized gerbils without GRE-EPI noise showed clearly delineated CBF increases due to 1-2 kHz FM tone stimulation in the subcortical structures LL, IC and MGB, as well as in AC in typical tonotopic bands. In comparison, distinct CBF increase due to the 1-2 FM tones with concurring EPI-noise only manifested in the AC. There the activation patterns did not show in the form of typical tonotopic bands (Thomas et al., 1993) but in local spots of activation within A1 and increased higher order AC involvement, especially in the 1st implementation of these CBF SPECT measurements, where the placement of the earphones had not been optimized yet.

Comparably, *in vivo* measurements of changes in glucose metabolism induced by FM tone stimulation with FDG-PET showed much higher IC than AC or MGB involvement within the auditory system of awake and anaesthetized gerbils (Kessler et al., 2018). Our lack of observed FM tones induced IC activation over GRE-EPI background noise might lie in the already very high activation in this region through the MR noise. Percent CBF changes are limited by ceiling levels

and depend strongly on the “baseline” activation in the comparison of two states (Whittaker et al., 2016). $\Delta\text{CBF}\%$ values in the visual system described in literature do rarely surpass the 40 % CBF increase we observed in left and right IC through EPI noise stimulation (Fox & Raichle, 1984; Griffeth et al., 2015; Liang et al., 2013; Whittaker et al., 2016), controversy to this theory, some do (Ances et al., 2008). However, the technical equipment in the MR scanner room already presents an ambient noise level without concurrent GRE-EPI acquisition, with reported average noise levels of 55 – 80 dB SPL (Cho et al., 1997; Ravicz et al., 2000). In our small animal MR scanner cabin, sound measurements with a handheld sound level meter amounted to 51 dB SPL right next to the inactive scanner. Consequently, medetomidine-anaesthetized gerbils placed in the MR scanner probably already had some heightened activation within IC without GRE-EPI noise. Additionally, active adaptation processing to the GRE-EPI noise might lead to heightened levels of activation in IC neurons that exceeds the activation induced by the 1-2 kHz FM stimulation tones (Rocchi & Ramachandran, 2018, 2020; Yuan et al., 2014). Similarly to what we observed in the low activation increases in the awake gerbils, processing of the GRE-EPI noise might have masked activation changes occurring in MGB and IC.

In AC, the observed changes in auditory activation patterns through concurring fMRI background noise closely corresponds to what has been reported in human subjects in fMRI acquisitions. Similarly to what we observed in the Mongolian gerbils, multiple studies on humans reported decreases of activation in the frequency specific regions in A1 (Gaab et al., 2007; Hall et al., 1999; Langers et al., 2005; Talavage & Edmister, 2004), which is proposed to be brought on by masking effects on the stimulus (Moelker & Pattynama, 2003; Talavage et al., 1998).

Some human fMRI studies also reported additional activation in higher order AC through concurring scanner noise (Bandettini et al., 1998; Robson et al., 1998; Talavage et al., 1999), which we observed with CBF SPECT in Mongolian gerbils as well and is probably necessary as executive support for the perception of the auditory stimulus (Peelle, 2014). Our CBF SPECT confirms the findings, that the effect of fMRI background noise does not occur in a linear additive fashion (Talavage & Edmister, 2004), and therefore cannot simply be removed by post-measurement arithmetics. In our optimized auditory fMRI protocol for Mongolian gerbils, the produced background noise non-negligibly affects the measured auditory activation patterns along the auditory pathway, which has to be considered for any scientific interpretation.

2.4.3. Comparison of fMRI and SPECT data

While auditory fMRI and condition 3 of the CBF SPECT measurements were performed sequentially, the acquired images of both modalities depict the same time span and experimental condition. Despite methodological differences between the optimized auditory fMRI for Mongolian gerbils and CBF SPECT imaging, both methods produced similar peak activation patterns in AC.

Differences in patterns were mainly observed in MGB and IC, where auditory stimulation induced activation only stood out with auditory fMRI, although also with lower activation than measured in AC.

Generally, with the two methods we look at different time frames of activation changes. The auditory activation patterns acquired with SPECT with concurring GRE-EPI noise show the differences in CBF of the entire 12 min of tracer injection with and without regularly repeated block-wise stimulation of 1-2 kHz tones. Auditory fMRI activation patterns are based on statistical comparison of a modelled theoretical signal changes to the actual occurring signal time course. Slight differences in activation patterns might reflect different sensitivity of the methods to the timing of the stimulation blocks ([van Ackooij et al., 2022](#)), as well as to starting and ending of the auditory stimulations, the on and off-responses ([Harms et al., 2005](#); [Harms & Melcher, 2002](#); [Phillips et al., 2002](#)).

The lower significance in measured MGB and IC activation with CBF SPECT in comparison to auditory fMRI, however, most likely originated from the difference in sample size. Statistically, with the implemented stimulation design, the auditory fMRI within an animal is run with 15 repetitions of the stimulus block (n=15). CBF increase is measured with only one static image depicting the whole duration of the experimental trial, resulting in n=1 per animal. It is not surprising, that this leads to far lower statistical noise and higher SNR in the group-wise fMRI activation patterns in comparison to grouped analysis of CBF SPECT. Additional repetitions of the CBF SPECT for GRE-EPI background noise condition with and without auditory stimulation could reduce the static noise and consequently show similar activation changes in MGB and IC, to those observed with the concurring fMRI measurements.

The co-localization of peak CBF increases and BOLD signal change in AC, as well as the lower or lacking activation in MGB and IC, validates the spatial distribution and signal strength of the newly established auditory fMRI in Mongolian gerbils. Over and beyond that, with CBF SPECT we were able to identify a serious issue with the transmission of the auditory stimulation in the newly established setup. This facilitated an improvement in headphone fixation and ultimately raised the quality of auditory activation patterns in a 2nd implementation of the fMRI-SPECT experiments and in all following auditory fMRI measurements presented in this dissertation.

3. Effects of auditory learning revealed by auditory fMRI in the Mongolian gerbil

3.1. Introduction

The main goal and reason behind establishing and evaluating auditory fMRI in the Mongolian gerbil was to enable investigation of auditory learning processes *in vivo* on the level of the whole brain, thus providing a tool for the translation of findings in rodent research to humans.

Auditory learning has shown to induce plasticity changes in rodents in the auditory cortex and other learning related areas such as MGB, prefrontal cortex, amygdala and hippocampus using various paradigms like fear conditioning and tone discrimination learning. While monitoring of learning-related changes in the brain is usually limited by its invasiveness in human research, in rodents a wide range of techniques for direct and indirect monitoring of neural activity, plasticity and neuro-physiological changes are available. Many of these methods offer great insight into the information processing during learning but on the downside are highly invasive or localized in application, and lack direct translatability to human research.

With application of auditory fMRI in Mongolian gerbil, we are not only able to non-invasively monitor auditory-evoked activation patterns throughout the whole brain at multiple stages of a learning process within the same animal, but are able to present different stimulation tones within the same fMRI measurement session and compare relative activation changes of those as well. This allowed us the investigation of auditory-evoked brain activation patterns throughout discrimination learning which revealed: (i) general learning-induced changes in brain activation patterns; (ii) variations in activation pattern changes due to performance differences of the individual animals in the learning task; and (iii) differences in performance and activation patterns caused by application of additional punishment to the training paradigm.

In the following, a short introduction into the topics of conditioning and discrimination learning, and previously observed discrimination learning-induced brain plasticity changes by means of experiments on rodents is given.

3.1.1. Investigation of learning processes via conditioning

In neurobiological research, behavioural learning processes are often studied by conditioning, where association between an unconditioned stimulus (UCS) that results in a reflex or a particular response, and a new stimulus is learned. After learning, presentation of this new stimulus, referred to as conditioned stimulus (CS), elicits the same response or conditioned response (CR), without coincidental UCS presentation. The most widely known experiment for classical conditioning is “Pavlov’s Dogs Experiment”, where dogs were conditioned to salivate at the sound of a bell that was usually scheduled before they were given food (Pavlov & Anrep, 1927; Rehman et al., 2023). Nowadays, learning and memory in rodents is often investigated with aversive

learning through fear conditioning. In classical fear conditioning, the UCS presented to the subject is an aversive stimulus, usually in the form of pain through an electric shock, which is presented with a coincidental thus far meaningless stimulus. Afterwards, the CS elicits a fear response in absence of the UCS, manifesting in freezing of the animals, high blood pressure and tachycardia (Oitzl, 2007). Interpretation of the learning effectiveness is done by evaluation of the freezing behaviour of animals when the CS is played without presentation of the UCS, and by how long extinction of this fear memory takes; in other words how often the CS has to be presented without UCS until the animal no longer displays freezing.

An alternative to classical conditioning is instrumental conditioning introduced by Skinner. It focuses on the learning and shaping of behaviour through consequences; therein association between stimuli and “reinforcers” are reflected instead of stimulus-stimulus associations (Litvin et al., 2009; Skinner, 1948). In aversive instrumental conditioning, the unpleasant reinforcement or punishment, most commonly applied in the form of a mild electrical shock, can be evaded by learned responses of the animals.

In active aversive conditioning, the animals can escape reinforcement by a particular action. In the simplest paradigm of active avoidance, the one-way active avoidance, animals have to go towards one direction upon CS presentation to escape reinforcement (Driscoll, 2018). In the beginning of the learning process, animals initially go through a fear conditioning response to the CS, which throughout the training process with increasing performance of the animals slowly declines concomitant with avoidance of the reinforcement UCS (Choi et al., 2010; Sidman, 1953). Standardized behavioural training of animals can be performed with two-way avoidance by implementing a shuttlebox, a slightly more complex task where the animals are required to shuttle between the two compartments upon CS to escape reinforcement (Theios & Dunaway, 1964). This box automatically registers the animal’s position and switches between compartments, which are separated by a narrow pathway or a hurdle to prevent frequent switches without CS presentation. An illustration of an exemplary shuttlebox is provided with Figure 23.



Figure 23: Scheme of a shuttlebox in an aversive avoidance paradigm

The animal is presented with a cue, i.e. tone, followed by a mild reinforcement shock that encourages the animal to change compartments. Over multiple trials, the animal learns to change compartments upon cue presentation before the shock is turned on and avoids the reinforcement.

In passive avoidance, the animal has to abstain from an action to prevent punishment; in the case of shuttlebox experiments by staying in the current box compartment upon CS presentation (Driscoll, 2018; Litvin et al., 2009).

Already in relatively simple paradigms of active avoidance, animals have shown differential performance in learning tasks, enabling identification of good and bad learners by their responses to the task (Brush, 1966; de Oliveira et al., 2016). One explanation for the diverse responses is some individual animals lapsing into a paradigm of learned helplessness (Seligman, 1972). This paradigm can be deliberately implemented through a combination of classical and instrumental conditioning, where the animal is first exposed to a classical fear conditioning paradigm, and later on subjected to an instrumental conditioning paradigm with the same surrounding and CS presentation but with a chance of escaping the UCS. There, the animals have impaired learning of the escape response or active avoidance due to the initial fear conditioning ("Learned Helplessness," 2009; Silveira & Joca, 2023). Similarly to this behaviour, subpopulations identified as bad learners in instrumental active avoidance conditioning exhibit low active avoidance rates and a lot of freezing (Choi et al., 2010; Lázaro-Muñoz et al., 2010; Martinez et al., 2013).

3.1.2. Discrimination learning

Discrimination between similar stimuli is crucial for cognitive functioning and is associated with memory accuracy (O'Reilly & McClelland, 1994). Failure of discrimination of aversive and non-aversive stimuli implies lowered memory resolution or generalized fear (Vieira et al., 2014). This fear generalization for similar stimuli can lead to psychological disorders like PTSD and phobias (Concina et al., 2018; Mahan & Ressler, 2012; Morey et al., 2015). Therefore, memory accuracy to a CS is an important factor to consider in preclinical studies concerning learning and memory.

In instrumental discrimination learning, a subject or animal has to not only learn the association of CS presentation to a particular action, but to differentiate between similar stimuli and learn to react differently to each stimulus. In the case of aversive conditioning, this learning task can be promoted by an active avoidance task with reinforcement for one tone and no consequence for others. For this procedural learning, a shuttlebox can be easily implemented as well in a GO/noGo procedure. For example, in auditory discrimination learning, the animal is presented with two stimulation tones, one representing the GO tone, upon which the animal has to change the compartment; and a noGo tone where it does not. Tones can differ in their features, such as duration, amplitude, frequency and modulation of frequencies (FM).

A standard auditory discrimination learning task often implemented at the Leibniz Institute for Neurobiology is the discrimination of FM direction in a shuttlebox with Mongolian gerbils, following an active avoidance instrumental conditioning approach (Ohl et al., 1999). Through application of this learning paradigm, many interesting auditory information-processing aspects of learning were investigated. For example, implementation of this learning task in combination

with focal lesions in AC led to discovery of lateralization of FM direction discrimination to the right AC in Mongolian gerbils (Wetzel et al., 2008; Wetzel, Ohl, et al., 1998), which is one of many known hemispheric functional asymmetries occurring in humans (Herve et al., 2013). Such lateralization effects rarely had been observed in rodents at that time.

However, the observed individual performance of the animals was very diverse (Wetzel, Wagner, et al., 1998). Through application of additional punishment (aP) for changing compartments upon noGo tone stimulation to the paradigm, the experimenters pursued more consistency in the behavioural performances and higher discrimination levels (Wetzel et al., 2008; Wetzel, Wagner, et al., 1998).

3.1.3. Changes in brain plasticity through auditory discrimination learning

Procedural learning and memory involves the acquisition, consolidation, and retrieval of individual information processing that is behaviourally expressed in a consistent manner (Packard, 2009), which necessitates the involvement of multiple functional networks. Sensory perception and learning are shaped by the emotional state (Phelps, 2004; Tyng et al., 2017).

Aversive conditioning, independent of the nature of the CS, induces similar processing in certain key regions of the brain across many species of mammals, schematically portrayed for humans and mice in Figure 24, which makes aversive learning especially appropriate for translational studies (Flores et al., 2018; Headley et al., 2019).

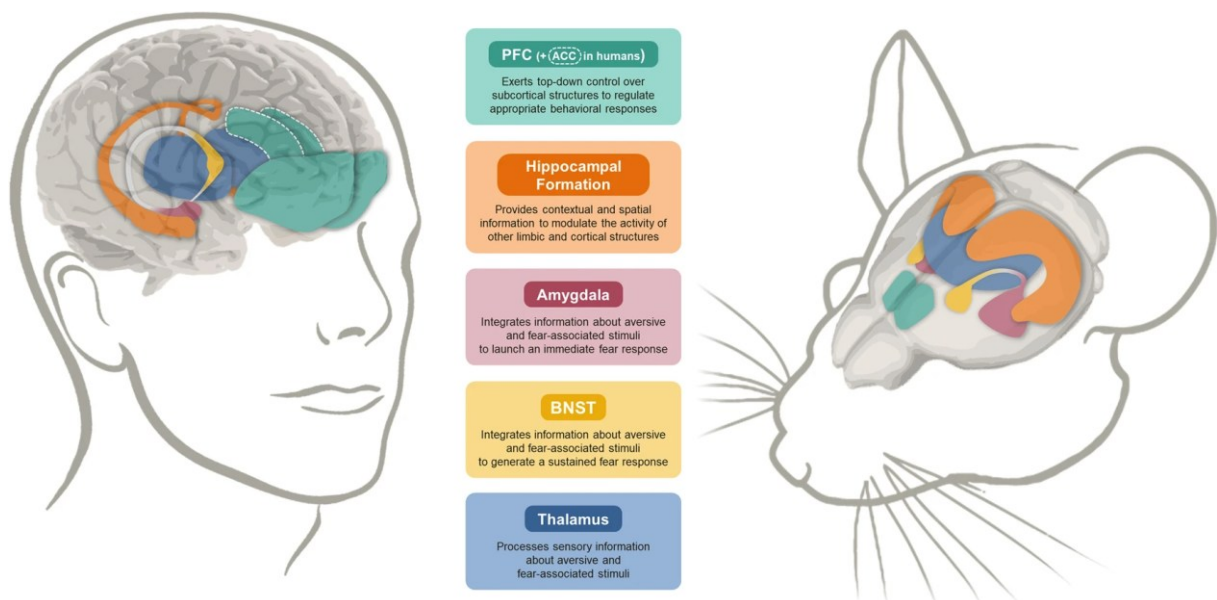


Figure 24: Key regions in rodent and human involved in aversive processing*

Similar processing for fear-mediated responses is induced in prefrontal cortex (PFC) and anterior cingulate cortex (ACC) in humans, hippocampal formation, thalamus, and cerebral nuclei with amygdala and bed nucleus of stria terminalis (BNST).

*Figure published in "Lost in translation: how to upgrade fear memory research", Flores et al, Springer Nature Molecular Psychiatry, Volume 23, Macmillan Publishers Limited, reproduced with permission from SNCSC (Flores et al., 2018)

With different paradigms of auditory conditioning in rodents, auditory learning has shown to induce frequency-specific plasticity changes in structures of the central auditory pathway: more precisely in the primary and higher order AC (Bakin & Weinberger, 1990; Edeline et al., 1993; Grosso et al., 2015; Ohl & Scheich, 1996; Weinberger et al., 1993), MGB (Edeline, 1990; Hennevin et al., 1993; Lennartz & Weinberger, 1992; Pardi et al., 2020; Taylor et al., 2021) and IC (Ayala et al., 2013; Szczepaniak & Møller, 1996).

In the course of the learning process of auditory discrimination tasks, participation and activation of neuromodulatory, associative brain regions have been reported as well; including amongst others, amygdala (Grewe et al., 2017; Lázaro-Muñoz et al., 2010; McCullough et al., 2016; Park et al., 2016), dorsal striatum (Xiong et al., 2015; Znamenskiy & Zador, 2013), hippocampus (Freeman et al., 1996), prefrontal cortex (Concina et al., 2018; Vieira et al., 2015) and limbic thalamus (Gabriel et al., 1991; Smith et al., 2002). Convergence of differential sensory input during auditory learning can additionally induce plasticity changes in other, multisensory regions such as the superior colliculus (Hu & Dan, 2022; Lesicko et al., 2020).

The implementation of FM direction discrimination tasks in Mongolian gerbils has facilitated the observation of a number of interesting learning-induced plasticity and brain activation changes. To name a few; increased dopamine concentration in prefrontal cortex was found during learning acquisition of the task (Stark et al., 2004), an increase of coherence in cortico-striatal projections detected (Schulz et al., 2015), the influence of β -adreno-receptors activation on long-term memory consolidation in AC deciphered (Schicknick et al., 2019), and the necessity of hemispheric interaction for this type of discrimination learning ascertained (Saldeitis et al., 2022).

In summary, these individual studies on relatively local and selective structures suggest widespread changes in activation and plasticity induced by auditory discrimination learning, reaching throughout the entire gerbil brain.

This circumstance is supported by the anatomy of the gerbil brain, as discussed in a review by Budinger & Scheich (Budinger & Scheich, 2009). There they describe the results of multiple histological studies on neuronal projections to and from primary AC in gerbils (Budinger et al., 2006; Budinger et al., 2000a, 2000b; Budinger et al., 2008), encompassing connections to numerous auditory, neuromodulatory and multisensory brain structures located in isocortex, basal forebrain, thalamus/hypothalamus, midbrain and hindbrain.

Auditory-stimulated fMRI could offer insight into whole brain activation changes throughout different stages of auditory discrimination learning with repeated measurements of the same animals.

However, extensive research into literature via PubMed did not show any studies that report on auditory learning-induced activation changes in the rodent brain by utilization of auditory fMRI.

3.2. Methods

3.2.1. Experimental animals

FM direction discrimination learning experiments were performed on 33 young adult male Mongolian gerbils (*Meriones unguiculatus*, bred in-house or purchased from Charles River, Italy) with a starting age of 11-12 weeks. The animals were housed in groups of up to three animals per cage in a temperature-controlled room with 12h/12h dark/light cycle (6:00/18:00) with food in the form of rodent pellets and sunflower seeds, and water *ad libitum*. All of the following animal experiments were approved by the ethics committee of Saxony-Anhalt (No. 42502- 2-1591 LIN).

Motion during the fMRI measurement led to the exclusion of all datasets of two animals and one dataset of another two animals. Additionally, one animal showed signs of reversal learning during the FM direction discrimination task, was outlier-tested in its negative behavioural score, and excluded accordingly. This leaves overall 30 animals included in the analysis of the study.

3.2.2. Experimental design

18 gerbils were trained to discriminate between rising (GO: 1-2kHz) and falling (noGo: 2-1kHz) FMs in ten daily sessions, promoted through reinforcement with a mild electrical foot shock for a “Miss”. Prior, after 3 and after 10 sessions auditory-stimulated BOLD fMRI was performed; Figure 25 shows a scheme of the measurement and training timeline. Through the exclusion criteria of motion during the fMRI acquisition (see chapter 3.2.5), 16 animals of this group ended up in the final analysis. A second group of 15 animals underwent the same experimental procedures, the only difference being additional punishment (aP) during the direction discrimination training; there, the animals received an additional shock for a “False Alarm”. One animal was to be excluded from this second aP group, due to reversal learning, leading to a sample size of N = 14 for the final analysis.



Figure 25: Timeline of the performed fMRI measurements throughout the course of the FM direction discrimination training

Note that all animals got a day of recovery after each fMRI measurement (blue); each training period was performed daily without breaks (green).

All gerbils underwent one more fMRI measurement 3-4 weeks prior to the experiments presented above. An additional surgical intervention was performed on 24 of the FM direction discrimination learning experiment animals, which is described in the supplements under “(i) Information on the additional surgical interventions” starting on page Q. The intention was to

selectively lesion interhemispheric connections of the AC. However, this method was not successful (Figure S 8) and did not show any impact on behaviour (Figure S 9 and Figure S 10) or fMRI derived auditory brain activation patterns (Figure S 11) in comparison to control animals. In compliance with the “3R principle”, these unaffected animals were deemed naïve and included in the analysis of the direction discrimination learning studies.

3.2.3. FM direction discrimination training

The gerbils were trained to discriminate between FM tones of different modulation direction in a shuttlebox controlled with the Graph State Suite (version 4, Coulbourn Instruments, USA) and the Coulbourn H02-01 Habitest Link (Coulbourn Instruments, USA). Prior to the initial FM direction discrimination training, the animals were habituated to the two-compartment shuttle box (38 x 22.5 x 19 cm³ divided by a hurdle of 4 cm height, Hasomed GmbH, Germany) for 20 min. For the discrimination training, speakers mounted above each compartment presented the CS in repeated loops of 200 ms FM tones (5 ms rise/decay times; 60 - 70 dB) with 300 ms inter-stimulus intervals (ISI). Rising 1-2 kHz FM tones represented the animals' cue to cross the hurdle within 6 s (CS+, GO tone). Correct behavioural responses of the animal to the GO tone were counted as “Hit” (correct response, CR+). Falling 2-1 kHz FM tones served as the cue to stay in the current compartment of the box for at least 10 s (CS-, noGo tone); a correct response was counted as “Correct Rejection”. Failing to cross the hurdle during the GO tone presentation was interpreted as a “Miss”, reinforced by an electrical foot shock that was applied through the electrical grid floor. This electrical foot shock served as UCS, which was applied until the animal crossed the hurdle or for a maximum of 4 s with ongoing GO tone presentation. A second group of animals underwent FM direction discrimination training with additional punishment (aP) for crossing the hurdle during noGo tone presentation (“False Alarm”; incorrect response, CR-) with application of the UCS until the animal returned to the original compartment or for a maximum of 1.5 s. The foot shock strength was initially set to 300 µA at the connected shock generator (Coulbourn Precision Animal Shocker, Coulbourn Instruments, USA). Throughout the training, the animals were closely observed and the shock strength adjusted by up to ± 100 µA if deemed necessary. In the discrimination training without aP, “False Alarms” were of no consequence for the animal.

Training was carried out in ten daily sessions consisting of 60 trials each, where the CS were presented in a Gellerman pseudorandom schedule, interleaved by 20 s inter trial periods. After the initial three training sessions, the training was suspended for two days to acquire fMRI and a subsequent recovery day for the animals (Figure 25).

3.2.4. Auditory fMRI measurements

The overall auditory measurement was implemented in accordance with the protocol for auditory fMRI of the Mongolian gerbil described in chapter 1.3.2. In the following, only the most

essential key settings and alterations of the standard protocol that served to investigate discrimination-learning effects are described in detail. The 9.4 T MRI scanner was implemented with the accompanying acquisition software ParaVision Acquisition Workplace (version 7). The standard ^1H -transmit-receive volume coil with inner diameter of 86 mm combined with the custom-made ^1H planar receive-only surface coil with 15 mm diameter was used for all MRI measurements of this study. All of the animal preparation was done according to the standard protocol with meticulous placement and fixation of the earphones. Medetomidine anaesthesia was started at 0.3 mg/kg/h and increased to 0.4 mg/kg/h after 45 min.

MRI measurements

MRI measurements were started after 1 h of medetomidine uptake. At this, scout scans were run and the volume resonator was manually matched and tuned. For high resolution anatomical images, we ran the TurboRARE sequence with TR/TE 2200/8 ms in 20 contiguous frontal slices of 0.8 mm thickness and 85 μm in-plane resolution (image matrix 355 x 234, FoV 30x20 mm^2 ; RARE-factor 8; 2 avg). Shimming was performed on basis of a previously run B0-map, the 3 FoV saturation slices adjusted according to the animals' position. The sequence was repeated at the very end of the MRI measurement with 6 avg under 1.5 % isoflurane anaesthesia for higher image quality.

For functional imaging, the optimized gradient echo EPI sequence was run within the same FoV/slices position with an in-plane resolution 400 μm and TR/TE of 1000/15 ms (image matrix 75 x 50, FoV 30x20 mm^2). The sequence was run with 300 reps as warm-up of the gradient system.

Discrimination learning fMRI

For the discrimination learning experiments, two functional scans were recorded, one with 1020 reps and the second with 1080 reps. During the first acquisition, a stimulation protocol was presented binaurally in a block design with 120 s baseline and 30 x [10 s stimulation and 20 s rest], with 3 pseudo-randomly alternating stimulation tones, visualized in Figure 26A.

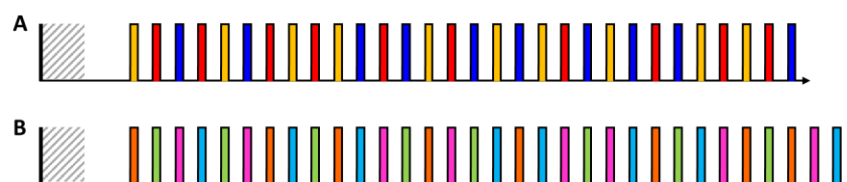


Figure 26: Auditory stimulation protocols for discrimination learning fMRI

A. Block design of the stimulation protocol applied on fMRI measurements with 1020 reps; with pseudorandomized binaural presentation of GO tone (red; 1-2 kHz rising), noGo tone (blue; 2-1 kHz falling) and control tone (yellow, alternating 3-6 kHz rising and 6-3 kHz falling). **B.** Block design for a contralateral noise procedure acquired with 1080 reps, designed for the investigation of lateralization effects in AC; with pseudorandomized presentation of GO tone to left ear (orange), GO tone to right ear (green), GO tone to left ear with contralateral white noise (pink), and GO tone to right ear with contralateral white noise (light blue).

Those tones consisted of repeated 200 ms ramped sweeps and 300 ms ISI with frequencies of 1-2kHz (red, GO tone), 2-1 kHz (blue, noGo tone), and 3-6 kHz alternating with 6-3 kHz (yellow, control tone).

A second functional scan was run with another stimulation protocol in block design with 120 s baseline and 32 x [10 s stim and 20 s rest], presenting 4 different pseudo-randomly alternating auditory stimulation types (Figure 26B). The stimulation tone again consisted of 200 ms ramped sweeps with a frequency of 1-2 kHz and 300 ms ISI, but presented monaurally in combination with coinciding contralateral white noise: sweeps left ear (orange), sweeps right ear (green), sweeps left with contralateral noise (pink), and sweeps right with contralateral noise (blue).

After conclusion of the MRI measurement, the animal was released from the MR setup, injected s.c. with 0.4 mg/kg atipamezole and returned to its home cage.

3.2.5. Data analysis

Analysis of the discrimination training

For an estimation of the animals' performance in the FM direction discrimination training, the CR difference was calculated by subtraction of the CR- ("False Alarm") from the CR+ ("Hit"): *CR difference = (CR+) - (CR-)* for each training session. In addition, the d-prime (d') was calculated to enable comparison to other behavioural learning experiments. This was achieved by subtraction of the z-transform of the rate of CR- from CR+ ($d' = z(CR+) - z(CR-)$). Z-transforms of CR+ and CR- were performed according to the signal-detection-theory (Green & Swets, 1966), with conversion of absolute rates of CR+ and CR- to relative values to the number of presented CS+ and CS-, and transformation to corresponding z-scores via look-up tables provided in Macmillan and Creelman's "Detection Theory: A User's Guide" (Macmillan & Creelman, 2005). The learning speed of each animal was estimated according to the description of Schulze et al. (Schulze et al., 2014), where a fourfold χ^2 test (2-sided, $p < 0.01$) was implemented on the outcome of each session of each animal with GraphPad Prism (version 10, GraphPad Software, Inc., USA). The speed of learning to discriminate the CS+ from CS- was defined as the first of two consecutive significant sessions with this test.

As the interindividual behavioural variation of the animals was extremely high, the animals were separated into equal sized groups of good and bad learners according to their average CR difference in the second block of their discrimination training, from session 4 to session 7. Statistical comparison of the groups of good and bad learners as well as between behavioural outcomes of gerbils, trained with and without aP respectively, was achieved with Holm-Šídák corrected Whitney-Mann U statistics with GraphPad prism.

Analysis of fMRI data

In the scope of this thesis, only the first stimulation paradigm alternately presenting GO, noGo and control tone to the animals will be presented.

Preprocessing and analysis of the fMRI data was mainly performed with BrainVoyager (version 20.6, Brain Innovation, Maastricht, Netherlands). The exported DICOM images were loaded into the imaging analysis program with 55 volumes skipped in addition to a 5 s delay occurring due to the dummy scan duration at the start of each GRE-EPI-sequence, leaving a 1 min baseline for the analysis.

For preprocessing of the imaging data, a slice time correction with a cubic spline interpolation was performed, as well as 3D motion correction trilinear/sinc interpolation to the first EPI-image, smoothing by a FWHM of 0.8 mm in space domain and temporal filtering with a Gaussian high pass filter (2 cos/sin of data points). If the spontaneous voxel displacement was bigger than the recorded voxel size (0.4 mm), either the dataset was cut short if the displacement occurred in a time window that left most of the data intact (at least 8 repetitions of each stimulation tone) or the scan was excluded from the analysis. Due to these exclusion criteria, all datasets of two animals were excluded from further analysis, as their functional MR images consistently showed motion artefacts throughout the study. Additionally, one dataset after 3 days of training and one dataset after 10 days of training were excluded, an example is shown in Figure 27.

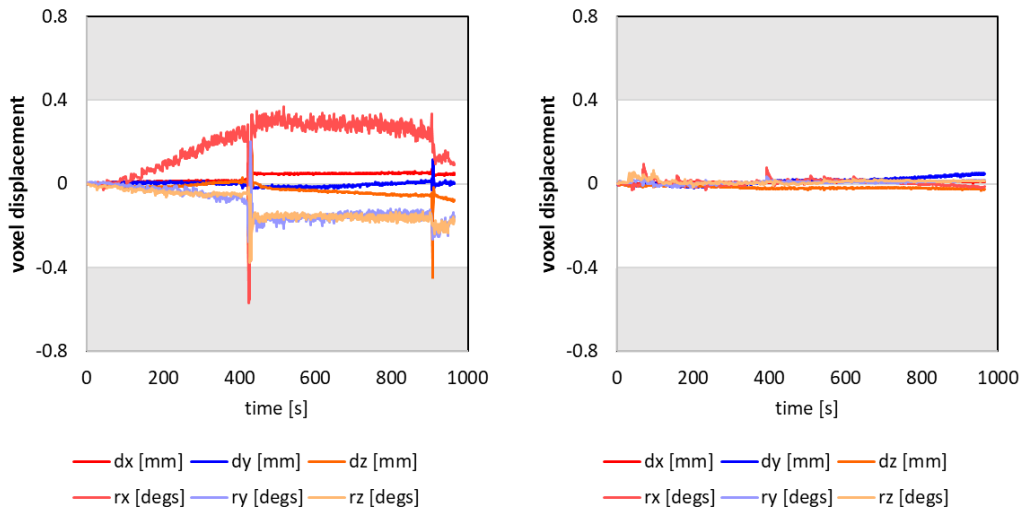


Figure 27: Motion correction (3 translations, 3 rotations) of two MR scans performed in the same animal
The scan in the left was excluded as the voxel displacement was bigger than the recorded voxel size (> 0.4 mm), leaving not enough of the data intact for a conclusive GLM analysis. The right shows the typical amount of motion occurring during an fMRI measurement without acute movement of the animal.

Each measurement was evaluated with an individual GLM, the two-gamma HRF applied to the stimulation protocol of each run adjusted with time to response peak of 3 s and time to undershoot peak of 10 s. To enable group analysis, the high quality anatomy of each scan was manually coregistered to a high definition 3D-anatomical template of a gerbil brain (*in vivo* measurement of 4 h performed by Patricia Wenk, 48 h after injection of a manganese-chloride

contrast agent). The coregistration parameters were applied to the corresponding functional scans, converting them to 3D VTC data in the same native space.

Multi subject GLMs, based on the single study GLMs design model, were run on the VTC data of each measurement time individually; performed with correction for serial correlation, %-transformation and separate subject predictors. Differential activation patterns were obtained by overlaying the resulting GLM-contrasts as an overview, combining all stimulation tones, or only applying each stimulation tone condition individually as positive contrast. For direct visual comparison between measurement time points, another multi subject/multi study GLM was run with all measurement time points combined. Here, the baseline measurement was subtracted from the time points after 3 days of training and after 10 days of training. For each of those contrasts, FDR and Bonferroni corrected thresholds were noted respectively, and images exported to NIfTI format for image presentation with MRICroGL (version 20, ([MRICroGL, 2019](#))), which was also used for 3D rendering of the activation patterns.

Through region of interest (ROI) analysis with the gerbil brain atlas (described in detail in chapter 1.2.6, BETA values (single subject, %-transformed) of the statistical maps were extracted from auditory structures and structures known to be involved in learning and memory. Regions definitions of this implemented gerbil brain atlas are appended in Table 4. The STC of each animal and measurement was additionally extracted and used to calculate ERA within the same ROI with Excel (Microsoft Office Standard 2016, Microsoft Corporation, USA). For the comparability of the results, the average baseline for each scan was calculated, and the STC normalized to 0 % by averaging the pre-period before each stimulus (from -4 s to -1 s) and dividing each data point by that value. An ERA for each stimulation tone condition was calculated by averaging the signal over all its repetitions per time point from -4 s to + 24 s (t = 0 s defined as stimulus onset).

Direct comparison of extracted BETA values (GLM-based; single subject, %-transformed) of each VOI for different time points and performance of the animals was achieved through mixed-model ANOVAs with Geisser-Greenhouse sphericity correction and Bonferroni's multiple comparison correction with GraphPad Prism.

Correlation of behavioural and fMRI data

To investigate the correlation of individual FM direction discrimination performance against the auditory brain activation patterns, linear regressions were performed with GraphPad Prism. In the course of this, the average performance of each animal in the second half of their training (mean of training block two, 7 last sessions) was plotted against their individual BETA values in the final fMRI measurement after the full 10 days of FM direction discrimination training. Linear regressions were performed for GO, noGo and control tone stimulation BETAs for all regions of the gerbil brain atlas, for the group without and with aP respectively.

3.3. Results

3.3.1. Auditory-evoked brain activation patterns

Analysis of the pre-training functional MRI data of all 30 animals included in the discrimination training studies resulted in activation of the central auditory system for the three stimulation tones, including bilateral activation in the AC, the MGB, and the IC. Figure 28 shows an overview of the activation patterns for all three stimulation tones derived from a group-GLM combining the animal group trained with and without aP (Bonferroni correction $p < 0.001$; $N=30$) prior to any behavioural training.

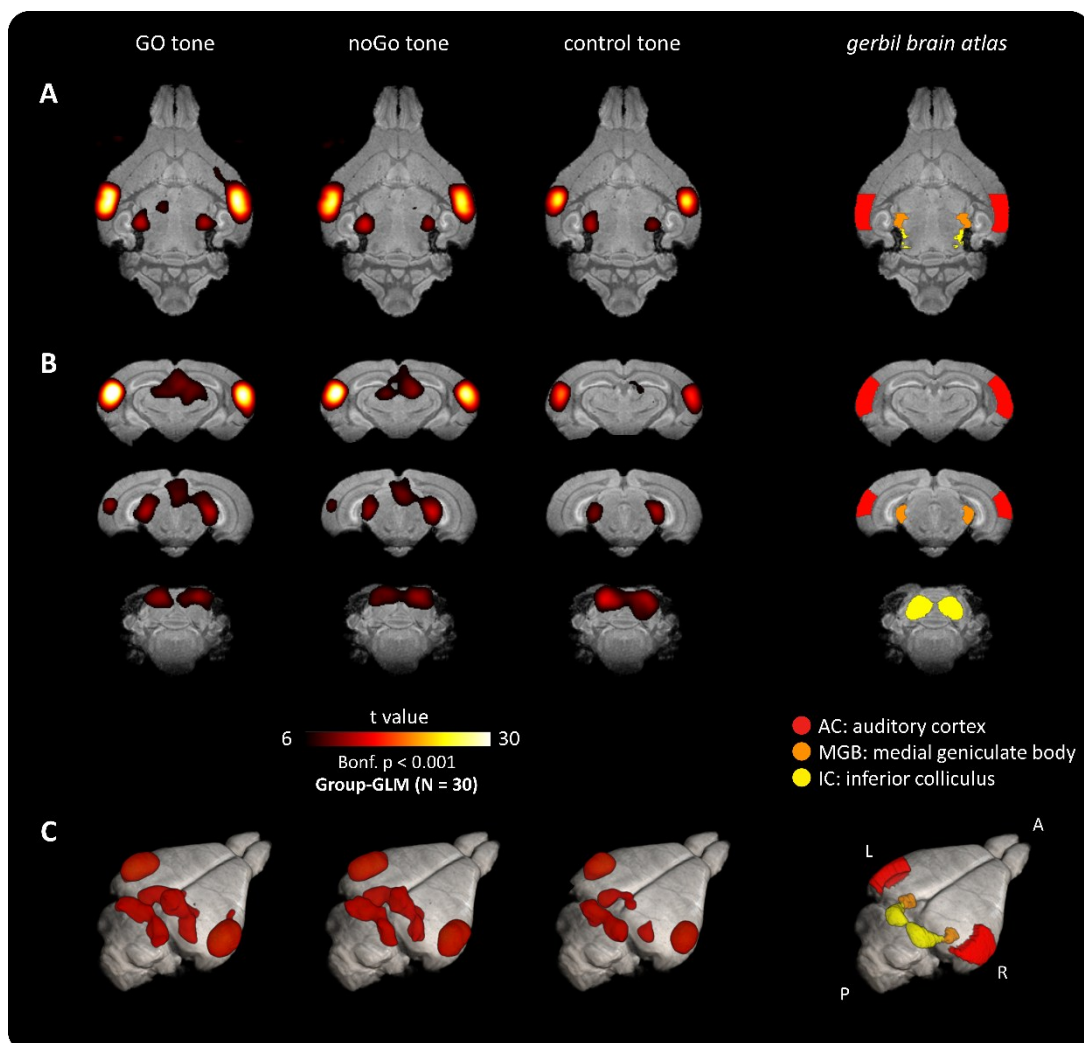


Figure 28: Brain activation patterns to the three different stimulation tones prior to the direction discrimination training

A. Horizontal images showing the activation in the AC, and MGB. **B.** Coronal images in region of the AC, MGB and the IC from top to bottom. **C.** 3D-rendered brain activation patterns, all overlaid on a high-resolution 3D-anatomical image of the gerbil brain. On the right corresponding images of the gerbil brain atlas, showing the structures of the central auditory pathway with AC in red, MGB in orange and IC in yellow. (Group-GLM of $N=30$ gerbils with threshold at Bonferroni correction of $p < 0.001$)

The control tone led to slightly less activation in the AC and MGB, and slightly stronger activation in the IC in comparison to the GO and noGo tone, which can be easily seen in both the horizontal

(Figure 28A) and coronal sections (Figure 28B) of the gerbil brain. Auditory stimulation also caused signal increase in some other regions.

To simplify the further comparison of the differences in brain activation patterns, most of the results are displayed in form of 3D-rendered images (Figure 28C); these do not show activation strength but rather the activation patterns throughout the brain and regions that become significantly active (Bonferroni or FDR correction of the data) through stimulation with the different tones.

Figure 29 illustrates extracted STCs (A) with corresponding ERAs (B) and BETA values (C) in the region of AC, MGB and IC of the central auditory pathway.

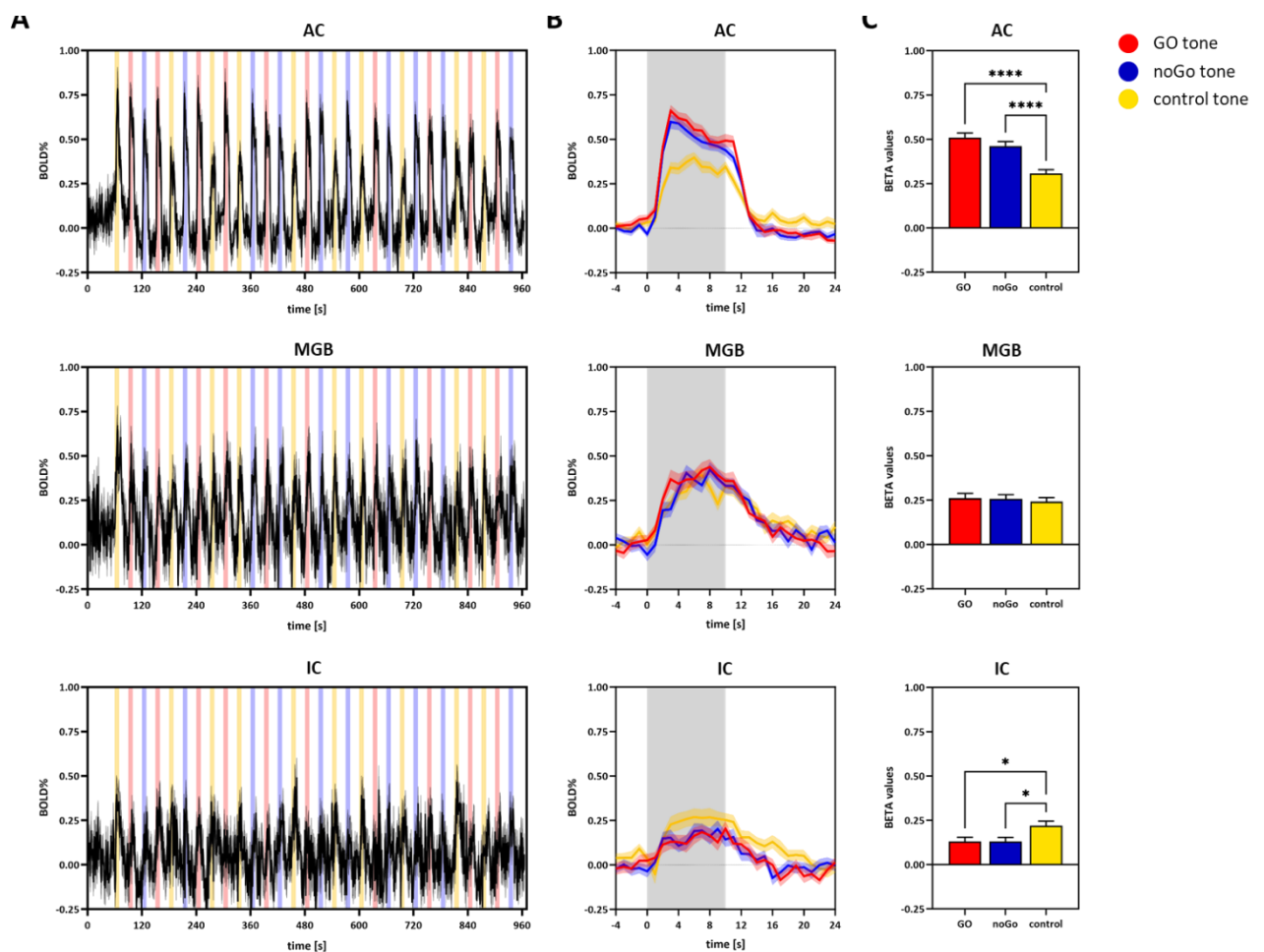


Figure 29: STC, ERA and BETA values for the three stimulation tones prior to the discrimination training Signal time courses (A) and event related averages (B) of the three stimulation tones GO (red), noGo (blue) and control tone (yellow) prior to the direction discrimination training in the central auditory pathway; averages of $N=30$ animals, onset and duration of auditory stimulation is indicated by shaded blocks in the background of time courses and event-related averages. C. BETA values for the different stimulation tones extracted from the Group-GLM.

The ERA curves show that the typical shape of the stimulation block convoluted with the gerbils' HRF is most closely reached in the AC (Figure 29B, top) with corresponding BETA values of 0.51 ± 0.03 % for GO, 0.46 ± 0.03 % for noGo, and significantly lower 0.31 ± 0.02 % for the control tone stimulation (Figure 29C, top). Comparatively, the MGB show a flatter ascend to the initial

response peak with lower BETA values of 0.26 ± 0.03 % for GO tone, 0.26 ± 0.02 % for noGo tone and 0.24 ± 0.02 % for control tone stimulation (Figure 29B&C, middle). The response curve in the IC is even more gradual in increase and decrease than the other structures (Figure 29B, bottom). Within, the BOLD response results in BETA values of 0.13 ± 0.02 % for GO and noGo tone, and significantly higher 0.22 ± 0.03 % for control tone (Figure 29C, bottom).

3.3.2. Changes in activation patterns induced by discrimination learning without aP

Gerbils that received no aP shock after “False Alarm”, surpassed a CR difference of 10 (maximal score 30) on average in their second FM direction discrimination training session, with no further improvement throughout the remainder of the training (Figure 30A). The behavioural score d' shows considerable error bars throughout the 10 sessions of FM direction discrimination training (SEM, Figure 30B), reflecting a widespread variation in behavioural performance of the individual animals. During each session, the animals received around 12 reinforcement shocks for failing to cross the hurdle upon GO tone presentation (Misses, Figure 30C). The learning speed definition shown in Figure 30D, indicates that only 75% of the animals learned discrimination between GO and noGo tone throughout the ten days of direction discrimination training.

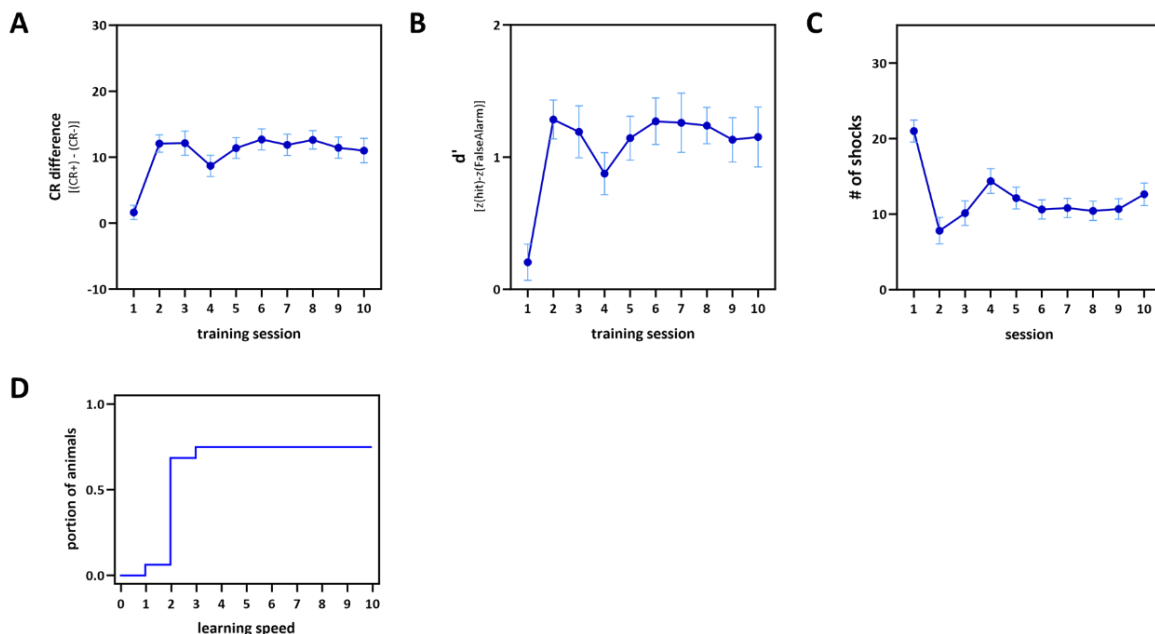


Figure 30: Behavioural scores of the gerbils during their discrimination training without aP

(A) CR difference calculated from $((CR+) - (CR-))$ and (B) corresponding d' values presenting relatively large error bars. C. Average number of reinforcement received in each session approximately halved after the initial training session. D. Estimation of learning speed of the animals shows, according to the applied definition not all animals learned to discriminate the tones after 10 days of training. ($N = 16$, mean \pm SEM)

The auditory fMRI from the pre-training measurement shows positive BOLD contrast in the complete central auditory pathway including AC, MGB and IC for all stimulation tones (Figure 31A-C, upper row). After 3 training sessions, increased and more widespread activity with additional BOLD activation in IC, thalamic regions, most prominently in MGB and thalamus

dorsalis (Th), as well as retrosplenial (RSC) and medial prefrontal cortex (mPFC) was observed for the GO and noGo tone. This activation increase persisted with 7 additional days of FM direction discrimination training (Figure 31A-C, lower row), alongside some activation increase at this time point for control tone stimulation. Extracted BETA values within these regions are listed in Table 3.

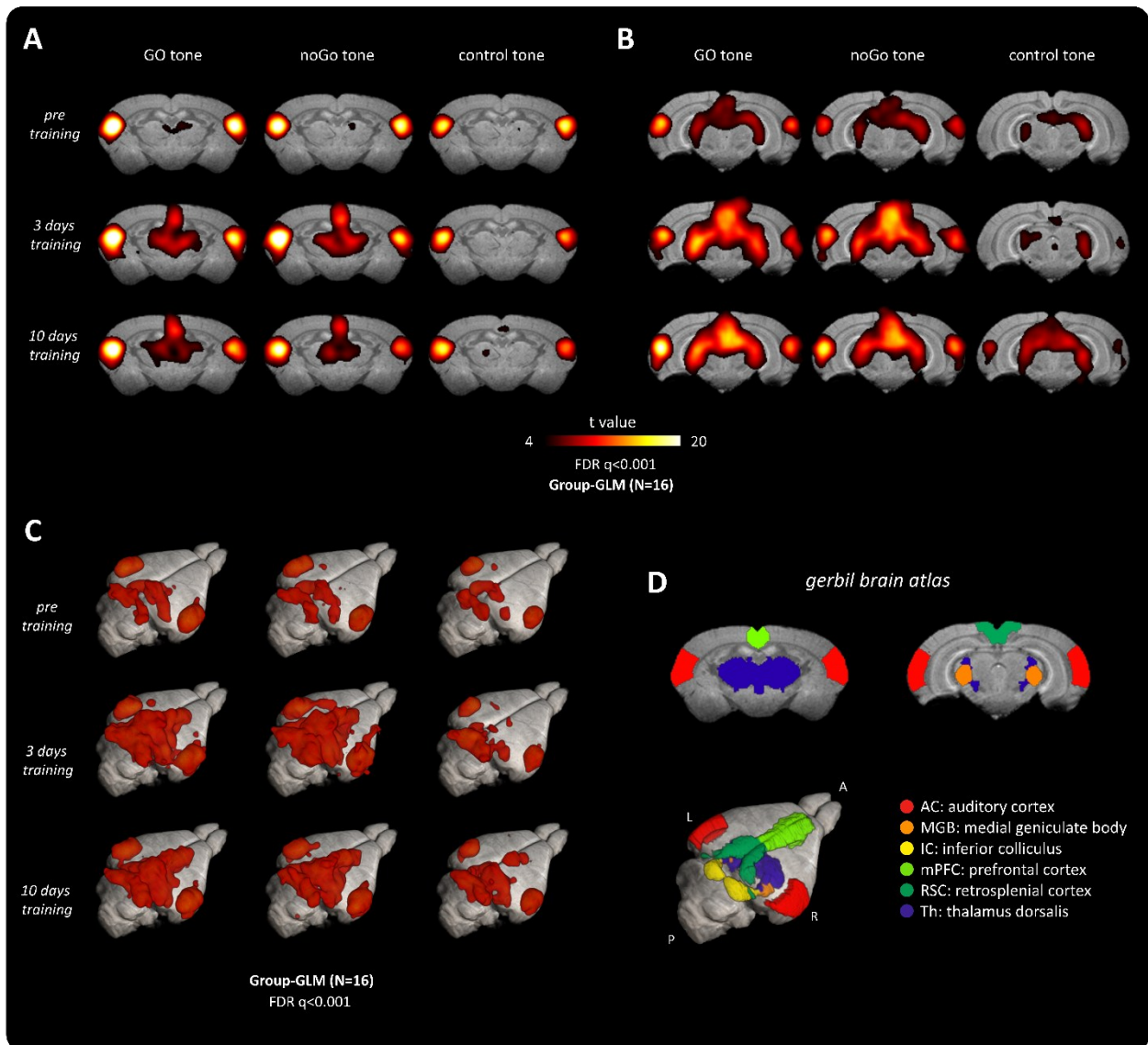


Figure 31: Brain activation changes induced by FM direction discrimination learning without aP

Results of group GLMs of the pre training measurement, after 3 days and after 10 days of training without aP (rows top to bottom) overlaid on coronal sections of a high-resolution 3D-anatomical template of the gerbil brain. **A.** Activation increase is visible for GO and NoGo tone stimulation in Th and mPFC after 3 and 10 days of FM direction discrimination training without aP. **B.** Similar activation increases occurred in RSC and MGB. **C.** 3D-rendered Global brain activation patterns for the different stimulation tones throughout discrimination training. **D.** Volumes of interest defined in the gerbil brain atlas overlaid on the same sections of the template. (Group-GLM of N=16 with FDR correction of $q < 0.001$)

i: Exclusion of one animal from 3-days-training measurement analysis due to motion artefacts

Similar to the behavioural scores d' , the amount of activation increase varied widely for the individual animals, especially in their final fMRI measurement after 10 full days of training, as can be seen in the standard errors Table 3, especially in mPFC and RSC. Nevertheless, mixed-model

ANOVAs performed on these values reported significant effects of FM direction discrimination training duration on the acquired BETA values in MGB ($p = 0.04$), IC ($p = 0.03$), mPFC ($p = 0.0004$), and Th ($p = 0.04$) of the listed regions. Apart from those regions that already stand out visibly through the activation patterns, similar effects were discovered in olfactory and orbital cortical areas, subiculum and retrohippocampal areas of the hippocampal formation, septal nuclei, epithalamus, and tegmental and tectal areas of the midbrain. While the tectal midbrain (*tectum mesencephalon*) contains the subregion IC, which also showed significant BETA value increases by itself, the effect was stronger for the entire structure with $p = 0.01$, the activation surplus being mostly localized in region of the superior colliculi.

Table 3: Exemplary BETA values for brain structures showing activation changes due to the direction discrimination training without aP

Activation changes (BETA values in %) to the previous measurement that are larger than the SEM are marked by \uparrow for BETA increase and \downarrow for BETA decrease. Note the standard error increase, especially after 10 days of training. ($N=16$; i : Exclusion of one animal from 3-days-training measurement analysis due to motion artefacts)

	training	GO	noGo	control
		mean \pm SEM	mean \pm SEM	mean \pm SEM
AC	pre	0.50 \pm 0.035	0.42 \pm 0.037	0.26 \pm 0.031
	3 days	0.47 \pm 0.040	0.46 \pm 0.051	\downarrow 0.22 \pm 0.032
	10 days	\uparrow 0.55 \pm 0.057	0.49 \pm 0.052	\uparrow 0.34 \pm 0.051
rAC	pre	0.41 \pm 0.034	0.36 \pm 0.039	0.24 \pm 0.038
	3 days	0.39 \pm 0.036	0.39 \pm 0.051	0.21 \pm 0.033
	10 days	0.42 \pm 0.051	0.39 \pm 0.046	\uparrow 0.27 \pm 0.049
lAC	pre	0.60 \pm 0.043	0.50 \pm 0.048	0.30 \pm 0.034
	3 days	0.56 \pm 0.061	\uparrow 0.56 \pm 0.067	\downarrow 0.24 \pm 0.037
	10 days	\uparrow 0.70 \pm 0.078	0.61 \pm 0.069	\uparrow 0.41 \pm 0.068
MGB	pre	0.25 \pm 0.036	0.27 \pm 0.034	0.23 \pm 0.038
	3 days	\uparrow 0.45 \pm 0.037	\uparrow 0.37 \pm 0.031	0.22 \pm 0.039
	10 days	0.41 \pm 0.040	\downarrow 0.33 \pm 0.039	\uparrow 0.29 \pm 0.045
IC	pre	0.12 \pm 0.031	0.14 \pm 0.033	0.19 \pm 0.037
	3 days	\uparrow 0.23 \pm 0.018	\uparrow 0.21 \pm 0.030	\uparrow 0.29 \pm 0.030
	10 days	\downarrow 0.22 \pm 0.028	0.21 \pm 0.034	0.28 \pm 0.023
mPFC	pre	-0.01 \pm 0.024	-0.02 \pm 0.021	-0.02 \pm 0.024
	3 days	\uparrow 0.11 \pm 0.031	\uparrow 0.11 \pm 0.043	0.01 \pm 0.023
	10 days	\uparrow 0.19 \pm 0.052	\uparrow 0.16 \pm 0.045	\uparrow 0.08 \pm 0.032
RSC	pre	0.14 \pm 0.033	0.13 \pm 0.027	0.05 \pm 0.047
	3 days	\uparrow 0.22 \pm 0.030	\uparrow 0.23 \pm 0.039	0.04 \pm 0.029
	10 days	0.22 \pm 0.046	0.21 \pm 0.045	\uparrow 0.11 \pm 0.036
Th	pre	0.11 \pm 0.018	0.10 \pm 0.018	0.08 \pm 0.018
	3 days	\uparrow 0.20 \pm 0.017	\uparrow 0.20 \pm 0.030	\downarrow 0.05 \pm 0.024
	10 days	0.18 \pm 0.029	0.18 \pm 0.029	\uparrow 0.10 \pm 0.025

3.3.3. Differences in performance are reflected in the brain activation patterns

As remarked upon, the interindividual variation of the behavioural scores was considerably high throughout the FM direction discrimination training without aP, as can be seen in the individual

CR difference scores in the left panel of Figure 32A. Coincidentally, the brain activation patterns observed in the individual animals, especially after the full 10 days of training also showed high variance. Investigating whether this variance in activation could be attributed to the learning performance of the animals in the FM direction discrimination task, the animals were separated into a group of “good learners” and a group of “bad learners” of equal size according to their average behavioural score throughout the training. The behavioural differences between those two groups is further elaborated in Figure 32.

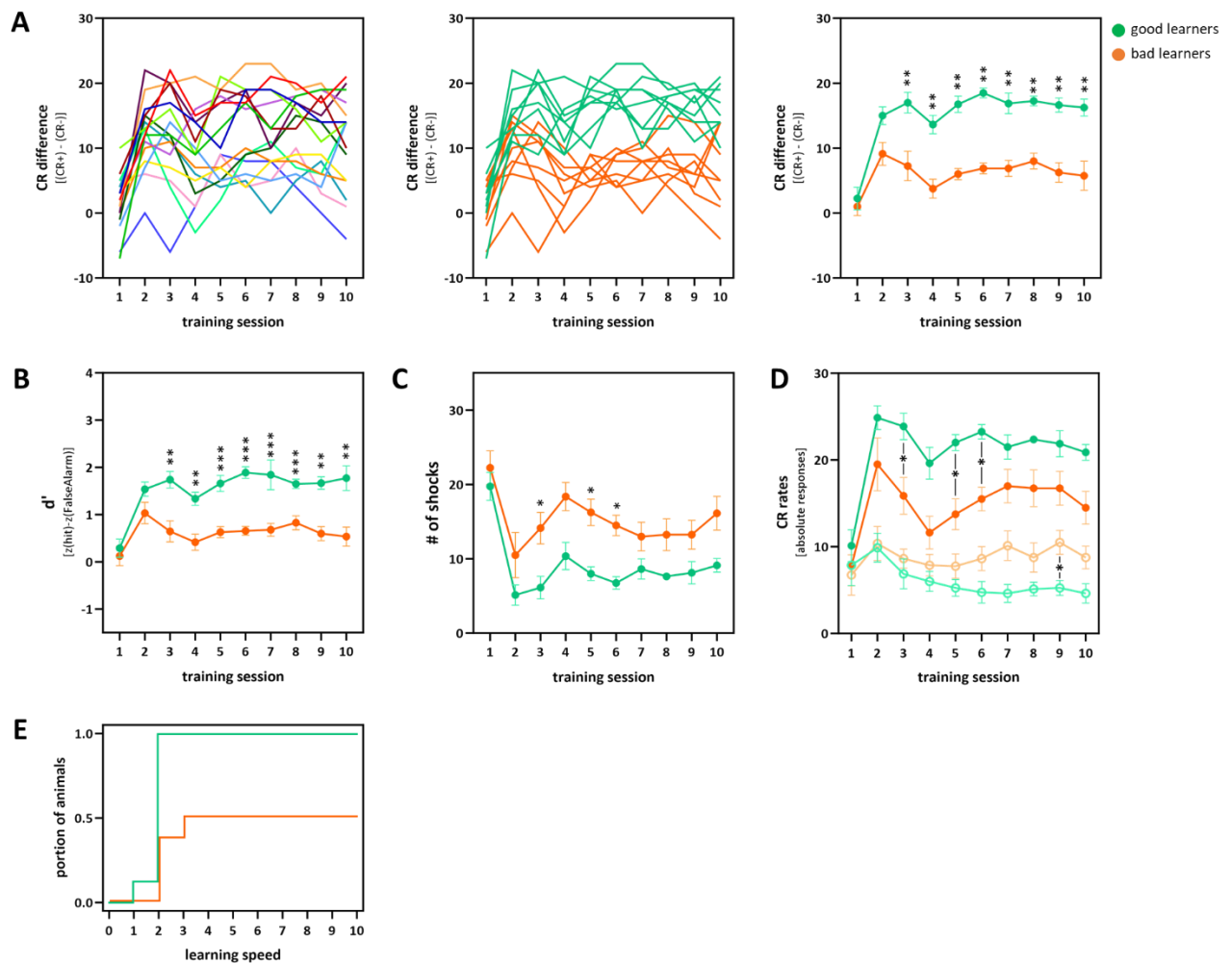


Figure 32: Separation into groups of good and bad learners by average discrimination performance in FM direction discrimination training without aP

A. Separation into groups of good and bad learners is shown from left to right. Left: the CR difference of the individual animals, middle: allocation of the individuals to good learners (green) and bad learners (orange), right: the resulting mean and SEM for each group with significantly higher learning score for good learners. **B.** Corresponding d' values present similar differences between good and bad learners. **C.** Average number of reinforcement shocks received throughout training. **D.** CR+ rates (bolder shades, closed circles) are significantly higher for good learners in earlier training sessions, while CR- rates (lighter shades, open circles) are significantly different in session 9, towards the end of the training. **E.** Learning speed of the animals: here only half of the bad learners reached criteria for discrimination learning. Statistical comparison between groups performed with Mann-Whitney tests with Holm-Šidák multiple comparison correction. (Adjusted p -values indicated by * $p < 0.05$; ** $p < 0.01$; *** $p < 0.001$)

Already in their third training session, the good and bad learners significantly varied in their CR difference score (Figure 32A, right panel). From the 4th session onwards, the good learners averagely scored with a CR difference of 16.6 ± 0.6 , while the bad learners reached average scores of 6.2 ± 0.6 (maximal score of 30, mean and SEM, N=8 each). These scores correspond to d' values of 1.7 ± 0.1 for good and 0.6 ± 0.1 for bad learners (Figure 32B, mean and SEM, N=8 each).

The number of received reinforcement shocks was always higher for bad learners in the FM direction discrimination training without aP although significantly different only in session 3, 5 and 6 (Figure 32C).

Figure 32D shows the comparison of the absolute CR rates for GO and noGo tone individually. CR+ rates (Hits) diverge more in the first half of the training with significantly higher values for the good learners in session 3, 5 and 6. This shows that bad learners took slightly longer to learn to cross the hurdle upon GO tone presentation. Good learners displayed continued decrease of CR- (False Alarms) after the initial 2 training sessions, presenting an improvement in discrimination abilities between the rising and falling tones, especially since there was no negative consequence for a False Alarm in the training without aP. Comparatively, bad learners CR- rate slightly increased in the later training sessions, resulting in significant difference between good and bad learners in session 9. The CR rates overall demonstrate that bad learners gradually learn to jump upon GO tone presentation due to the reinforcement, but do not improve in their FM direction discrimination abilities.

The learning speed reflecting on the performance difference between groups is shown in Figure 32E. According to the definition of Schulze et al. (Schulze et al., 2014), all of the good learners were able to discriminate between the upwards modulated GO and downwards modulated noGo tone by their 2nd session. Half of the bad learners learned to discriminate the tones by their 3rd session; however, the other half did not learn to discriminate in the ten days of discrimination training.

In auditory brain activation patterns, presented in Figure 33, the good learners show slightly more activation in the central auditory pathway in the pre training measurement for all three stimulation tones, especially in thalamus and midbrain. After 3 sessions of direction discrimination training (Figure 33A&B, middle row), both groups show a similar pattern for the GO tone stimulation with an increase of activity in thalamus and midbrain and additional activity in mPFC and RSC. For the noGo tone stimulation, the bad learners show more widespread and intense activation increase, which becomes more obvious in the differential group-GLM images in Figure 33C&D.

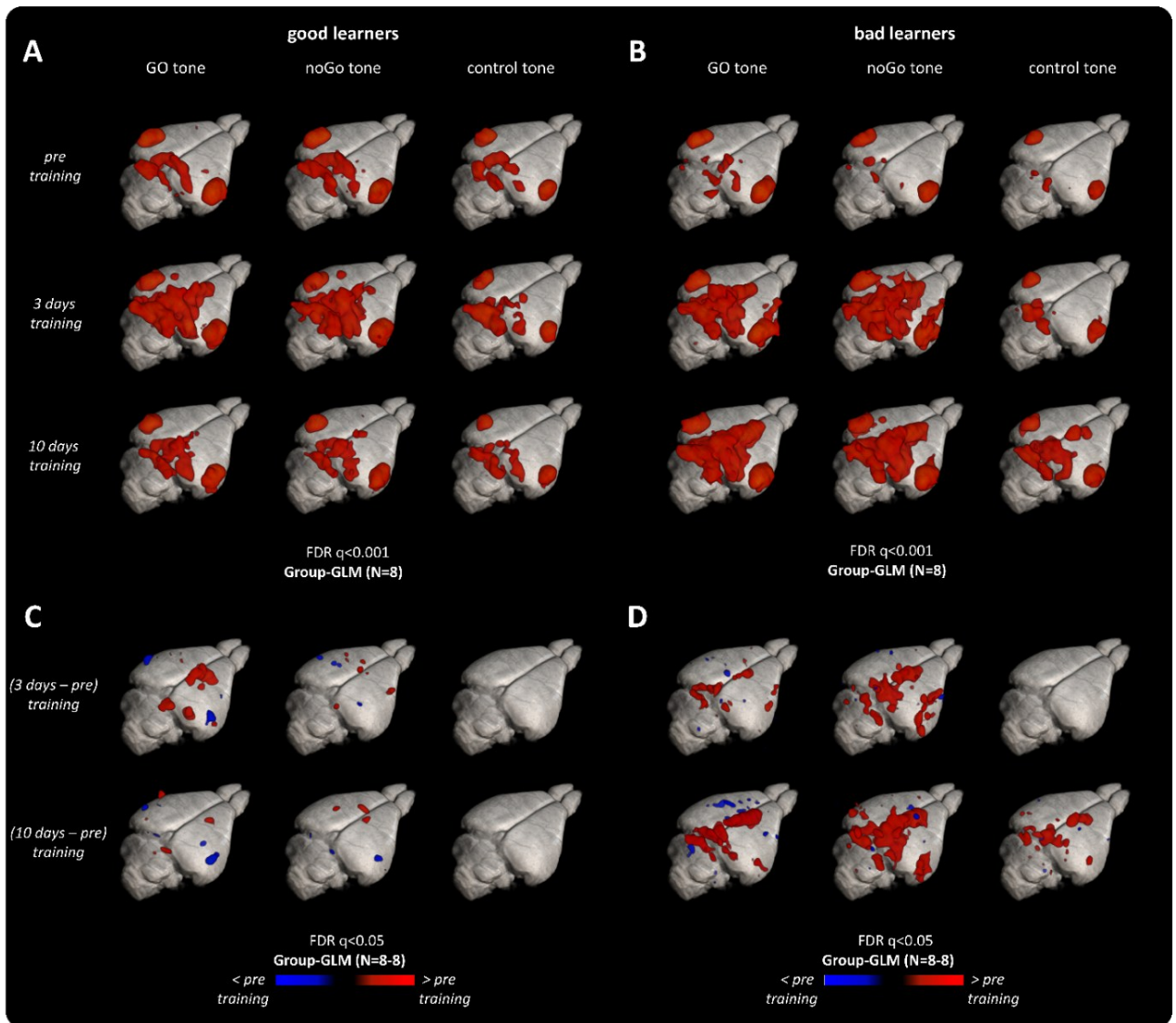


Figure 33: Auditory brain activation patterns of good and bad learners throughout discrimination training FM direction training performed without aP. Results of Group-GLMs of good (A) and bad (B) learners with FDR correction of $q < 0.001$ ($N=8$). Both groups show visibly increased activation in the midbrain, RSC and mPFC for GO and noGo tone stimulation after 3 days of training (A&B, middle row). After 10 days of training the activation patterns differ between groups, with brain activation returning to a state close to pre training for the good learners (A, lower row), while the bad learners show further activation increase in all stated structures for GO, noGo and even control tone stimulation (B, lower row). Differential Group-GLM images between the post and the pre training measurements show even differences between the (C) good and (D) bad learners more clearly (group-GLM of $N=8-8$ with FDR correction of $q < 0.05$).

i: Exclusion of one bad learner from 3-days-training measurement analysis due to motion artefacts

The biggest activation pattern difference between the groups occurred after the full 10 days of FM direction discrimination training. Here, the good learners show brain activation patterns that closely resemble their pre training baseline patterns, while the bad learners have the most widespread activation for the GO and noGo tone of the entire study. At this time point, bad learners additionally present a distinct activation increase for the control tone stimulation. For a more detailed comparison, supplementary Figure S 2 shows the BOLD contrast in exemplary coronal sections for the GO tone stimulation after the full 10 days of training.

Figure 34 illustrates the statistical comparison of BETA values within the visibly activated areas (Figure 33) for good (green) and bad learners (orange). Further areas that showed statistical differences throughout the discrimination training are appended in Figure S 3, as well as accompanying BETA values for all stimulation tones and measurement time points (Table 5).

As visible in Figure 34, good learners presented notable changes in BETA values for the GO tone stimulation after 3 days of training, with significant increases in MGB from $0.27 \pm 0.05 \%$ to $0.49 \pm 0.05 \%$, in mPFC from $-0.02 \pm 0.02 \%$ to $0.12 \pm 0.04 \%$, and in Th from $0.10 \pm 0.02 \%$ to $0.19 \pm 0.02 \%$. Similarly but non-significantly, increase of BETA values occurred also in IC from $0.16 \pm 0.03 \%$ to $0.25 \pm 0.03 \%$, and in RSC from $0.13 \pm 0.03 \%$ to $0.20 \pm 0.04 \%$. In the meantime, in rAC (shown instead of AC due to the lateralized processing of FM tones in this hemisphere; AC and IAC are included in supplemental Figure S 3), a slight and also non-significant activation decrease occurred from $0.42 \pm 0.04 \%$ to $0.37 \pm 0.05 \%$. After the full 10 days of training, the good learners' brain activity declined to a state more closely resembling the baseline activity (MGB: $0.31 \pm 0.04 \%$, IC: $0.20 \pm 0.04 \%$, mPFC: $0.06 \pm 0.02 \%$, RSC: $0.10 \pm 0.03 \%$, Th: $0.11 \pm 0.02 \%$), with exception in rAC with slightly further decreased activation (rAC: $0.35 \pm 0.04 \%$, not significant).

The bad learners showed similar BETA value increases for the GO tone after 3 days of training, but this was not significant (MGB: $0.22 \pm 0.05 \%$ to $0.41 \pm 0.05 \%$, mPFC: $0.01 \pm 0.04 \%$ to $0.10 \pm 0.05 \%$, IC: $0.08 \pm 0.05 \%$ to $0.22 \pm 0.02 \%$, RSC $0.15 \pm 0.06 \%$ to $0.24 \pm 0.04 \%$, Th $0.12 \pm 0.03 \%$ to $0.20 \pm 0.02 \%$). In rAC, in contrast to good learners, bad learners showed a slight increase of BETA values from $0.39 \pm 0.06 \%$ to $0.42 \pm 0.05 \%$ for the GO tone stimulation (not significant).

In contrast to good learners, bad learners' brain activation to GO tone stimulation even further increased with the additional training (i.e. after 10 days of training), resulting in significantly increased BETA values of $0.52 \pm 0.05 \%$ in MGB and $0.31 \pm 0.08 \%$ in mPFC. In the other brain areas visualized in Figure 34 this further activation increase occurred similarly although non-significantly, with BETA values of $0.49 \pm 0.09 \%$ in rAC, and $0.23 \pm 0.04 \%$ in IC, $0.34 \pm 0.06 \%$ in RSC, and $0.26 \pm 0.04 \%$ in Th for GO tone stimulation after 10 days of training.

BETA values for noGo tone stimulation progressed similarly to GO tone stimulation throughout the FM direction discrimination training. For good learners, the BETA value increases to noGo tone after 3 days of training were slightly lower than the described increases to the GO tone stimulation, overall lacking significance. For bad learners, BETA value increase in many of the described regions was even higher for noGo tone stimulation after 3 days of training, but reached similar levels to the GO tone after completion of the training. After 10 training sessions, bad learners' training-induced activation increase was significant in mPFC, RSC and Th for noGo tone.

BETA values to the presented control tone did not significantly change throughout the FM direction discrimination training without aP. However, the values are visibly increased for bad learners in MGB, mPFC, RSC and Th after 10 days of training (Figure 34).

After 10 days of training, the good and bad learners showed significant brain activation differences in mPFC, RSC, MGB and Th for GO and noGo tone stimulation, as well as in rAC for the noGo tone stimulation, highlighted by asterisks and square brackets in Figure 34. Apart from these brain regions that stand out in the fMRI activation patterns with relatively high threshold values (Figure 33), some other brain regions presented similar changes of BETA values. Graphs of those are attached in supplemental Figure S 3, showcasing amongst others significant differences between good and bad learners in subthalamus, epithalamus and septal nuclei.

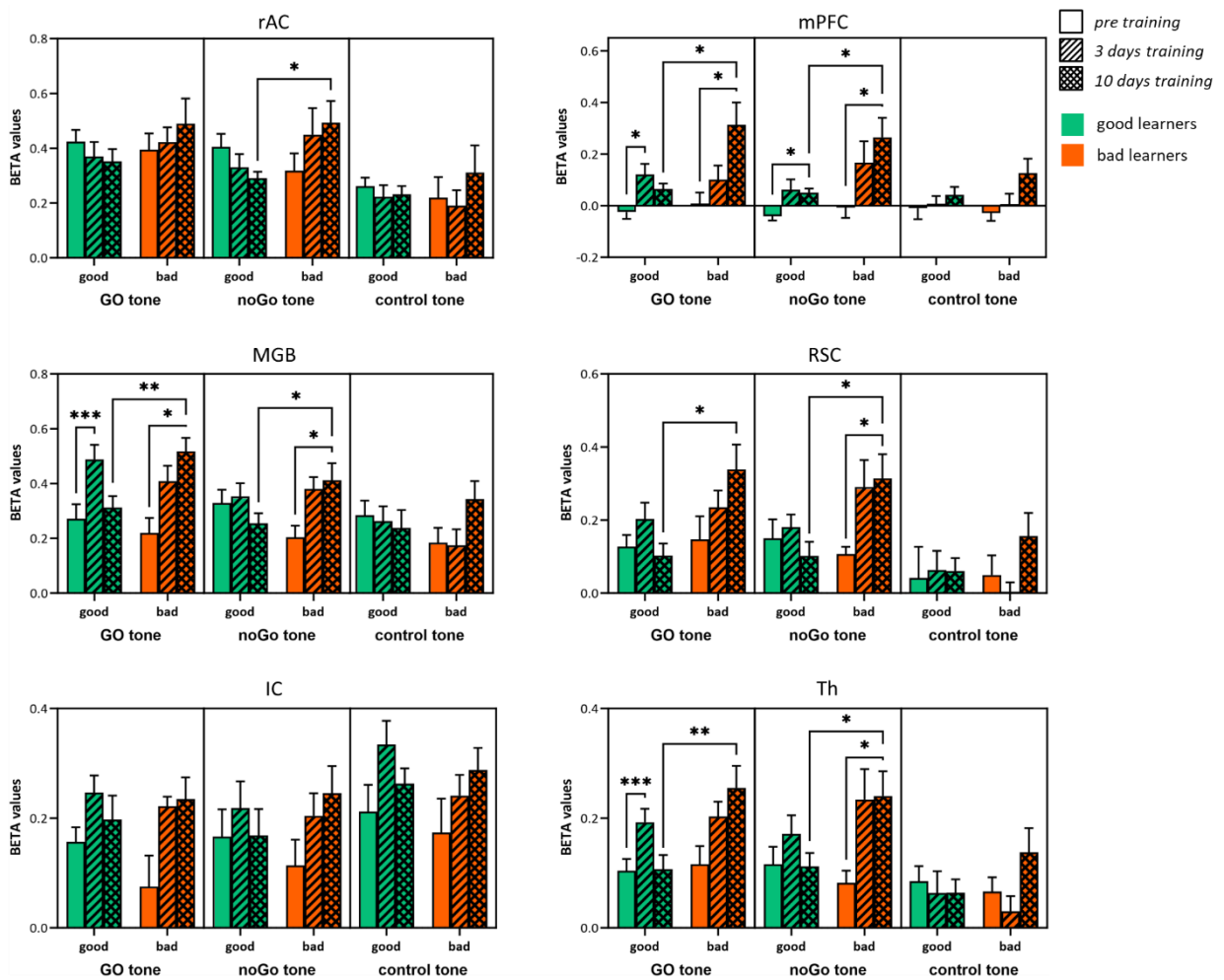


Figure 34: Statistical comparison of good and bad learners throughout discrimination training without aP

*In the comparison of BETA values, significant differences between good and bad learners are showing after 10 sessions of training, occurring most prominently in MGB of the auditory system, and the extra-auditory structures mPFC, RSC and Th. (Mixed-model ANOVAs with Bonferroni multiple comparisons correction; N=8 per group; * $p < 0.05$; ** $p < 0.01$; *** $p < 0.001$)*

i: Exclusion of one bad learner from 3-days-training measurement analysis due to motion artefacts

These significant differences between the groups of good and bad learners in region specific areas demonstrate performance dependency in changes of brain activation patterns through FM direction discrimination training. However, they do not represent the wide range of individual behavioral outcomes we observed in the left panel of Figure 32A. Through linear regression of the individual CR differences (average of day 4 to day 10 of training) against the corresponding BETA

values acquired in the final fMRI measurement, we were able to observe correlation of individual performance and region-specific brain activation, illustrated in Figure 35.

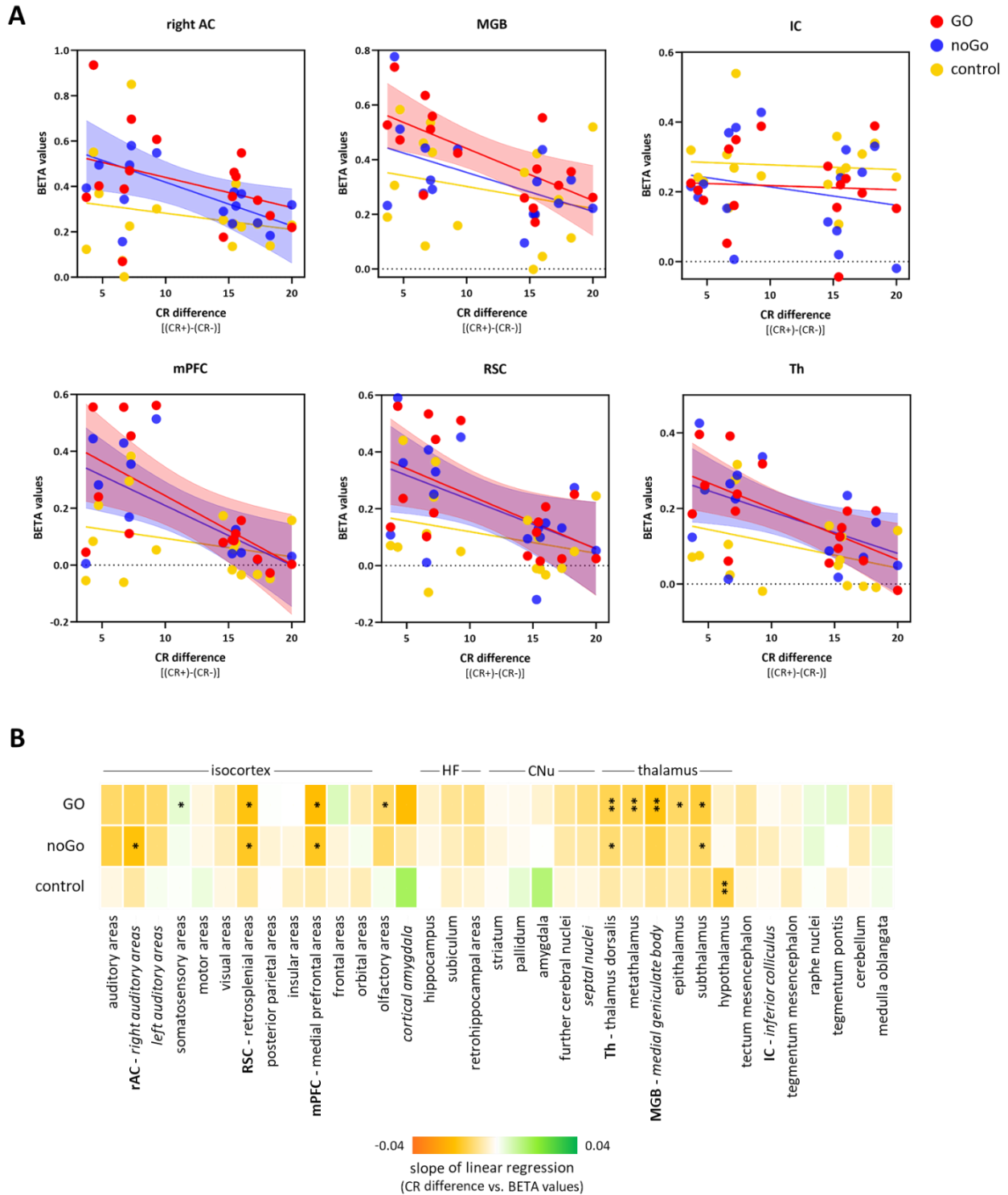


Figure 35: Correlation of learning performance in discrimination training and brain activation

A. BETA values against CR difference in last 7 days of FM direction discrimination training without aP in the auditory regions rAC, MGB and IC; and in extra-auditory regions mPFC, RSC, and Th for GO (red), noGo (blue) and control tone (yellow). Linear regressions that resulted in statistically significant non-zero slopes are indicated by semi-transparent areas within the 95% confidence intervals of the line ($p < 0.05$). **B.** Summarized outcome of linear regressions of all regions of the gerbil brain atlas, slope indicated by colour range, orange implying higher BETAs in bad learners; green higher BETAs in good learners. Level of significance is denoted by * for $p < 0.05$ and ** for $p < 0.01$; $N = 16$.

Such regressions show significant correlation of individual behavior to the measured brain activation in rAC (noGo 0.32 R²), MGB (GO 0.43 R²), mPFC (GO 0.29 R²; noGo 0.27 R²), RSC (GO 0.31 R²; noGo 0.27 R²) and Th (GO 0.41 R²; noGo 0.27 R²). Similar to the general ANOVA outcome, IC showed no such correlation.

The correlation of average CR difference to measured brain activity are additionally shown for all brain regions of the gerbil brain atlas in Figure 35B. Again, significant correlation, ergo statistically significant non-zero slopes, were evident in the previously listed brain regions subthalamus (GO 0.39 R²; noGo 0.28 R²) and epithalamus (GO 0.39 R²).

Changes in activation patterns at time of reinforcement shock onset in gerbils trained without aP

Not only onset of the auditory stimulation elicited BOLD activation in the trained gerbils, but also the expected reinforcement shock. In the GO trials of the FM direction discrimination training, the GO tone was presented to the gerbils for 6 s before the reinforcement shock was turned on in cases of a “Miss”, when they failed to cross the hurdle. When analyzing the acquired fMRI data with a shift of the hemodynamic response function by those 6 s, the brain activation patterns of the trained gerbils show activation in some additional regions. Comparatively, the pre training measurement of all animals and the measurement after 10 days of training in good learners shows very little to none BOLD contrast, as can be seen in the 3D-rendered images in Figure 36.

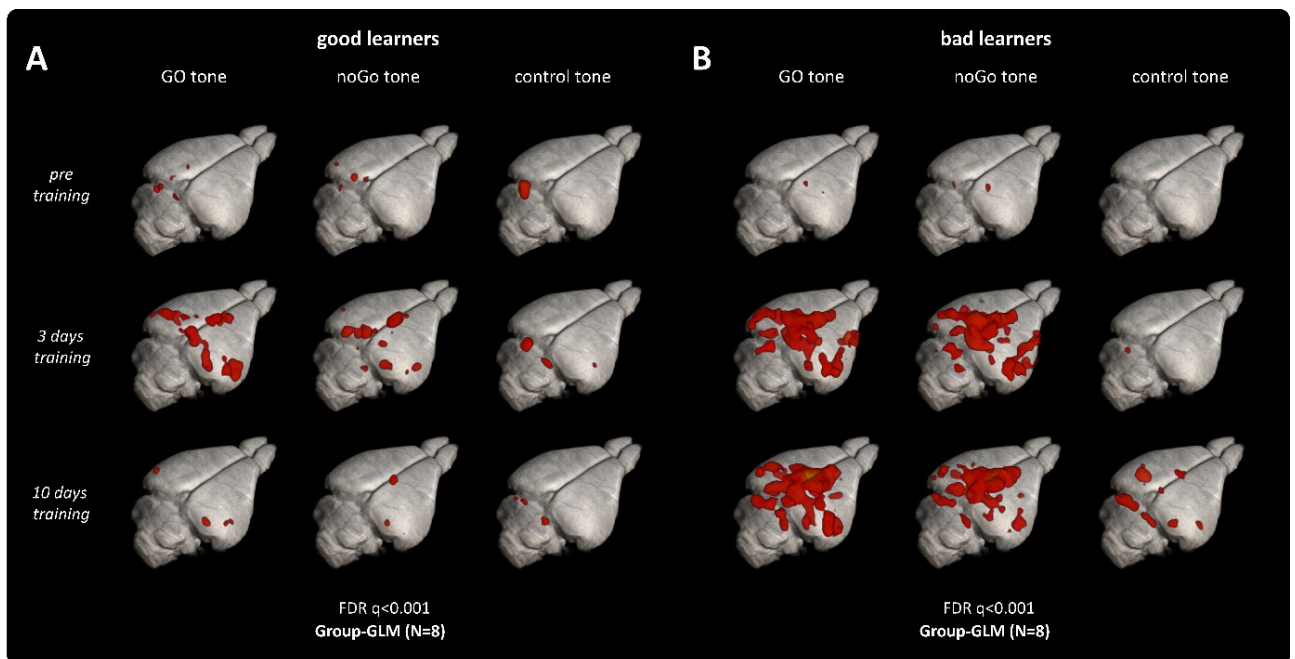


Figure 36: Brain activation at expected time of reinforcement shock in animals trained without aP

Applying the hemodynamic response function with a 6 s shift shows BOLD activation for good learners (A) predominantly after 3 days of training, with a more widespread pattern for GO tone stimulation. B. For bad learners, strong BOLD activation is visible after 3 days and after 10 days of FM direction discrimination training for GO and noGo tone stimulation. (FDR corrected Group-GLMs of N = 8 with q < 0.001)

i: Exclusion of one bad learner from 3-days-training measurement analysis due to motion artefacts

Most prominently, new activation occurred in bad learners after 10 days of training. This becomes visible in posterior parietal association cortex, motor cortex, somatosensory areas in the

region of fore and hind limbs, and insular areas of the isocortex. In the AC, activation shows only in higher order areas (AuD and AuV). Exemplary coronal slices showing activation in these regions are presented for the bad learners in Figure 37.

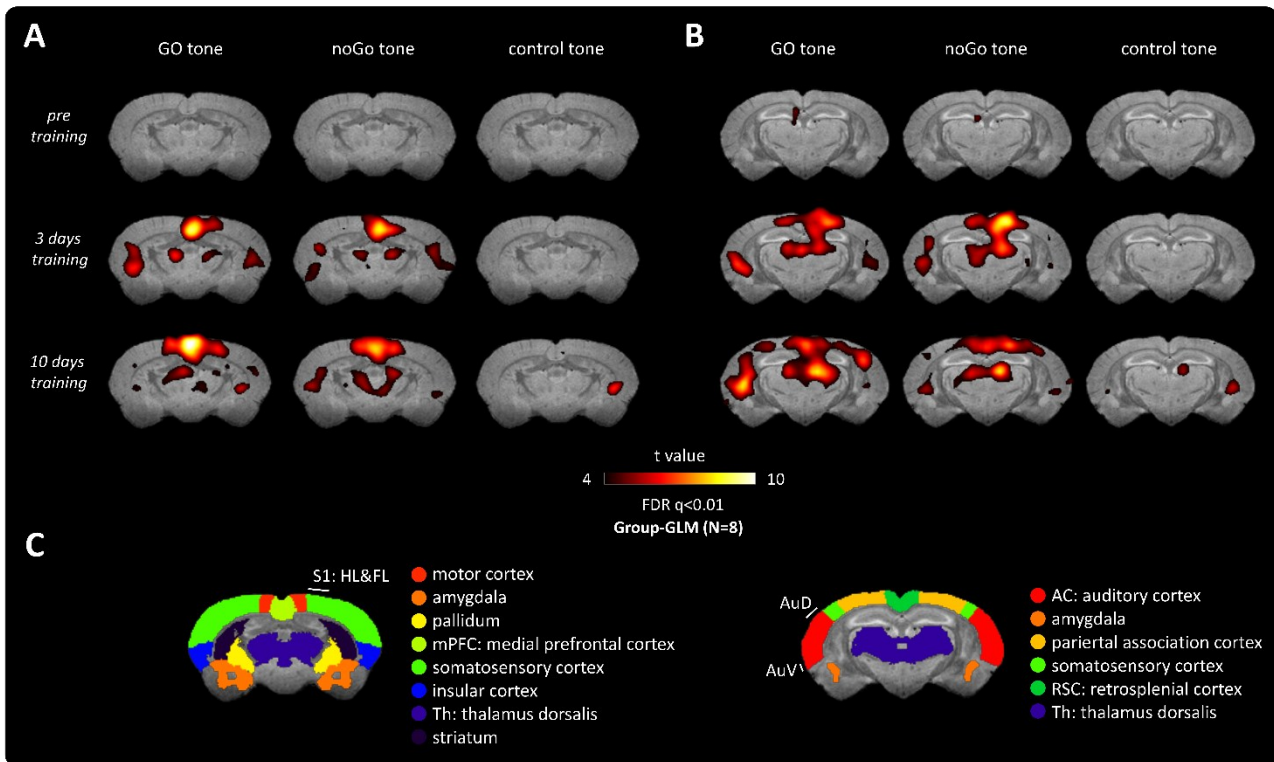


Figure 37: Brain activation at time of reinforcement shock for bad learners trained without aP

In comparison to the stimulation-tone onset analysis, additional activation is visible in: A. motor cortex, primary somatosensory cortex in region of the fore and hind limbs (S1: HL&FL) and insular cortex for GO and noGo tone stimulation after 3 and 10 days of training. And in B. parietal association cortex and in higher order AC, AuD (secondary AC, dorsal area) and AuV (secondary AC, ventral area). (Group-GLMs with N=8, FDR corrected with $q < 0.01$)

i: Exclusion of one bad learner from 3-days-training measurement analysis due to motion artefacts

In comparison to the originally applied design matrices without time shift, the 6 s shifted design matrix showed additional, significant activation increases of BETA values in bad learners in posterior parietal association cortex, motor cortex, and the structures of the hippocampal formation (HF) for noGo tone stimulation. For GO tone, this effect in bad learners was significant only in subiculum. The BETA values to these additional areas are listed in the supplements in Table 6. For instance, in posterior parietal association cortex the BOLD activation for bad learners progressed (non-significantly) from $0.07 \pm 0.03 \%$ to $0.17 \pm 0.03 \%$ for GO tone, and changed significantly from $0.04 \pm 0.03 \%$ to $0.18 \pm 0.03 \%$ for noGo tone stimulation from pre training to 10 days of direction discrimination training.

With linear regressions of individual BETA values and the corresponding CR differences, only few brain areas exhibit significant correlation of performance and brain activation after 10 days of training; in comparison to analysis emphasizing on stimulation tone onsets, new correlation is observable in motor cortex (noGo $0.32 R^2$) and posterior parietal cortex (noGo $0.35 R^2$) for noGo

tone stimulation. (Correlations for all areas of the gerbil brain atlas are visualized in panel A of Figure 46).

3.3.4. Discrimination learning and brain activation patterns with aP

The variation of individual behavioural scores was also high with application of aP in the FM direction discrimination training, as can be seen in Figure 38A. However, here the separation into groups of good and bad learners did not reach as high statistical significance of the CR difference as was the case with the animals trained without aP (for comparison see Figure 32).

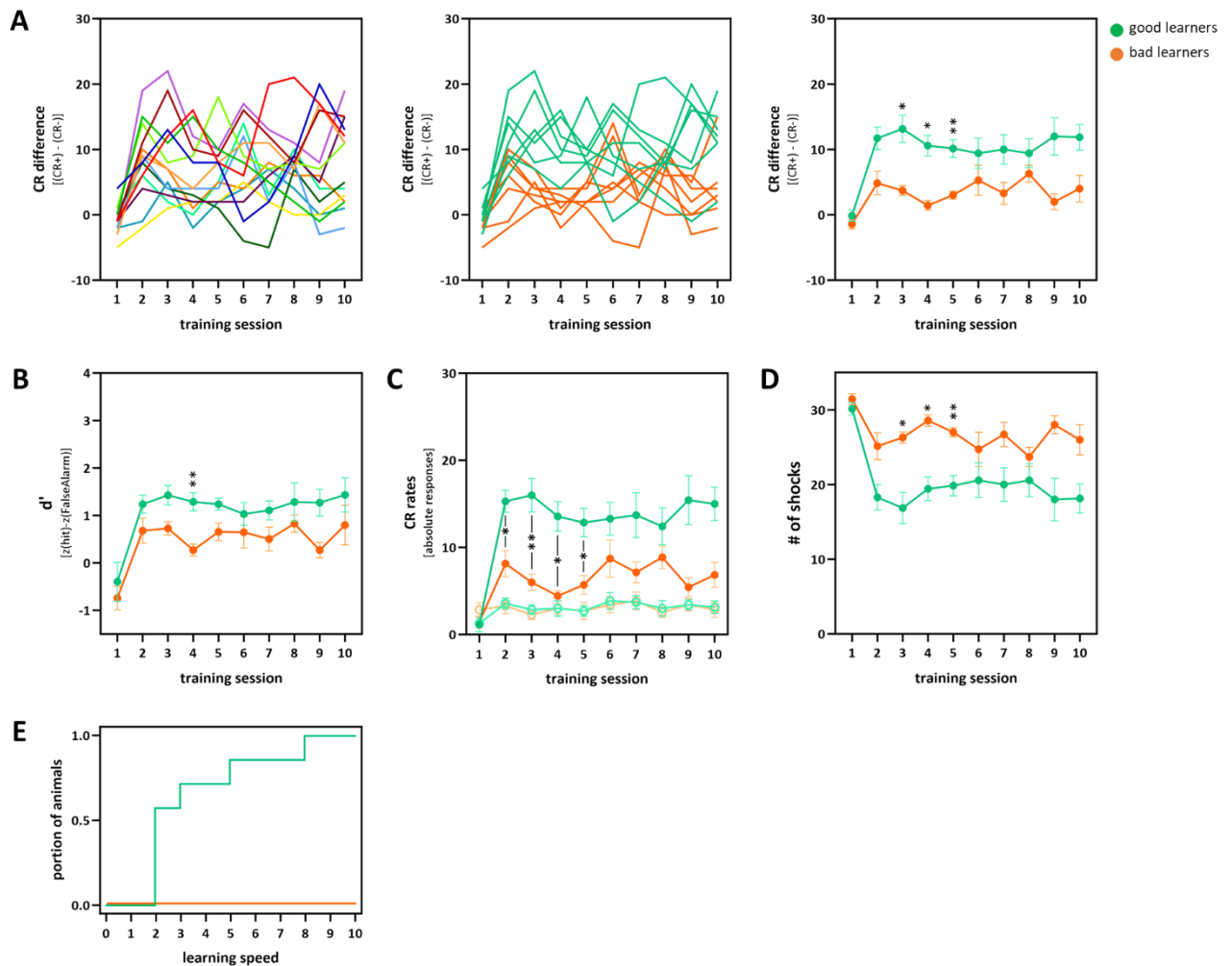


Figure 38: Performance of gerbils in discrimination training with aP

A. left: CR difference of the individual animals, middle: allocation of the individuals to good (green) and bad (orange) learners, right: the resulting mean for each group showing significant differences between good and bad learners in session 3-5. **B.** Corresponding d' values are significantly lower for bad learners in session 4. **C.** CR+ rates (bolder shade, closed circle) are significantly higher for good learners in earlier training sessions, while CR- rates (lighter shades, open circle) of both groups stayed equally low throughout the training. **D.** Number of reinforcement and punishment shocks in training with aP was high throughout the training for both, good and bad learners, with significantly higher numbers for bad learners from day 3 to 5. **E.** None of the bad learners were able to discriminate between GO and noGo tone, according to the learning speed. Statistical comparison between groups performed with Mann-Whitney tests with Holm-Šidák multiple comparison correction. (Adjusted p -values indicated by * $p < 0.05$; ** $p < 0.01$)

Still, the first significant distinction between good and bad learners showed in the third training session as well. The CR difference of the last 7 days of training averaged at 10.5 ± 1.1 for the good learners versus 3.6 ± 0.6 for the bad learners (maximal score of 30, mean and SEM, N=7 each). This corresponds to d' values of 1.24 ± 0.12 for good learners and 0.57 ± 0.11 for bad learners (Figure 38B).

CR+ rate was significantly higher for good learners from the second to the fifth session (Figure 38C, bolder shades, closed circles); CR- was very low and similar in both groups (Figure 38C, lighter shades, open circles). The amount of shocks for reinforcement and punishment received by the bad learners per training session was relatively high, as shown in Figure 38D, surpassing in average 26 per session after the initial training day; due to the low CR- rate only on average 3 of these shocks served as punishment for a “False Alarm”. The good learners in average received 19 shocks per session after the first, roughly 17 of them as reinforcement for “Miss”.

A lack of discrimination ability in bad learners is very clearly reflected in the learning speed of the groups in Figure 38E: here, the good learners gradually learned to differentiate between GO and noGo tones, with the last animal of the group learning after 8 sessions. According to the learning speed definition presented by Schulze et al. (Schulze et al., 2014), not one of the bad learners sufficiently learned to discriminate the tones throughout the 10 days of training.

Figure 39 shows the progression of brain activation patterns for good and bad learners throughout the FM direction discrimination training with aP. The pre training fMRI measurement presents similar brain activation patterns in good and bad learners for the three stimulation tones, with slightly more subcortical activation in the group of bad learners (Figure 39A&B, upper row).

After 3 days of FM direction discrimination training with aP, good learners have more widespread activation in the patterns than bad learners (Figure 39A&B, middle row), especially visible in midbrain, thalamic regions, mPFC and RSC for the GO tone stimulation. This amount to BETA value increases from 0.22 ± 0.04 % to 0.29 ± 0.06 % in MGB, from 0.08 ± 0.03 % to 0.16 ± 0.09 % in IC, from 0.03 ± 0.02 % to 0.20 ± 0.09 % in mPFC, from 0.10 ± 0.03 % to 0.28 ± 0.11 % in RSC, and from 0.10 ± 0.03 % to 0.15 ± 0.04 % in Th (although not significant). After the full 10 days of training, the activation patterns look very similar to the ones acquired prior to the discrimination training, easily observable in Figure 39A, with brain activation returned to the original rates (MGB: 0.14 ± 0.02 %, IC: 0.12 ± 0.04 %, mPFC: 0.04 ± 0.02 %, RSC: 0.05 ± 0.02 %, Th: 0.06 ± 0.03 %). Differential images (Figure 39C) report this circumstance even more plainly: there is no significant additional activation (in red) in the fMRI measurement post 10 days of training in comparison to the pre training measurement for the good learners. For noGo tone stimulation, progression of the activation patterns proceeds similarly throughout the discrimination training, but to a lesser extent. Corresponding BETA values are appended in Table 7.

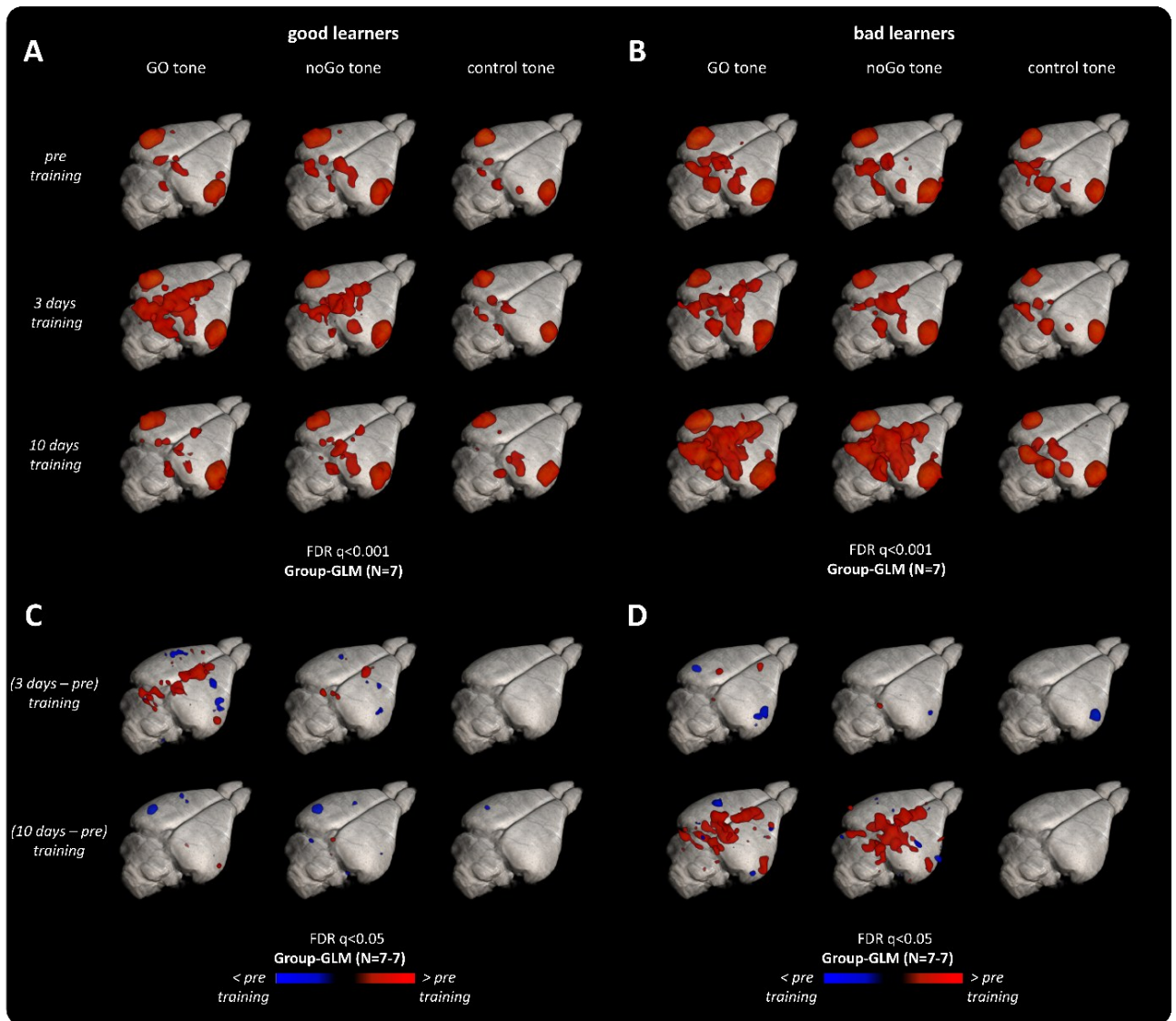


Figure 39: Brain activation of good and bad learners throughout discrimination training with aP

3D-rendered activation patterns with FDR correction of $q = 0.001$ ($N=7$) show slightly more activation increase in mPFC, RSC, thalamus and midbrain after 3 days of direction discrimination training with aP for (A) good learners than for (B) bad learners. After 10 training sessions, good learners' brain activation returned to the levels of pre training, while bad learners' patterns exhibited the biggest areas of activation at that time point. C&D. Differential group-GLMs between the trained state and the pre training measurement show activation differences between the (C) good and (D) bad learners more clearly (group-GLM of $N=7-7$ with FDR correction of $q < 0.05$).

i: Exclusion of one good learner from 10-days-training measurement analysis due to motion artefacts

Against the good learners, the bad learners' brain activation patterns show only little difference after 3 days of FM direction discrimination training with aP (Figure 39B&D). In contrast, after the full 10 days of training, the patterns of bad learners show plenty of additional activation in mPFC, RSC, thalamic areas and midbrain. For instance, the BETA value for GO tone stimulation increased from $0.13 \pm 0.06\%$ to $0.16 \pm 0.03\%$ in RSC after 3 days of training, and significantly further to $0.31 \pm 0.05\%$ after 10 days of training. Similarly but non-significantly, the activation changed from $0.34 \pm 0.06\%$ to $0.33 \pm 0.05\%$ to $0.48 \pm 0.07\%$ in MGB, from $0.21 \pm 0.06\%$ to $0.20 \pm 0.07\%$ to $0.34 \pm 0.02\%$ in IC, from $0.03 \pm 0.03\%$ to $0.14 \pm 0.02\%$ to $0.22 \pm 0.05\%$ in mPFC, and from $0.14 \pm 0.03\%$, to $0.15 \pm 0.02\%$ to $0.24 \pm 0.04\%$ in Th for GO tone stimulation. Similar changes

occurred for bad learners for the noGo tone. BETA values extracted from these regions for all stimulation tones are listed in the supplements in Table 7.

In these visibly active regions, statistical comparison of good and bad learners, presented in Figure 40, again demonstrates a distinct difference between good and bad learners after 10 days of direction discrimination training with aP. For the GO and noGo tone stimulation the significant differences between good and bad learners after 10 days of discrimination training occurred in MGB, IC, mPFC, RSC and Th.

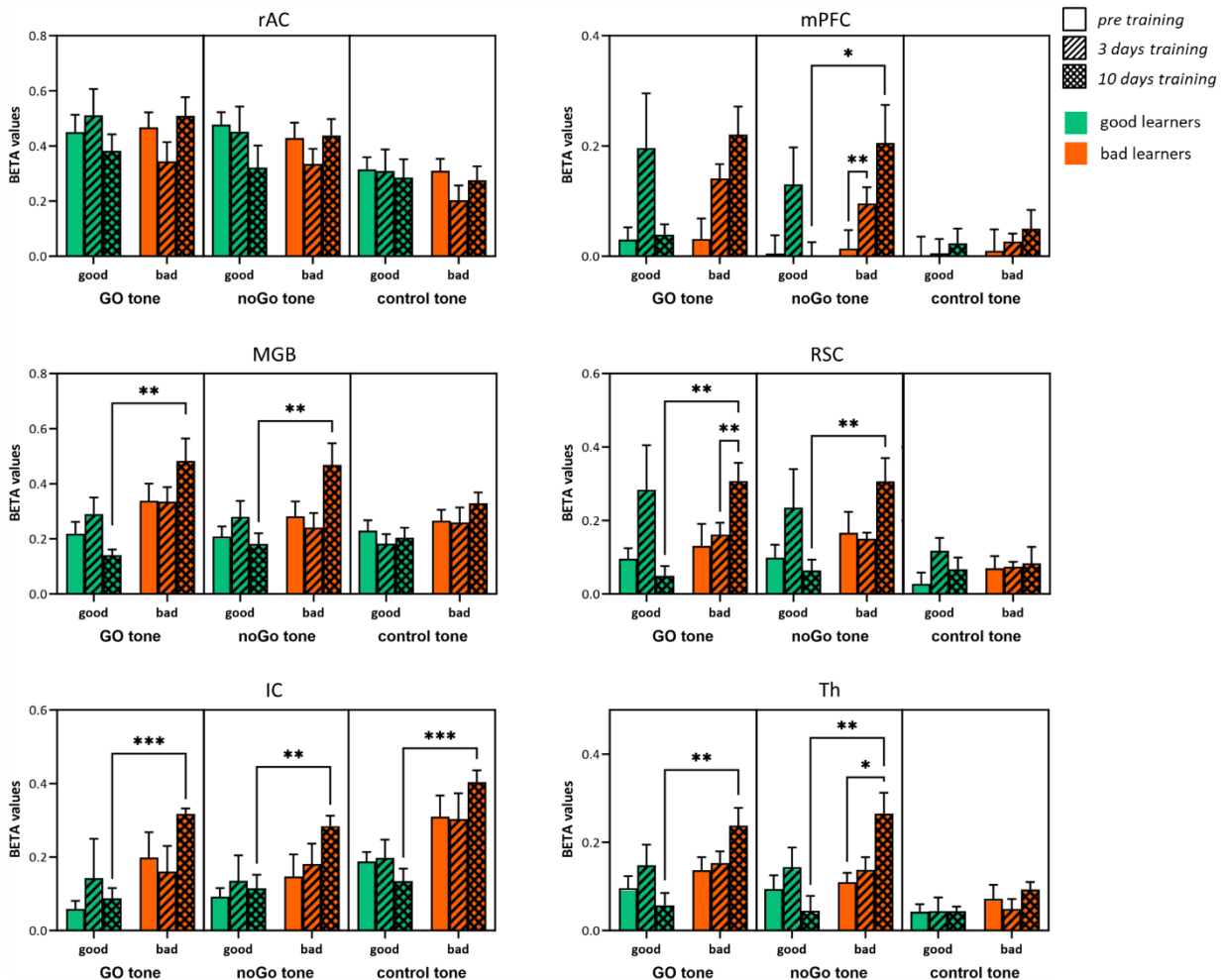


Figure 40: Statistical comparison of good and bad learners in discrimination training with aP
*In the comparison of BETA values, significant differences between good and bad learners are showing most intensely after 10 sessions of training in MGB, IC, mPFC, RSC and Th. (Mixed-model ANOVAs with Bonferroni multiple comparisons correction; N=7 per group, * $p < 0.05$; ** $p < 0.01$; *** $p < 0.001$)*
i: Exclusion of one good learner from 10-days-training measurement analysis due to motion artefacts

Further areas that showed statistical differences throughout the discrimination training are appended in Figure S 5, as well as accompanying BETA values for all stimulation tones and measurement time points (Table 7). Amongst them are the insular cortex, amygdala, hippocampus, subiculum, and septal nuclei with significantly larger BETA values for GO tone stimulation in bad learners after 10 training sessions. The same is the case for both, GO and noGo tone, in epithalamus, subthalamus, metathalamus and tectal area of the midbrain.

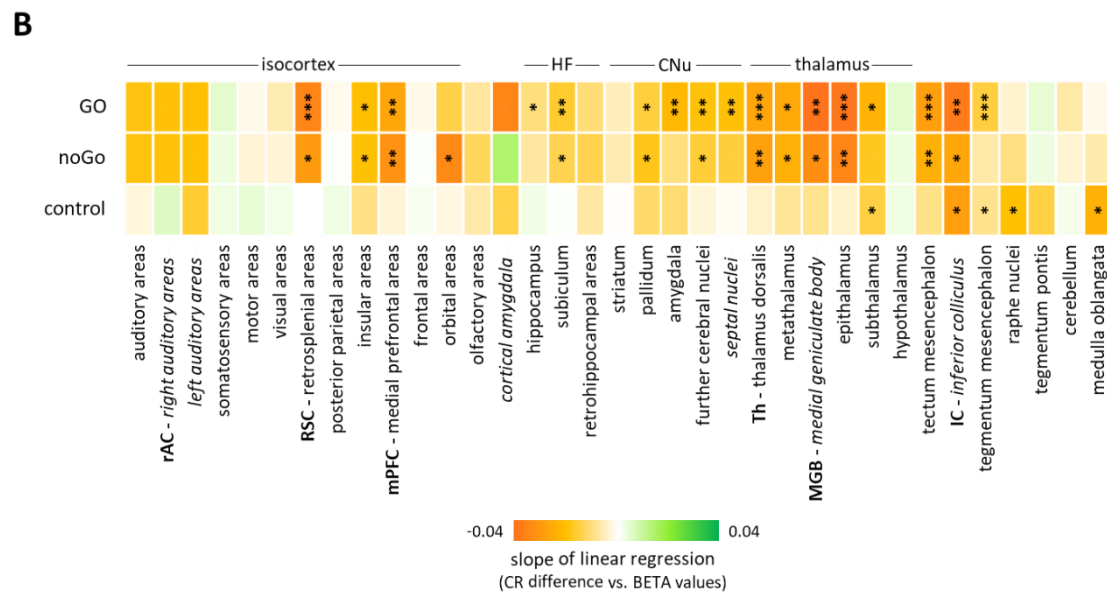
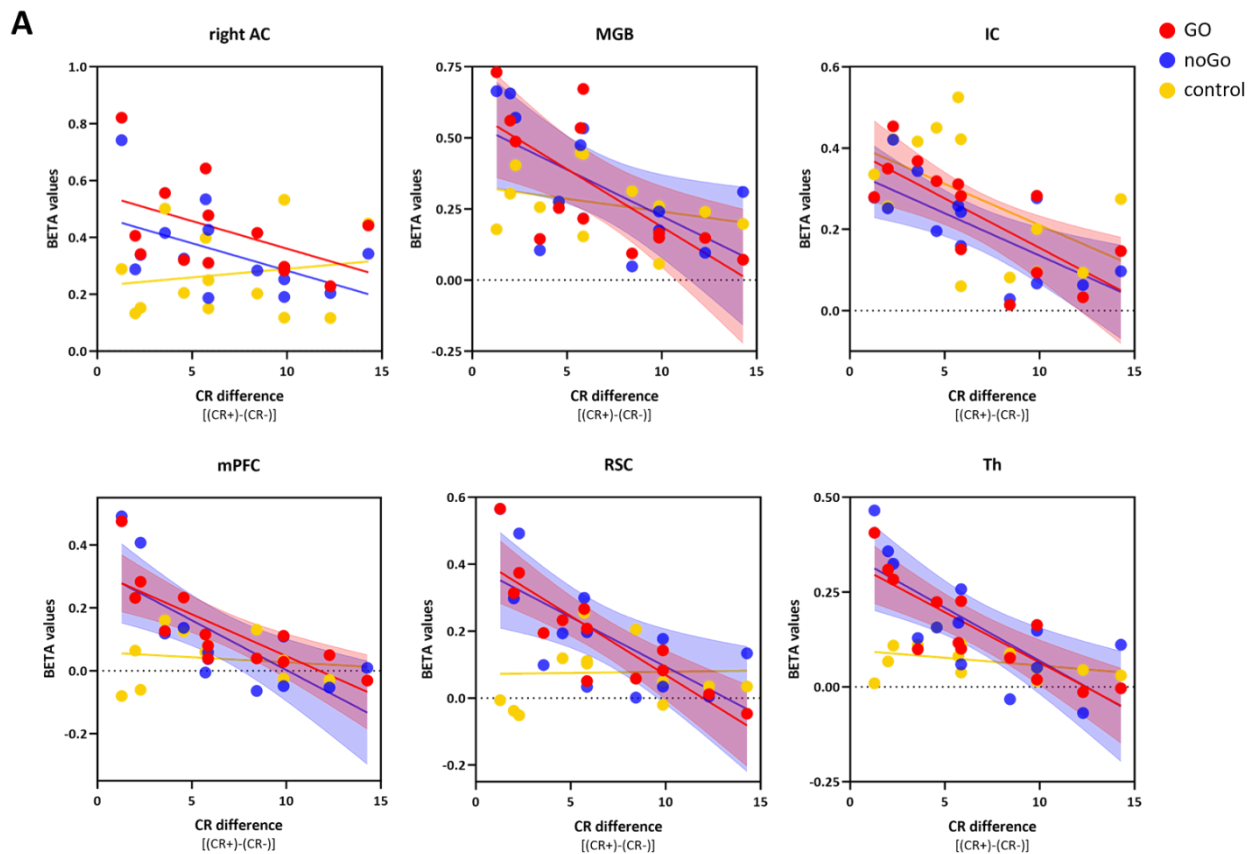


Figure 41: Correlation of learning performance in discrimination training with aP and brain activation

A. BETA values against CR difference in last 7 days of direction discrimination training in the auditory regions rAC, MGB and IC; and in extra-auditory regions mPFC, RSC, and Th for GO (red), noGo (blue) and control tone (yellow). Linear regressions that resulted in statistically significant non-zero slopes are indicated by semi-transparent areas within the 95% confidence intervals of the line ($p < 0.05$). **B.** Summarized outcome of linear regressions of all regions of the gerbil brain atlas, slope indicated by colour range, orange implies higher BETAs in bad learners; green higher BETAs in good learners, level of significance denoted by * for $p < 0.05$, ** for $p < 0.01$ and *** for $p < 0.001$; $N = 13$. Note the high levels of correlation throughout the brain compared to animals trained without aP (Figure 35).

i: Exclusion of one animal due to motion artefacts in final fMRI

With linear regression of the average CR differences (from day 4 to 10) of FM direction discrimination training with application of aP against corresponding BETA values acquired in the final fMRI measurement, a high degree of correlation between behavior and brain activity in many regions is visible (Figure 41).

Significant correlation is occurring for GO and noGo tone stimulation in MGB (GO 0.49 R²; noGo 0.37 R²), IC (GO 0.64 R²; noGo 0.47 R²), mPFC (GO 0.63 R²; noGo 0.55 R²), RSC (GO 0.73 R²; noGo 0.45 R²), and Th (GO 0.70 R²; noGo 0.55 R²). rAC showed no significant correlation.

An overview of significances and slopes from all brain areas is provided in Figure 41B. Similar to the ANOVAs performed on other brain structures, significant correlation also occurred in insular cortex (GO 0.43 R²; noGo 0.43 R²), amygdala (GO 0.54 R²), hippocampus (GO 0.42 R²), the subiculum of the HF (GO 0.56 R²), and in additional thalamic structures.

Changes in activation patterns at time of reinforcement shock onset in gerbils trained with aP

Again, there are additional active areas to be found in the brain activation patterns when the HRF is shifted by 6 s, from stimulation tone onset to the time point the gerbils would have received a reinforcement shock for missing to cross the hurdle upon GO tone presentation. Figure 42 serves as general overview of the active brain areas in group-GLMs applied with a 6 s shift for both, good and bad learners, throughout their discrimination training with aP (for comparison without aP see Figure 36).

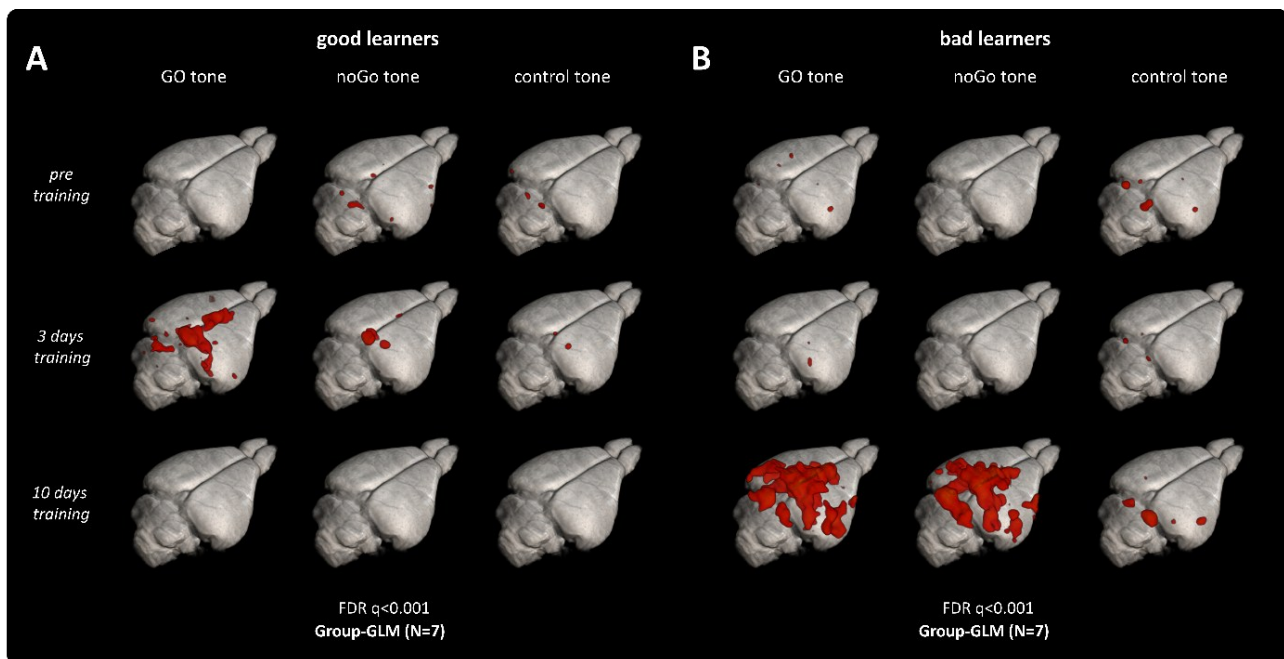


Figure 42: Brain activation at the time of reinforcement shock in discrimination training with aP
A. Good learners show visibly increased activation in RSC and mPFC for GO tone stimulation after the initial 3 days of training. **B.** After 10 days of training bad learners show a widespread area of increased activation for GO, noGo tone stimulation. (Group-GLMs of N=7 with FDR correction of $q < 0.001$)

i: Exclusion of one good learner from 10-days-training measurement analysis due to motion artefacts

Good learners only show significant brain activation in the measurement after 3 days of training, mostly in mPFC and RSC for GO tone stimulation, and to a lesser extent in RSC for noGo tone stimulation. Whereas in bad learners, big areas of brain activation only appear after 10 days of training, for 6 s after GO and noGo tone stimulation onset, but all the more pronounced.

Exemplarily, the precise location of activation in bad learners is presented in coronal slices with a FDR corrected threshold of $q < 0.01$ in Figure 43. Here, after 10 days of direction discrimination training, activation for the GO tone stimulation shows strongly in mPFC, RSC and Th, and moderately in additional areas: in somatosensory cortex in region of the fore and hind limbs, motor cortex, parietal association cortex and higher order auditory areas, the AuD and AuV. Comparatively, 6 s after noGo tone stimulation onset the activation in these regions is not as high, apart from mPFC.

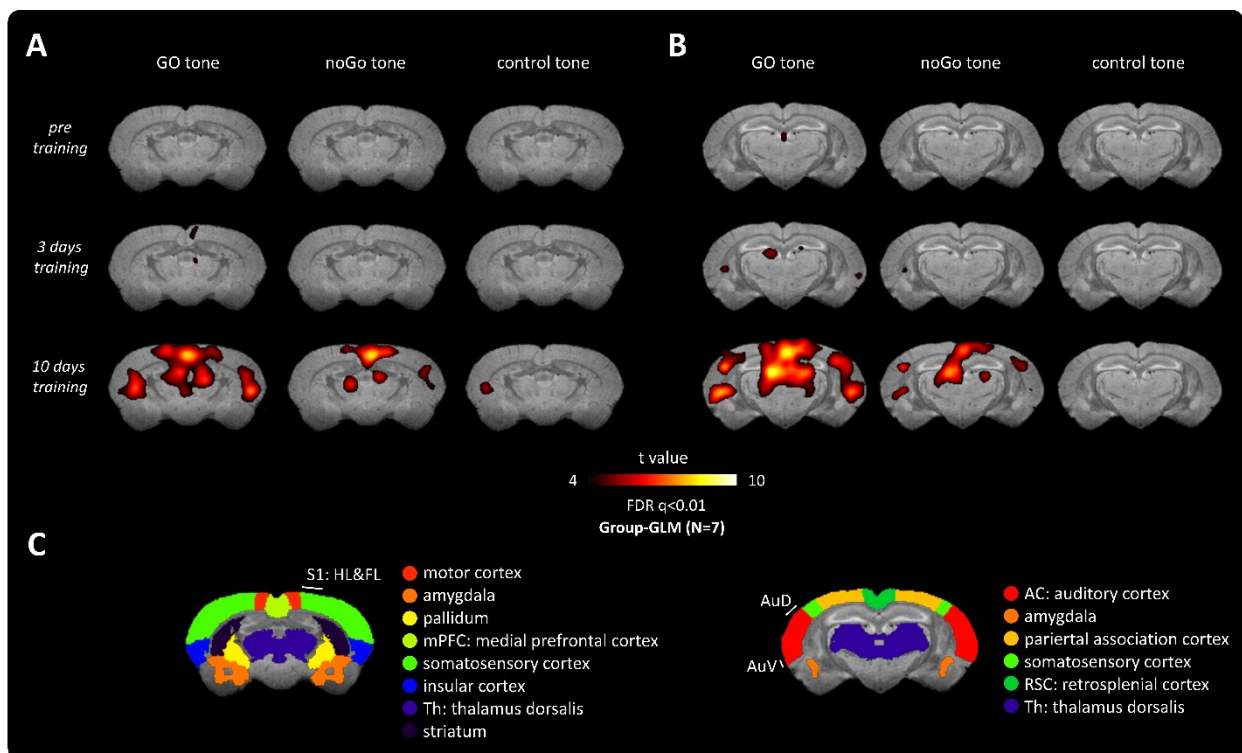


Figure 43: Brain activation at time of reinforcement for bad learners in discrimination training without aP

A. Additional activation in motor cortex, primary somatosensory cortex in region of the fore and hind limbs (S1: HL&FL) and insular cortex for GO and noGo tone stimulation only after 10 days of training. **B.** Additional activation in parietal association cortex; activation in auditory cortex is focused on higher order areas AuD and AuV. (Group-GLMs with $N=8$, FDR correction with $q < 0.01$)

Similar to the striking differences in activation patterns of good and bad learners at time of reinforcement (Figure 42), ANOVAs report significant differences between good and bad learners on BETA value level as well (supplements Figure S 6), corresponding BETA values are appended in Table 8. For example, in posterior parietal areas this activation amounts to 0.18 ± 0.03 % for GO and 0.16 ± 0.04 % for noGo tone in bad learners after 10 days of training, versus 0.04 ± 0.03 % for GO tone and 0.07 ± 0.03 % for noGo tone in good learners. In somatosensory cortex to 0.09 ± 0.02 % for GO and noGo tone in bad learners, versus -0.01 ± 0.02 % for GO tone and 0.01 ± 0.02 % for noGo

tone in good learners. Compared to the analysis at stimulation tone onset, further significant differences between BETA values of good and bad learners were observable in auditory cortex, visual cortex, motor cortex, and striatum; generally with higher statistical significance 6 s after onset of GO tone than after noGo tone onset (supplemental Figure S 6).

Linear regression of the shifted BETA values from final fMRI measurement against the learning score (CR difference average of last 7 days of FM direction discrimination training with aP) evidences correlation of learning performance to brain activity in many regions, especially 6 s after GO tone onset. An overview of significances and slopes of the regressions is featured in panel B of Figure 46. In comparison to the same kind of analysis performed on the fMRI data without time shift, correlations are especially noticeable in isocortex, the cerebral nuclei (CNU, GO tone only), the hippocampal formation (HF), and thalamus.

3.3.5. Comparison of gerbils trained with and without aP

Comparing the learning of these animals trained with aP with the animals trained without aP in the otherwise identical task, learning scores in the form of CR differences do not result in significant dissimilarity (Figure 44A); neither do d' values (data not shown).

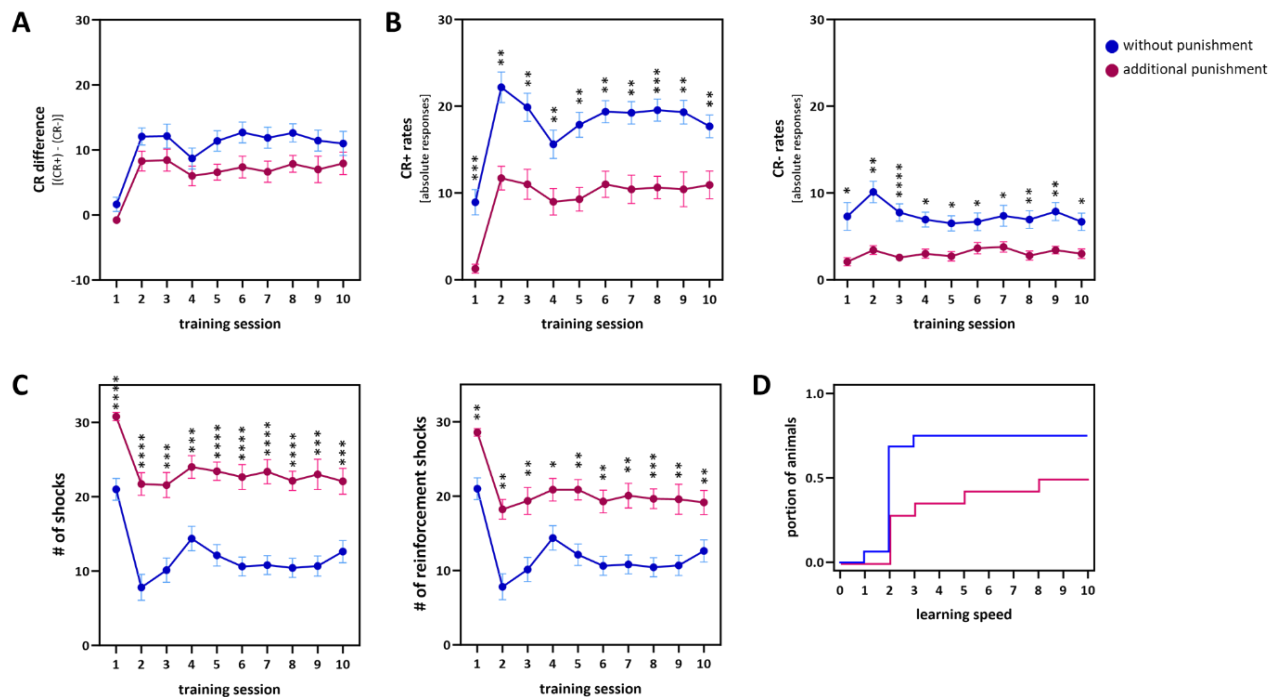


Figure 44: Effect of aP on outcome of direction discrimination training

Statistical comparison of the entire groups of animals trained with aP (magenta) and (blue) animals trained without. (A) CR difference, (B) CR+ and CR- rates (left to right), (C) # of shocks received throughout training, and (D) learning speed of the animals. Statistical comparison between groups performed with Mann-Whitney tests with Holm-Šidák multiple comparison correction. (Adjusted p -values indicated by * $p < 0.05$; ** $p < 0.01$; *** $p < 0.001$; **** $p < 0.0001$; animals trained without aP $N = 16$, with aP $N = 14$)

When applying the same separation into groups of good and bad learners, good learners that received aP reach significantly lower scores in session 6 with an adjusted p value of 0.015 (good learners with aP 9.4 ± 2.3 (N=7) vs. good learners without aP 18.5 ± 0.8 (N=8)). Bad learners did not vary significantly in their CR difference or d' in any session.

Comparison of the CR rates elicits far more differences between behaviour of gerbils trained with and without aP (Figure 44B): both, CR+ and CR-, are significantly higher for animals trained without aP in every single session. This means, while the animals trained without aP were much more likely to cross the hurdle correctly upon GO tone stimulation, they were also much more likely to cross the hurdle when they were not supposed to. These two circumstances resulted in significantly more shocks applied to the aP animals in all training sessions, even though only few of them were applied as aP for “False Alarm” (Figure 44C).

Comparing the fMRI results of gerbils trained without aP to those of the animals trained with aP, the good learners share a similar brain activation pattern development throughout the discrimination training (Figure 33 vs. Figure 39). Starting with an initial increase in activation in midbrain, thalamic regions, mPFC and RSC after 3 days of training, followed by the same return to original brain activation in the final fMRI after 10 days of training.

Meanwhile, the biggest distinction between brain patterns of animals trained with and without aP emerged for bad learners in the measurement after 3 days training: bad learners trained without aP show an excessive surplus of brain activation compared to bad learners trained with aP that showed comparatively little activation increase at that time. These differences are easily visible in a direct side by side comparison of the activation patterns, presented in Figure 45, and especially prominent for the noGo tone.

After the full 10 days of training all bad learners distinctly showed their most widespread brain activation. For both, GO tone and noGo tone stimulation, bad learners trained with and without aP reach very similar BETA values for the main areas of activation changes. For control tone stimulation, bad learners that experienced aP show decidedly lower BETA values in mPFC, RSC and Th, but similar activation increase in the auditory system than animals trained without aP.

Besides these differences that are visible in the brain activation patterns, for both, ANOVAs of BETA values throughout the discrimination training as well as the linear regressions, animals trained with aP show more activation increase (Figure S 3 vs. Figure S 5) and correlation to learning (Figure 35 vs. Figure 41) in insular cortex and areas of the limbic system, such as in amygdala, hippocampus and subiculum.

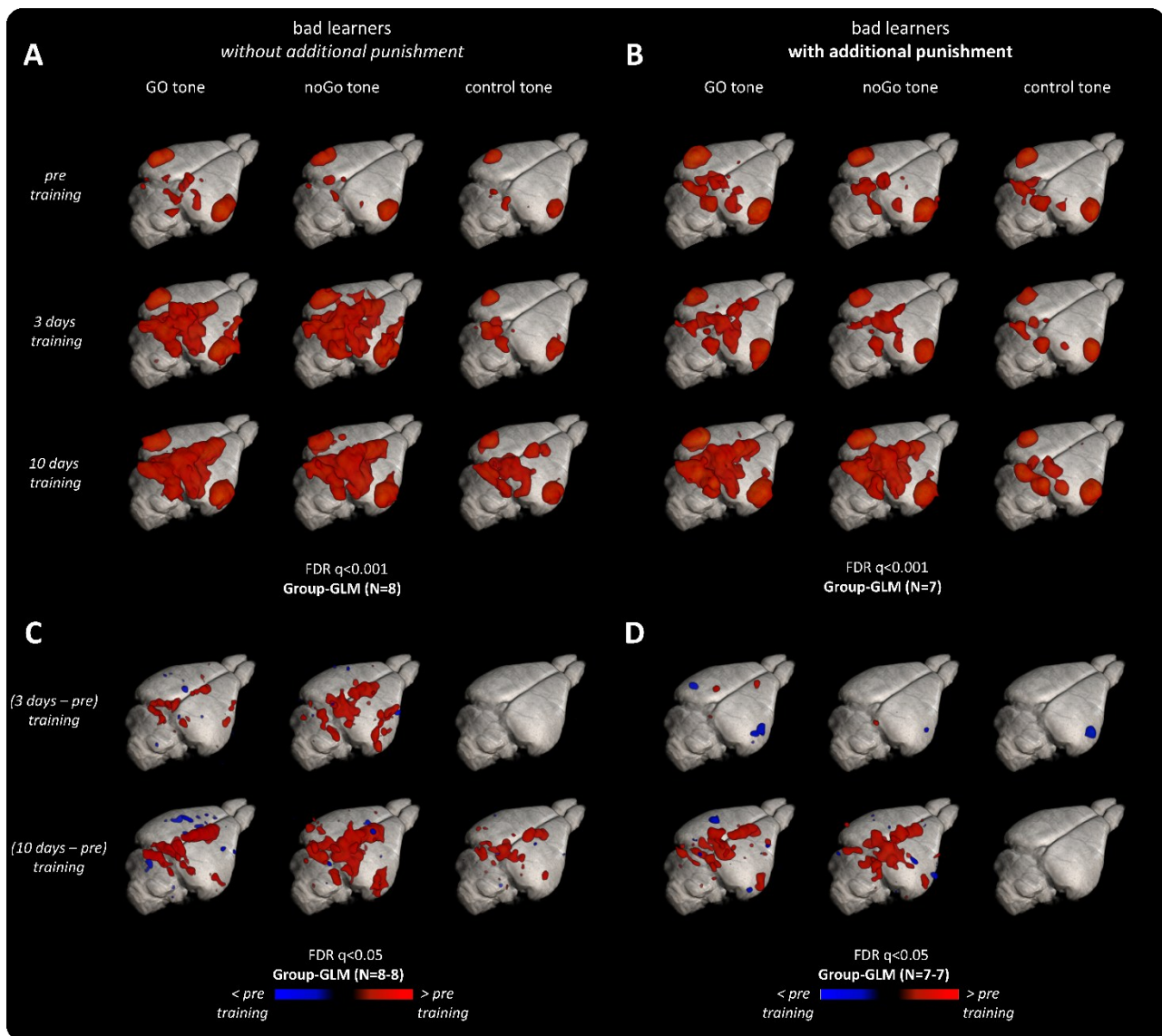


Figure 45: Effect of aP in discrimination training on brain activation patterns in bad learners

Auditory activation patterns of bad learners in direction discrimination training without (A) and with aP (B) show earlier increase of activation for animals without reinforcement. C&D. Differential activation patterns (post – pre training) highlight the earlier activation increase in training without reinforcement, but also more activation for the noGo and control tone.

i: Exclusion of one bad learner without aP from 3-days-training measurement analysis due to motion artefacts

With analysis of the fMRI data focused on the onset of the aversive reinforcement applied to the animals during training, even bigger differences between animals trained with and without aP attract attention for in the final fMRI measurement. This shows especially in the linear regression analysis with more correlation between learning scores and brain activation in isocortex, HF, basal ganglia, and thalamus in the training with aP, an overview is presented in Figure 46. Beyond that, the bad learners trained with aP show higher brain activation and correlation to behaviour 6 s after GO tone than 6 s after noGo tone stimulus onset, while bad learners trained without aP do not demonstrate this tendency.

3.4. Discussion

3.4.1. Auditory-evoked brain activation patterns

Auditory brain activation patterns recorded prior to the direction discrimination training feature bilateral activation throughout the central auditory pathway for all three stimulation tones.

The activation in AC was significantly stronger for GO and noGo tone than control tone stimulation. This indicates either differences in masking effects of the fMRI background noise for the different stimulation tones, or inherently differential neuronal processing of the FM tones in range of 1 – 2 kHz and 3 – 6 kHz in Mongolian gerbils, independent of background noise.

The frequency profile of the GRE-EPI sequence (chapter 1, Figure 11) shows higher SPL in the 3-6 kHz range than the 1-2 kHz range, which could potentially result in stronger masking effects for that frequency. However, the control tone led to the highest activation increase in IC, the lowest auditory structure measurable with the optimized auditory fMRI setup. In comparison, a distinctly higher BOLD signal appeared in IC after headphone position was improved in the CBF SPECT study. Therefore, the explanation of a stronger masking effect for the control tone is unconvincing.

The more likely explanation lies in the area size of FM presentation for the different frequency ranges in the AC of Mongolian gerbils. Studies implementing FM tones for tonotopy measurements in the region of the AC with 2-deoxyglucose (Scheich et al., 1993) and epidural electrocortico-graphy (Ohl et al., 2000) report larger areas for the representation of FM tones around 1 and 2 kHz than those of higher frequency tones in gerbils. Hence, the significantly higher BOLD contrast for GO and noGo tones can be explained by a higher number of neurons being activated in these larger frequency-specific areas of AC.

3.4.2. Brain areas involved in auditory discrimination learning

FM direction discrimination training with and without aP caused big changes in the brain wide activation patterns, especially pronounced for GO and noGo tone that were presented in the behavioural training. Most prominently visible in the fMRI activation patterns, the training induced activation increases in the auditory structures MGB and IC, and in the extra-auditory structures Th, mPFC and RSC. In addition, significant BETA value increases were discovered in olfactory and orbital cortical areas, subiculum and retrohippocampal areas of the hippocampal formation, septal nuclei, epithalamus, and tegmental area of the midbrain, and in the tectal midbrain in region of superior colliculus.

Segregated analysis of animals dependent on their performance additionally showed significant activation differences in most of these areas, as well as in subthalamus and rAC.

With the implementation of the task with aP for CR-, further activation changes showed in the insular cortex, hippocampus and amygdala.

Analysis of the data with a shift to onset time of the reinforcement highlighted additional activation in motor cortex, posterior parietal cortex, and higher order AC areas in animals trained without aP. Same analysis applied to animals trained with aP showed performance-dependent activation increase throughout the brain with high correlation of activation to the performance of the individual animals in numerous structures of isocortex, CNu, HF and thalamus, as well as tegmental and tectal area of the midbrain.

Activation in the auditory system

For many years, plasticity and neuronal activation have been recognized and studied during and after learning processes of rodents. In the context of auditory learning, within the auditory system these changes were observed in AC, MGB and IC.

With auditory fMRI in the Mongolian gerbil, we were able to observe such changes as well, with significant BOLD activation increase in IC and MGB after 3 days of FM direction discrimination training, for both GO and noGo tone stimulation.

AC: In AC, recorded activation changes differed dependent on the hemisphere. Counterintuitively to the lateralization side for discrimination of FM direction ([Wetzel et al., 2008](#); [Wetzel, Ohl, et al., 1998](#)), rAC did not show significant activation changes for animals trained without aP. However, with separation of the animals by their performance, good learners showed slight rAC activation decrease, while bad learners showed an increase. In contrast, in gerbils trained with aP, the observed activation changes in rAC were reversed for good and bad learners in comparison to gerbils trained without aP. In numerous preclinical studies on rodents and human subjects, plasticity changes of AC were induced by auditory learning ([Bakin & Weinberger, 1990](#); [Brechmann & Scheich, 2005](#); [Edeline et al., 1993](#); [Grosso et al., 2015](#); [Ohl & Scheich, 1996](#); [Pantev & Herholz, 2011](#); [Rutkowski & Weinberger, 2005](#); [Scheich et al., 2007](#); [Weinberger et al., 1993](#)).

Our observation of rather low and controversial BOLD activation changes in AC in comparison to changes in other structures might be a result of the changed signal processing caused by the coinciding GRE-EPI background noise, as discussed in chapter 2.4.2 on page 55. Nevertheless, according to histological studies in the Mongolian gerbil, all structures we observed significant activation changes in are sharing a direct connection to A1 ([Budinger et al., 2006](#); [Budinger et al., 2000a, 2000b](#); [Budinger et al., 2008](#)), and may therefore indirectly report on plasticity changes in this region.

More importantly, analysis of the data shifted to the expected onset time of the reinforcement uncovered delayed significant activation for both ACs in the higher order auditory areas for both training paradigms.

Activation in the limbic system

The limbic system comprises phylogenetically old structures of the brain that serve important functions dealing with survival and adaptation (Bruce & Braford, 2009; Walker, 2009), such as emotions, motivation, behaviour and memory. There is no mutual agreement to which precise structures belong to this system, but it is composed of several interconnected regions that can include the cingulate cortex, the HF, amygdala, septal nuclei, as well as hypothalamus and limbic thalamus (Kalivas & Volkow, 2005; Papez, 1937; Rajmohan & Mohandas, 2007; Roxo et al., 2011; Taber et al., 2004).

Cingulate cortex: mPFC, in which we observed a strongly significant BOLD increase for GO and noGo tones, is often referred to as its substructures cingulate, prelimbic and infralimbic areas. Its involvement has been reported in fear and aversive avoidance conditioning (Concina et al., 2018; Corcoran & Quirk, 2007; Gongwer et al., 2023; Stark et al., 2004; Vieira et al., 2015), as well as in reward-promoted, appetitive conditioning of rodents (Capuzzo & Floresco, 2020; Petykó et al., 2015; Riaz et al., 2019). Many studies report the mPFC as facilitator for attention (Birrell & Brown, 2000; Broersen, 2000; Dias et al., 1996; Ragozzino, 2007; Ragozzino et al., 1999) and decision-making (Clark et al., 2008; Sul et al., 2010). In the particular context of active avoidance, mPFC is a key region that promotes the transition from freezing behaviour to avoidance behaviour (LeDoux et al., 2017; Moscarello & LeDoux, 2013).

HF: Significant BOLD signal increase was observed in hippocampus and especially the subiculum and retrohippocampal area of the HF after discrimination training. The HF is widely accepted to play an important role in encoding, consolidation and retrieval of learning and memory. In discrimination learning in rodents, however, its involvement is a highly controversial subject. Some researchers emphasise its necessity for this type of learning (Oleksiak et al., 2021; Tang et al., 2003). Others interpret higher importance of other structures such as the RSC (Smith et al., 2012) and the dorsal striatum for its memory (Broadbent et al., 2007), arguing that the nature of the task is more strongly based on habit formation than declarative or episodic learning. However, with our observation of performance-dependent HF activation differences throughout the FM direction discrimination training, we can confirm that the HF is involved in this kind of learning process as well.

Septal nuclei also showed significant BOLD signal increase after our FM direction discrimination training; they have been reported to contribute to fear conditioning before (Holschneider et al., 2006; Zhang et al., 2018). The septal nuclei provide an interface between the phylogenetically old and the newer brain structures and are well-positioned to modulate many behavioural functions such as emotion, movement, motivation, attention, cognition and memory (Numan, 2012).

Amygdala: The amygdala is the brain structure most commonly associated with fearful and anxious emotions (Janak & Tye, 2015). As described before in the introduction to different types of conditioning, animals exposed to aversive avoidance conditioning initially go through a fear

conditioning response to the CS (Choi et al., 2010; Sidman, 1953). Their avoidance reaction is the performance of a specific motor response to a conditioned threat (Moscarello & LeDoux, 2013). Since our paradigm of FM direction discrimination is aversively reinforced with a mild electrical shock, activation increase in fear related areas would hardly be unexpected. Discrimination training implemented with aP did induce measurable amygdala activation upon GO tone presentation in our fMRI experiments. In comparison, stimulation with the GO tone did not induce significant activation in amygdala for the animals trained without aP. While aversive and avoidance conditioning in rodents is highly associated with amygdala-involvement (Maren & Quirk, 2004; Sangha et al., 2020; Zhang et al., 2021), comparative studies on human subjects only rarely report on activation in amygdala, which can be explained by attenuation throughout the repeated stimulus presentations during non-invasive imaging like fMRI (Yin et al., 2018). In contrast, after visual fear conditioning studies on rodents, fMRI revealed high activation in the amygdala (Brydges et al., 2013; Harris et al., 2015). An *ex vivo* autoradiography study also presented CBF increase in parts of amygdala of rats after auditory promoted fear conditioning (Holschneider et al., 2006). Our lack of observed amygdala activation in the training paradigm without aP could be explained by signal bleed-out in ventral brain regions caused by our measurement setup and the *bullae* of the gerbils, thoroughly discussed in chapter 1.4.2. Animals trained with aP received significantly more reinforcement shocks throughout the discrimination training. Therefore, the less aversive nature of the training without aP might have caused signal changes that were below fMRI resolution in this ventral region. The same applies for the general lack of observed hypothalamus activation changes.

Th: Standard fMRI analysis for the auditory stimulation onset showed high activation increases in the Th. The defined atlas region Th comprises of a collection of numerous thalamic nuclei, including anterior nuclei, ventral nuclei, dorsal nuclei, midline and intralaminar nuclei (see Table 4 in the supplements), which per different definitions are nuclei belonging to the “limbic thalamus” (Taber et al., 2004; Vogt et al., 1992). Through lesioning studies, limbic thalamus function has been implicated in attention modulation, as well as in training-induced activity propagation to cingulate cortex (Gabriel et al., 1989; Smith et al., 2002). Our observed prominent training-induced activation increase in this area, affirm the importance of Th for aversive avoidance learning process.

Activation in the basal ganglia

The basal ganglia is comprised of striatum, globus pallidus, subthalamic nucleus and substantia nigra, and refers to a widespread group of subcortical nuclei that are primarily responsible for motor control, but also have other roles such as motor learning, executive functions and behaviours, and emotions (Foster et al., 2021; Lanciego et al., 2012). While activity in the basal ganglia does not induce movement, it facilitates movement control through inhibitory and

excitatory circuit projections to the motor cortex through the thalamus. Therefore it plays a significant role in procedural learning (Packard, 2009).

Striatum: Generally, all types of sensory stimuli evoke striatum responses: tactile, olfactory, visual and auditory (Cromwell et al., 2007; Glynn & Ahmad, 2002; LeDoux et al., 1991; Pidoux et al., 2011; Schulz et al., 2011; Schulz et al., 2009; Syed et al., 2011; Wieland et al., 2015; Woldeit et al., 2012). Through appetitive auditory learning the cortico-striatal plasticity during acquisition of auditory discrimination learning task increases in rats (Xiong et al., 2015; Znamenskiy & Zador, 2013). This also heightened coherence of AC and striatum activity was also observed during acquisition of aversive FM direction discrimination learning in Mongolian gerbils (Schulz et al., 2015), where it is involved in the dopaminergic signalling that promotes the internal reinforcement of the active avoidance task (Dombrowski et al., 2013; Ilango et al., 2014; Ilango et al., 2012).

The other structures of the basal ganglia that are known to be involved in motor control, were not individually resolved with the atlas regions implemented for the auditory fMRI analysis in our study, since many of these regions are below reasonable spatial resolution with the used GRE-EPI sequence and applied smoothing. However, in the linear regression analysis the larger regions encompassing these structures all showed significant performance-dependent activation differences in the discrimination training with aP at the time of the expected reinforcement shock: Pallidum containing globus pallidus, subthalamus the subthalamic nucleus, and tegmentum mesencephalon consisting largely of the substantia nigra.

Motor cortex: Within the motor cortex, the structure ultimately responsible for movement induction (Yip & Lui, 2023), significantly higher activation in bad learners in comparison to good learners after 10 days of discrimination training with and without aP was observed at the time of the expected reinforcement. This indicates that bad learners of our study learned to prepare to jump just after 6s of tone presentation, directly after onset of the reinforcement shock.

Activation in other brain regions

RSC: We observed prominent and significant activation increases induced by the direction discrimination training in RSC. In rodent studies, the RSC is best known in the context of spatial learning and spatial navigation tasks (Miller et al., 2014; Vann et al., 2009; Vedder et al., 2017). Beyond that, RSC has also shown to be involved in object recognition (de Landeta et al., 2020; Haijima & Ichtani, 2012), in integration of multiple sensory stimuli (Castiello et al., 2021; Keene & Bucci, 2008; Robinson et al., 2011), remote fear memory retrieval (Todd et al., 2016), and in learning of some discrimination tasks (Smith et al., 2012). In these discrimination tasks, RSC plays a role in encoding for cues that predict reinforcement and for error correction (Alexander et al., 2023; Gabriel, 1993; Smith et al., 2012). The cingulate area of mPFC merges into the RSC (Radtke-Schuller et al., 2016). Both structures are highly connected to each other (Monko & Heilbronner, 2021) and connected to the anterior thalamus via the cingulum bundle fibres (Bubb et al., 2020).

Therefore, it is not surprising that both structures show coincidental activation in our auditory-stimulated fMRI after discrimination learning.

Epithalamus: In epithalamus, we observed significant activation increase in epithalamus for bad learners after 10 days of training in both training paradigms for GO and noGo tone. This thalamic region contains the habenula. The habenula has shown to be essential to negatively motivated behaviour (Hu et al., 2020). In fear conditioning of rats it has been proposed to select relevant information that predicts danger (Durieux et al., 2020) and to be required for the formation of independent cued fear memories (Sachella et al., 2022). It is strongly connected to both the limbic and the basal ganglia system (Hu et al., 2020).

Mesencephalic tectum: Significant activation changes through the discrimination training and correlation of individual learning performance to the activation in tectal area of the midbrain, in region of the superior colliculus, after 10 days of discrimination training with aP was recorded with auditory fMRI. Superior colliculus is connected to several structures of the auditory pathway including IC, MGB, and AC, and is thought to moderate several acoustic-motor behaviours (Ding et al., 2019; Huffman & Henson, 1990; Lesicko et al., 2020; Syka & Straschill, 1970).

Insular cortex: Insular cortex showed activation increase after FM direction discrimination training with aP. In rodents, the insular cortex has shown to modulate anxiety (Gehrlach et al., 2019; Méndez-Ruette et al., 2019) and shown activation in studies on aversive avoidance (Gabriel, 1993; Guzman-Ramos & Bermudez-Rattoni, 2012). In humans, the structure has been reported to be involved in decision making under risk (Clark et al., 2008; McGregor & LaLumiere, 2023), which has also been shown through lesioning of this structure in rats (Ishii et al., 2012).

Beyond those regions, other cortical structures also showed some extent of involvement in learning in the FM direction discrimination tasks, such as the somatosensory cortex in region of front and hind legs, representing the body regions of the gerbils that had exposure to the reinforcement and punishment shocks during the FM direction discrimination task. Or the posterior parietal association cortex, which is known to be involved in directing attention (Shomstein, 2012). While plasticity changes in these regions have been implicated in aversive avoidance and discrimination learning as well, activation increase in these structures was not high and their possible roles in the discrimination learning will not be discussed in more detail.

Generally, detection of FM direction discrimination learning induced activation changes in all of the structures mentioned above confirms that auditory fMRI is a valuable method for monitoring learning-induced activity changes. Our results indicate brain-wide information processing with focal activation hotspots in multiple structures that are engaged in the learning course of the FM direction discrimination task of gerbils. Many individual structures and networks, which have previously been observed in the context of fear memory and avoidance conditioning, showed involvement in this learning process alongside the auditory structures necessary for perception and cognition of the auditory cues.

3.4.3. Performance dependent activation changes

Both, implementation of FM direction discrimination training with and without aP, led to a wide variation in behavioural scores. The animals were separated into groups of “good” and “bad” learners according to their average CR difference score, which produced multiple significant behavioural dissimilarities of these two groups besides the CR difference itself. In both, training with and without aP, the performance difference showed the greatest contrast in the final fMRI after ten days of discrimination training, with good learners presenting significantly less activation in many brain structures than bad learners for all three stimulation tones.

Aversive avoidance conditioning is interpreted to undergo at least 3 stages of learning. (i) the initial fear conditioning where the animals learn to associate the UCS with the CS, (ii) learning of the escape strategy, where the animal notices the compartment change stops the reinforcement shock, and (iii) the active avoidance strategy, where the animal learns the UCS can be prevented by early change of compartment (Kozma et al., 2021; Maia, 2010).

Internal emotional responses to avoidance conditioning can be described by theoretic mathematical models, the two-factor theory (Mowrer, 1951) and the similar “actor-critic”-model (Maia, 2010) as follows. The initial stage of learning is marked by a pronounced fear response of the animals (Coover & Ursin, 1973; Freeman et al., 1996; Kamin et al., 1963; Solomon et al., 1953; Solomon & Wynne, 1953). Throughout the learning acquisition phase, with the appearance of avoidance responses, this fear is released after successful avoidance of the reinforcement shock and offset of the CS presentation, and dopaminergic signalling occurs that produces a positive internal reinforcement (Dombrowski et al., 2013; Ilango et al., 2014; Ilango et al., 2012). This leads to stable avoidance responses even without further UCS presentation (Levis, 1966; Levis & Boyd, 1979; Litvin et al., 2009; Solomon et al., 1953; Solomon & Wynne, 1953; Williams & Levis, 1991). With continued avoidance, the emotional responses fade away (two-factor theory) or decrease to a low state only slightly above pre-condition states (actor-critic model), which signifies the change from fear-elicited avoidance behaviour to formation of a habit (Cain, 2019; LeDoux et al., 2017). For instance, in auditory avoidance conditioning performed in rabbits, plasticity changes were observed with initial high neuronal firing responses in limbic thalamus, cingulate areas of mPFC and hippocampus, that at discrimination ability level were decreasing with training continuation or “overtraining” (Freeman et al., 1996). Similarly, in an FM tone avoidance task performed on Mongolian gerbils, increase of extracellular dopamine in prefrontal cortex occurred solely during acquisition of the avoidance strategy (Stark et al., 1999; Stark et al., 2004). The development of the fMRI acquired activation changes in good learners corresponds very well to these theories throughout the FM direction discrimination training with and without application of aP, which shows that they learned to discriminate the tones and have consolidated the task after the 10 days of training.

The bad learners, in contrast, showed further increase of activation in the limbic system with continued training, without improvement or retrogression of their discrimination abilities.

Diverse performance in active avoidance in rodents is well-established (Brush, 1966; Choi et al., 2010; de Oliveira et al., 2016; Galatzer-Levy et al., 2014; Martinez et al., 2013). Similar behavioural diversity has also been reported in the Mongolian gerbil with implementation of the FM direction discrimination task (Wetzel, Ohl, et al., 1998). For a long time, animals that performed poorly on such tasks were simply excluded from the studies, leading for example to exclusion rates of approximately 20 % in active avoidance paradigms in rats (Brush, 1966, 2003). While complete exclusion of the animals leads to a warped understanding on how learning processes proceed, the distinction of performance differences in animals is important to understand normal and abnormal functioning of neuronal circuits (Galatzer-Levy et al., 2014). A fact that we can absolutely back up with the differential auditory activation patterns acquired for good and bad learners with auditory fMRI. As demonstrated in the analysis of all animals trained without aP (chapter 3.3.2), without the separation of the animals into groups of good and bad learners, activation changes occurring after the initial 3 days of training would have been completely overlooked through the coincidence in brain activation decrease in good and brain activation increase in bad learners.

The spectrum of different performance groups in rodents varies widely in different reports. Some researchers identify “good” and “poor” performers (Choi et al., 2010; de Oliveira et al., 2016), as we did for our activation patterns and ANOVA analysis. Others make out multiple different learning groups according to their learning speed (Galatzer-Levy et al., 2014). With our linear regression analysis approach, we went a step further, and looked into the correlation of individual behavioural scores to the extent of brain activation in different structures. Here, we were able to find significant negative correlation of performance and behaviour in mPFC, RSC and different thalamic regions upon GO and noGo tone presentation after 10 days of training with and without aP. Linear correlations comparable to ours were found in freezing rates of mice after auditory fear conditioning with functional connectivity in the limbic system, acquired with functional ultrasound (Grohs-Metz et al., 2022). In contrast to our findings, post visual avoidance training c-fos expression, a gene transcription factor commonly used as marker for neuronal activation, correlated positively to performance in rats’ prelimbic and infralimbic cortex (Martinez et al., 2013). In this regard, the good learners of this study showed performance improvement in their last avoidance training session, and therefore presumably still were in a learning acquisition stage. Besides this, we did not look into the individual substructures of mPFC with our VOI analysis, and concurring cingulate cortex activation could have superimposed inverse changes in infralimbic and prelimbic cortex. In the future, a more detailed parcellation in mPFC might be beneficial for the auditory fMRI analysis.

As described before, mPFC and Th also commonly show activation after fear conditioning in rodents. Subpopulations identified as bad learners in instrumental active avoidance conditioning have been reported to exhibit a lot of freezing (Choi et al., 2010; de Oliveira et al., 2016; Lázaro-Muñoz et al., 2010; Martinez et al., 2013). This behaviour is akin to what is observed in rodents after successful fear conditioning (Oitzl, 2007), and corresponds to emotional fear responses in the first stage of the proposed learning stage of aversive avoidance conditioning (Kozma et al., 2021; Maia, 2010; Mowrer, 1951). Bad learners, due to their continued poor performance, are experiencing frequent foot shocks throughout the continued training and may never reach the stage of avoidance that is necessary for the diminishing of the emotional responses of fear and relieve (Maia, 2010; Mowrer, 1951) and formation of a habit (Cain, 2019; LeDoux et al., 2017).

Explanations for bad performance revolve around defective circuitry in mPFC and amygdala, which makes the animals unable to perform the required instrumental responses (Choi et al., 2010; Corcoran & Quirk, 2007; Lázaro-Muñoz et al., 2010; Martinez et al., 2013; Moscarello & LeDoux, 2013). For instance, through selective lesioning of the central amygdala in bad learners, their discrimination ability was restored (Lázaro-Muñoz et al., 2010). Interestingly, we observed a relatively high (although not significant) amygdala activation increase in good learners after three days of training with aP, while bad learners showed comparatively lower activation in this area after the full ten days of training. Coincidental mPFC activation was similar for good learners after 3 days and bad learners after 10 days. This could be an indicator that the interaction of these areas was indeed involved in the poor performance of our bad learners.

Another explanation to performance variation in aversive discrimination learning can be found in the initial stress level of the animals during the first training phase, making the differential results not a matter of learning ability but of anxiety (Brush, 2003; de Oliveira et al., 2016). In these observed bad learners, displayed behavioural fear responses of bad learners were accompanied with lowered corticosterone levels after 7 days of aversive avoidance training, as a result of the continuous exposure to the foot shock (de Oliveira et al., 2016). While acute exposure to a foot shock induces the release of corticosterone (dos Santos Corrêa et al., 2019; Marchand et al., 2007), hypocortisolism is a good indicator for chronic stress (Heim et al., 2000; Xu et al., 2015). The presence of corticosterone facilitates extinction learning in auditory fear conditioning (Cordero et al., 1998; Lesuis et al., 2018), which can be loosely compared to the reduction of emotional responses in fear avoidance conditioning. Lowered corticosterone levels due to chronic stress induced by the discrimination training may also explain the absence of further improvement in the task and the persistence of the emotional response in bad learners.

Beyond the fear-related responses, a lower BOLD signal in the auditory system correlated with higher learning scores of the gerbils as well. Better performance necessitates a lower amount of activation, which has been reported for many associative brain areas (Buckner et al., 2000; Gerlach et al., 1999). In human auditory fMRI studies on FM categorization, activation in posterior

part and lateral surface areas of the planum temporale (higher order AC area) is reportedly also inversely proportional to the performance in the task (Brechmann & Scheich, 2005). This effect can be explained with a theory proposed by Desimone, which states that the specificity of a stimulus is improved by suppression of neurons that have a low stimulus selectivity (Desimone, 1992). In the gerbil auditory cortex this theory was substantiated with electrophysiological measurements during auditory conditioning, where the main area of activation showed activation increases and its' neighbourhood activation decreases (Ohl & Scheich, 1997). Today, it is widely accepted that learning can be driven by response suppression (Poort et al., 2022).

Another interesting insight found in human fMRI is that aversive reinforcement reportedly worsens tone discrimination thresholds (Resnik et al., 2011). Resnik et al. theorized that the aversive experience possibly leads to wider stimulus generalization by modulating perceptual thresholds. This fear generalization theory could explain the additional activation increase in structures of the auditory and limbic networks for control tone stimulation in bad learners after ten days of FM direction discrimination training with and without aP.

The observance of good and bad learning in the Mongolian gerbils accompanied by performance-dependent differences in brain activation patterns is consistent with related findings reported in literature. While the wide range of performance differences in healthy animals is often ignored in behavioural learning tasks, our observed performance-dependent activation differences in many brain areas proves that they should receive attention in any research question. Beyond that, the effects of auditory discrimination performance differences in rodents on brain-wide activation have not been published so far.

3.4.4. Effect of additional punishment

Theoretically, the application of aP can lead to a better discrimination performance in animals. This was shown by Wetzell et al in 1998, where one gerbil that did not show any discrimination abilities throughout 6 sessions of FM direction discrimination training, improved rapidly when aP was introduced to the training paradigm (Wetzell, Wagner, et al., 1998). In the analogical FM direction discrimination task of our auditory fMRI studies, the application of aP from the beginning of the training, however, led to no improvement of learning scores. Instead, it led to significantly lower CR+ and CR- rates in every single session, a significantly higher amount of electrical foot shocks applied to the gerbils per session, as well as a general decrease in learning speed. Multiple differences in brain activation patterns were found in gerbils trained with and without aP.

For both, good and bad learners, the application of aP led to a measurable recruitment of amygdala and insular cortex. The amygdala, as stated before, is distinctly associated with emotions, especially fear, while the insular cortex is involved in risky decision-making. Their interaction may store information of aversive memory (Gehrlach et al., 2019; Guzman-Ramos &

Bermudez-Rattoni, 2012). The strength of mPFC, amygdala and insular cortex connection correlates positively with levels of anxiety in humans (Williams, 2017). Since the gerbils that were trained with aP experienced significantly more aversive reinforcement shocks in comparison to animals trained without aP, higher involvement of structures that process anxiety, fear and risk is plausible. In classical fear conditioning paradigms, an increase of shock strength leads to higher amount of freezing (dos Santos Corrêa et al., 2019; Pietersen et al., 2006), as does a higher number of applied shocks (Haubrich & Nader, 2023; Lesuis et al., 2018; Marchand et al., 2007). Positive linear correlations were found in freezing rates of mice after auditory fear conditioning with functional connectivity in the limbic system as well (Grohs-Metz et al., 2022). It can therefore be concluded that the higher amygdala and insular cortex involvement we observed in the more aversive discrimination training paradigm overall makes sense.

The biggest difference between animals trained with and without aP showed in bad learners, with an earlier activation increase in training without aP, but also more activation for the noGo tone stimulation. This circumstance is somewhat unexpected, since in the training paradigm with aP both CS, GO and noGo tones, are connoted with an aversive stimulus for committing an error. Similar to active avoidance, the hippocampus, and several areas of isocortex such as mPFC have shown involvement in aversive passive avoidance (Baarendse et al., 2008; Baldi et al., 1999; Burwell et al., 2004; Fukushima et al., 2021; McGaugh, 2004; Santos-Anderson & Routtenberg, 1976). Therefore, a higher activation in these regions would have been expected in gerbils trained with aP than without aP for noGo tone stimulation instead. However, Schulz et al. found no significant cortico-striatal coherence for noGo tone in the FM direction discrimination task with aP in gerbils as well, arguing that overall low CR- rates were responsible for less induced coherence for that tone (Schulz et al., 2015). Likewise, we observed very low CR- rates, and as a result, only few aP shocks were applied to the animals, which could be the reason for the comparatively lower brain activation to the noGo tone.

The higher activation to noGo tones and control tones in animals trained without aP suggests more generalization and lower internal discrimination abilities of the gerbils trained without aP in comparison to gerbils trained with aP. The similarity of CR differences and d' values for gerbils trained with and without aP arose from the fact, that the gerbils trained without aP were crossing the hurdle much more often upon GO tone presentation and noGo presentation. The outcome is logical, as there was no (aversive) consequence for erroneous hurdle crossing in that training paradigm. This possibly led to similar meaning assignment for GO and noGo tone and a generally higher degree of generalization in the discrimination task without aP.

Beyond that, aP additionally resulted in a much higher correlation of the performance/learning values to measured brain activation. It would make sense that application of extra foot shocks would result in higher brain activation in the limbic system, as was observed in e.g. higher freezing

rates of classically fear conditioned animals (Haubrich & Nader, 2023; Lesuis et al., 2018; Marchand et al., 2007). However, this was only the case for the amygdala and insular cortex, while other brain areas on average did not show higher amounts of activation in good or bad learners. Instead it seems that the CR difference and d' values give a better account on the actual learning performance of the animals when aP is applied in the discrimination training, due the lowered CR-rates and fewer irrelevant hurdle-crossings upon noGo tone presentation.

Therefore, in learning studies with scientific hypotheses that depend on precise learning scores and performance outcomes, the discrimination training paradigm would benefit greatly from application of aP for CR-.

3.4.5. Summary of auditory learning-induced effects observed with auditory fMRI

With application of auditory fMRI in Mongolian gerbil, we were able to monitor auditory-evoked activation patterns at multiple stages of FM direction discrimination training. Three major observations were made about FM direction discrimination learning, summarily visualized in Figure 47.

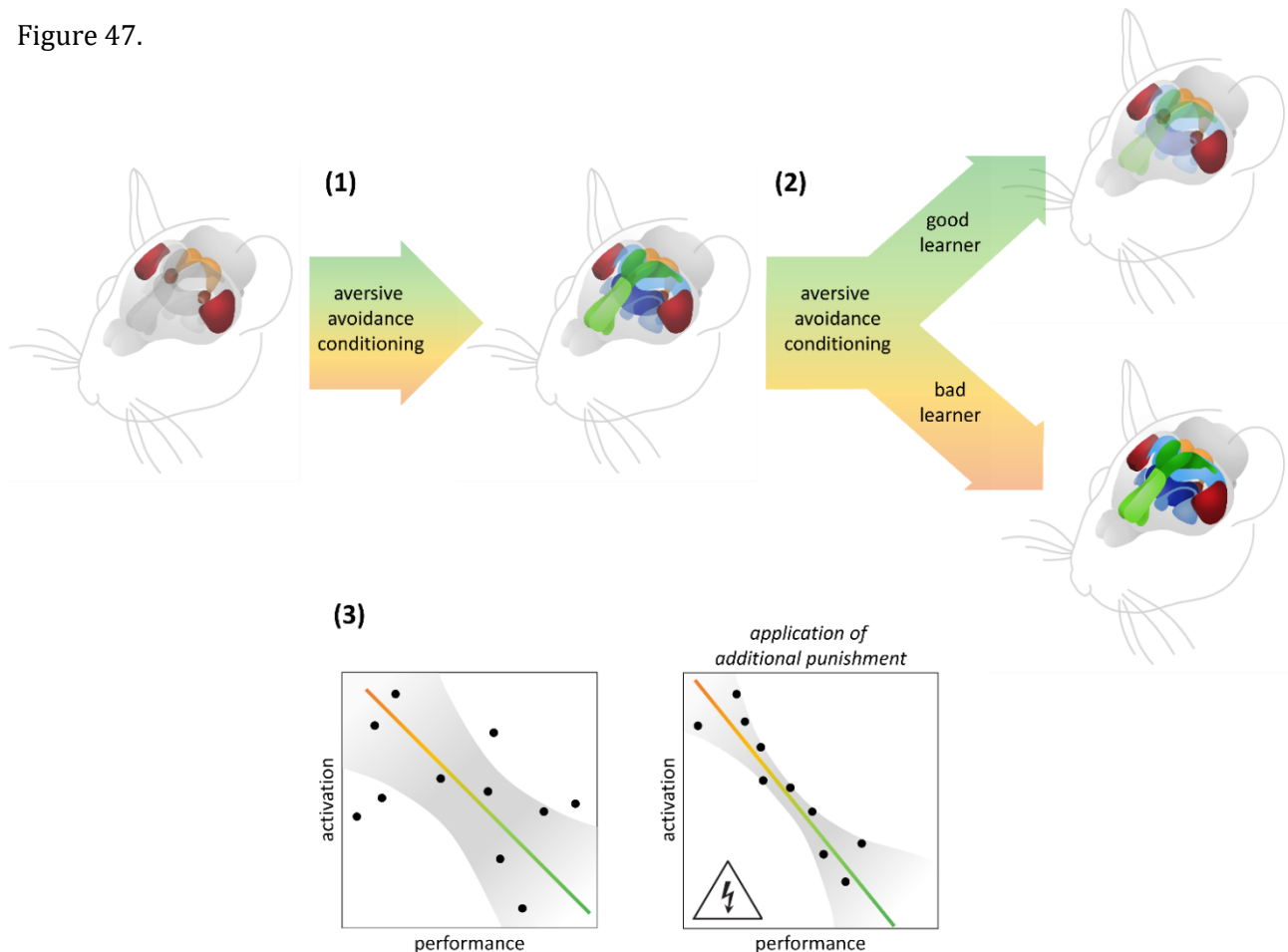


Figure 47: Overview of discrimination learning effects in Mongolian gerbils acquired with auditory fMRI

Effect (1): Auditory discrimination learning induces significant activation increase in several auditory, associative and neuromodulatory brain areas. **Effect (2):** activation patterns vary performance-dependently after prolonged training, with significantly higher activation throughout the brain of bad learners in comparison to good learners. **Effect (3):** application of additional punishment to the discrimination training paradigm leads to higher correlation between individual learning scores and brain activation levels.

General discussion

Optimization of the auditory setup, anaesthesia protocol and fMRI sequence parameters enabled brain-wide acquisition of auditory-stimulated brain activation patterns and auditory learning-induced changes with auditory fMRI in the Mongolian gerbil.

Our results indicate global information processing with focal activation hotspots in multiple structures that are engaged in the learning course of the FM direction discrimination task in gerbils. Many individual structures, networks and circuits that have previously been observed in the context of fear memory and avoidance conditioning showed involvement in this learning process alongside the auditory structures necessary for perception and cognition of the auditory cues.

Through our repeated fMRI measurements, we were able to distinguish activation changes and consolidation processes in various brain structures with a clear and significant performance dependency. The addition of punishment in the training paradigm led to higher correlation of the animals' behaviour to the activation level of isocortex, the CNu, such as the amygdala of the limbic system and striatum and pallidum of the basal ganglia, and thalamic regions. The fact that we observed highly congruent activation patterns in good and bad learners in two independent groups of gerbils trained with a similar FM direction discrimination task, one without and one with additional punishment, validates the genuineness of the observed activation changes, in particular in the structures MGB, IC, mPFC, RSC and Th.

Our optimized anaesthesia approach does not only largely support motion-free and non-invasive imaging of brain activation, but ensures that the animals do not experience additional stress and fear through the fMRI acquisition itself, which would be the case in awake fMRI (Han et al., 2019; López-Moraga et al., 2022; Low et al., 2016; Mandino et al., 2023). In these awake measurements, the acquisition-related fear response can potentially entangle with the actual fear-responses brought on with the aversive or fear conditioning.

Challenges and Limitations

Several limitations on the application of auditory fMRI in Mongolian gerbils and the performed studies on auditory learning can be identified.

First and foremost and quite general to any method that measures neuronal activation based on neurovascular coupling, the observation of the changes in CBF, CBV and blood oxygenation gives no direct information on the nature of the underlying cell activation and circuit dynamics. BOLD signal change occurs for both excitatory and inhibitory neuronal activity. The results of this auditory fMRI, and for the same reasons of the CBF SPECT, are limited to localization of activation changes. Auditory fMRI additionally provides information on the onset time of these activation changes.

We checked on obvious confounds of applied medetomidine anaesthesia and MR background noise with CBF SPECT. This additional imaging approach indicated that effects of medetomidine were minor with the application of the newly established medetomidine anaesthesia protocol for Mongolian gerbils. Theoretically, α_2 -adrenoceptor agonists are capable of reducing neuronal activation in thalamus, prefrontal cortex, orbital cortex, parietal association cortex, and posterior cingulate cortex (Bonhomme et al., 2008). Nevertheless, with our optimized medetomidine anaesthesia protocol, we were able to measure learning-induced activation changes in all of these regions throughout the performed auditory learning studies.

The acoustic background noise caused by the fMRI acquisition with the optimized GRE-EPI sequences, however, had a non-negligible effect on the auditory processing in AC, MGB and IC. This became easily visible in the activation patterns acquired in the CBF SPECT study. In the application of auditory fMRI for investigation of auditory learning effects, significant, learning-induced changes of activation were observed in all these structures anyways. This attests to the stimulation tones being perceived by the gerbils and distinguished from the high GRE-EPI background noise. Nevertheless, the activation acquired in AC, MGB and IC of the Mongolian gerbils was considerably altered by the concurring GRE-EPI noise.

Already during the establishment phase, signal loss in GRE-EPI images towards the brain periphery was observed, despite sequence optimizations. Consequently, structures located far to the ventral, anterior and posterior direction within the gerbils' brain may not have had a sufficient SNR to acquire reliable signal changes. In the performed auditory learning experiments, this was in all likelihood the case for hypothalamus, which reportedly is highly involved in aversive avoidance conditioning (Lazaridis et al., 2019; Trusel et al., 2019; Weera et al., 2021) but did not show coherent activation changes in the auditory fMRI acquired throughout the learning process. Additionally, literature describes smaller structures of the brain being involved in aversive avoidance learning (Martinez et al., 2013) and fear conditioning (Grohs-Metz et al., 2022) than what was resolved in the gerbil brain atlas implemented for ROI analysis. For future evaluation of the auditory fMRI data, the interpretation might benefit from further parcellation of the larger structures such as the mPFC.

Generally, in rodent brain anatomy precise structure borders and nomenclature varies between and within species and differs to common nomenclature of human analogues (Bota & Swanson, 2008; Bubb et al., 2020; Paxinos & Watson, 2006; Swanson, 2015; Vogt & Paxinos, 2014). This aggravated the literature search on specific brain regions and, hence, comparison to results from previously published studies. Common paradigms of different learning and conditioning approaches are also referred to by a variety of terms (Brown, 1998).

Outlook and implications for future research

The fMRI data acquired throughout the auditory FM direction discrimination training additionally contains information on the timing of the activation onset within the different structures, which could be detected on a small scale by shift of the GLM analysis to the later onset time of the reinforcement. Here we observed recruitment of additional brain structures with a time delay, indicating a time dependent activation cascade within the trials of the discrimination learning paradigm. Theoretically, the data could additionally be analysed for precise latencies of activation onset of all the involved structures, allowing for a time-resolved analysis of activation propagation through neuronal circuits, which has been reported with lower time resolution fMRI in the mouse auditory pathway before (Blazquez Freches et al., 2018). Once required pipelines are set up in our lab, a connectivity analysis will be implemented on the already collected data as well, to show changes in the connections between different brain structures, and thus constituting a bigger picture of how the brain plasticity changes during a procedural learning process.

In the scope of the hereby-presented dissertation, auditory fMRI has shown to facilitate the investigation of neuronal activation changes throughout the brain of Mongolian gerbils under mild medetomidine anaesthesia. Dependent on the research question, the background noise produced by the GRE-EPI sequence may seriously affect the informative value of this measurement methodology. Nevertheless, the newly established method offers time-resolved brain-wide imaging that allows non-invasive observation of brain activation brought on by auditory learning. This enables a direct comparison to ongoing human studies investigated with auditory fMRI. To maximise the usefulness of this method, it should be combined with other research methods that give additional information on the underlying nature of the observed brain activation such as calcium imaging or electrophysiology, as others have successfully done before (Angenstein et al., 2009; Schwalm et al., 2017). Alternatively, auditory fMRI in the Mongolian gerbil could be combined with invasive procedures such as lesioning of auditory structures (Saldeitis et al., 2022) to answer research questions that are unfeasible in human subjects.

The combination of auditory fMRI and FM direction discrimination training has shown that differences in performance have a huge impact on the progression of brain-wide activation patterns and therefore should be taken into account in the analysis of any kind of learning-induced changes. Additional punishment may lead to slightly worse discrimination scores in the training and a retardation in learning of the task, but ultimately to a better correlation of these behavioural learning scores to ongoing brain activation changes. In any case, the findings described in this dissertation thesis provide important information on auditory discrimination training effects that will facilitate the experimental design and analysis of future discrimination studies.

Citations

- Alexander, A. S., Place, R., Starrett, M. J., Chrastil, E. R., & Nitz, D. A. (2023). Rethinking retrosplenial cortex: Perspectives and predictions. *Neuron*, *111*(2), 150-175. <https://doi.org/https://doi.org/10.1016/j.neuron.2022.11.006>
- Amaro Jr., E., Williams, S. C. R., Shergill, S. S., Fu, C. H. Y., MacSweeney, M., Picchioni, M. M., Brammer, M. J., & McGuire, P. K. (2002). Acoustic noise and functional magnetic resonance imaging: Current strategies and future prospects. *Journal of Magnetic Resonance Imaging*, *16*(5), 497-510. <https://doi.org/https://doi.org/10.1002/jmri.10186>
- Ances, B. M., Leontiev, O., Perthen, J. E., Liang, C., Lansing, A. E., & Buxton, R. B. (2008). Regional differences in the coupling of cerebral blood flow and oxygen metabolism changes in response to activation: Implications for BOLD-fMRI. *Neuroimage*, *39*(4), 1510-1521. <https://doi.org/https://doi.org/10.1016/j.neuroimage.2007.11.015>
- Angeloni, C. F., Mlynarski, W., Piasini, E., Williams, A. M., Wood, K. C., Garami, L., Hermundstad, A. M., & Geffen, M. N. (2023). Dynamics of cortical contrast adaptation predict perception of signals in noise. *Nature Communications*, *14*(1), 4817. <https://doi.org/10.1038/s41467-023-40477-6>
- Angenstein, F., Kammerer, E., & Scheich, H. (2009). The BOLD Response in the Rat Hippocampus Depends Rather on Local Processing of Signals than on the Input or Output Activity. A Combined Functional MRI and Electrophysiological Study. *The Journal of Neuroscience*, *29*(8), 2428-2439. <https://doi.org/10.1523/jneurosci.5015-08.2009>
- Angenstein, N., & Brechmann, A. (2013a). Division of labor between left and right human auditory cortices during the processing of intensity and duration. *Neuroimage*, *83*, 1-11. <https://doi.org/10.1016/j.neuroimage.2013.06.071>
- Angenstein, N., & Brechmann, A. (2013b). Left auditory cortex is involved in pairwise comparisons of the direction of frequency modulated tones. *Front Neurosci*, *7*, 115. <https://doi.org/10.3389/fnins.2013.00115>
- Angenstein, N., & Brechmann, A. (2015). Auditory intensity processing: Categorization versus comparison. *Neuroimage*, *119*, 362-370. <https://doi.org/10.1016/j.neuroimage.2015.06.074>
- Angenstein, N., & Brechmann, A. (2017). Effect of sequential comparison on active processing of sound duration. *Hum Brain Mapp*, *38*(9), 4459-4469. <https://doi.org/10.1002/hbm.23673>
- Ayala, Y., Pérez-González, D., Duque, D., Nelken, I., & Malmierca, M. (2013). Frequency discrimination and stimulus deviance in the inferior colliculus and cochlear nucleus [Original Research]. *Frontiers in Neural Circuits*, *6*. <https://doi.org/10.3389/fncir.2012.00119>
- Azevedo, F. A. C., Carvalho, L. R. B., Grinberg, L. T., Farfel, J. M., Ferretti, R. E. L., Leite, R. E. P., Filho, W. J., Lent, R., & Herculano-Houzel, S. (2009). Equal numbers of neuronal and nonneuronal cells make the human brain an isometrically scaled-up primate brain. *Journal of Comparative Neurology*, *513*(5), 532-541. <https://doi.org/https://doi.org/10.1002/cne.21974>
- Baarendse, P. J. J., van Groothoest, G., Jansen, R. F., Pieneman, A. W., Ögren, S. O., Verhage, M., & Stiedl, O. (2008). Differential involvement of the dorsal hippocampus in passive avoidance in C57Bl/6J and DBA/2J mice. *Hippocampus*, *18*(1), 11-19. <https://doi.org/https://doi.org/10.1002/hipo.20356>
- Baker, N. J., Schofield, J. C., Caswell, M. D., & McLellan, A. D. (2011). Effects of early atipamezole reversal of medetomidine-ketamine anesthesia in mice. *J Am Assoc Lab Anim Sci*, *50*(6), 916-920.
- Bakin, J. S., & Weinberger, N. M. (1990). Classical conditioning induces CS-specific receptive field plasticity in the auditory cortex of the guinea pig. *Brain Res*, *536*(1-2), 271-286. [https://doi.org/10.1016/0006-8993\(90\)90035-a](https://doi.org/10.1016/0006-8993(90)90035-a)
- Baldi, E., Ambrogi Lorenzini, C., Sacchetti, B., Tassoni, G., & Bucherelli, C. (1999). Effects of combined medial septal area, fimbria-fornix and entorhinal cortex tetrodotoxin inactivations on passive avoidance response consolidation in the rat. *Brain Res*, *821*(2), 503-510. [https://doi.org/10.1016/s0006-8993\(99\)01116-6](https://doi.org/10.1016/s0006-8993(99)01116-6)
- Bandettini, P. A., Jesmanowicz, A., Van Kylen, J., Birn, R. M., & Hyde, J. S. (1998). Functional MRI of brain activation induced by scanner acoustic noise. *Magn Reson Med*, *39*(3), 410-416. <https://doi.org/10.1002/mrm.1910390311>
- Barron, H. C., Mars, R. B., Dupret, D., Lerch, J. P., & Sampaio-Baptista, C. (2021). Cross-species neuroscience: closing the explanatory gap. *Philos Trans R Soc Lond B Biol Sci*, *376*(1815), 20190633. <https://doi.org/10.1098/rstb.2019.0633>
- Batchelder, M., Keller, L. S., Sauer, M. B., & L. West, W. (2012). Chapter 52 - Gerbils. In M. A. Suckow, K. A. Stevens, & R. P. Wilson (Eds.), *The Laboratory Rabbit, Guinea Pig, Hamster, and Other Rodents* (pp. 1131-1155). Academic Press. <https://doi.org/https://doi.org/10.1016/B978-0-12-380920-9.00052-3>
- Behler, O., & Uppenkamp, S. (2016). Auditory fMRI of Sound Intensity and Loudness for Unilateral Stimulation. In P. van Dijk, D. Başkent, E. Gaudrain, E. de Kleine, A. Wagner, & C. Lanting, *Physiology, Psychoacoustics and Cognition in Normal and Impaired Hearing* Cham.
- Belliveau, J. W., Kennedy, D. N., McKinstry, R. C., Buchbinder, B. R., Weiskoff, R. M., Cohen, M. S., Vevea, J. M., Brady, T. J., & Rosen, B. R. (1991). Functional Mapping of the Human Visual Cortex by Magnetic Resonance Imaging. *254*(5032), 716-719. <https://doi.org/doi:10.1126/science.1948051>
- BioPAL, I. (2013). *Iron MRI imaging contrast agents (USPIO) - technical information*. <https://www.biopal.com/molday-ion.htm>
- Birrell, J. M., & Brown, V. J. (2000). Medial frontal cortex mediates perceptual attentional set shifting in the rat. *J Neurosci*, *20*(11), 4320-4324. <https://doi.org/10.1523/jneurosci.20-11-04320.2000>
- Bjørnerud, A. (2008a). *The Physics of Magnetic Resonance Imaging: Contrast Agents*. University of Oslo <https://www.uio.no/studier/emner/matnat/fys/FYS-KJM4740/v14/kompendium/kompendium-mri-feb-2009.pdf>
- Bjørnerud, A. (2008b). *The Physics of Magnetic Resonance Imaging: Pulse Sequences - An Introduction*. University of Oslo <https://www.uio.no/studier/emner/matnat/fys/FYS-KJM4740/v14/kompendium/kompendium-mri-feb-2009.pdf>
- Blamire, A. M., Ogawa, S., Ugurbil, K., Rothman, D., McCarthy, G., Ellermann, J. M., Hyder, F., Rattner, Z., & Shulman, R. G. (1992). Dynamic mapping of the human visual cortex by high-speed magnetic resonance imaging. *Proc Natl Acad Sci U S A*, *89*(22), 11069-11073. <https://doi.org/10.1073/pnas.89.22.11069>
- Blazquez Freches, G., Chavarrias, C., & Shemesh, N. (2018). BOLD-fMRI in the mouse auditory pathway. *Neuroimage*, *165*, 265-277. <https://doi.org/10.1016/j.neuroimage.2017.10.027>
- Bol, C., Danhof, M., Stanski, D. R., & Mandema, J. W. (1997). Pharmacokinetic-pharmacodynamic characterization of the cardiovascular, hypnotic, EEG and ventilatory responses to dexmedetomidine in the rat. *J Pharmacol Exp Ther*, *283*(3), 1051-1058.
- Bonhomme, V., Maquet, P., Phillips, C., Plenevaux, A., Hans, P., Luxen, A., Lamy, M., & Laureys, S. (2008). The Effect of Clonidine Infusion on Distribution of Regional Cerebral Blood Flow in Volunteers. *Anesthesia & Analgesia*, *106*(3), 899-909. <https://doi.org/10.1213/ane.0b013e3181619685>
- Bonnici, H. M., Richter, F. R., Yazar, Y., & Simons, J. S. (2016). Multimodal Feature Integration in the Angular Gyrus during Episodic and Semantic Retrieval. *J Neurosci*, *36*(20), 5462-5471. <https://doi.org/10.1523/jneurosci.4310-15.2016>
- Bota, M., & Swanson, L. W. (2008). BAMS Neuroanatomical Ontology: Design and Implementation. *Front Neuroinform*, *2*, 2. <https://doi.org/10.3389/neuro.11.002.2008>
- Brechmann, A., & Angenstein, N. (2019). The impact of task difficulty on the lateralization of processing in the human auditory cortex. *40*(18), 5341-5353. <https://doi.org/10.1002/hbm.24776>
- Brechmann, A., Baumgart, F., & Scheich, H. (2002). Sound-level-dependent representation of frequency modulations in human auditory cortex: a low-noise fMRI study. *J Neurophysiol*, *87*(1), 423-433. <https://doi.org/10.1152/jn.00187.2001>
- Brechmann, A., & Scheich, H. (2005). Hemispheric shifts of sound representation in auditory cortex with conceptual listening. *Cereb Cortex*, *15*(5), 578-587. <https://doi.org/10.1093/cercor/bhh159>
- Broadbent, N. J., Squire, L. R., & Clark, R. E. (2007). Rats depend on habit memory for discrimination learning and retention. *Learn Mem*, *14*(3), 145-151. <https://doi.org/10.1101/lm.455607>
- Broersen, L. M. (2000). Attentional processes and learning and memory in rats: the prefrontal cortex and hippocampus compared. *Prog Brain Res*, *126*, 79-94. [https://doi.org/10.1016/s0079-6123\(00\)26008-1](https://doi.org/10.1016/s0079-6123(00)26008-1)
- Brown, A. D., Hayward, T., Portfors, C. V., & Coffin, A. B. (2023). On the value of diverse organisms in auditory research: From fish to flies to humans. *Hear Res*, *432*, 108754. <https://doi.org/10.1016/j.heares.2023.108754>
- Brown, G. D. (1998). Operational terminology for stimulus exposure (SE) conditioning. *Behav Brain Res*, *95*(2), 143-150. [https://doi.org/10.1016/s0166-4328\(98\)00071-0](https://doi.org/10.1016/s0166-4328(98)00071-0)
- Brown, R. M., & Penhune, V. B. (2018). Efficacy of Auditory versus Motor Learning for Skilled and Novice Performers. *Journal of Cognitive Neuroscience*, *30*(11), 1657-1682. https://doi.org/10.1162/jocn_a.01309
- Bruce, L. L., & Braford, M. R. (2009). Evolution of the Limbic System.
- Brush, F. R. (1966). On the differences between animals that learn and do not learn to avoid electric shock. *Psychonomic Science*, *5*(3), 123-124. <https://doi.org/10.3758/BF03328312>
- Brush, F. R. (2003). Selection for Differences in Avoidance Learning: The Syracuse Strains Differ in Anxiety, Not Learning Ability. *Behavior Genetics*, *33*(6), 677-696. <https://doi.org/10.1023/A:1026135231594>
- Bruyant, P. P. (2002). Analytic and Iterative Reconstruction Algorithms in SPECT. *Journal of Nuclear Medicine*, *43*(10), 1343-1358. <https://jnm.snmjournals.org/content/jnumed/43/10/1343.full.pdf>

- Brydges, N. M., Whalley, H. C., Jansen, M. A., Merrifield, G. D., Wood, E. R., Lawrie, S. M., Wynne, S. M., Day, M., Fleetwood-Walker, S., Steele, D., Marshall, I., Hall, J., & Holmes, M. C. (2013). Imaging conditioned fear circuitry using awake rodent fMRI. *PLoS One*, *8*(1), e54197. <https://doi.org/10.1371/journal.pone.0054197>
- Bubb, E. J., Nelson, A. J. D., Cozens, T. C., & Aggleton, J. P. (2020). Organisation of cingulum bundle fibres connecting the anterior thalamic nuclei with the rodent anterior cingulate and retrosplenial cortices. *Brain and Neuroscience Advances*, *4*, 2398212820957160. <https://doi.org/10.1177/2398212820957160>
- Buckner, R. L., Koutstaal, W., Schacter, D. L., & Rosen, B. R. (2000). Functional MRI evidence for a role of frontal and inferior temporal cortex in amodal components of priming. *Brain*, *123*(3), 620-640. <https://doi.org/10.1093/brain/123.3.620>
- Budinger, E., Heil, P., Hess, A., & Scheich, H. (2006). Multisensory processing via early cortical stages: Connections of the primary auditory cortical field with other sensory systems. *Neuroscience*, *143*(4), 1065-1083. <https://doi.org/10.1016/j.neuroscience.2006.08.035>
- Budinger, E., Heil, P., & Scheich, H. (2000a). Functional organization of auditory cortex in the Mongolian gerbil (*Meriones unguiculatus*). III. Anatomical subdivisions and corticocortical connections. *Eur J Neurosci*, *12*(7), 2425-2451. <https://www.ncbi.nlm.nih.gov/pubmed/10947821>
- Budinger, E., Heil, P., & Scheich, H. (2000b). Functional organization of auditory cortex in the Mongolian gerbil (*Meriones unguiculatus*). IV. Connections with anatomically characterized subcortical structures. *Eur J Neurosci*, *12*(7), 2452-2474. <https://doi.org/10.1046/j.1460-9568.2000.00143.x>
- Budinger, E., Laszcz, A., Lison, H., Scheich, H., & Ohl, F. W. (2008). Non-sensory cortical and subcortical connections of the primary auditory cortex in Mongolian gerbils: bottom-up and top-down processing of neuronal information via field AI. *Brain Res*, *1220*, 2-32. <https://doi.org/10.1016/j.brainres.2007.07.084>
- Budinger, E., & Scheich, H. (2009). Anatomical connections suitable for the direct processing of neuronal information of different modalities via the rodent primary auditory cortex. *Hear Res*, *258*(1-2), 16-27. <https://doi.org/10.1016/j.heares.2009.04.021>
- Bukhari, Q., Schroeter, A., Cole, D. M., & Rudin, M. (2017). Resting State fMRI in Mice Reveals Anesthesia Specific Signatures of Brain Functional Networks and Their Interactions [Original Research]. *Frontiers in Neural Circuits*, *11*. <https://doi.org/10.3389/fncir.2017.00005>
- Burwell, R. D., Sadoris, M. P., Bucci, D. J., & Wiig, K. A. (2004). Corticohippocampal contributions to spatial and contextual learning. *J Neurosci*, *24*(15), 3826-3836. <https://doi.org/10.1523/jneurosci.0410-04.2004>
- Buxton, R. B., & Frank, L. R. (1997). A model for the coupling between cerebral blood flow and oxygen metabolism during neural stimulation. *J Cereb Blood Flow Metab*, *17*(1), 64-72. <https://doi.org/10.1097/00004647-199701000-00009>
- Cabral, J., Fernandes, F. F., & Shemesh, N. (2023). Intrinsic macroscale oscillatory modes driving long range functional connectivity in female rat brains detected by ultrafast fMRI. *Nature Communications*, *14*(1), 375. <https://doi.org/10.1038/s41467-023-36025-x>
- Cain, C. K. (2019). Avoidance problems reconsidered. *Current Opinion in Behavioral Sciences*, *26*, 9-17. <https://doi.org/https://doi.org/10.1016/j.cobeha.2018.09.002>
- Capuzzo, G., & Floresco, S. B. (2020). Prelimbic and Infralimbic Prefrontal Regulation of Active and Inhibitory Avoidance and Reward-Seeking. *J Neurosci*, *40*(24), 4773-4787. <https://doi.org/10.1523/jneurosci.0414-20.2020>
- Castiello, S., Zhang, W., & Delamater, A. R. (2021). The retrosplenial cortex as a possible "sensory integration" area: A neural network modeling approach of the differential outcomes effect in negative patterning. *Neurobiology of Learning and Memory*, *185*, 107527. <https://doi.org/https://doi.org/10.1016/j.nlm.2021.107527>
- Cauli, B., & Hamel, E. (2010). Revisiting the role of neurons in neurovascular coupling [Perspective]. *Frontiers in Neuroenergetics*, *2*. <https://doi.org/10.3389/fnene.2010.00009>
- Chamba, G., Weissmann, D., Rousset, C., Renaud, B., & Pujol, J. F. (1991). Distribution of alpha-1 and alpha-2 binding sites in the rat locus coeruleus. *Brain Research Bulletin*, *26*(2), 185-193. [https://doi.org/https://doi.org/10.1016/0361-9230\(91\)90225-9](https://doi.org/https://doi.org/10.1016/0361-9230(91)90225-9)
- Chen, H.-F., Lambers, H., Nagelmann, N., Sandbrink, M., Segelcke, D., Pogatzki-Zahn, E., Faber, C., & Pradier, B. (2023). Generation of a whole-brain hemodynamic response function and sex-specific differences in cerebral processing of mechano-sensation in mice detected by BOLD fMRI [Original Research]. *Frontiers in Neuroscience*, *17*. <https://doi.org/10.3389/fnins.2023.1187328>
- Chen, J. E., & Glover, G. H. (2015). Functional Magnetic Resonance Imaging Methods. *Neuropsychol Rev*, *25*(3), 289-313. <https://doi.org/10.1007/s11065-015-9294-9>
- Chen, J. J., & Pike, G. B. (2009). Origins of the BOLD post-stimulus undershoot. *Neuroimage*, *46*(3), 559-568. <https://doi.org/10.1016/j.neuroimage.2009.03.015>
- Chen, W., & Zhu, X. H. (1997). Suppression of physiological eye movement artifacts in functional MRI using slab presaturation. *Magn Reson Med*, *38*(4), 546-550. <https://doi.org/10.1002/mrm.1910380407>
- Chen, X., Tong, C., Han, Z., Zhang, K., Bo, B., Feng, Y., & Liang, Z. (2020). Sensory evoked fMRI paradigms in awake mice. *Neuroimage*, *204*, 116242. <https://doi.org/https://doi.org/10.1016/j.neuroimage.2019.116242>
- Cheng, J. T., Ghanad, I., Remenschneider, A., & Rosowski, J. (2021). The onset of nonlinear growth of middle-ear responses to high intensity sounds. *Hear Res*, *405*, 108242. <https://doi.org/10.1016/j.heares.2021.108242>
- Cheung, M. M., Lau, C., Zhou, I. Y., Chan, K. C., Cheng, J. S., Zhang, J. W., Ho, L. C., & Wu, E. X. (2012). BOLD fMRI investigation of the rat auditory pathway and tonotopic organization. *Neuroimage*, *60*(2), 1205-1211. <https://doi.org/10.1016/j.neuroimage.2012.01.087>
- Cheung, M. M., Lau, C., Zhou, I. Y., Chan, K. C., Zhang, J. W., Fan, S. J., & Wu, E. X. (2012). High fidelity tonotopic mapping using swept source functional magnetic resonance imaging. *Neuroimage*, *61*(4), 978-986. <https://doi.org/10.1016/j.neuroimage.2012.03.031>
- Cho, Z. H., Chung, S. C., Lim, D. W., & Wong, E. K. (1998). Effects of the acoustic noise of the gradient systems on fMRI: a study on auditory, motor, and visual cortices. *Magn Reson Med*, *39*(2), 331-335. <https://doi.org/10.1002/mrm.1910390224>
- Cho, Z. H., Park, S. H., Kim, J. H., Chung, S. C., Chung, S. T., Chung, J. Y., Moon, C. W., Yi, J. H., Sin, C. H., & Wong, E. K. (1997). Analysis of acoustic noise in MRI. *Magnetic Resonance Imaging*, *15*(7), 815-822. [https://doi.org/https://doi.org/10.1016/S0730-725X\(97\)00090-8](https://doi.org/https://doi.org/10.1016/S0730-725X(97)00090-8)
- Choi, J. S., Cain, C. K., & LeDoux, J. E. (2010). The role of amygdala nuclei in the expression of auditory signaled two-way active avoidance in rats. *Learn Mem*, *17*(3), 139-147. <https://doi.org/10.1101/lm.1676610>
- Clark, L., Bechara, A., Damasio, H., Aitken, M. R., Sahakian, B. J., & Robbins, T. W. (2008). Differential effects of insular and ventromedial prefrontal cortex lesions on risky decision-making. *Brain*, *131*(Pt 5), 1311-1322. <https://doi.org/10.1093/brain/awn066>
- Cohen, M. S., & Schmitt, F. (2012). Echo planar imaging before and after fMRI: a personal history. *Neuroimage*, *62*(2), 652-659. <https://doi.org/10.1016/j.neuroimage.2012.01.038>
- Concina, G., Cambiaghi, M., Renna, A., & Sacchetti, B. (2018). Coherent Activity between the Prelimbic and Auditory Cortex in the Slow-Gamma Band Underlies Fear Discrimination. *J Neurosci*, *38*(39), 8313-8328. <https://doi.org/10.1523/jneurosci.0540-18.2018>
- Constable, R. T., & Spencer, D. D. (2001). Repetition time in echo planar functional MRI. *Magnetic Resonance in Medicine*, *46*(4), 748-755. <https://doi.org/https://doi.org/10.1002/mrm.1253>
- Cooper, E. (2016). Human Auditory Pathway. In *AuditoryPathway_final.png* (Ed.).
- Coover, G. D., & Ursin, H. (1973). Plasma-corticosterone levels during active-avoidance learning in rats. *Journal of Comparative and Physiological Psychology*, *82*(1), 170-174. <https://doi.org/10.1037/h0033790>
- Corcoran, K. A., & Quirk, G. J. (2007). Activity in Prelimbic Cortex Is Necessary for the Expression of Learned, But Not Innate, Fears. *The Journal of Neuroscience*, *27*(4), 840-844. <https://doi.org/10.1523/jneurosci.5327-06.2007>
- Cordero, M. I., Merino, J. J., & Sandi, C. (1998). Correlational relationship between shock intensity and corticosterone secretion on the establishment and subsequent expression of contextual fear conditioning. *Behavioral neuroscience*, *112*(4), 885-891. <https://doi.org/10.1037/0735-7044.112.4.885>
- Correa-Sales, C., Rabin, B. C., & Maze, M. (1992). A hypnotic response to dexmedetomidine, an alpha 2 agonist, is mediated in the locus coeruleus in rats. *Anesthesiology*, *76*(6), 948-952. <https://doi.org/10.1097/0000542-199206000-00013>
- Costalupes, J. A., Young, E. D., & Gibson, D. J. (1984). Effects of continuous noise backgrounds on rate response of auditory nerve fibers in cat. *Journal of Neurophysiology*, *51*(6), 1326-1344.
- Counter, S. A., Olofsson, A., Grahn, H. F., & Borg, E. (1997). MRI acoustic noise: Sound pressure and frequency analysis. *7*(3), 606-611. <https://doi.org/https://doi.org/10.1002/jmri.1880070327>
- Cromwell, H. C., Klein, A., & Mears, R. P. (2007). Single unit and population responses during inhibitory gating of striatal activity in freely moving rats. *Neuroscience*, *146*(1), 69-85. <https://doi.org/10.1016/j.neuroscience.2007.01.025>
- Czoschke, S., Fischer, C., Bahador, T., Bledowski, C., & Kaiser, J. (2021). Decoding Concurrent Representations of Pitch and Location in Auditory Working Memory. *J Neurosci*, *41*(21), 4658-4666. <https://doi.org/10.1523/jneurosci.2999-20.2021>
- Damestani, N. L., O'Daly, O., Solana, A. B., Wiesinger, F., Lythgoe, D. J., Hill, S., de Lara Rubio, A., Makovac, E., Williams, S. C. R., & Zelaya, F. (2021). Revealing the mechanisms behind novel auditory stimuli discrimination: An evaluation of silent functional MRI using looping star. *Human Brain Mapping*, *42*(9), 2833-2850. <https://doi.org/https://doi.org/10.1002/hbm.25407>

- Danielsen, A., Otnæss, M. K., Jensen, J., Williams, S. C., & Ostberg, B. C. (2014). Investigating repetition and change in musical rhythm by functional MRI. *Neuroscience*, *275*, 469-476. <https://doi.org/10.1016/j.neuroscience.2014.06.029>
- Davis, M., Falls, W. A., Campeau, S., & Kim, M. (1993). Fear-potentiated startle: a neural and pharmacological analysis. *Behav Brain Res*, *58*(1-2), 175-198. [https://doi.org/10.1016/0166-4328\(93\)90102-v](https://doi.org/10.1016/0166-4328(93)90102-v)
- de Landeta, A. B., Pereyra, M., Medina, J. H., & Katche, C. (2020). Anterior retrosplenial cortex is required for long-term object recognition memory. *Scientific Reports*, *10*(1), 4002. <https://doi.org/10.1038/s41598-020-60937-z>
- de Oliveira, C. C., Gouveia, F. V., de Castro, M. C., Kuroki, M. A., dos Santos, L. C. T., Fonoff, E. T., Teixeira, M. J., Otoch, J. P., & Martinez, R. C. R. (2016). A Window on the Study of Aversive Instrumental Learning: Strains, Performance, Neuroendocrine, and Immunologic Systems [Original Research]. *Frontiers in Behavioral Neuroscience*, *10*. <https://doi.org/10.3389/fnbeh.2016.00162>
- Dean, I., Harper, N. S., & McAlpine, D. (2005). Neural population coding of sound level adapts to stimulus statistics. *Nature Neuroscience*, *8*(12), 1684-1689. <https://doi.org/10.1038/nn1541>
- Dean, I., Robinson, B. L., Harper, N. S., & McAlpine, D. (2008). Rapid neural adaptation to sound level statistics. *J Neurosci*, *28*(25), 6430-6438. <https://doi.org/10.1523/jneurosci.0470-08.2008>
- Desimone, R. (1992). The physiology of memory: Recordings of things past. *Science*, *258*(5080), 245-246. <https://doi.org/10.1126/science.1411523>
- Detre, J. A., Leigh, J. S., Williams, D. S., & Koretsky, A. P. (1992). Perfusion imaging. *MRI*, *23*(1), 37-45. <https://doi.org/10.1002/mrm.1910230106>
- Di Salle, F., Formisano, E., Seifritz, E., Linden, D. E., Scheffler, K., Saulino, C., Tedeschi, G., Zanella, F. E., Pepino, A., Goebel, R., & Marciano, E. (2001). Functional fields in human auditory cortex revealed by time-resolved fMRI without interference of EPI noise. *Neuroimage*, *13*(2), 328-338. <https://doi.org/10.1006/nimg.2000.0683>
- Dias, R., Robbins, T. W., & Roberts, A. C. (1996). Dissociation in prefrontal cortex of affective and attentional shifts. *Nature*, *380*(6569), 69-72. <https://doi.org/10.1038/380069a0>
- Ding, Y., Xu, N., Gao, Y., Wu, Z., & Li, L. (2019). The role of the deeper layers of the superior colliculus in attentional modulations of prepulse inhibition. *Behav Brain Res*, *364*, 106-113. <https://doi.org/10.1016/j.bbr.2019.01.052>
- Dinh, T. N. A., Jung, W. B., Shim, H.-J., & Kim, S.-G. (2021). Characteristics of fMRI responses to visual stimulation in anesthetized vs. awake mice. *Neuroimage*, *226*, 117542. <https://doi.org/https://doi.org/10.1016/j.neuroimage.2020.117542>
- Dombrowski, P. A., Maia, T. V., Boschen, S. L., Bortolanza, M., Wendler, E., Schwarting, R. K., Brandão, M. L., Winn, P., Blaha, C. D., & Da Cunha, C. (2013). Evidence that conditioned avoidance responses are reinforced by positive prediction errors signaled by tonic striatal dopamine. *Behav Brain Res*, *241*, 112-119. <https://doi.org/10.1016/j.bbr.2012.06.031>
- dos Santos Corrêa, M., Vaz, B. d. S., Grisanti, G. D. V., de Paiva, J. P. Q., Tiba, P. A., & Fornari, R. V. (2019). Relationship between footshock intensity, post-training corticosterone release and contextual fear memory specificity over time. *Psychoneuroendocrinology*, *110*, 104447. <https://doi.org/https://doi.org/10.1016/j.psyneuen.2019.104447>
- Driscoll, L. L. (2018). 6.20 - Cognitive Function*. In C. A. McQueen (Ed.), *Comprehensive Toxicology (Third Edition)* (pp. 376-392). Elsevier. <https://doi.org/https://doi.org/10.1016/B978-0-12-801238-3.02206-6>
- Drummond, John C., Dao, Andrew V., Roth, David M., Cheng, C.-R., Atwater, Benjamin I., Minokadeh, A., Pasco, Leonardo C., & Patel, Piyush M. (2008). Effect of Dexmedetomidine on Cerebral Blood Flow Velocity, Cerebral Metabolic Rate, and Carbon Dioxide Response in Normal Humans. *Anesthesiology*, *108*(2), 225-232. <https://doi.org/10.1097/01.anes.0000299576.00302.4c>
- Durieux, L., Mathis, V., Herbeaux, K., Muller, M. A., Barbelivien, A., Mathis, C., Schlichter, R., Hugel, S., Majchrzak, M., & Lecourtier, L. (2020). Involvement of the lateral habenula in fear memory. *Brain Struct Funct*, *225*(7), 2029-2044. <https://doi.org/10.1007/s00429-020-02107-5>
- Edeline, J.-M. (1990). Frequency-specific plasticity of single unit discharges in the rat medial geniculate body. *Brain Research*, *529*, 109-119.
- Edeline, J.-M., Pham, P., & Weinberger, N. M. (1993). Rapid development of learning-induced receptive field plasticity in the auditory cortex. *Behavioral neuroscience*, *107* 4, 539-551.
- Edelstein, W. A., Hedeen, R. A., Mallozzi, R. P., El-Hamamsy, S. A., Ackermann, R. A., & Havens, T. J. (2002). Making MRI quieter. *Magn Reson Imaging*, *20*(2), 155-163. [https://doi.org/10.1016/s0730-725x\(02\)00475-7](https://doi.org/10.1016/s0730-725x(02)00475-7)
- Elliott, M. R., Bowtell, R. W., & Morris, P. G. (1999). The effect of scanner sound in visual, motor, and auditory functional MRI. *Magn Reson Med*, *41*(6), 1230-1235. [https://doi.org/10.1002/\(sici\)1522-2594\(199906\)41:6<1230::aid-mrm20>3.0.co;2-1](https://doi.org/10.1002/(sici)1522-2594(199906)41:6<1230::aid-mrm20>3.0.co;2-1)
- Elster, A. D. (2023). *BOLD and Brain Activity - Does the BOLD response result from the firing of nerve cells?* Retrieved 26.11.2023 from MRIQuestions.com
- Farahani, K., Sinha, U., Sinha, S., Chiu, L. C., & Lufkin, R. B. (1990). Effect of field strength on susceptibility artifacts in magnetic resonance imaging. *Comput Med Imaging Graph*, *14*(6), 409-413. [https://doi.org/10.1016/0895-6111\(90\)90040-i](https://doi.org/10.1016/0895-6111(90)90040-i)
- Ferris, C. F., & Tenney, J. (2014). Chapter 3 - Functional Magnetic Resonance Imaging in Epilepsy: Methods and Applications Using Awake Animals. In C. L. Faingold & H. Blumenfeld (Eds.), *Neuronal Networks in Brain Function, CNS Disorders, and Therapeutics* (pp. 37-54). Academic Press. <https://doi.org/https://doi.org/10.1016/B978-0-12-415804-7.00003-4>
- Finck, A., Schneck, C. D., & Hartman, A. F. (1972). Development of cochlear function in the neonate Mongolian gerbil (*Meriones unguiculatus*). *J Comp Physiol Psychol*, *78*(3), 375-380. <https://doi.org/10.1037/h0032373>
- Flores, Á., Fullana, M. Á., Soriano-Mas, C., & Andero, R. (2018). Lost in translation: how to upgrade fear memory research. *Molecular Psychiatry*, *23*(11), 2122-2132. <https://doi.org/10.1038/s41380-017-0006-0>
- Foster, N. N., Barry, J., Korobkova, L., Garcia, L., Gao, L., Becerra, M., Sherafat, Y., Peng, B., Li, X., Choi, J.-H., Gou, L., Zingg, B., Azam, S., Lo, D., Khanjani, N., Zhang, B., Stanis, J., Bowman, I., Cotter, K., ... Dong, H.-W. (2021). The mouse cortico-basal ganglia-thalamic network. *Nature*, *598*(7879), 188-194. <https://doi.org/10.1038/s41586-021-03993-3>
- Fox, P. T., & Raichle, M. E. (1984). Stimulus rate dependence of regional cerebral blood flow in human striate cortex, demonstrated by positron emission tomography. *J Neurophysiol*, *51*(5), 1109-1120. <https://doi.org/10.1152/jn.1984.51.5.1109>
- Freeman, J. H., Jr., Cuppernell, C., Flannery, K., & Gabriel, M. (1996). Context-specific multi-site cingulate cortical, limbic thalamic, and hippocampal neuronal activity during concurrent discriminative approach and avoidance training in rabbits. *J Neurosci*, *16*(4), 1538-1549. <https://doi.org/10.1523/jneurosci.16-04-01538.1996>
- Friston, K., & Ashburner, J. (2020). SPM12 [computer program]. London, UK, Wellcome Centre for Human Neuroimaging, UCL Queen Square Institute of Neurology.
- Friston, K. J., Josephs, O., Rees, G., & Turner, R. (1998). Nonlinear event-related responses in fMRI. *Magnetic Resonance in Medicine*, *39*(1), 41-52. <https://doi.org/https://doi.org/10.1002/mrm.1910390109>
- Fukuda, M., Vazquez, A. L., Zong, X., & Kim, S.-G. (2013). Effects of the α -adrenergic receptor agonist dexmedetomidine on neural, vascular and BOLD fMRI responses in the somatosensory cortex. *European Journal of Neuroscience*, *37*(1), 80-95. <https://doi.org/https://doi.org/10.1111/ejn.12024>
- Fukushima, H., Zhang, Y., & Kida, S. (2021). Interactions between the amygdala and medial prefrontal cortex as upstream regulators of the hippocampus to reconsolidate and enhance retrieved inhibitory avoidance memory. *Molecular Brain*, *14*(1), 44. <https://doi.org/10.1186/s13041-021-00753-2>
- Gaab, N., Gabrieli, J. D., & Glover, G. H. (2007). Assessing the influence of scanner background noise on auditory processing. II. An fMRI study comparing auditory processing in the absence and presence of recorded scanner noise using a sparse design. *Hum Brain Mapp*, *28*(8), 721-732. <https://doi.org/10.1002/hbm.20299>
- Gabriel, M. (1993). Discriminative Avoidance Learning: A Model System. In B. A. Vogt & M. Gabriel (Eds.), *Neurobiology of Cingulate Cortex and Limbic Thalamus: A Comprehensive Handbook* (pp. 478-523). Birkhäuser Boston. https://doi.org/10.1007/978-1-4899-6704-6_18
- Gabriel, M., Sparenborg, S., & Kubota, Y. (1989). Anterior and medial thalamic lesions, discriminative avoidance learning, and cingulate cortical neuronal activity in rabbits. *Experimental Brain Research*, *76*(2), 441-457. <https://doi.org/10.1007/BF00247901>
- Gabriel, M., Vogt, B. A., Kubota, Y., Poremba, A., & Kang, E. (1991). Training-stage related neuronal plasticity in limbic thalamus and cingulate cortex during learning: a possible key to mnemonic retrieval. *Behavioural Brain Research*, *46*(2), 175-185. [https://doi.org/https://doi.org/10.1016/S0166-4328\(05\)80111-1](https://doi.org/https://doi.org/10.1016/S0166-4328(05)80111-1)
- Galatzer-Levy, I., Moscarello, J., Blessing, E., Klein, J., Cain, C., & Ledoux, J. (2014). Heterogeneity in signaled active avoidance learning: Substantive and methodological relevance of diversity in instrumental defensive responses to threat cues. *Frontiers in Systems Neuroscience*, *8*. <https://doi.org/10.3389/fnsys.2014.00179>
- Gao, P. P., Zhang, J. W., Fan, S.-J., Sanes, D. H., & Wu, E. X. (2015). Auditory midbrain processing is differentially modulated by auditory and visual cortices: An auditory fMRI study. *Neuroimage*, *123*, 22-32. <https://doi.org/https://doi.org/10.1016/j.neuroimage.2015.08.040>

- Gehrlach, D. A., Dolensek, N., Klein, A. S., Roy Chowdhury, R., Matthys, A., Junghänel, M., Gaitanos, T. N., Podgornik, A., Black, T. D., Reddy Vaka, N., Conzelmann, K. K., & Gogolla, N. (2019). Aversive state processing in the posterior insular cortex. *Nat Neurosci*, 22(9), 1424-1437. <https://doi.org/10.1038/s41593-019-0469-1>
- Gerlach, C., Law, I., Gade, A., & Paulson, O. B. (1999). Perceptual differentiation and category effects in normal object recognition: A PET study. *Brain*, 122(11), 2159-2170. <https://doi.org/10.1093/brain/122.11.2159>
- Gibson, D. J., Young, E. D., & Costalupes, J. A. (1985). Similarity of dynamic range adjustment in auditory nerve and cochlear nuclei. *Journal of Neurophysiology*, 53(4), 940-958. <https://doi.org/10.1152/jn.1985.53.4.940>
- Gleich, O., & Strutz, J. (2012). The Mongolian Gerbil as a Model for the Analysis of Peripheral and Central Age-Dependent Hearing Loss. In N. Sadaf (Ed.), *Hearing Loss* (pp. Ch. 4). IntechOpen. <https://doi.org/10.5772/33569>
- Glover, G. H. (2011). Overview of functional magnetic resonance imaging. *Neurosurg Clin N Am*, 22(2), 133-139, vii. <https://doi.org/10.1016/j.nec.2010.11.001>
- Glynn, G., & Ahmad, S. (2002). Three-dimensional electrophysiological topography of the rat corticostriatal system. *Journal of Comparative Physiology A*, 188(9), 695-703. <https://doi.org/10.1007/s00359-002-0341-7>
- Godenschweger, F., Kägebein, U., Stucht, D., Yarach, U., Sciarra, A., Yakupov, R., Lüsebrink, F., Schulze, P., & Speck, O. (2016). Motion correction in MRI of the brain. *Phys Med Biol*, 61(5), R32-56. <https://doi.org/10.1088/0031-9155/61/5/r32>
- Gongwer, M. W., Klune, C. B., Couto, J., Jin, B., Enos, A. S., Chen, R., Friedmann, D., & DeNardo, L. A. (2023). Brain-Wide Projections and Differential Encoding of Prefrontal Neuronal Classes Underlying Learned and Innate Threat Avoidance. *J Neurosci*, 43(32), 5810-5830. <https://doi.org/10.1523/jneurosci.0697-23.2023>
- Gorman, A. W., Deh, K. M., Schwiedrzik, C. M., White, J. R., Groman, E. V., Fisher, C. A., Gillen, K. M., Spincemille, P., Rasmussen, S., Prince, M. R., Voss, H. U., Freiwald, W. A., & Wang, Y. (2018). Brain Iron Distribution after Multiple Doses of Ultra-small Superparamagnetic Iron Oxide Particles in Rats. *Comp Med*, 68(2), 139-147.
- Green, D. M., & Swets, J. A. (1966). *Signal detection theory and psychophysics*. John Wiley.
- Grewe, B. F., Gründemann, J., Kitch, L. J., Lecoq, J. A., Parker, J. G., Marshall, J. D., Larkin, M. C., Jercog, P. E., Grenier, F., Li, J. Z., Lüthi, A., & Schnitzer, M. J. (2017). Neural ensemble dynamics underlying a long-term associative memory. *Nature*, 543(7647), 670-675. <https://doi.org/10.1038/nature21682>
- Griffith, V. E., Simon, A. B., & Buxton, R. B. (2015). The coupling of cerebral blood flow and oxygen metabolism with brain activation is similar for simple and complex stimuli in human primary visual cortex. *Neuroimage*, 104, 156-162. <https://doi.org/10.1016/j.neuroimage.2014.10.003>
- Grohs-Metz, G., Smausz, R., Gigg, J., Boeckers, T., & Hengerer, B. (2022). Functional ultrasound imaging of recent and remote memory recall in the associative fear neural network in mice. *Behavioural Brain Research*, 428, 113862. <https://doi.org/https://doi.org/10.1016/j.bbr.2022.113862>
- Grosso, A., Cambiaghi, M., Renna, A., Milano, L., Roberto Merlo, G., Sacco, T., & Sacchetti, B. (2015). The higher order auditory cortex is involved in the assignment of affective value to sensory stimuli. *Nat Commun*, 6, 8886. <https://doi.org/10.1038/ncomms9886>
- Gutierrez-Barragan, D., Singh, N. A., Alvino, F. G., Coletta, L., Rocchi, F., De Guzman, E., Galbusera, A., Uboldi, M., Panzeri, S., & Gozzi, A. (2022). Unique spatiotemporal fMRI dynamics in the awake mouse brain. *Curr Biol*, 32(3), 631-644.e636. <https://doi.org/10.1016/j.cub.2021.12.015>
- Guzman-Ramos, K., & Bermudez-Rattoni, F. (2012). Interplay of amygdala and insular cortex during and after associative taste aversion memory formation. *Rev Neurosci*, 23(5-6), 463-471. <https://doi.org/10.1515/revneuro-2012-0056>
- Haase, A., Frahm, J., Matthaei, D., Hancike, W., & Merboldt, K. D. (1986). FLASH imaging. Rapid NMR imaging using low flip-angle pulses. *Journal of Magnetic Resonance (1969)*, 67(2), 258-266. [https://doi.org/https://doi.org/10.1016/0022-2364\(86\)90433-6](https://doi.org/https://doi.org/10.1016/0022-2364(86)90433-6)
- Hajjima, A., & Ichitani, Y. (2012). Dissociable anterograde amnesic effects of retrosplenial cortex and hippocampal lesions on spontaneous object recognition memory in rats. *Hippocampus*, 22(9), 1868-1875. <https://doi.org/https://doi.org/10.1002/hipo.22021>
- Hall, D. A., Haggard, M. P., Akeroyd, M. A., Palmer, A. R., Summerfield, A. Q., Elliott, M. R., Gurney, E. M., & Bowtell, R. W. (1999). "sparse" temporal sampling in auditory fMRI. *Human Brain Mapping*, 7(3), 213-223. [https://doi.org/https://doi.org/10.1002/\(SICI\)1097-0193\(1999\)7:3<213::AID-HBM5>3.0.CO;2-N](https://doi.org/https://doi.org/10.1002/(SICI)1097-0193(1999)7:3<213::AID-HBM5>3.0.CO;2-N)
- Hall, D. A., Haggard, M. P., Summerfield, A. Q., Akeroyd, M. A., Palmer, A. R., & Bowtell, R. W. (2001). Functional magnetic resonance imaging measurements of sound-level encoding in the absence of background scanner noise. *J Acoust Soc Am*, 109(4), 1559-1570. <https://doi.org/10.1121/1.1345697>
- Hall, D. A., Summerfield, A. Q., Gonçalves, M. S., Foster, J. R., Palmer, A. R., & Bowtell, R. W. (2000). Time-course of the auditory BOLD response to scanner noise. *Magn Reson Med*, 43(4), 601-606. [https://doi.org/10.1002/\(sici\)1522-2594\(200004\)43:4<601::aid-mrm16>3.0.co;2-r](https://doi.org/10.1002/(sici)1522-2594(200004)43:4<601::aid-mrm16>3.0.co;2-r)
- Han, Z., Chen, W., Chen, X., Zhang, K., Tong, C., Zhang, X., Li, C. T., & Liang, Z. (2019). Awake and behaving mouse fMRI during Go/No-Go task. *Neuroimage*, 188, 733-742. <https://doi.org/10.1016/j.neuroimage.2019.01.002>
- Harms, M. P., John J. Guinan, J., Sigalovsky, I. S., & Melcher, J. R. (2005). Short-Term Sound Temporal Envelope Characteristics Determine Multisecond Time Patterns of Activity in Human Auditory Cortex as Shown by fMRI. *Journal of Neurophysiology*, 93(1), 210-222. <https://doi.org/10.1152/jn.00712.2004>
- Harms, M. P., & Melcher, J. R. (2002). Sound Repetition Rate in the Human Auditory Pathway: Representations in the Waveshape and Amplitude of fMRI Activation. *Journal of Neurophysiology*, 88(3), 1433-1450. <https://doi.org/10.1152/jn.2002.88.3.1433>
- Harris, A. P., Lennen, R. J., Marshall, I., Jansen, M. A., Pernet, C. R., Brydges, N. M., Duguid, I. C., & Holmes, M. C. (2015). Imaging learned fear circuitry in awake mice using fMRI. *Eur J Neurosci*, 42(5), 2125-2134. <https://doi.org/10.1111/ejn.12939>
- Harris, D. M., & Dallos, P. (1979). Forward masking of auditory nerve fiber responses. *Journal of Neurophysiology*, 42(4), 1083-1107.
- Haubrich, J., & Nader, K. (2023). Network-Level Changes in the Brain Underlie Fear Memory Strength. In: eLife Sciences Publications, Ltd.
- Hayat, H., Regev, N., Matosevich, N., Sales, A., Paredes-Rodriguez, E., Krom, A. J., Bergman, L., Li, Y., Lavigne, M., Kremer, E. J., Yizhar, O., Pickering, A. E., & Nir, Y. (2020). Locus coeruleus norepinephrine activity mediates sensory-evoked awakenings from sleep. *Science Advances*, 6(15), eaaz4232. <https://doi.org/doi:10.1126/sciadv.aaz4232>
- Hayes, C. E., & Axel, L. (1985). Noise performance of surface coils for magnetic resonance imaging at 1.5 T. *Med Phys*, 12(5), 604-607. <https://doi.org/10.1118/1.595682>
- Headley, D. B., Kanta, V., Kyriazi, P., & Paré, D. (2019). Embracing Complexity in Defensive Networks. *Neuron*, 103(2), 189-201. <https://doi.org/10.1016/j.neuron.2019.05.024>
- Hedeen, R. A., & Edelstein, W. A. (1997). Characterization and prediction of gradient acoustic noise in MR imagers. *Magn Reson Med*, 37(1), 7-10. <https://doi.org/10.1002/mrm.1910370103>
- Heim, C., Ehlert, U., & Hellhammer, D. H. (2000). The potential role of hypocortisolism in the pathophysiology of stress-related bodily disorders. *Psychoneuroendocrinology*, 25(1), 1-35. [https://doi.org/10.1016/s0306-4530\(99\)00035-9](https://doi.org/10.1016/s0306-4530(99)00035-9)
- Heismann, B., Ott, M., & Grodzki, D. (2015). Sequence-based acoustic noise reduction of clinical MRI scans. *Magn Reson Med*, 73(3), 1104-1109. <https://doi.org/10.1002/mrm.25229>
- Hennevin, E., Maho, C., Hars, B., & Dutrieux, G. (1993). Learning-induced plasticity in the medial geniculate nucleus is expressed during paradoxical sleep. *Behav Neurosci*, 107(6), 1018-1030. <https://doi.org/10.1037//0735-7044.107.6.1018>
- Hennig, J., Nauerth, A., & Friedburg, H. (1986). RARE imaging: A fast imaging method for clinical MR. *3(6)*, 823-833. <https://doi.org/https://doi.org/10.1002/mrm.1910030602>
- Herculano-Houzel, S., Mota, B., & Lent, R. (2006). Cellular scaling rules for rodent brains. *Proceedings of the National Academy of Sciences*, 103(32), 12138-12143. <https://doi.org/doi:10.1073/pnas.0604911103>
- Herve, P. Y., Zago, L., Petit, L., Mazoyer, B., & Tzourio-Mazoyer, N. (2013). Revisiting human hemispheric specialization with neuroimaging. *Trends Cogn Sci*, 17(2), 69-80. <https://doi.org/10.1016/j.tics.2012.12.004>
- Hess, A., Stiller, D., Kaulisch, T., Heil, P., & Scheich, H. (2000). New insights into the hemodynamic blood oxygenation level-dependent response through combination of functional magnetic resonance imaging and optical recording in gerbil barrel cortex. *J Neurosci*, 20(9), 3328-3338. <https://doi.org/10.1523/jneurosci.20-09-03328.2000>
- Hikishima, K., Tsurugizawa, T., Kasahara, K., Hayashi, R., Takagi, R., Yoshinaka, K., & Nitta, N. (2023). Functional ultrasound reveals effects of MRI acoustic noise on brain function. *Neuroimage*, 281, 120382. <https://doi.org/https://doi.org/10.1016/j.neuroimage.2023.120382>
- Hillman, E. M. (2014). Coupling mechanism and significance of the BOLD signal: a status report. *Annu Rev Neurosci*, 37, 161-181. <https://doi.org/10.1146/annurev-neuro-071013-014111>
- Holschneider, D. P., Yang, J., Sadler, T. R., Nguyen, P. T., Givrad, T. K., & Maarek, J. M. (2006). Mapping cerebral blood flow changes during auditory-cue conditioned fear in the nontethered, nonrestrained rat. *Neuroimage*, 29(4), 1344-1358. <https://doi.org/10.1016/j.neuroimage.2005.08.038>
- Hu, F., & Dan, Y. (2022). An inferior-superior colliculus circuit controls auditory cue-directed visual spatial attention. *Neuron*, 110(1), 109-119.e103. <https://doi.org/https://doi.org/10.1016/j.neuron.2021.10.004>
- Hu, H., Cui, Y., & Yang, Y. (2020). Circuits and functions of the lateral habenula in health and in disease. *Nature Reviews Neuroscience*, 21(5), 277-295. <https://doi.org/10.1038/s41583-020-0292-4>

- Hu, X., & Yacoub, E. (2012). The story of the initial dip in fMRI. *Neuroimage*, *62*(2), 1103-1108. <https://doi.org/10.1016/j.neuroimage.2012.03.005>
- Huang, S.-M., Wu, C.-Y., Lin, Y.-H., Hsieh, H.-H., Yang, H.-C., Chiu, S.-C., & Peng, S.-L. (2022). Differences in brain activity between normal and diabetic rats under isoflurane anesthesia: a resting-state functional MRI study. *BMC Medical Imaging*, *22*(1), 136. <https://doi.org/10.1186/s12880-022-00867-6>
- Huffman, R. F., & Henson, O. W. (1990). The descending auditory pathway and acousticomotor systems: connections with the inferior colliculus. *Brain Research Reviews*, *15*(3), 295-323. [https://doi.org/10.1016/0165-0173\(90\)90005-9](https://doi.org/10.1016/0165-0173(90)90005-9)
- Hutton, C., Bork, A., Josephs, O., Deichmann, R., Ashburner, J., & Turner, R. (2002). Image distortion correction in fMRI: A quantitative evaluation. *Neuroimage*, *16*(1), 217-240. <https://doi.org/10.1006/nimg.2001.1054>
- Ilango, A., Shumake, J., Wetzel, W., & Ohl, F. W. (2014). Contribution of Emotional and Motivational Neurocircuitry to Cue-Signaled Active Avoidance Learning [Opinion]. *Frontiers in Behavioral Neuroscience*, *8*. <https://doi.org/10.3389/fnbeh.2014.00372>
- Ilango, A., Shumake, J., Wetzel, W., Scheich, H., & Ohl, F. W. (2012). The Role of Dopamine in the Context of Aversive Stimuli with Particular Reference to Acoustically Signaled Avoidance Learning [Mini Review]. *Frontiers in Neuroscience*, *6*. <https://doi.org/10.3389/fnins.2012.00132>
- Ishii, H., Ohara, S., Tobler, P. N., Tsutsui, K., & Iijima, T. (2012). Inactivating anterior insular cortex reduces risk taking. *J Neurosci*, *32*(45), 16031-16039. <https://doi.org/10.1523/jneurosci.2278-12.2012>
- Ishiyama, T., Dohi, S., Iida, H., Watanabe, Y., & Shimonaka, H. (1995). Mechanisms of dexmedetomidine-induced cerebrovascular effects in canine in vivo experiments. *Anesth Analg*, *81*(6), 1208-1215. <https://doi.org/10.1097/0000539-199512000-00016>
- Janak, P. H., & Tye, K. M. (2015). From circuits to behaviour in the amygdala. *Nature*, *517*(7534), 284-292. <https://doi.org/10.1038/nature14188>
- Jäncke, L., Shah, N. J., Posse, S., Grosse-Ryken, M., & Müller-Gärtner, H. W. (1998). Intensity coding of auditory stimuli: an fMRI study. *Neuropsychologia*, *36*(9), 875-883. [https://doi.org/10.1016/s0028-3932\(98\)00019-0](https://doi.org/10.1016/s0028-3932(98)00019-0)
- Jang, D. P., Lee, K. M., Lee, S.-Y., Oh, J.-H., Park, C.-W., Kim, I. Y., Kim, Y.-B., & Cho, Z.-H. (2012). Auditory adaptation to sound intensity in conscious rats: 2-[F-18]-fluoro-2-deoxy-D-glucose PET study. *23*(4), 228-233. <https://doi.org/10.1097/WNR.0b013e32835022c7>
- Jiang, X., Chevillet, M. A., Rauschecker, J. P., & Riesenhuber, M. (2018). Training Humans to Categorize Monkey Calls: Auditory Feature- and Category-Selective Neural Tuning Changes. *Neuron*, *98*(2), 405-416.e404. <https://doi.org/10.1016/j.neuron.2018.03.014>
- Jonckers, E., Shah, D., Hamaide, J., Verhoye, M., & Van der Linden, A. (2015). The power of using functional fMRI on small rodents to study brain pharmacology and disease. *Front Pharmacol*, *6*, 231. <https://doi.org/10.3389/fphar.2015.00231>
- Juchter, C., Beutelmann, R., & Klump, G. M. (2022). Speech sound discrimination by Mongolian gerbils. *Hear Res*, *418*, 108472. <https://doi.org/10.1016/j.heares.2022.108472>
- Kalivas, P. W., & Volkow, N. D. (2005). The Neural Basis of Addiction: A Pathology of Motivation and Choice. *American Journal of Psychiatry*, *162*(8), 1403-1413. <https://doi.org/10.1176/appi.ajp.162.8.1403>
- Kalthoff, D., Seehafer, J. U., Po, C., Wiedermann, D., & Hoehn, M. (2011). Functional connectivity in the rat at 11.7T: Impact of physiological noise in resting state fMRI. *Neuroimage*, *54*(4), 2828-2839. <https://doi.org/10.1016/j.neuroimage.2010.10.053>
- Kamin, L. J., Brimer, C. J., & Black, A. H. (1963). Conditioned suppression as a monitor of fear of the CS in the course of avoidance training. *J Comp Physiol Psychol*, *56*, 497-501. <https://doi.org/10.1037/h0047966>
- Katsunuma, A., Takamori, H., Sakakura, Y., Hamamura, Y., Ogo, Y., & Katayama, R. (2002). Quiet MRI with novel acoustic noise reduction. *Magma*, *13*(3), 139-144. <https://doi.org/10.1007/bf02678588>
- Kawase, T., & Liberman, M. C. (1993). Antimasking effects of the olivocochlear reflex. I. Enhancement of compound action potentials to masked tones. *J Neurophysiol*, *70*(6), 2519-2532. <https://doi.org/10.1152/jn.1993.70.6.2519>
- Keene, C. S., & Bucci, D. J. (2008). Involvement of the retrosplenial cortex in processing multiple conditioned stimuli. *Behavioral neuroscience*, *122*(3), 651-658. <https://doi.org/10.1037/0735-7044.122.3.651>
- Kennerley, A. J., Mayhew, J. E., Redgrave, P., & Berwick, J. (2010). Vascular Origins of BOLD and CBV fMRI Signals: Statistical Mapping and Histological Sections Compared. *Open Neuroimaging J*, *4*, 1-8. <https://doi.org/10.2174/187444001004010001>
- Kessler, M., Mamach, M., Beutelmann, R., Bankstahl, J. P., Bengel, F. M., Klump, G. M., & Berding, G. (2018). Activation in the auditory pathway of the gerbil studied with [18F]-FDG PET: effects of anesthesia. *Brain Struct Funct*, *223*(9), 4293-4305. <https://doi.org/10.1007/s00429-018-1743-9>
- Khan, Z. P., Ferguson, C. N., & Jones, R. M. (1999). Alpha-2 and imidazoline receptor agonists: Their pharmacology and therapeutic role. *Anaesthesia*, *54*(2), 146-165. <https://doi.org/10.1046/j.1365-2044.1999.00659.x>
- Kim, S. G., Harel, N., Jin, T., Kim, T., Lee, P., & Zhao, F. (2013). Cerebral blood volume MRI with intravascular superparamagnetic iron oxide nanoparticles. *NMR Biomed*, *26*(8), 949-962. <https://doi.org/10.1002/nbm.2885>
- King, A. J., & Nelken, I. (2009). Unraveling the principles of auditory cortical processing: can we learn from the visual system? *Nature Neuroscience*, *12*(6), 698-701. <https://doi.org/10.1038/nn.2308>
- King, J. A., Garelick, T. S., Brevard, M. E., Chen, W., Messenger, T. L., Duong, T. Q., & Ferris, C. F. (2005). Procedure for minimizing stress for fMRI studies in conscious rats. *J Neurosci Methods*, *148*(2), 154-160. <https://doi.org/10.1016/j.jneumeth.2005.04.011>
- Kint, L. T., Seewoo, B. J., Hyndman, T. H., Clarke, M. W., Edwards, S. H., Rodger, J., Feindel, K. W., & Musk, G. C. (2020). The Pharmacokinetics of Medetomidine Administered Subcutaneously during Isoflurane Anaesthesia in Sprague-Dawley Rats. *Animals (Basel)*, *10*(6). <https://doi.org/10.3390/ani10061050>
- Kleinfeld, D., Blinder, P., Drew, P., Driscoll, J., Muller, A., Tsai, P., & Shih, A. (2011). A Guide to Delineate the Logic of Neurovascular Signaling in the Brain [Review]. *Frontiers in Neuroenergetics*, *3*. <https://doi.org/10.3389/fnene.2011.00001>
- Ko, J. (2004). Use of DOMITOR and ANTISEDAN in Small Animals (Pocket Pets). *DDA news*, *2/2004*, 1-3. https://www.researchgate.net/profile/Jon-Armeno/publication/278300324_Chemical_immobilization_of_zebra_slinks/557e875708aec87640dc69a6/Chemical-immobilization-of-zebras.pdf
- Kosslyn, S. M. (1999). If neuroimaging is the answer, what is the question? *Philos Trans R Soc Lond B Biol Sci*, *354*(1387), 1283-1294. <https://doi.org/10.1098/rstb.1999.0479>
- Kozma, R., Hu, S., Sokolov, Y., Wanger, T., Schulz, A. L., Woldeit, M. L., Gonçalves, A. I., Ruzsínkó, M., & Ohl, F. W. (2021). State Transitions During Discrimination Learning in the Gerbil Auditory Cortex Analyzed by Network Causality Metrics [Hypothesis and Theory]. *Frontiers in Systems Neuroscience*, *15*. <https://doi.org/10.3389/fnsys.2021.641684>
- Lambers, H., Segeroth, M., Albers, F., Wachsmuth, L., van Alst, T. M., & Faber, C. (2020). A cortical rat hemodynamic response function for improved detection of BOLD activation under common experimental conditions. *Neuroimage*, *208*, 116446. <https://doi.org/10.1016/j.neuroimage.2019.116446>
- Lanciego, J. L., Luquin, N., & Obeso, J. A. (2012). Functional neuroanatomy of the basal ganglia. *Cold Spring Harb Perspect Med*, *2*(12), a009621. <https://doi.org/10.1101/cshperspect.a009621>
- Langers, D. R., Van Dijk, P., & Backes, W. H. (2005). Interactions between hemodynamic responses to scanner acoustic noise and auditory stimuli in functional magnetic resonance imaging. *Magn Reson Med*, *53*(1), 49-60. <https://doi.org/10.1002/mrm.20315>
- Larsen, B., Sydnor, V. J., Keller, A. S., Yeo, B. T. T., & Satterthwaite, T. D. (2023). A critical period plasticity framework for the sensorimotor-association axis of cortical neurodevelopment. *Trends Neurosci*, *46*(10), 847-862. <https://doi.org/10.1016/j.tins.2023.07.007>
- Lazaridis, I., Tzortzi, O., Weglage, M., Martin, A., Xuan, Y., Parent, M., Johansson, Y., Fuzik, J., Fürth, D., Fenko, L. E., Ramakrishnan, C., Silberberg, G., Deisseroth, K., Carlén, M., & Meletis, K. (2019). A hypothalamus-habenula circuit controls aversion. *Molecular Psychiatry*, *24*(9), 1351-1368. <https://doi.org/10.1038/s41380-019-0369-5>
- Lázaro-Muñoz, G., LeDoux, J. E., & Cain, C. K. (2010). Sidman instrumental avoidance initially depends on lateral and basal amygdala and is constrained by central amygdala-mediated Pavlovian processes. *Biol Psychiatry*, *67*(12), 1120-1127. <https://doi.org/10.1016/j.biopsych.2009.12.002>
- Learned Helplessness. (2009). In M. D. Binder, N. Hirokawa, & U. Windhorst (Eds.), *Encyclopedia of Neuroscience* (pp. 2123-2123). Springer Berlin Heidelberg. https://doi.org/10.1007/978-3-540-29678-2_2738
- LeDoux, J. E., Farb, C. R., & Romanski, L. M. (1991). Overlapping projections to the amygdala and striatum from auditory processing areas of the thalamus and cortex. *Neuroscience Letters*, *134*(1), 139-144. [https://doi.org/10.1016/0304-3940\(91\)90526-Y](https://doi.org/10.1016/0304-3940(91)90526-Y)
- LeDoux, J. E., Moscarello, J., Sears, R., & Campese, V. (2017). The birth, death and resurrection of avoidance: a reconceptualization of a troubled paradigm. *Molecular Psychiatry*, *22*(1), 24-36. <https://doi.org/10.1038/mp.2016.166>
- Lennartz, R. C., & Weinberger, N. M. (1992). Frequency-specific receptive field plasticity in the medial geniculate body induced by pavlovian fear conditioning is expressed in the anesthetized brain. *Behavioral neuroscience*, *106*(3), 484-497.
- Lesicko, A. M. H., Sons, S. K., & Llano, D. A. (2020). Circuit Mechanisms Underlying the Segregation and Integration of Parallel Processing Streams in the Inferior Colliculus. *The Journal of Neuroscience*, *40*(33), 6328-6344. <https://doi.org/10.1523/jneurosci.0646-20.2020>
- Lesuis, S. L., Catsburg, L. A. E., Lucassen, P. J., & Krugers, H. J. (2018). Effects of corticosterone on mild auditory fear conditioning and extinction; role of sex and training paradigm. *Learn Mem*, *25*(10), 544-549. <https://doi.org/10.1101/lm.047811.118>

- Levis, D. J. (1966). Effects of serial CS presentation and other characteristics of the CS on the conditioned avoidance response. *Psychological Reports*, *18*(3), 755-766. <https://doi.org/10.2466/pr0.1966.18.3.755>
- Levis, D. J., & Boyd, T. L. (1979). Symptom maintenance: An infrahuman analysis and extension of the conservation of anxiety principle. *Journal of Abnormal Psychology*, *88*(2), 107-120. <https://doi.org/10.1037/0021-843X.88.2.107>
- Liang, C. L., Ances, B. M., Perthen, J. E., Moradi, F., Liau, J., Buracas, G. T., Hopkins, S. R., & Buxton, R. B. (2013). Luminance contrast of a visual stimulus modulates the BOLD response more than the cerebral blood flow response in the human brain. *Neuroimage*, *64*, 104-111. <https://doi.org/10.1016/j.neuroimage.2012.08.077>
- Lin, S.-P., & Brown, J. J. (2007). MR contrast agents: Physical and pharmacologic basics. *Journal of Magnetic Resonance Imaging*, *25*(5), 884-899. <https://doi.org/doi:10.1002/jmri.20955>
- Litvin, Y., Blanchard, D. C., Arakawa, H., & Blanchard, R. J. (2009). Aversive Learning. In M. D. Binder, N. Hirokawa, & U. Windhorst (Eds.), *Encyclopedia of Neuroscience* (pp. 293-296). Springer Berlin Heidelberg. https://doi.org/10.1007/978-3-540-29678-2_500
- Ljungberg, E., Damestani, N. L., Wood, T. C., Lythgoe, D. J., Zelaya, F., Williams, S. C. R., Solana, A. B., Barker, G. J., & Wiesinger, F. (2021). Silent zero TE MR neuroimaging: Current state-of-the-art and future directions. *Progress in Nuclear Magnetic Resonance Spectroscopy*, *123*, 73-93. <https://doi.org/https://doi.org/10.1016/j.pnmrs.2021.03.002>
- Loenneker, T., Hennel, F., Ludwig, U., & Hennig, J. (2001). Silent BOLD imaging. *Magma*, *13*(2), 76-81. <https://doi.org/10.1007/bf02668155>
- López-Moraga, A., Beckers, T., & Luyten, L. (2022). The effects of stress on avoidance in rodents: An unresolved matter. *Front Behav Neurosci*, *16*, 983026. <https://doi.org/10.3389/fnbeh.2022.983026>
- Low, L. A., Bauer, L. C., Pitcher, M. H., & Bushnell, M. C. (2016). Restraint training for awake functional brain scanning of rodents can cause long-lasting changes in pain and stress responses. *Pain*, *157*(8), 1761-1772. <https://doi.org/10.1097/j.pain.0000000000000579>
- Macmillan, N. A., & Creelman, C. D. (2005). *Detection theory: A user's guide*, 2nd ed. Lawrence Erlbaum Associates Publishers.
- Magnuson, M. E., Thompson, G. J., Pan, W.-J., & Keilholz, S. D. (2014). Time-dependent effects of isoflurane and dexmedetomidine on functional connectivity, spectral characteristics, and spatial distribution of spontaneous BOLD fluctuations. *NMR in Biomedicine*, *27*(3), 291-303. <https://doi.org/https://doi.org/10.1002/nbm.3062>
- Mahan, A. L., & Ressler, K. J. (2012). Fear conditioning, synaptic plasticity and the amygdala: implications for posttraumatic stress disorder. *Trends Neurosci*, *35*(1), 24-35. <https://doi.org/10.1016/j.tins.2011.06.007>
- Maia, T. V. (2010). Two-factor theory, the actor-critic model, and conditioned avoidance. *Learning & Behavior*, *38*(1), 50-67. <https://doi.org/10.3758/LB.38.1.50>
- Malmierca, M. S. (2013). Anatomy and Physiology of the Mammalian Auditory System. In D. Jaeger & R. Jung (Eds.), *Encyclopedia of Computational Neuroscience* (pp. 1-36). Springer New York. https://doi.org/10.1007/978-1-4614-7320-6_286-1
- Malmierca, M. S., Cristaudo, S., Pérez-González, D., & Covey, E. (2009). Stimulus-specific adaptation in the inferior colliculus of the anesthetized rat. *J Neurosci*, *29*(17), 5483-5493. <https://doi.org/10.1523/jneurosci.4153-08.2009>
- Mandeville, J. B., Marota, J. J., Kosofsky, B. E., Keltner, J. R., Weissleder, R., Rosen, B. R., & Weiskoff, R. M. (1998). Dynamic functional imaging of relative cerebral blood volume during rat forepaw stimulation. *Magn Reson Med*, *39*(4), 615-624. <https://doi.org/10.1002/mrm.1910390415>
- Mandeville, J. B., & Marota, J. J. A. (1999). Vascular filters of functional MRI: Spatial localization using BOLD and CBV contrast. *Magnetic Resonance in Medicine*, *42*(3), 591-598. [https://doi.org/https://doi.org/10.1002/\(SICI\)1522-2594\(199909\)42:3<591::AID-MRM23>3.0.CO;2-8](https://doi.org/https://doi.org/10.1002/(SICI)1522-2594(199909)42:3<591::AID-MRM23>3.0.CO;2-8)
- Mandino, F., Vujic, S., Grandjean, J., & Lake, E. M. R. (2023). Where do we stand on fMRI in awake mice? *Cerebr Cortex*. <https://doi.org/10.1093/cercor/bhad478>
- Mansfield, P. (1977). Multi-planar image formation using NMR spin echoes. *Journal of Physics C: Solid State Physics*, *10*(3), L55. <https://doi.org/10.1088/0022-3719/10/3/004>
- Marchand, A. R., Barbelivien, A., Seillier, A., Herbeaux, K., Sarrieau, A., & Majchrzak, M. (2007). Contribution of corticosterone to cue versus contextual fear in rats. *Behavioural Brain Research*, *183*(1), 101-110. <https://doi.org/https://doi.org/10.1016/j.bbr.2007.05.034>
- Maren, S., & Quirk, G. J. (2004). Neuronal signalling of fear memory. *Nature reviews Neuroscience*, *5*(11), 844-852. <https://doi.org/10.1038/nrn1535>
- Markicevic, M., Savvateev, I., Grimm, C., & Zerbi, V. (2021). Emerging imaging methods to study whole-brain function in rodent models. *Translational Psychiatry*, *11*(1), 457. <https://doi.org/10.1038/s41398-021-01575-5>
- Martinez, R. C., Gupta, N., Lázaro-Muñoz, G., Sears, R. M., Kim, S., Moscarello, J. M., LeDoux, J. E., & Cain, C. K. (2013). Active vs. reactive threat responding is associated with differential c-Fos expression in specific regions of amygdala and prefrontal cortex. *Learn Mem*, *20*(8), 446-452. <https://doi.org/10.1101/lm.031047.113>
- Masamoto, K., Kim, T., Fukuda, M., Wang, P., & Kim, S.-G. (2006). Relationship between Neural, Vascular, and BOLD Signals in Isoflurane-Anesthetized Rat Somatosensory Cortex. *Cerebral Cortex*, *17*(4), 942-950. <https://doi.org/10.1093/cercor/bhl005>
- Mason, M. J. (2016). Structure and function of the mammalian middle ear. I: Large middle ears in small desert mammals. *J Anat*, *228*(2), 284-299. <https://doi.org/10.1111/joa.12313>
- Mateos-Aparicio, P., & Rodríguez-Moreno, A. (2019). The Impact of Studying Brain Plasticity [Opinion]. *Frontiers in Cellular Neuroscience*, *13*. <https://doi.org/10.3389/fncel.2019.00066>
- McCullough, K. M., Choi, D., Guo, J., Zimmerman, K., Walton, J., Rainnie, D. G., & Ressler, K. J. (2016). Molecular characterization of Thyl1 expressing fear-inhibiting neurons within the basolateral amygdala. *Nature Communications*, *7*(1), 13149. <https://doi.org/10.1038/ncomms13149>
- McGaugh, J. L. (2004). The amygdala modulates the consolidation of memories of emotionally arousing experiences. *Annual Review of Neuroscience*, *27*(1), 1-28. <https://doi.org/10.1146/annurev.neuro.27.070203.144157>
- McGregor, M. S., & LaLumiere, R. T. (2023). Still a "hidden island"? The rodent insular cortex in drug seeking, reward, and risk. *Neuroscience & Biobehavioral Reviews*, *153*, 105334. <https://doi.org/https://doi.org/10.1016/j.neubiorev.2023.105334>
- McPherson, R. W., Koehler, R. C., Kirsch, J. R., & Traystman, R. J. (1997). Intraventricular dexmedetomidine decreases cerebral blood flow during normoxia and hypoxia in dogs. *Anesth Analg*, *84*(1), 139-147. <https://doi.org/10.1097/0000539-199701000-00026>
- Meléndez, J. C., & McCrank, E. (1993). Anxiety-related reactions associated with magnetic resonance imaging examinations. *Jama*, *270*(6), 745-747. <https://doi.org/10.1001/jama.1993.03510060091039>
- Méndez-Ruette, M., Linsambarth, S., Moraga-Amaro, R., Quintana-Donoso, D., Méndez, L., Tamburini, G., Cornejo, F., Torres, R. F., & Stehberg, J. (2019). The Role of the Rodent Insula in Anxiety [Original Research]. *Frontiers in Physiology*, *10*. <https://doi.org/10.3389/fphys.2019.00330>
- Miller, A. M. P., Vedder, L. C., Law, L. M., & Smith, D. M. (2014). Cues, context, and long-term memory: the role of the retrosplenial cortex in spatial cognition [Review]. *Frontiers in Human Neuroscience*, *8*. <https://doi.org/10.3389/fnhum.2014.00586>
- Moelker, A., & Pattynama, P. M. (2003). Acoustic noise concerns in functional magnetic resonance imaging. *Hum Brain Mapp*, *20*(3), 123-141. <https://doi.org/10.1002/hbm.10134>
- Monko, M. E., & Heilbronner, S. R. (2021). Retrosplenial Cortical Connectivity with Frontal Basal Ganglia Networks. *J Cogn Neurosci*, *33*(6), 1096-1105. https://doi.org/10.1162/jocn_a.01699
- Monti, M. M. (2011). Statistical Analysis of fMRI Time-Series: A Critical Review of the GLM Approach. *Front Hum Neurosci*, *5*, 28. <https://doi.org/10.3389/fnhum.2011.00028>
- Moore, B. C. J. (2012). *An Introduction to the Psychology of Hearing*. Emerald. <https://books.google.de/books?id=LM9U8e28pLMC>
- Morey, R. A., Dunsmoor, J. E., Haswell, C. C., Brown, V. M., Vora, A., Weiner, J., Stjepanovic, D., Wagner, H. R., 3rd, & LaBar, K. S. (2015). Fear learning circuitry is biased toward generalization of fear associations in posttraumatic stress disorder. *Transl Psychiatry*, *5*(12), e700. <https://doi.org/10.1038/tp.2015.196>
- Moscarello, J. M., & LeDoux, J. E. (2013). Active avoidance learning requires prefrontal suppression of amygdala-mediated defensive reactions. *J Neurosci*, *33*(9), 3815-3823. <https://doi.org/10.1523/jneurosci.2596-12.2013>
- Mowrer, O. H. (1951). Two-factor learning theory: summary and comment. *Psychological Review*, *58*(5), 350-354. <https://doi.org/10.1037/h0058956>
- MRICroGL*. In. (2019). (Version version 20 (v1.2.20220720)) NITRIC - Neuroimaging Tools & Resources Collaboratory.
- Nairne, J. S., Vasconcelos, M., & Pandeirada, J. N. S. (2012). Adaptive Memory and Learning. In N. M. Seel (Ed.), *Encyclopedia of the Sciences of Learning* (pp. 118-121). Springer US. https://doi.org/10.1007/978-1-4419-1428-6_1636
- Nasrallah, F. A., Tan, J., & Chuang, K. H. (2012). Pharmacological modulation of functional connectivity: α 2-adrenergic receptor agonist alters synchrony but not neural activation. *Neuroimage*, *60*(1), 436-446. <https://doi.org/10.1016/j.neuroimage.2011.12.026>
- Neirinkx, R. D., Burke, J. F., Harrison, R. C., Forster, A. M., Andersen, A. R., & Lassen, N. A. (1988). The Retention Mechanism of Technetium-99m-HM-PAO: Intracellular Reaction with Glutathione. *Journal of Cerebral Blood Flow & Metabolism*, *8*(1_suppl), S4-S12. <https://doi.org/10.1038/jcbfm.1988.27>
- Nelken, I., & Ahissar, M. (2006). High-Level and Low-Level Processing in the Auditory System: The Role of Primary Auditory Cortex. *IOS Press*.

- Nelson, Laura E., Lu, J., Guo, T., Saper, Clifford B., Franks, Nicholas P., & Maze, M. (2003). The α -2-Adrenoceptor Agonist Dexmedetomidine Converges on an Endogenous Sleep-promoting Pathway to Exert Its Sedative Effects. *Anesthesiology*, *98*(2), 428-436. <https://doi.org/10.1097/0000542-200302000-00024>
- Nishiyama, K., Kobayashi, K., & Riquimaroux, H. (2009). Ultrasonic upward FM vocalization of Mongolian gerbils, *Meriones unguiculatus*. *The Journal of the Acoustical Society of America*, *125*(4, Supplement), 2508-2508. <https://doi.org/10.1121/1.4808754>
- Nuernberger, M., Schaller, D., Klingner, C., Witte, O., & Brodoehl, S. (2022). Acoustic Stimuli Can Improve and Impair Somatosensory Perception [Original Research]. *Frontiers in Neuroscience*, *16*. <https://doi.org/10.3389/fnins.2022.930932>
- Numan, R. (2012). *The Behavioral Neuroscience of the Septal Region*. Springer New York. <https://books.google.de/books?id=JTzABwAAQBAJ>
- Nuñez, A., & Malmierca, E. (2007). Corticofugal modulation of sensory information. *Adv Anat Embryol Cell Biol*, *187*, 1 p following table of contents, 1-74.
- O'Reilly, R. C., & McClelland, J. L. (1994). Hippocampal conjunctive encoding, storage, and recall: avoiding a trade-off. *Hippocampus*, *4*(6), 661-682. <https://doi.org/10.1002/hipo.450040605>
- Oelschlegel, A., & Goldschmidt, J. (2020). Functional Neuroimaging in Rodents Using Cerebral Blood Flow SPECT. *Frontiers in Physics*, *8*. <https://doi.org/10.3389/fphy.2020.00152>
- Oertel, D. (1999). The role of timing in the brain stem auditory nuclei of vertebrates. *Annu Rev Physiol*, *61*, 497-519. <https://doi.org/10.1146/annurev.physiol.61.1.497>
- Ogawa, S., Lee, T. M., Kay, A. R., & Tank, D. W. (1990). Brain magnetic resonance imaging with contrast dependent on blood oxygenation. *Proc Natl Acad Sci U S A*, *87*(24), 9868-9872. <https://doi.org/10.1073/pnas.87.24.9868>
- Ohl, F. W., & Scheich, H. (1996). Differential Frequency Conditioning Enhances Spectral Contrast Sensitivity of Units in Auditory Cortex (Field A1) of the Alert Mongolian Gerbil. *European Journal of Neuroscience*, *8*(5), 1001-1017. <https://doi.org/https://doi.org/10.1111/j.1460-9568.1996.tb01587.x>
- Ohl, F. W., & Scheich, H. (1997). Learning-induced dynamic receptive field changes in primary auditory cortex of the anaesthetized Mongolian gerbil. *J Comp Physiol A*, *181*(6), 685-696. <https://doi.org/10.1007/s003590050150>
- Ohl, F. W., Scheich, H., & Freeman, W. J. (2001). Change in pattern of ongoing cortical activity with auditory category learning. *Nature*, *412*(6848), 733-736. <https://doi.org/10.1038/35089076>
- Ohl, F. W., Schulze, H., Scheich, H., & Freeman, W. J. (2000). Spatial representation of frequency-modulated tones in gerbil auditory cortex revealed by epidural electrocorticography. *J Physiol Paris*, *94*(5-6), 549-554. [https://doi.org/10.1016/s0928-4257\(00\)01091-3](https://doi.org/10.1016/s0928-4257(00)01091-3)
- Ohl, F. W., Wetzel, W., Wagner, T., Rech, A., & Scheich, H. (1999). Bilateral ablation of auditory cortex in Mongolian gerbil affects discrimination of frequency modulated tones but not of pure tones. *Learn Mem*, *6*(4), 347-362. <https://www.ncbi.nlm.nih.gov/pubmed/10509706>
- Oitzl, M. S. (2007). Avoidance*. In G. Fink (Ed.), *Encyclopedia of Stress (Second Edition)* (pp. 297-301). Academic Press. <https://doi.org/https://doi.org/10.1016/B978-012373947-6.00050-7>
- Oleksiak, C. R., Ramanathan, K. R., Miles, O. W., Perry, S. J., Maren, S., & Moscarello, J. M. (2021). Ventral hippocampus mediates the context-dependence of two-way signaled avoidance in male rats. *Neurobiology of Learning and Memory*, *183*, 107458. <https://doi.org/https://doi.org/10.1016/j.nlm.2021.107458>
- Oliver, D. L., & Huerta, M. F. (1992). Inferior and Superior Colliculi.
- Paasonen, J., Salo, R. A., Huttunen, J. K., & Grohn, O. (2017). Resting-state functional MRI as a tool for evaluating brain hemodynamic responsiveness to external stimuli in rats. *Magn Reson Med*, *78*(3), 1136-1146. <https://doi.org/10.1002/mrm.26496>
- Paasonen, J., Salo, R. A., Shatillo, A., Forsberg, M. M., Narvainen, J., Huttunen, J. K., & Grohn, O. (2016). Comparison of seven different anesthesia protocols for nicotine pharmacologic magnetic resonance imaging in rat. *Eur Neuropsychopharmacol*, *26*(3), 518-531. <https://doi.org/10.1016/j.euroneuro.2015.12.034>
- Paasonen, J., Stenroos, P., Salo, R. A., Kiviniemi, V., & Grohn, O. (2018). Functional connectivity under six anesthesia protocols and the awake condition in rat brain. *Neuroimage*, *172*, 9-20. <https://doi.org/10.1016/j.neuroimage.2018.01.014>
- Packard, M. G. (2009). Procedural Learning in Animals. In L. R. Squire (Ed.), *Encyclopedia of Neuroscience* (pp. 1077-1081). Academic Press. <https://doi.org/https://doi.org/10.1016/B978-008045046-9.00782-8>
- Pan, W.-J., Billings, J., Grooms, J., Shakil, S., & Keilholz, S. (2015). Considerations for resting state functional MRI and functional connectivity studies in rodents [Review]. *Frontiers in Neuroscience*, *9*. <https://doi.org/10.3389/fnins.2015.00269>
- Pandya, D. N., & Seltzer, B. (1982). Association areas of the cerebral cortex. *Trends in Neurosciences*, *5*, 386-390. [https://doi.org/https://doi.org/10.1016/0166-2236\(82\)90219-3](https://doi.org/https://doi.org/10.1016/0166-2236(82)90219-3)
- Pantev, C., & Herholz, S. C. (2011). Plasticity of the human auditory cortex related to musical training. *Neuroscience & Biobehavioral Reviews*, *35*(10), 2140-2154. <https://doi.org/https://doi.org/10.1016/j.neubiorev.2011.06.010>
- Papez, J. W. (1937). A Proposed Mechanism of Emotion. *Archives of Neurology & Psychiatry*, *38*(4), 725-743. <https://doi.org/10.1001/archneurpsyc.1937.02260220069003>
- Papini, M. R. (2012). Evolution of Learning. In N. M. Seel (Ed.), *Encyclopedia of the Sciences of Learning* (pp. 1188-1192). Springer US. https://doi.org/10.1007/978-1-4419-1428-6_302
- Pardi, M. B., Vogenstahl, J., Dalmay, T., Spanò, T., Pu, D. L., Naumann, L. B., Kretschmer, F., Sprekeler, H., & Letzkus, J. J. (2020). A thalamocortical top-down circuit for associative memory. *Science*, *370*(6518), 844-848. <https://doi.org/10.1126/science.abc2399>
- Park, S., Lee, J., Park, K., Kim, J., Song, B., Hong, I., Kim, J., Lee, S., & Choi, S. (2016). Sound tuning of amygdala plasticity in auditory fear conditioning. *Scientific Reports*, *6*(1), 31069. <https://doi.org/10.1038/srep31069>
- Pavlov, I. P., & Anrep, G. V. (1927). *Conditioned reflexes; an investigation of the physiological activity of the cerebral cortex*. Oxford University Press: Humphrey Milford.
- Pawela, C. P., Biswal, B. B., Hudetz, A. G., Schulte, M. L., Li, R., Jones, S. R., Cho, Y. R., Matloub, H. S., & Hyde, J. S. (2009). A protocol for use of medetomidine anesthesia in rats for extended studies using task-induced BOLD contrast and resting-state functional connectivity. *Neuroimage*, *46*(4), 1137-1147. <https://doi.org/10.1016/j.neuroimage.2009.03.004>
- Paxinos, G., & Watson, C. (2006). *The Rat Brain in Stereotaxic Coordinates: Hard Cover Edition*. Elsevier Science. <https://books.google.de/books?id=0prYfdBbh58C>
- Peelle, J. E. (2014). Methodological challenges and solutions in auditory functional magnetic resonance imaging. *Front Neurosci*, *8*, 253. <https://doi.org/10.3389/fnins.2014.00253>
- Pellegrino, G., Schuler, A.-L., Arcara, G., Di Pino, G., Piccione, F., & Kobayashi, E. (2022). Resting state network connectivity is attenuated by fMRI acoustic noise. *Neuroimage*, *247*, 118791. <https://doi.org/https://doi.org/10.1016/j.neuroimage.2021.118791>
- Peng, X., Mao, Y., Tai, Y., Luo, B., Dai, Q., Wang, X., Wang, H., Liang, Y., Guan, R., Liu, C., Guo, Y., Chen, L., Zhang, Z., & Wang, H. (2023). Characterization of Anxiety-Like Behaviors and Neural Circuitry following Chronic Moderate Noise Exposure in Mice. *Environ Health Perspect*, *131*(10), 107004. <https://doi.org/10.1289/ehp.12532>
- Pereira, A. G., Farias, M., & Moita, M. A. (2020). Thalamic, cortical, and amygdala involvement in the processing of a natural sound cue of danger. *PLoS Biol*, *18*(5), e3000674. <https://doi.org/10.1371/journal.pbio.3000674>
- Petrinovic, M. M., Hankov, G., Schroeter, A., Bruns, A., Rudin, M., von Kienlin, M., Künnecke, B., & Mueggler, T. (2016). A novel anesthesia regime enables neurofunctional studies and imaging genetics across mouse strains. *Scientific Reports*, *6*(1), 24523. <https://doi.org/10.1038/srep24523>
- Petykó, Z., Gálósi, R., Tóth, A., Máté, K., Szabó, I., Szabó, I., Karádi, Z., & Lénárd, L. (2015). Responses of rat medial prefrontal cortical neurons to Pavlovian conditioned stimuli and to delivery of appetitive reward. *Behav Brain Res*, *287*, 109-119. <https://doi.org/10.1016/j.bbr.2015.03.034>
- Phelps, E. A. (2004). Human emotion and memory: interactions of the amygdala and hippocampal complex. *Curr Opin Neurobiol*, *14*(2), 198-202. <https://doi.org/10.1016/j.conb.2004.03.015>
- Phillips, A. A., Chan, F. H., Zheng, M. M., Krassioukov, A. V., & Ainslie, P. N. (2016). Neurovascular coupling in humans: Physiology, methodological advances and clinical implications. *J Cereb Blood Flow Metab*, *36*(4), 647-664. <https://doi.org/10.1177/0271678X15617954>
- Phillips, D. P. (1985). Temporal response features of cat auditory cortex neurons contributing to sensitivity to tones delivered in the presence of continuous noise. *Hearing Research*, *19*(3), 253-268. [https://doi.org/https://doi.org/10.1016/0378-5955\(85\)90145-5](https://doi.org/https://doi.org/10.1016/0378-5955(85)90145-5)
- Phillips, D. P., Hall, S. E., & Boehnke, S. E. (2002). Central auditory onset responses, and temporal asymmetries in auditory perception. *Hearing Research*, *167*(1), 192-205. [https://doi.org/https://doi.org/10.1016/S0378-5955\(02\)00393-3](https://doi.org/https://doi.org/10.1016/S0378-5955(02)00393-3)
- Pidoux, M., Mahon, S., Deniau, J. M., & Charpier, S. (2011). Integration and propagation of somatosensory responses in the corticostriatal pathway: an intracellular study in vivo. *J Physiol*, *589*(Pt 2), 263-281. <https://doi.org/10.1113/jphysiol.2010.199646>
- Pietersen, C. Y., Bosker, F. J., Postema, F., & den Boer, J. A. (2006). Fear conditioning and shock intensity: the choice between minimizing the stress induced and reducing the number of animals used. *Lab Anim*, *40*(2), 180-185. <https://doi.org/10.1258/002367706776319006>
- Pinardi, M., Schuler, A.-L., Arcara, G., Ferreri, F., Marinazzo, D., Di Pino, G., & Pellegrino, G. (2023). Reduced connectivity of primary auditory and motor cortices during exposure to auditory white noise. *Neuroscience Letters*, *804*, 137212. <https://doi.org/https://doi.org/10.1016/j.neulet.2023.137212>

- Plewes, D. B., & Kucharczyk, W. (2012). Physics of MRI: A primer. *35*(5), 1038-1054. <https://doi.org/https://doi.org/10.1002/jmri.23642>
- Poort, J., Wilmes, K. A., Blot, A., Chadwick, A., Sahani, M., Clopath, C., Mrsic-Flogel, T. D., Hofer, S. B., & Khan, A. G. (2022). Learning and attention increase visual response selectivity through distinct mechanisms. *Neuron*, *110*(4), 686-697.e686. <https://doi.org/10.1016/j.neuron.2021.11.016>
- Pradier, B., Wachsmuth, L., Nagelmann, N., Segelcke, D., Kreitz, S., Hess, A., Pogatzki-Zahn, E. M., & Faber, C. (2021). Combined resting state-fMRI and calcium recordings show stable brain states for task-induced fMRI in mice under combined ISO/MED anesthesia. *Neuroimage*, *245*, 118626. <https://doi.org/https://doi.org/10.1016/j.neuroimage.2021.118626>
- Prielipp, R. C., Wall, M. H., Tobin, J. R., Groban, L., Cannon, M. A., Fahey, F. H., Gage, H. D., Stump, D. A., James, R. L., Bennett, J., & Butterworth, J. (2002). Dexmedetomidine-Induced Sedation in Volunteers Decreases Regional and Global Cerebral Blood Flow. *Anesthesia & Analgesia*, *95*(4), 1052-1059. <https://doi.org/10.1213/0000539-200210000-00048>
- Puderbaugh, M., & Emmady, P. D. (2023). Neuroplasticity. In *StatPearls*. StatPearls Publishing
- Copyright © 2023, StatPearls Publishing LLC.
- Purves, D., Augustine, G. J., Fitzpatrick, D., Hall, W. C., LaMantia, A.-S., McNamara, J. O., & Williams, S. M. (2004). The Auditory Thalamus. In *Neuroscience* (Third Edition ed., pp. 283-314). Sinauer Associates, Inc.
- Quirk, M. E., Letendre, A. J., Ciotton, R. A., & Lingley, J. F. (1989). Anxiety in patients undergoing MR imaging. *Radiology*, *170*(2), 463-466. <https://doi.org/10.1148/radiology.170.2.2911670>
- Radtke-Schuller, S., Schuller, G., Angenstein, F., Gresser, O. S., Goldschmidt, J., & Budinger, E. (2016). Brain atlas of the Mongolian gerbil (*Meriones unguiculatus*) in CT/MRI-aided stereotaxic coordinates. *Brain Struct Funct*, *221* Suppl 1, 1-272. <https://doi.org/10.1007/s00429-016-1259-0>
- Ragozzino, M. E. (2007). The contribution of the medial prefrontal cortex, orbitofrontal cortex, and dorsomedial striatum to behavioral flexibility. *Ann N Y Acad Sci*, *1121*, 355-375. <https://doi.org/10.1196/annals.1401.013>
- Ragozzino, M. E., Detrick, S., & Kesner, R. P. (1999). Involvement of the prelimbic-infralimbic areas of the rodent prefrontal cortex in behavioral flexibility for place and response learning. *J Neurosci*, *19*(11), 4585-4594. <https://doi.org/10.1523/jneurosci.19-11-04585.1999>
- Raichle, M. E. (1998). Behind the scenes of functional brain imaging: A historical and physiological perspective. *Proceedings of the National Academy of Sciences*, *95*(3), 765-772. <https://doi.org/doi:10.1073/pnas.95.3.765>
- Rajmohan, V., & Mohandas, E. (2007). The limbic system. *Indian J Psychiatry*, *49*(2), 132-139. <https://doi.org/10.4103/0019-5545.33264>
- Rauschecker, J. P., & Tian, B. (2000). Mechanisms and streams for processing of "what" and "where" in auditory cortex. *Proc Natl Acad Sci U S A*, *97*(22), 11800-11806. <https://doi.org/10.1073/pnas.97.22.11800>
- Ravicz, M. E., Melcher, J. R., & Kiang, N. Y. (2000). Acoustic noise during functional magnetic resonance imaging. *J Acoust Soc Am*, *108*(4), 1683-1696. <https://doi.org/10.1121/1.1310190>
- Rees, A., & Palmer, A. R. (1988). Rate-intensity functions and their modification by broadband noise for neurons in the guinea pig inferior colliculus. *The Journal of the Acoustical Society of America*, *83*(4), 1488-1498. <https://doi.org/10.1121/1.395904>
- Rehman, I., Mahabadi, N., Sanvictores, T., & Rehman, C. I. (2023, 14.08.2023). *Classical Conditioning*. StatPearls Publishing. <https://www.ncbi.nlm.nih.gov/books/NBK470326/>
- Resnik, J., Sobel, N., & Paz, R. (2011). Auditory aversive learning increases discrimination thresholds. *Nat Neurosci*, *14*(6), 791-796. <https://doi.org/10.1038/nn.2802>
- Riaz, S., Puveendrakumaran, P., Khan, D., Yoon, S., Hamel, L., & Ito, R. (2019). Prelimbic and infralimbic cortical inactivations attenuate contextually driven discriminative responding for reward. *Sci Rep*, *9*(1), 3982. <https://doi.org/10.1038/s41598-019-40532-7>
- Ritvo, V. J. H., Turk-Browne, N. B., & Norman, K. A. (2019). Nonmonotonic Plasticity: How Memory Retrieval Drives Learning. *Trends Cogn Sci*, *23*(9), 726-742. <https://doi.org/10.1016/j.tics.2019.06.007>
- Robinson, S., Keene, C. S., Iaccarino, H. F., Duan, D., & Bucci, D. J. (2011). Involvement of retrosplenial cortex in forming associations between multiple sensory stimuli. *Behavioral neuroscience*, *125*(4), 578-587. <https://doi.org/10.1037/a0024262>
- Robles, L., & Ruggero, M. A. (2001). Mechanics of the mammalian cochlea. *Physiol Rev*, *81*(3), 1305-1352. <https://doi.org/10.1152/physrev.2001.81.3.1305>
- Robson, M. D., Dorosz, J. L., & Gore, J. C. (1998). Measurements of the temporal fMRI response of the human auditory cortex to trains of tones. *Neuroimage*, *7*(3), 185-198. <https://doi.org/10.1006/nimg.1998.0322>
- Rocchi, F., & Ramachandran, R. (2018). Neuronal adaptation to sound statistics in the inferior colliculus of behaving macaques does not reduce the effectiveness of the masking noise. *Journal of Neurophysiology*, *120*(6), 2819-2833. <https://doi.org/10.1152/jn.00875.2017>
- Rocchi, F., & Ramachandran, R. (2020). Foreground stimuli and task engagement enhance neuronal adaptation to background noise in the inferior colliculus of macaques. *Journal of Neurophysiology*, *124*(5), 1315-1326. <https://doi.org/10.1152/jn.00153.2020>
- Rosowski, J. J., Ravicz, M. E., Teoh, S. W., & Flandermeier, D. (1999). Measurements of middle-ear function in the Mongolian gerbil, a specialized mammalian ear. *Audiol Neurootol*, *4*(3-4), 129-136. <https://doi.org/10.1159/000013831>
- Roxo, M. R., Franceschini, P. R., Zubaran, C., Kleber, F. D., & Sander, J. W. (2011). The Limbic System Conception and Its Historical Evolution. *TheScientificWorldJOURNAL*, *11*, 157150. <https://doi.org/10.1100/2011/157150>
- Russo, G., Helluy, X., Behroozi, M., & Manahan-Vaughan, D. (2021). Gradual Restraint Habituation for Awake Functional Magnetic Resonance Imaging Combined With a Sparse Imaging Paradigm Reduces Motion Artifacts and Stress Levels in Rodents. *Front Neurosci*, *15*, 805679. <https://doi.org/10.3389/fnins.2021.805679>
- Rutkowski, R. G., & Weinberger, N. M. (2005). Encoding of learned importance of sound by magnitude of representational area in primary auditory cortex. *Proceedings of the National Academy of Sciences*, *102*(38), 13664-13669. <https://doi.org/doi:10.1073/pnas.0506838102>
- Ryan, A. (1976). Hearing sensitivity of the mongolian gerbil, *Meriones unguiculatus*. *J Acoust Soc Am*, *59*(5), 1222-1226. <https://doi.org/10.1121/1.380961>
- Sachella, T. E., Ihidoype, M. R., Proulx, C. D., Pafundo, D. E., Medina, J. H., Mendez, P., & Piriz, J. (2022). A novel role for the lateral habenula in fear learning. *Neuropsychopharmacology*, *47*(6), 1210-1219. <https://doi.org/10.1038/s41386-022-01294-5>
- Saldeitis, K., Jeschke, M., Michalek, A., Henschke, J. U., Wetzell, W., Ohl, F. W., & Budinger, E. (2022). Selective Interruption of Auditory Interhemispheric Cross Talk Impairs Discrimination Learning of Frequency-Modulated Tone Direction But Not Gap Detection and Discrimination. *J Neurosci*, *42*(10), 2025-2038. <https://doi.org/10.1523/JNEUROSCI.0216-21.2022>
- Sampathkumar, V., Miller-Hansen, A., Sherman, S. M., & Kasthuri, N. (2021). Integration of signals from different cortical areas in higher order thalamic neurons. *Proceedings of the National Academy of Sciences*, *118*(30), e2104137118. <https://doi.org/doi:10.1073/pnas.2104137118>
- Sangha, S., Diehl, M. M., Bergstrom, H. C., & Drew, M. R. (2020). Know safety, no fear. *Neuroscience & Biobehavioral Reviews*, *108*, 218-230. <https://doi.org/https://doi.org/10.1016/j.neubiorev.2019.11.006>
- Santos-Anderson, R. M., & Routtenberg, A. (1976). Stimulation of rat medial or sulcal prefrontal cortex during passive avoidance learning selectively influences retention performance. *Brain Res*, *103*(2), 243-259. [https://doi.org/10.1016/0006-8993\(76\)90797-6](https://doi.org/10.1016/0006-8993(76)90797-6)
- Savola, J. M. (1989). Cardiovascular actions of medetomidine and their reversal by atipamezole. *Acta Vet Scand Suppl*, *85*, 39-47.
- Scarff, C. J., Dort, J. C., Eggermont, J. J., & Goodyear, B. G. (2004). The effect of MR scanner noise on auditory cortex activity using fMRI. *Hum Brain Mapp*, *22*(4), 341-349. <https://doi.org/10.1002/hbm.20043>
- Schaefer, K.-P., Süß, K.-J., & Fiebig, E. (1981). Acoustic-Induced Eye Movements. *Annals of the New York Academy of Sciences*, *374*(1), 674-688. <https://doi.org/https://doi.org/10.1111/j.1749-6632.1981.tb30910.x>
- Scheich, H., Brechmann, A., Brosch, M., Budinger, E., & Ohl, F. W. (2007). The cognitive auditory cortex: task-specificity of stimulus representations. *Hear Res*, *229*(1-2), 213-224. <https://doi.org/10.1016/j.heares.2007.01.025>
- Scheich, H., Heil, P., & Langner, G. (1993). Functional organization of auditory cortex in the mongolian gerbil (*Meriones unguiculatus*). II. Tonotopic 2-deoxyglucose. *Eur J Neurosci*, *5*(7), 898-914. <https://doi.org/10.1111/j.1460-9568.1993.tb00941.x>
- Schicknick, H., Henschke, J. U., Budinger, E., Ohl, F. W., Gundelfinger, E. D., & Tschmeyer, W. (2019). β -adrenergic modulation of discrimination learning and memory in the auditory cortex. *European Journal of Neuroscience*, *50*(7), 3141-3163. <https://doi.org/https://doi.org/10.1111/ejn.14480>
- Schindelin, J., Arganda-Carreras, I., Frise, E., Kaynig, V., Longair, M., Pietzsch, T., Preibisch, S., Rueden, C., Saalfeld, S., Schmid, B., Tinevez, J.-Y., White, D. J., Hartenstein, V., Eliceiri, K., Tomancak, P., & Cardona, A. (2012). Fiji: an open-source platform for biological-image analysis. *Nature Methods*, *9*(7), 676-682. <https://doi.org/10.1038/nmeth.2019>
- Schlegel, F., Schroeter, A., & Rudin, M. (2015). The hemodynamic response to somatosensory stimulation in mice depends on the anesthetic used: Implications on analysis of mouse fMRI data. *Neuroimage*, *116*, 40-49. <https://doi.org/10.1016/j.neuroimage.2015.05.013>

- Schroeter, A., Schlegel, F., Seuwen, A., Grandjean, J., & Rudin, M. (2014). Specificity of stimulus-evoked fMRI responses in the mouse: the influence of systemic physiological changes associated with innocuous stimulation under four different anesthetics. *Neuroimage*, *94*, 372-384. <https://doi.org/10.1016/j.neuroimage.2014.01.046>
- Schulz, A. L., Woldeit, M. L., Goncalves, A. I., Saldeitis, K., & Ohl, F. W. (2015). Selective Increase of Auditory Cortico-Striatal Coherence during Auditory-Cued Go/NoGo Discrimination Learning. *Front Behav Neurosci*, *9*, 368. <https://doi.org/10.3389/fnbeh.2015.00368>
- Schulz, J. M., Oswald, M. J., & Reynolds, J. N. J. (2011). Visual-Induced Excitation Leads to Firing Pauses in Striatal Cholinergic Interneurons. *The Journal of Neuroscience*, *31*(31), 11133-11143. <https://doi.org/10.1523/jneurosci.0661-11.2011>
- Schulz, J. M., Redgrave, P., Mehring, C., Aertsen, A., Clements, K. M., Wickens, J. R., & Reynolds, J. N. (2009). Short-latency activation of striatal spiny neurons via subcortical visual pathways. *J Neurosci*, *29*(19), 6336-6347. <https://doi.org/10.1523/jneurosci.4815-08.2009>
- Schulze, H., Deutscher, A., Tziridis, K., & Scheich, H. (2014). Unilateral auditory cortex lesions impair or improve discrimination learning of amplitude modulated sounds, depending on lesion side. *PLoS One*, *9*(1), e87159. <https://doi.org/10.1371/journal.pone.0087159>
- Schulze, K., Mueller, K., & Koelsch, S. (2013). Auditory stroop and absolute pitch: an fMRI study. *Hum Brain Mapp*, *34*(7), 1579-1590. <https://doi.org/10.1002/hbm.22010>
- Schwalm, M., Schmid, F., Wachsmuth, L., Backhaus, H., Kronfeld, A., Aedo Jury, F., Prouvot, P.-H., Fois, C., Albers, F., van Alst, T., Faber, C., & Stroh, A. (2017). Cortex-wide BOLD fMRI activity reflects locally-recorded slow oscillation-associated calcium waves. *eLife*, *6*, e27602. <https://doi.org/10.7554/eLife.27602>
- Seehafer, J. U., Kalthoff, D., Farr, T. D., Wiedermann, D., & Hoehn, M. (2010). No increase of the blood oxygenation level-dependent functional magnetic resonance imaging signal with higher field strength: implications for brain activation studies. *J Neurosci*, *30*(15), 5234-5241. <https://doi.org/10.1523/JNEUROSCI.0844-10.2010>
- Seligman, M. E. (1972). Learned helplessness. *Annu Rev Med*, *23*, 407-412. <https://doi.org/10.1146/annurev.me.23.020172.002203>
- Shah, N. J., Jäncke, L., Grosse-Ruyken, M.-L., & Müller-Gärtner, H. W. (1999). Influence of acoustic masking noise in fMRI of the auditory cortex during phonetic discrimination. *Journal of Magnetic Resonance Imaging*, *9*(1), 19-25. [https://doi.org/https://doi.org/10.1002/\(SICI\)1522-2586\(199901\)9:1<19::AID-JMRI3>3.0.CO;2-K](https://doi.org/https://doi.org/10.1002/(SICI)1522-2586(199901)9:1<19::AID-JMRI3>3.0.CO;2-K)
- Shih, I., & MacKinnon, M. J. (2020). *Stimulating and Recording Neuronal Activity During Traditional fMRI, and The Benefits When Doing This at "Zero" Echo Time*. Bruker Biospin MRI. <https://event.on24.com/wcc/r/2775158/039384F3E087F0D94159EBBB2C850D36?partnerref=ISWeb>
- Shih, Y. Y., Wey, H. Y., De La Garza, B. H., & Duong, T. Q. (2011). Striatal and cortical BOLD, blood flow, blood volume, oxygen consumption, and glucose consumption changes in noxious forepaw electrical stimulation. *J Cereb Blood Flow Metab*, *31*(3), 832-841. <https://doi.org/10.1038/jcbfm.2010.173>
- Shim, H.-J., Jung, W. B., Schlegel, F., Lee, J., Kim, S., Lee, J., & Kim, S.-G. (2018). Mouse fMRI under ketamine and xylazine anesthesia: Robust contralateral somatosensory cortex activation in response to forepaw stimulation. *Neuroimage*, *177*, 30-44. <https://doi.org/https://doi.org/10.1016/j.neuroimage.2018.04.062>
- Shomstein, S. (2012). Cognitive functions of the posterior parietal cortex: top-down and bottom-up attentional control [Mini Review]. *Frontiers in Integrative Neuroscience*, *6*. <https://doi.org/10.3389/fnint.2012.00038>
- Sidman, M. (1953). Avoidance Conditioning with Brief Shock and No Exteroceptive Warning Signal. *Science*, *118*(3058), 157-158. <https://doi.org/doi:10.1126/science.118.3058.157>
- Silveira, K. M., & Joca, S. (2023). Learned Helplessness in Rodents. In J. Harro (Ed.), *Psychiatric Vulnerability, Mood, and Anxiety Disorders: Tests and Models in Mice and Rats* (pp. 161-184). Springer US. https://doi.org/10.1007/978-1-0716-2748-8_9
- Sinex, D. G., & Geisler, C. D. (1981). Auditory-nerve fiber responses to frequency-modulated tones. *Hear Res*, *4*(2), 127-148. [https://doi.org/10.1016/0378-5955\(81\)90001-0](https://doi.org/10.1016/0378-5955(81)90001-0)
- Sirmpllatze, N., Baudewig, J., & Boretius, S. (2019). Temporal stability of fMRI in medetomidine-anesthetized rats. *Sci Rep*, *9*(1), 16673. <https://doi.org/10.1038/s41598-019-53144-y>
- Siveke, I., Myoga, M. H., Grothe, B., & Felmy, F. (2021). Ambient noise exposure induces long-term adaptations in adult brainstem neurons. *Scientific Reports*, *11*(1), 5139. <https://doi.org/10.1038/s41598-021-84230-9>
- Skinner, B. F. (1948). Superstition in the pigeon. *J Exp Psychol*, *38*(2), 168-172. <https://doi.org/10.1037/h0055873>
- Smith, D. M., Barredo, J., & Mizumori, S. J. Y. (2012). Complimentary roles of the hippocampus and retrosplenial cortex in behavioral context discrimination. *Hippocampus*, *22*(5), 1121-1133. <https://doi.org/https://doi.org/10.1002/hipo.20958>
- Smith, D. M., John H. Freeman, J., Nicholson, D., & Gabriel, M. (2002). Limbic Thalamic Lesions, Appetitively Motivated Discrimination Learning, and Training-Induced Neuronal Activity in Rabbits. *The Journal of Neuroscience*, *22*(18), 8212-8221. <https://doi.org/10.1523/jneurosci.22-18-08212.2002>
- Smith, R. L. (1979). Adaptation, saturation, and physiological masking in single auditory-nerve fibers. *The Journal of the Acoustical Society of America*, *65*(1), 166-178.
- Solomon, R. L., Kamin, L. J., & Wynne, L. C. (1953). Traumatic avoidance learning: the outcomes of several extinction procedures with dogs. *J Abnorm Psychol*, *48*(2), 291-302. <https://doi.org/10.1037/h0058943>
- Solomon, R. L., & Wynne, L. C. (1953). Traumatic avoidance learning: Acquisition in normal dogs. *Psychological Monographs: General and Applied*, *67*(4), 1-19. <https://doi.org/10.1037/h0093649>
- Stadler, A., Schima, W., Ba-Ssalamah, A., Kettenbach, J., & Eisenhuber, E. (2007). Artifacts in body MR imaging: their appearance and how to eliminate them. *Eur Radiol*, *17*(5), 1242-1255. <https://doi.org/10.1007/s00330-006-0470-4>
- Stark, H., Bischof, A., & Scheich, H. (1999). Increase of extracellular dopamine in prefrontal cortex of gerbils during acquisition of the avoidance strategy in the shuttle-box. *Neuroscience Letters*, *264*(1), 77-80. [https://doi.org/https://doi.org/10.1016/S0304-3940\(99\)00174-3](https://doi.org/https://doi.org/10.1016/S0304-3940(99)00174-3)
- Stark, H., Rothe, T., Wagner, T., & Scheich, H. (2004). Learning a new behavioral strategy in the shuttle-box increases prefrontal dopamine. *Neuroscience*, *126*(1), 21-29. <https://doi.org/10.1016/j.neuroscience.2004.02.026>
- Stringer, C., Wang, T., Michaelos, M., & Pachitariu, M. (2021). Cellpose: a generalist algorithm for cellular segmentation. *Nature Methods*, *18*(1), 100-106. <https://doi.org/10.1038/s41592-020-01018-x>
- Sul, J. H., Kim, H., Huh, N., Lee, D., & Jung, M. W. (2010). Distinct roles of rodent orbitofrontal and medial prefrontal cortex in decision making. *Neuron*, *66*(3), 449-460. <https://doi.org/10.1016/j.neuron.2010.03.033>
- Sullender, C. T., Richards, L. M., He, F., Luan, L., & Dunn, A. K. (2022). Dynamics of isoflurane-induced vasodilation and blood flow of cerebral vasculature revealed by multi-exposure speckle imaging. *J Neurosci Methods*, *366*, 109434. <https://doi.org/10.1016/j.jneumeth.2021.109434>
- Swanson, L. W. (2015). Brain maps online: Toward open access atlases and a pan-mammalian nomenclature. *Journal of Comparative Neurology*, *523*(15), 2272-2276. <https://doi.org/https://doi.org/10.1002/cne.23788>
- Swift, K. M., Gross, B. A., Frazer, M. A., Bauer, D. S., Clark, K. J. D., Vazey, E. M., Aston-Jones, G., Li, Y., Pickering, A. E., Sara, S. J., & Poe, G. R. (2018). Abnormal Locus Coeruleus Sleep Activity Alters Sleep Signatures of Memory Consolidation and Impairs Place Cell Stability and Spatial Memory. *Current Biology*, *28*(22), 3599-3609.e3594. <https://doi.org/10.1016/j.cub.2018.09.054>
- Syed, E. C., Sharott, A., Moll, C. K., Engel, A. K., & Kral, A. (2011). Effect of sensory stimulation in rat barrel cortex, dorsolateral striatum and on corticostriatal functional connectivity. *Eur J Neurosci*, *33*(3), 461-470. <https://doi.org/10.1111/j.1460-9568.2010.07549.x>
- Syka, J., & Straschill, M. (1970). Activation of superior colliculus neurons and motor responses after electrical stimulation of the inferior colliculus. *Experimental Neurology*, *28*(3), 384-392. [https://doi.org/https://doi.org/10.1016/0014-4886\(70\)90175-5](https://doi.org/https://doi.org/10.1016/0014-4886(70)90175-5)
- Szczepaniak, W. S., & Möller, A. R. (1996). Evidence of neuronal plasticity within the inferior colliculus after noise exposure: a study of evoked potentials in the rat. *Electroencephalography and clinical neurophysiology*, *100* 2, 158-164.
- Taber, K. H., Wen, C., Khan, A., & Hurley, R. A. (2004). The Limbic Thalamus. *The Journal of Neuropsychiatry and Clinical Neurosciences*, *16*(2), 127-132. <https://doi.org/10.1176/jnp.16.2.127>
- Talavage, T., Edmister, W., Ledden, P., & Weisskoff, R. (1998). Quantification of the impact of fMRI scanner noise on auditory cortex. Proceedings of the 6th Annual meeting of the International Society for Magnetic Resonance in Medicine. p.
- Talavage, T. M., & Edmister, W. B. (2004). Nonlinearity of FMRI responses in human auditory cortex. *Hum Brain Mapp*, *22*(3), 216-228. <https://doi.org/10.1002/hbm.20029>
- Talavage, T. M., Edmister, W. B., Ledden, P. J., & Weisskoff, R. M. (1999). Quantitative assessment of auditory cortex responses induced by imager acoustic noise. *Hum Brain Mapp*, *7*(2), 79-88. [https://doi.org/10.1002/\(SICI\)1097-0193\(1999\)7:2<#x0003c;79::AID-HBM1>#x0003e;3.0.CO;2-R](https://doi.org/10.1002/(SICI)1097-0193(1999)7:2<#x0003c;79::AID-HBM1>#x0003e;3.0.CO;2-R)
- Tang, J., Wagner, S., Schachner, M., Dityatev, A., & Wotjak, C. T. (2003). Potentiation of amygdaloid and hippocampal auditory-evoked potentials in a discriminatory fear-conditioning task in mice as a function of tone pattern and context. *European Journal of Neuroscience*, *18*(3), 639-650. <https://doi.org/https://doi.org/10.1046/j.1460-9568.2003.02758.x>
- Taylor, J. A., Hasegawa, M., Benoit, C. M., Freire, J. A., Theodore, M., Ganea, D. A., Innocenti, S. M., Lu, T., & Gründemann, J. (2021). Single cell plasticity and population coding stability in auditory thalamus upon associative learning. *Nature Communications*, *12*(1), 2438. <https://doi.org/10.1038/s41467-021-22421-8>

- Teoh, S. W., Flandermeier, D. T., & Rosowski, J. J. (1997). Effects of pars flaccida on sound conduction in ears of Mongolian gerbil: acoustic and anatomical measurements. *Hear Res*, *106*(1-2), 39-65. [https://doi.org/10.1016/S0378-5955\(97\)00002-6](https://doi.org/10.1016/S0378-5955(97)00002-6)
- Theios, J., & Dunaway, J. E. (1964). One-way versus shuttle avoidance conditioning. *Psychonomic Science*, *1*(1), 251-252. <https://doi.org/10.3758/BF03342894>
- Thomas, H., Tillein, J., Heil, P., & Scheich, H. (1993). Functional organization of auditory cortex in the mongolian gerbil (*Meriones unguiculatus*). I. Electrophysiological mapping of frequency representation and distinction of fields. *Eur J Neurosci*, *5*(7), 882-897. <https://doi.org/10.1111/j.1460-9568.1993.tb00940.x>
- Todd, T. P., Mehlman, M. L., Keene, C. S., DeAngeli, N. E., & Bucci, D. J. (2016). Retrosplenial cortex is required for the retrieval of remote memory for auditory cues. *Learn Mem*, *23*(6), 278-288. <https://doi.org/10.1101/lm.041822.116>
- Tomasi, D., Caparelli, E. C., Chang, L., & Ernst, T. (2005). fMRI-acoustic noise alters brain activation during working memory tasks. *Neuroimage*, *27*(2), 377-386. <https://doi.org/10.1016/j.neuroimage.2005.04.010>
- Trevino, M., Zang, A., & Lobarinas, E. (2023). The middle ear muscle reflex: Current and future role in assessing noise-induced cochlear damage. *The Journal of the Acoustical Society of America*, *153*(1), 436-445. <https://doi.org/10.1121/10.0016853>
- Trusel, M., Nuno-Perez, A., Lecca, S., Harada, H., Lalive, A. L., Congiu, M., Takemoto, K., Takahashi, T., Ferraguti, F., & Mamei, M. (2019). Punishment-Predictive Cues Guide Avoidance through Potentiation of Hypothalamus-to-Habenula Synapses. *Neuron*, *102*(1), 120-127.e124. <https://doi.org/10.1016/j.neuron.2019.01.025>
- Tsurugizawa, T., Tamada, K., Debacker, C., Zalesky, A., & Takumi, T. (2021). Cranioplastic Surgery and Acclimation Training for Awake Mouse fMRI. *Bio-protocol*, *11*(7), e3972. <https://doi.org/10.21769/BioProtoc.3972>
- Tyng, C. M., Amin, H. U., Saad, M. N. M., & Malik, A. S. (2017). The Influences of Emotion on Learning and Memory [Review]. *Frontiers in Psychology*, *8*. <https://doi.org/10.3389/fpsyg.2017.01454>
- van Ackooij, M., Paul, J. M., van der Zwaag, W., van der Stoep, N., & Harvey, B. M. (2022). Auditory timing-tuned neural responses in the human auditory cortices. *Neuroimage*, *258*, 119366. <https://doi.org/https://doi.org/10.1016/j.neuroimage.2022.119366>
- Van Audenhaege, K., Van Holen, R., Vandenberghe, S., Vanhove, C., Metzler, S. D., & Moore, S. C. (2015). Review of SPECT collimator selection, optimization, and fabrication for clinical and preclinical imaging. *Med Phys*, *42*(8), 4796-4813. <https://doi.org/10.1118/1.4927061>
- Van Egroo, M., Koshmanova, E., Vandewalle, G., & Jacobs, H. I. L. (2022). Importance of the locus coeruleus-norepinephrine system in sleep-wake regulation: Implications for aging and Alzheimer's disease. *Sleep Medicine Reviews*, *62*, 101592. <https://doi.org/https://doi.org/10.1016/j.smrv.2022.101592>
- Vann, S. D., Aggleton, J. P., & Maguire, E. A. (2009). What does the retrosplenial cortex do? *Nature reviews Neuroscience*, *10*(11), 792-802. <https://doi.org/10.1038/nrn2733>
- Vedder, L. C., Miller, A. M. P., Harrison, M. B., & Smith, D. M. (2017). Retrosplenial Cortical Neurons Encode Navigational Cues, Trajectories and Reward Locations During Goal Directed Navigation. *Cereb Cortex*, *27*(7), 3713-3723. <https://doi.org/10.1093/cercor/bhw192>
- Vetter, D. E. (2015). Cellular signaling protective against noise-induced hearing loss – A role for novel intrinsic cochlear signaling involving corticotropin-releasing factor? *Biochem Pharmacol*, *97*(1), 1-15. <https://doi.org/10.1016/j.bcp.2015.06.011>
- Vieira, P. A., Corches, A., Lovelace, J. W., Westbrook, K. B., Mendoza, M., & Korzus, E. (2015). Prefrontal NMDA receptors expressed in excitatory neurons control fear discrimination and fear extinction. *Neurobiology of Learning and Memory*, *119*, 52-62. <https://doi.org/https://doi.org/10.1016/j.nlm.2014.12.012>
- Vieira, P. A., Lovelace, J. W., Corches, A., Rashid, A. J., Josselyn, S. A., & Korzus, E. (2014). Prefrontal consolidation supports the attainment of fear memory accuracy. *Learn Mem*, *21*(8), 394-405. <https://doi.org/10.1101/lm.036087.114>
- Vogt, B. A., & Paxinos, G. (2014). Cytoarchitecture of mouse and rat cingulate cortex with human homologies. *Brain Structure and Function*, *219*(1), 185-192. <https://doi.org/10.1007/s00429-012-0493-3>
- Vogt, L. J., Vogt, B. A., & Sikes, R. W. (1992). Limbic thalamus in rabbit: architecture, projections to cingulate cortex and distribution of muscarinic acetylcholine, GABA, and opioid receptors. *J Comp Neurol*, *319*(2), 205-217. <https://doi.org/10.1002/cne.903190203>
- Walker, J. J. (2009). Overview of limbic system anatomy and organization. *The FASEB Journal*, *23*(S1), 301.301-301.301. https://doi.org/https://doi.org/10.1096/fasebj.23.1_supplement.301.1
- Webb, A. G. (2003). *Introduction to Biomedical Imaging*. Wiley. https://books.google.de/books?id=WcQ_DwAAQBAJ
- Weber, R., Ramos-Cabrer, P., Wiedermann, D., van Camp, N., & Hoehn, M. (2006). A fully noninvasive and robust experimental protocol for longitudinal fMRI studies in the rat. *Neuroimage*, *29*(4), 1303-1310. <https://doi.org/https://doi.org/10.1016/j.neuroimage.2005.08.028>
- Weera, M. M., Shackett, R. S., Kramer, H. M., Middleton, J. W., & Gilpin, N. W. (2021). Central Amygdala Projections to Lateral Hypothalamus Mediate Avoidance Behavior in Rats. *J Neurosci*, *41*(1), 61-72. <https://doi.org/10.1523/jneurosci.0236-20.2020>
- Weinberger, N. M., Javid, R., & Lapan, B. (1993). Long-term retention of learning-induced receptive-field plasticity in the auditory cortex. *Proceedings of the National Academy of Sciences*, *90*(6), 2394-2398. <https://doi.org/doi:10.1073/pnas.90.6.2394>
- Weishaupt, D., Froehlich, J. M., Nanz, D., Köchli, V. D., Prüßmann, K. P., & Marincek, B. (2009). *Wie funktioniert MRI?: Eine Einführung in Physik und Funktionsweise der Magnetresonanztomographie*. Springer Berlin Heidelberg. <https://books.google.de/books?id=vCjy1QecdekC>
- Westerman, L. A., & Smith, R. L. (1984). Rapid and short-term adaptation in auditory nerve responses. *Hearing Research*, *15*(3), 249-260. [https://doi.org/https://doi.org/10.1016/0378-5955\(84\)90032-7](https://doi.org/https://doi.org/10.1016/0378-5955(84)90032-7)
- Wetzel, W., Ohl, F. W., & Scheich, H. (2008). Global versus local processing of frequency-modulated tones in gerbils: an animal model of lateralized auditory cortex functions. *Proc Natl Acad Sci U S A*, *105*(18), 6753-6758. <https://doi.org/10.1073/pnas.0707844105>
- Wetzel, W., Ohl, F. W., Wagner, T., & Scheich, H. (1998). Right auditory cortex lesion in Mongolian gerbils impairs discrimination of rising and falling frequency-modulated tones. *Neurosci Lett*, *252*(2), 115-118. <https://www.ncbi.nlm.nih.gov/pubmed/9756335>
- Wetzel, W., Wagner, T., Ohl, F. W., & Scheich, H. (1998). Categorical discrimination of direction in frequency-modulated tones by Mongolian gerbils. *Behav Brain Res*, *91*(1-2), 29-39. [https://doi.org/10.1016/S0166-4328\(97\)00099-5](https://doi.org/10.1016/S0166-4328(97)00099-5)
- Whittaker, J. R., Driver, I. D., Bright, M. G., & Murphy, K. (2016). The absolute CBF response to activation is preserved during elevated perfusion: Implications for neurovascular coupling measures. *Neuroimage*, *125*, 198-207. <https://doi.org/https://doi.org/10.1016/j.neuroimage.2015.10.023>
- Wieland, S., Schindler, S., Huber, C., Köhr, G., Oswald, M. J., & Kelsch, W. (2015). Phasic Dopamine Modifies Sensory-Driven Output of Striatal Neurons through Synaptic Plasticity. *J Neurosci*, *35*(27), 9946-9956. <https://doi.org/10.1523/jneurosci.0127-15.2015>
- Wilkinson, F. (1986). Eye and brain growth in the Mongolian gerbil (*Meriones unguiculatus*). *Behav Brain Res*, *19*(1), 59-69. [https://doi.org/10.1016/0166-4328\(86\)90048-3](https://doi.org/10.1016/0166-4328(86)90048-3)
- Williams, L. M. (2017). Defining biotypes for depression and anxiety based on large-scale circuit dysfunction: a theoretical review of the evidence and future directions for clinical translation. *Depression and Anxiety*, *34*(1), 9-24. <https://doi.org/https://doi.org/10.1002/da.22556>
- Williams, R. W., & Levis, D. J. (1991). A demonstration of persistent human avoidance in extinction. *Bulletin of the Psychonomic Society*, *29*(2), 125-127. <https://doi.org/10.3758/BF0335212>
- Willmore, B. D. B., & King, A. J. (2023). Adaptation in auditory processing. *Physiological Reviews*, *103*(2), 1025-1058. <https://doi.org/10.1152/physrev.00011.2022>
- Wolak, T., Ciesla, K., Wojcik, J., & Skarzynski, H. (2017). Effect of Sound Intensity on Level of Activation in Auditory Cortex as Measured by fMRI [journal article]. *Journal of Hearing Science*, *7*(4), 20-27. <https://doi.org/10.17430/1002807>
- Woldeit, M. L., Schulz, A. L., & Ohl, F. W. (2012). Phase de-synchronization effects auditory gating in the ventral striatum but not auditory cortex. *Neuroscience*, *216*, 70-81. <https://doi.org/10.1016/j.neuroscience.2012.04.058>
- Wolff, S., & Brechmann, A. (2023). Dorsal posterior cingulate cortex responds to negative feedback information supporting learning and relearning of response policies. *Cereb Cortex*, *33*(10), 5947-5956. <https://doi.org/10.1093/cercor/bhac473>
- Xie, R., Gittelman, J. X., Li, N., & Pollak, G. D. (2008). Whole cell recordings of intrinsic properties and sound-evoked responses from the inferior colliculus. *Neuroscience*, *154*(1), 245-256. <https://doi.org/https://doi.org/10.1016/j.neuroscience.2008.02.039>
- Xiong, Q., Znamenskiy, P., & Zador, A. M. (2015). Selective corticostriatal plasticity during acquisition of an auditory discrimination task. *Nature*, *521*(7552), 348-351. <https://doi.org/10.1038/nature14225>
- Xu, N., LaGrow, T. J., Anumba, N., Lee, A., Zhang, X., Yousefi, B., Bassil, Y., Clavijo, G. P., Khalilzad Sharghi, V., Maltbie, E., Meyer-Baese, L., Nezafati, M., Pan, W.-J., & Keilholz, S. (2022). Functional Connectivity of the Brain Across Rodents and Humans [Review]. *Frontiers in Neuroscience*, *16*. <https://doi.org/10.3389/fnins.2022.816331>
- Xu, Y. Y., Ge, J. F., Qin, G., Peng, Y. N., Zhang, C. F., Liu, X. R., Liang, L. C., Wang, Z. Z., Chen, F. H., & Li, J. (2015). Acute, but not chronic, stress increased the plasma concentration and hypothalamic mRNA expression of NUCB2/nesfatin-1 in rats. *Neuropeptides*, *54*, 47-53. <https://doi.org/10.1016/j.npep.2015.08.003>
- Yang, Q. X., Smith, M. B., & Wang, J. (2006). Magnetic Susceptibility Effects in High Field MRI. In *Ultra High Field Magnetic Resonance Imaging* (pp. 249-284). Springer US. https://doi.org/10.1007/978-0-387-49648-1_9

- Yin, S., Liu, Y., Petro, N. M., Keil, A., & Ding, M. (2018). Amygdala Adaptation and Temporal Dynamics of the Salience Network in Conditioned Fear: A Single-Trial fMRI Study. *eNeuro*, 5(1). <https://doi.org/10.1523/eneuro.0445-17.2018>
- Yip, D. W., & Lui, F. (2023). Physiology, Motor Cortical. In *StatPearls*. StatPearls Publishing. Copyright © 2023, StatPearls Publishing LLC.
- Yoo, P. E., John, S. E., Farquharson, S., Cleary, J. O., Wong, Y. T., Ng, A., Mulcahy, C. B., Grayden, D. B., Ordidge, R. J., Opie, N. L., O'Brien, T. J., Oxley, T. J., & Moffat, B. A. (2018). 7T-fMRI: Faster temporal resolution yields optimal BOLD sensitivity for functional network imaging specifically at high spatial resolution. *Neuroimage*, 164, 214-229. <https://doi.org/https://doi.org/10.1016/j.neuroimage.2017.03.002>
- Yoshida, K., Mimura, Y., Ishihara, R., Nishida, H., Komaki, Y., Minakuchi, T., Tsurugizawa, T., Mimura, M., Okano, H., Tanaka, K. F., & Takata, N. (2016). Physiological effects of a habituation procedure for functional MRI in awake mice using a cryogenic radiofrequency probe. *J Neurosci Methods*, 274, 38-48. <https://doi.org/10.1016/j.jneumeth.2016.09.013>
- Yoshida, N., & Liberman, M. C. (2000). Sound conditioning reduces noise-induced permanent threshold shift in mice. *Hearing Research*, 148(1), 213-219. [https://doi.org/https://doi.org/10.1016/S0378-5955\(00\)00161-1](https://doi.org/https://doi.org/10.1016/S0378-5955(00)00161-1)
- Yost, W. A. (2002). Auditory Perception. In V. S. Ramachandran (Ed.), *Encyclopedia of the Human Brain* (pp. 303-320). Academic Press. <https://doi.org/https://doi.org/10.1016/B0-12-227210-2/00047-9>
- Yu, X., Wadghiri, Y. Z., Sanes, D. H., & Turnbull, D. H. (2005). In vivo auditory brain mapping in mice with Mn-enhanced MRI. *Nature Neuroscience*, 8(7), 961-968. <https://doi.org/10.1038/nn1477>
- Yuan, C. W., Khouri, L., Grothe, B., & Leibold, C. (2014). Neuronal adaptation translates stimulus gaps into a population code. *PLoS One*, 9(4), e95705. <https://doi.org/10.1371/journal.pone.0095705>
- Zatorre, R. J., Belin, P., & Penhune, V. B. (2002). Structure and function of auditory cortex: music and speech. *Trends Cogn Sci*, 6(1), 37-46. <https://www.ncbi.nlm.nih.gov/pubmed/11849614>
- Zerarka, S., Pellerin, L., Slosman, D., & Magistretti, P. J. (2001). Astrocytes as a predominant cellular site of (99m)Tc-HMPAO retention. *J Cereb Blood Flow Metab*, 21(4), 456-468. <https://doi.org/10.1097/00004647-200104000-00014>
- Zerbi, V., Grandjean, J., Rudin, M., & Wenderoth, N. (2015). Mapping the mouse brain with rs-fMRI: An optimized pipeline for functional network identification. *Neuroimage*, 123, 11-21. <https://doi.org/10.1016/j.neuroimage.2015.07.090>
- Zhang, G. W., Sun, W. J., Zingg, B., Shen, L., He, J., Xiong, Y., Tao, H. W., & Zhang, L. I. (2018). A Non-canonical Reticular-Limbic Central Auditory Pathway via Medial Septum Contributes to Fear Conditioning. *Neuron*, 97(2), 406-417.e404. <https://doi.org/10.1016/j.neuron.2017.12.010>
- Zhang, W.-H., Zhang, J.-Y., Holmes, A., & Pan, B.-X. (2021). Amygdala Circuit Substrates for Stress Adaptation and Adversity. *Biological Psychiatry*, 89(9), 847-856. <https://doi.org/https://doi.org/10.1016/j.biopsych.2020.12.026>
- Zhao, F., Wang, P., Hendrich, K., Ugurbil, K., & Kim, S.-G. (2006). Cortical layer-dependent BOLD and CBV responses measured by spin-echo and gradient-echo fMRI: Insights into hemodynamic regulation. *Neuroimage*, 30(4), 1149-1160. <https://doi.org/https://doi.org/10.1016/j.neuroimage.2005.11.013>
- Znamenskiy, P., & Zador, A. M. (2013). Corticostriatal neurons in auditory cortex drive decisions during auditory discrimination. *Nature*, 497(7450), 482-485. <https://doi.org/10.1038/nature12077>

Appendix

List of Figures

Figure 1: Structures of the auditory pathway in human and rodent brain.....	2
Figure 2: Hearing range of humans, rats, mice and gerbils.....	4
Figure 3: Radiofrequency signal after excitation with an RF pulse with 90° flip angle	6
Figure 4: Hemodynamic response function to sensory stimulation	8
Figure 5: Protocol for auditory stimulations with pulsed presentation of the stimulation tone.....	15
Figure 6: Stability of different anaesthesia regimes during fMRI acquisition	17
Figure 7: fMRI image quality of different optimized sequence types acquired with a 20 mm surface coil.....	18
Figure 8: Functional images acquired with optimized mode of GRE-EPI acquisition.....	19
Figure 9: Auditory activation patterns acquired with GRE-EPI after sequence optimization	20
Figure 10: Auditory activation patterns acquired with ZTE sequence after SPIO injection	21
Figure 11: Sound profiles of different stimulation tones vs. GRE-EPI noise	22
Figure 12: Overview of final auditory fMRI measurement setup.....	23
Figure 13: Auditory-evoked brain activation in the Mongolian gerbil with optimized auditory fMRI	26
Figure 14: Auditory stimulation protocol for CBF SPECT study on medetomidine anaesthesia and GRE-EPI noise effects.....	40
Figure 15: CBF distribution in the brain of awake gerbils with and without auditory stimulation	45
Figure 16: Comparison of AC activation to auditory stimulation with 1-2 kHz FM tones in awake and medetomidine-anaesthetized gerbils.....	46
Figure 17: Subcortical activation to auditory stimulation with 1-2 kHz in awake and medetomidine- anaesthetized animals.....	47
Figure 18: Auditory-evoked BOLD response measured with fMRI during simultaneous CBF-tracer injection.....	48
Figure 19: Mean CBF of medetomidine-anaesthetized animals under different conditions with and without 1-2 kHz stimulation	49
Figure 20: 1-2 kHz stimulation induced CBF increase under different conditions and GRE-EPI effect.....	50
Figure 21: 3D-rendered auditory-evoked CBF increase due to 1-2 kHz stimulation shows a shift of peak activation with concurring GRE-EPI noise in rAC.....	51
Figure 22: Direct comparison of patterns for auditory-evoked CBF and BOLD increase	53
Figure 23: Scheme of a shuttlebox in an aversive avoidance paradigm.....	60
Figure 24: Key regions in rodent and human involved in aversive processing*.....	62
Figure 25: Timeline of the performed fMRI measurements throughout the course of the FM direction discrimination training.....	64
Figure 26: Auditory stimulation protocols for discrimination learning fMRI	66
Figure 27: Motion correction (3 translations, 3 rotations) of two MR scans performed in the same animal.....	68
Figure 28: Brain activation patterns to the three different stimulation tones prior to the direction discrimination training.....	70
Figure 29: STC, ERA and BETA values for the three stimulation tones prior to the discrimination training.....	71
Figure 30: Behavioural scores of the gerbils during their discrimination training without aP	72

Figure 31: Brain activation changes induced by FM direction discrimination learning without aP	73
Figure 32: Separation into groups of good and bad learners by average discrimination performance in FM direction discrimination training without aP	75
Figure 33: Auditory brain activation patterns of good and bad learners throughout discrimination training..	77
Figure 34: Statistical comparison of good and bad learners throughout discrimination training without aP...	79
Figure 35: Correlation of learning performance in discrimination training and brain activation	80
Figure 36: Brain activation at expected time of reinforcement shock in animals trained without aP	81
Figure 37: Brain activation at time of reinforcement shock for bad learners trained without aP	82
Figure 38: Performance of gerbils in discrimination training with aP	83
Figure 39: Brain activation of good and bad learners throughout discrimination training with aP	85
Figure 40: Statistical comparison of good and bad learners in discrimination training with aP	86
Figure 41: Correlation of learning performance in discrimination training with aP and brain activation	87
Figure 42: Brain activation at the time of reinforcement shock in discrimination training with aP	88
Figure 43: Brain activation at time of reinforcement for bad learners in discrimination training without aP ..	89
Figure 44: Effect of aP on outcome of direction discrimination training	90
Figure 45: Effect of aP in discrimination training on brain activation patterns in bad learners	92
Figure 46: Correlation of learning performance and brain activation at time of reinforcement.....	93
Figure 47: Overview of discrimination learning effects in Mongolian gerbils acquired with auditory fMRI ...	105
Figure S 1: Loudspeakers and headphones for auditory stimulation delivery into the MRI scanner.....	C
Figure S 2: Coronal sections of the gerbil brain showing the auditory brain activation patterns of (A) bad and (B) good learners after 10 days of discrimination training without aP for the GO tone stimulation F	
Figure S 3: Other brain areas showing differences between good and bad learners during discrimination training without aP	H
Figure S 4: Brain areas showing additional statistically significant differences due to discrimination training without aP at time of reinforcement.....	J
Figure S 5: Other brain areas showing differences between good and bad learners during discrimination training with aP	N
Figure S 6: Brain areas showing additional statistically significant differences due to discrimination training with aP at time of reinforcement.....	O
Figure S 7: There is no impact of injection of e6-chlorine-conjugated retrobeads as shown here in exemplary animals of the FM direction discrimination training group with aP	S
Figure S 8: There is no impact of photolytic lesioning on neuronal density (NeuN staining)	T
Figure S 9: There is no impact of surgical interventions on animals' behaviour in the direction discrimination training without aP	U
Figure S 10: There is no impact of surgical interventions on animals' behaviour in the direction discrimination training of the animals with aP	V
Figure S 11: There is no impact of the tracer injections on the brain activation pattern recorded with auditory fMRI of animals trained without aP	W

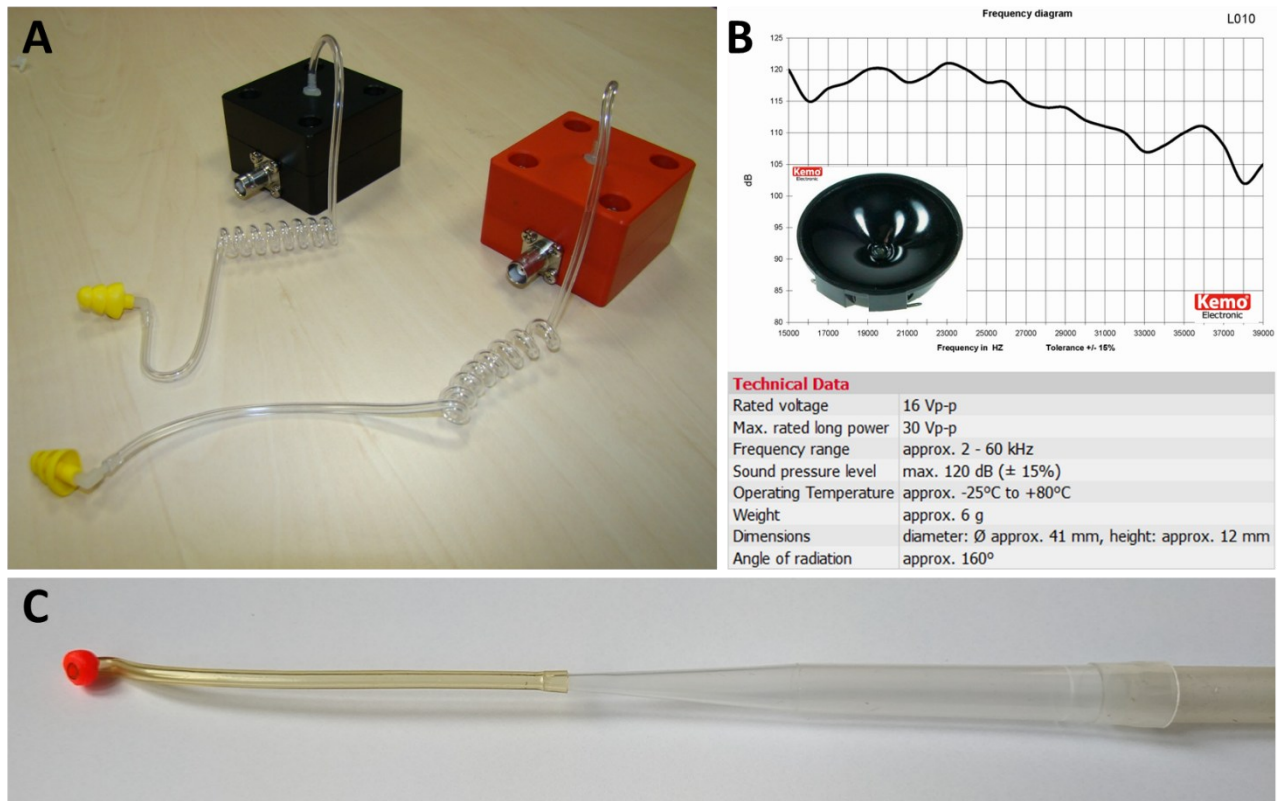


Figure S 1: Loudspeakers and headphones for auditory stimulation delivery into the MRI scanner
A. Overall sound delivery system for fMRI built in-house by Andreas Fügner with **(B)** piezo loudspeakers (L010, Kemo Electronic GmbH, Germany). **C.** Adjusted headphones for small animal fMRI application, tips of sound delivery tubes enveloped with pliable earplug mass (Pillow Soft Silicone Putty Earplugs, Mack's, USA) to enable a tight fit and dampen the MR scanner noise during fMRI acquisition.

Table 4: Gerbil brain atlas regions used for VOI-based fMRI analysis

Grouped regions implemented for VOI-analysis are marked bold writing. Hierarchy of the regions decreases from left to right, for better understanding of the grouping of some ambiguous areas their substructures are explicitly stated in the list.

endbrain	cerebral cortex	isocortex	auditory areas (AC)	<i>primary auditory cortex</i> <i>secondary auditory cortex, dorsal area</i> <i>secondary auditory cortex, ventral area</i> <i>temporal association cortex</i>
			somatosensory areas	
			motor areas	
			visual areas	
			retrosplenial areas (RSC)	
			posterior parietal areas	
			insular areas	
			medial prefrontal areas (mPFC)	<i>infralimbic cortex</i> <i>prelimbic cortex</i> <i>cingulate cortex</i>
			frontal areas	
			orbital areas	
			olfactory areas	olfactory bulb accessory olfactory bulb anterior olfactory nucleus cortical amygdala ...
			hippocampal formation	hippocampus
	subiculum			
	retrohippocampal areas			
cerebral nuclei	striatum	dorsal striatum		
		ventral striatum		
	pallidum	dorsal pallidum		
		ventral pallidum		
	amygdala			
further cerebral nuclei	septal nuclei	claustrum endopiriform nucleus bed nucleus of stria terminalis ...		

--- Table 4 continued on following page ---

--- Table 4 continued from previous page ---

interbrain	thalamus dorsalis (Th)	anterior group medial group ventral group dorsal group posterior group intralaminar group median group reticular thalamic nucleus
	metathalamus	medial geniculate body (MGB) lateral geniculate body ventral geniculate body
	epithalamus	habenula pretectal nuclei
	subthalamus	zona incerta subthalamic nucleus
	hypothalamus	anterior hypothalamus preoptic hypothalamus dorsal hypothalamus lateral hypothalamus para-/periventricular hypothalamus posterior hypothalamus ventral hypothalamus mammillary region of hypothalamus
midbrain	tectum mesencephalon	inferior colliculus (IC) superior colliculus nucleus of the posterior commissure precommissural nucleus tectal grey
	tegmentum mesencephalon	periaqueductal gray ventral tegmental area substantia nigra red nucleus ...
(hindbrain & midbrain)		raphe nuclei
hindbrain	pons	superior olivary complex nuclei of lateral lemniscus parabrachial nuclei locus coeruleus ...
	cerebellum	cerebellar lobuli cerebellar nuclei cerebellar peduncles
	medulla oblongata	cochlear nuclei inferior olive restibular nuclei reticular nuclei myelencephalic ...

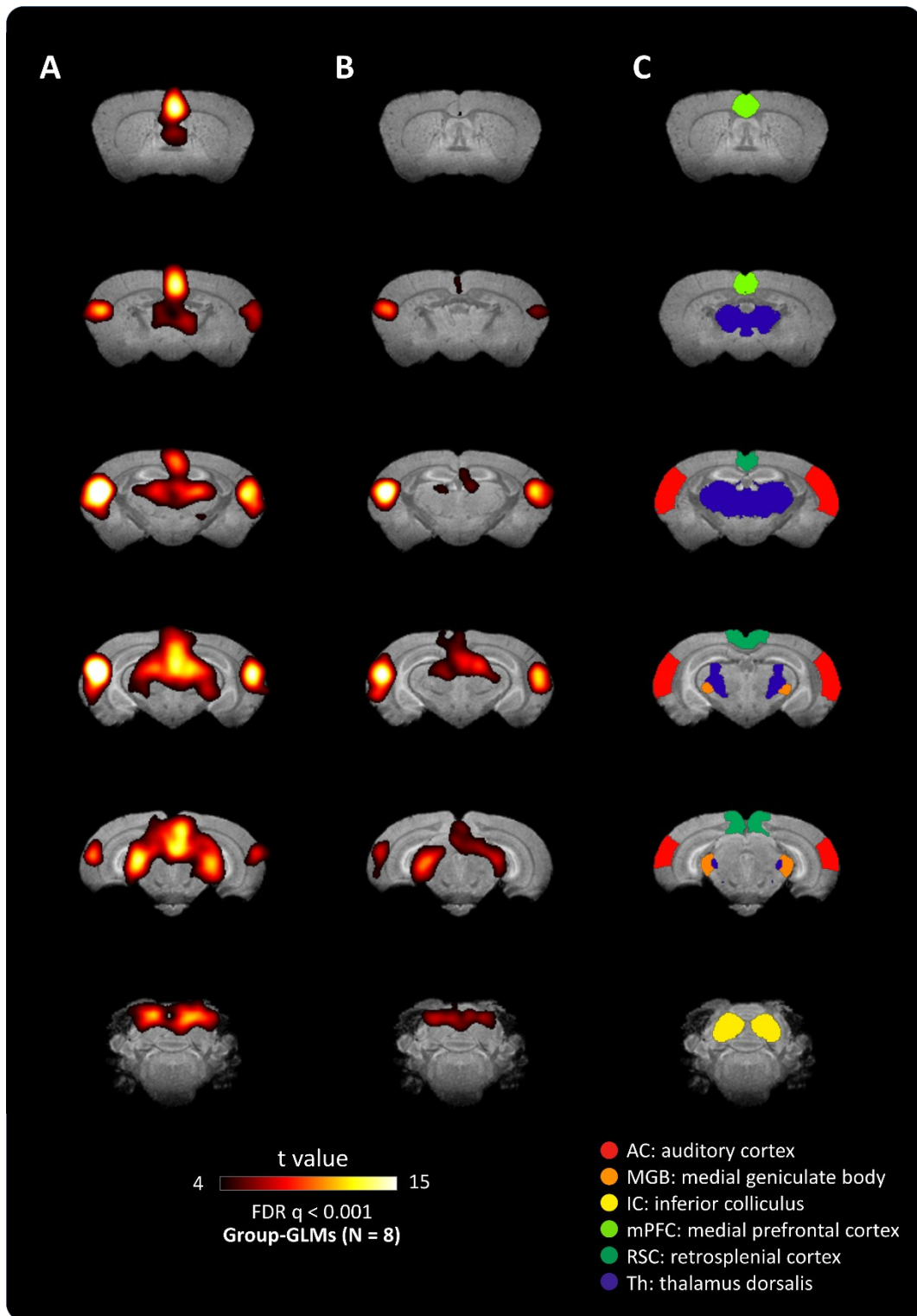


Figure S 2: Coronal sections of the gerbil brain showing the auditory brain activation patterns of (A) bad and (B) good learners after 10 days of discrimination training without aP for the GO tone stimulation
Bad learners show a lot more activation in the midbrain (including Th and MGB) and the neuromodulatory cortical brain structures mPFC and RSC.

Table 5: BETA values for good and bad learners trained without aP

Changes to the previous measurement that are bigger than the previous SEM are marked with ↓ for decrease and with ↑ for increase in BETA values. All values are given as mean and SEM in % (N=8 per group; i: Exclusion of one bad learner from 3-days-training measurement analysis due to motion artefacts).

		BETA values (%) of <i>good learners</i>			BETA values (%) of <i>bad learners</i>		
	training	GO mean ± SEM	nGo mean ± SEM	control mean ± SEM	GO mean ± SEM	noGo mean ± SEM	control mean ± SEM
AC	pre	0.54 ± 0.02	0.48 ± 0.04	0.29 ± 0.03	0.46 ± 0.06	0.37 ± 0.06	0.24 ± 0.06
	3 days	↓ 0.45 ± 0.03	↓ 0.41 ± 0.03	↓ 0.25 ± 0.04	0.49 ± 0.07	↑ 0.52 ± 0.10	0.20 ± 0.05
	10 days	↑ 0.48 ± 0.03	0.41 ± 0.04	↑ 0.32 ± 0.07	↑ 0.62 ± 0.10	0.57 ± 0.09	↑ 0.36 ± 0.08
rAC	pre	0.42 ± 0.04	0.41 ± 0.04	0.26 ± 0.03	0.39 ± 0.06	0.32 ± 0.06	0.22 ± 0.07
	3 days	↓ 0.37 ± 0.05	↓ 0.33 ± 0.04	↓ 0.22 ± 0.04	0.42 ± 0.05	↑ 0.45 ± 0.08	0.19 ± 0.05
	10 days	0.35 ± 0.04	0.29 ± 0.02	0.23 ± 0.03	↑ 0.49 ± 0.09	0.49 ± 0.07	↑ 0.31 ± 0.09
lAC	pre	0.66 ± 0.04	0.56 ± 0.07	0.31 ± 0.05	0.53 ± 0.07	0.44 ± 0.06	0.28 ± 0.05
	3 days	↓ 0.52 ± 0.03	↓ 0.49 ± 0.04	↓ 0.26 ± 0.05	↑ 0.61 ± 0.12	↑ 0.63 ± 0.13	↓ 0.21 ± 0.06
	10 days	↑ 0.62 ± 0.06	↑ 0.54 ± 0.06	↑ 0.40 ± 0.11	↑ 0.79 ± 0.14	0.67 ± 0.12	↑ 0.43 ± 0.08
MGB	pre	0.27 ± 0.05	0.33 ± 0.05	0.28 ± 0.05	0.22 ± 0.05	0.20 ± 0.04	0.18 ± 0.05
	3 days	↑ 0.49 ± 0.05	0.35 ± 0.05	0.26 ± 0.05	↑ 0.41 ± 0.05	↑ 0.38 ± 0.04	0.17 ± 0.05
	10 days	↓ 0.31 ± 0.04	↓ 0.26 ± 0.03	0.24 ± 0.06	↑ 0.52 ± 0.05	0.41 ± 0.06	↑ 0.34 ± 0.06
IC	pre	0.16 ± 0.03	0.17 ± 0.05	0.21 ± 0.05	0.08 ± 0.05	0.11 ± 0.04	0.17 ± 0.06
	3 days	↑ 0.25 ± 0.03	↑ 0.22 ± 0.05	↑ 0.33 ± 0.04	↑ 0.22 ± 0.02	↑ 0.20 ± 0.04	↑ 0.24 ± 0.03
	10 days	↓ 0.20 ± 0.04	↓ 0.17 ± 0.04	↓ 0.26 ± 0.03	0.23 ± 0.04	↑ 0.25 ± 0.05	↑ 0.29 ± 0.04
mPFC	pre	-0.02 ± 0.02	-0.04 ± 0.02	-0.01 ± 0.04	0.01 ± 0.04	-0.01 ± 0.04	-0.03 ± 0.03
	3 days	↑ 0.12 ± 0.04	↑ 0.06 ± 0.04	0.01 ± 0.03	↑ 0.10 ± 0.05	↑ 0.17 ± 0.07	0.01 ± 0.03
	10 days	↓ 0.06 ± 0.02	0.05 ± 0.02	↑ 0.04 ± 0.03	↑ 0.31 ± 0.08	↑ 0.26 ± 0.07	↑ 0.13 ± 0.05
RSC	pre	0.13 ± 0.03	0.15 ± 0.05	0.04 ± 0.08	0.15 ± 0.06	0.11 ± 0.02	0.05 ± 0.05
	3 days	↑ 0.20 ± 0.04	0.18 ± 0.03	0.06 ± 0.05	↑ 0.24 ± 0.04	↑ 0.29 ± 0.06	0.00 ± 0.02
	10 days	↓ 0.10 ± 0.03	↓ 0.10 ± 0.04	0.06 ± 0.03	↑ 0.34 ± 0.06	0.31 ± 0.06	↑ 0.16 ± 0.06
Th	pre	0.10 ± 0.02	0.12 ± 0.03	0.09 ± 0.03	0.12 ± 0.03	0.08 ± 0.02	0.07 ± 0.02
	3 days	↑ 0.19 ± 0.02	↑ 0.17 ± 0.03	0.06 ± 0.04	↑ 0.20 ± 0.02	↑ 0.23 ± 0.05	↓ 0.03 ± 0.02
	10 days	↓ 0.11 ± 0.02	↓ 0.11 ± 0.02	0.06 ± 0.02	↑ 0.26 ± 0.04	0.24 ± 0.04	↑ 0.14 ± 0.04
septal nuclei	pre	0.03 ± 0.01	0.04 ± 0.03	0.02 ± 0.03	0.07 ± 0.03	0.06 ± 0.02	0.03 ± 0.01
	3 days	↑ 0.14 ± 0.04	↑ 0.08 ± 0.03	0.04 ± 0.02	↑ 0.12 ± 0.02	↑ 0.18 ± 0.05	0.03 ± 0.02
	10 days	↓ 0.06 ± 0.01	0.07 ± 0.02	0.03 ± 0.03	↑ 0.19 ± 0.04	0.17 ± 0.03	↑ 0.07 ± 0.03
subiculum	pre	0.09 ± 0.02	0.11 ± 0.02	0.05 ± 0.03	0.03 ± 0.02	0.02 ± 0.02	-0.02 ± 0.02
	3 days	↑ 0.14 ± 0.03	0.12 ± 0.02	0.05 ± 0.03	↑ 0.12 ± 0.02	↑ 0.14 ± 0.03	-0.02 ± 0.03
	10 days	↓ 0.08 ± 0.03	↓ 0.09 ± 0.02	0.04 ± 0.01	↑ 0.18 ± 0.04	0.16 ± 0.04	↑ 0.09 ± 0.03
epithalamus	pre	0.18 ± 0.04	0.20 ± 0.04	0.16 ± 0.05	0.13 ± 0.04	0.11 ± 0.03	0.06 ± 0.03
	3 days	↑ 0.27 ± 0.03	↑ 0.25 ± 0.03	↓ 0.12 ± 0.05	↑ 0.30 ± 0.03	↑ 0.33 ± 0.05	0.08 ± 0.04
	10 days	↓ 0.20 ± 0.03	↓ 0.21 ± 0.03	0.14 ± 0.04	↑ 0.35 ± 0.05	0.32 ± 0.05	↑ 0.23 ± 0.04
subthalamus	pre	0.10 ± 0.04	0.22 ± 0.05	0.05 ± 0.02	0.16 ± 0.03	0.07 ± 0.03	0.12 ± 0.04
	3 days	↑ 0.23 ± 0.06	↓ 0.14 ± 0.04	↑ 0.09 ± 0.04	↑ 0.20 ± 0.03	↑ 0.17 ± 0.06	↓ 0.04 ± 0.05
	10 days	↓ 0.12 ± 0.05	0.12 ± 0.04	0.08 ± 0.03	↑ 0.27 ± 0.03	↑ 0.24 ± 0.03	↑ 0.16 ± 0.06

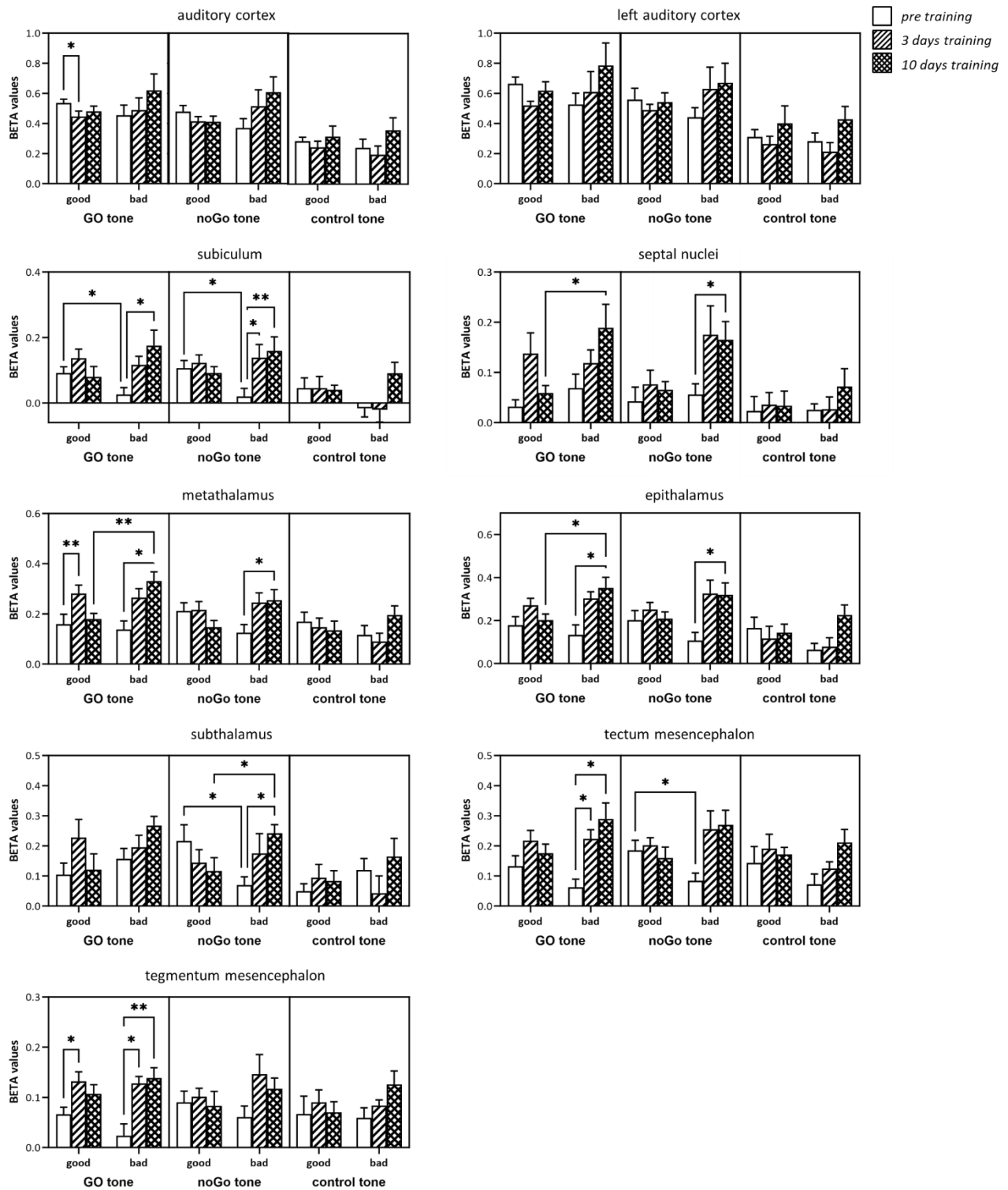


Figure S 3: Other brain areas showing differences between good and bad learners during discrimination training without aP

*In the comparison of BETA values, significant differences between good and bad learners are mostly showing after 10 sessions of training (Mixed-model ANOVAs with Bonferroni multiple comparisons correction; N=8 per group; * $p < 0.05$; ** $p < 0.01$)*

i: Exclusion of one bad learner from 3-days-training measurement analysis due to motion artefacts

Table 6: BETA values at time of reinforcement for good and bad learners trained without aP

Brain areas that show additional changes at time of reinforcement. Changes to the previous measurement that are bigger than the previous SEM are marked with ↓ for decrease and with ↑ for increase in BETA values. All values are given as mean and SEM in % (N=7 per group; i: Exclusion of one good learner from 10-days-training measurement analysis due to motion artefacts).

	training	BETA values (%) of <i>good learners</i>			BETA values (%) of <i>bad learners</i>		
		GO mean ± SEM	nGo mean ± SEM	control mean ± SEM	GO mean ± SEM	noGo mean ± SEM	control mean ± SEM
AC	pre	0.10 ± 0.03	0.07 ± 0.04	0.04 ± 0.04	0.10 ± 0.04	0.05 ± 0.04	0.01 ± 0.04
	3 days	↑ 0.17 ± 0.04	0.10 ± 0.05	0.06 ± 0.02	↑ 0.24 ± 0.03	↑ 0.20 ± 0.04	0.03 ± 0.04
	10 days	0.15 ± 0.04	0.11 ± 0.03	↑ 0.11 ± 0.03	0.26 ± 0.05	0.20 ± 0.05	↑ 0.13 ± 0.06
rAC	pre	0.10 ± 0.03	0.11 ± 0.04	0.07 ± 0.05	0.10 ± 0.04	0.07 ± 0.04	0.03 ± 0.04
	3 days	↑ 0.17 ± 0.03	0.12 ± 0.03	0.10 ± 0.02	↑ 0.24 ± 0.03	↑ 0.19 ± 0.04	0.07 ± 0.04
	10 days	↓ 0.11 ± 0.05	↓ 0.08 ± 0.03	0.12 ± 0.03	0.24 ± 0.05	0.21 ± 0.05	↑ 0.17 ± 0.05
lAC	pre	0.08 ± 0.03	0.03 ± 0.04	-0.01 ± 0.04	0.08 ± 0.05	0.01 ± 0.05	-0.03 ± 0.04
	3 days	↑ 0.19 ± 0.04	0.07 ± 0.07	0.03 ± 0.02	↑ 0.22 ± 0.04	↑ 0.21 ± 0.06	-0.05 ± 0.04
	10 days	0.19 ± 0.03	↑ 0.14 ± 0.04	↑ 0.10 ± 0.05	↑ 0.30 ± 0.06	0.20 ± 0.06	↑ 0.09 ± 0.09
motor cortex	pre	0.00 ± 0.01	0.01 ± 0.01	0.02 ± 0.01	-0.01 ± 0.01	0.00 ± 0.02	0.00 ± 0.01
	3 days	↑ 0.04 ± 0.01	↑ 0.04 ± 0.01	0.02 ± 0.02	↑ 0.02 ± 0.02	↑ 0.04 ± 0.03	0.00 ± 0.03
	10 days	↓ 0.01 ± 0.01	↓ 0.01 ± 0.01	0.03 ± 0.01	↑ 0.10 ± 0.04	↑ 0.08 ± 0.02	↑ 0.03 ± 0.01
posterior parietal cortex	pre	0.07 ± 0.02	0.04 ± 0.02	0.05 ± 0.02	0.07 ± 0.03	0.04 ± 0.03	-0.01 ± 0.01
	3 days	↑ 0.10 ± 0.04	↑ 0.09 ± 0.03	0.04 ± 0.01	↑ 0.15 ± 0.02	↑ 0.16 ± 0.04	↑ 0.02 ± 0.02
	10 days	0.07 ± 0.02	↓ 0.05 ± 0.03	0.05 ± 0.02	0.17 ± 0.03	0.18 ± 0.03	↑ 0.09 ± 0.03
hippocampus	pre	0.03 ± 0.01	0.04 ± 0.01	0.01 ± 0.01	0.05 ± 0.01	0.03 ± 0.01	0.02 ± 0.01
	3 days	↑ 0.07 ± 0.02	↑ 0.05 ± 0.02	↑ 0.03 ± 0.01	↑ 0.09 ± 0.01	↑ 0.10 ± 0.02	0.01 ± 0.02
	10 days	↓ 0.04 ± 0.01	0.05 ± 0.01	↓ 0.01 ± 0.01	0.10 ± 0.02	0.08 ± 0.01	↑ 0.04 ± 0.02
subiculum	pre	0.06 ± 0.02	0.07 ± 0.02	0.05 ± 0.02	0.04 ± 0.02	0.02 ± 0.02	0.03 ± 0.02
	3 days	↑ 0.11 ± 0.04	↑ 0.12 ± 0.03	0.03 ± 0.01	↑ 0.14 ± 0.02	↑ 0.14 ± 0.02	↓ 0.00 ± 0.03
	10 days	↓ 0.06 ± 0.03	0.09 ± 0.03	0.04 ± 0.02	0.15 ± 0.02	0.12 ± 0.02	↑ 0.08 ± 0.05
retrohippocampal areas	pre	0.06 ± 0.04	0.05 ± 0.02	0.08 ± 0.03	0.09 ± 0.03	0.03 ± 0.05	-0.02 ± 0.03
	3 days	↑ 0.13 ± 0.05	0.04 ± 0.02	↓ 0.04 ± 0.02	↑ 0.21 ± 0.05	↑ 0.19 ± 0.05	↑ 0.03 ± 0.03
	10 days	↓ 0.07 ± 0.05	0.05 ± 0.04	↑ 0.09 ± 0.03	0.22 ± 0.04	0.20 ± 0.06	↑ 0.15 ± 0.05

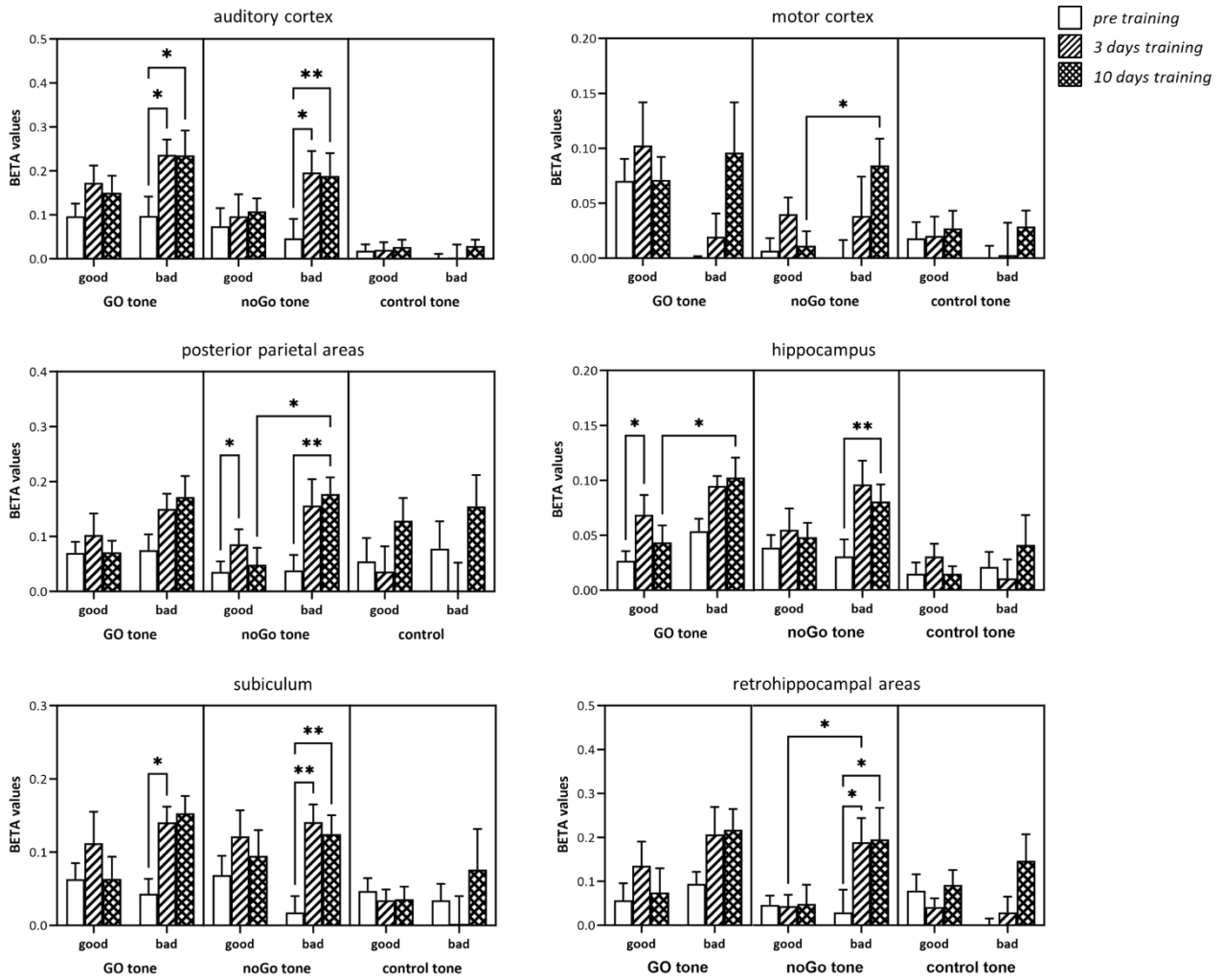


Figure S 4: Brain areas showing additional statistically significant differences due to discrimination training without aP at time of reinforcement

*Bad learners show significant activation increase in several brain areas at time of reinforcement throughout the discrimination training, most pronounced for noGo tone stimulation. (Mixed-model ANOVAs with Bonferroni multiple comparisons correction; N=8 per group; *p < 0.05; **p < 0.01)*

i: Exclusion of one bad learner from 3-days-training measurement analysis due to motion artefacts

Table 7: BETA values for good and bad learners in discrimination training with aP

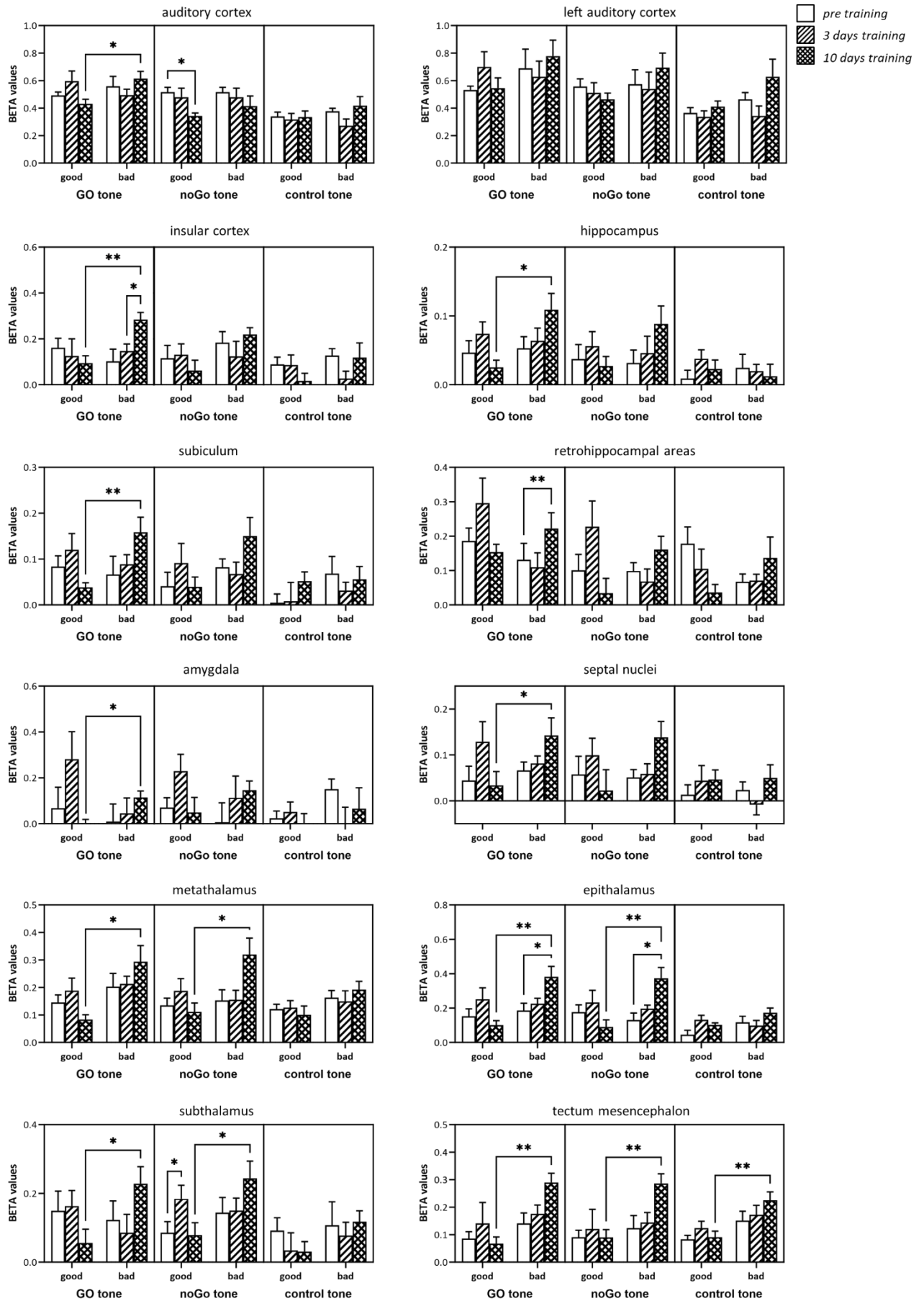
Changes to the previous measurement that are bigger than the previous SEM are marked with ↓ for decrease and with ↑ for increase in BETA values. All values are given as mean and SEM in % (N=7; i: Exclusion of one good learner from 10-days-training measurement analysis due to motion artefacts).

	training	BETA values (%) of <i>good learners</i>			BETA values (%) of <i>bad learners</i>		
		GO mean ± SEM	nGo mean ± SEM	control mean ± SEM	GO mean ± SEM	noGo mean ± SEM	control mean ± SEM
AC	pre	0.49 ± 0.02	0.52 ± 0.03	0.34 ± 0.03	0.56 ± 0.07	0.49 ± 0.05	0.38 ± 0.02
	3 days	↑ 0.60 ± 0.07	↓ 0.48 ± 0.06	0.32 ± 0.04	0.50 ± 0.04	0.45 ± 0.07	↓ 0.27 ± 0.04
	10 days	↓ 0.48 ± 0.05	↓ 0.41 ± 0.07	0.35 ± 0.04	↑ 0.62 ± 0.05	↑ 0.54 ± 0.05	↑ 0.42 ± 0.06
rAC	pre	0.45 ± 0.06	0.48 ± 0.04	0.31 ± 0.04	0.47 ± 0.05	0.43 ± 0.05	0.31 ± 0.04
	3 days	↑ 0.51 ± 0.09	0.45 ± 0.08	0.31 ± 0.07	↓ 0.34 ± 0.06	↓ 0.33 ± 0.05	↓ 0.20 ± 0.05
	10 days	↓ 0.33 ± 0.03	↓ 0.24 ± 0.02	0.26 ± 0.07	↑ 0.51 ± 0.06	↑ 0.44 ± 0.05	↑ 0.28 ± 0.05
lAC	pre	0.53 ± 0.03	0.56 ± 0.05	0.36 ± 0.04	0.69 ± 0.13	0.57 ± 0.10	0.46 ± 0.05
	3 days	↑ 0.70 ± 0.10	0.51 ± 0.07	0.34 ± 0.04	0.63 ± 0.10	0.54 ± 0.11	↓ 0.34 ± 0.07
	10 days	↓ 0.59 ± 0.07	0.53 ± 0.07	↑ 0.42 ± 0.03	↑ 0.78 ± 0.11	↑ 0.69 ± 0.10	↑ 0.63 ± 0.12
MGB	pre	0.22 ± 0.04	0.21 ± 0.03	0.23 ± 0.03	0.34 ± 0.06	0.28 ± 0.05	0.27 ± 0.04
	3 days	↑ 0.29 ± 0.06	↑ 0.28 ± 0.05	↓ 0.18 ± 0.03	0.33 ± 0.05	0.24 ± 0.05	0.26 ± 0.05
	10 days	↓ 0.14 ± 0.02	↓ 0.18 ± 0.04	0.20 ± 0.03	↑ 0.48 ± 0.07	↑ 0.47 ± 0.07	↑ 0.33 ± 0.04
IC	pre	0.08 ± 0.03	0.09 ± 0.02	0.19 ± 0.02	0.21 ± 0.06	0.15 ± 0.06	0.31 ± 0.05
	3 days	↑ 0.16 ± 0.09	↑ 0.14 ± 0.06	0.20 ± 0.05	0.20 ± 0.07	0.18 ± 0.05	0.30 ± 0.07
	10 days	0.12 ± 0.04	0.11 ± 0.03	↓ 0.13 ± 0.03	↑ 0.34 ± 0.02	↑ 0.28 ± 0.03	↑ 0.40 ± 0.03
mPFC	pre	0.03 ± 0.02	0.00 ± 0.03	0.00 ± 0.03	0.03 ± 0.03	0.01 ± 0.03	0.01 ± 0.04
	3 days	↑ 0.20 ± 0.09	↑ 0.13 ± 0.06	0.01 ± 0.02	↑ 0.14 ± 0.02	↑ 0.10 ± 0.03	0.03 ± 0.01
	10 days	↓ 0.04 ± 0.02	↓ 0.00 ± 0.03	0.02 ± 0.02	↑ 0.22 ± 0.05	↑ 0.21 ± 0.06	↑ 0.05 ± 0.03
RSC	pre	0.10 ± 0.03	0.10 ± 0.03	0.03 ± 0.03	0.13 ± 0.06	0.17 ± 0.05	0.07 ± 0.03
	3 days	↑ 0.28 ± 0.11	↑ 0.24 ± 0.10	↑ 0.12 ± 0.03	0.16 ± 0.03	0.15 ± 0.02	0.07 ± 0.01
	10 days	↓ 0.05 ± 0.02	↓ 0.06 ± 0.03	↓ 0.07 ± 0.03	↑ 0.31 ± 0.05	↑ 0.31 ± 0.06	0.08 ± 0.04
Th	pre	0.10 ± 0.03	0.09 ± 0.03	0.04 ± 0.02	0.14 ± 0.03	0.11 ± 0.02	0.07 ± 0.03
	3 days	↑ 0.15 ± 0.04	↑ 0.14 ± 0.04	0.04 ± 0.03	0.15 ± 0.02	↑ 0.14 ± 0.03	0.05 ± 0.02
	10 days	↓ 0.06 ± 0.03	↓ 0.04 ± 0.03	0.04 ± 0.01	↑ 0.24 ± 0.04	↑ 0.27 ± 0.04	↑ 0.09 ± 0.02
insular cortex	pre	0.16 ± 0.04	0.12 ± 0.05	0.09 ± 0.03	0.10 ± 0.05	0.18 ± 0.04	0.13 ± 0.03
	3 days	0.13 ± 0.07	0.13 ± 0.04	0.09 ± 0.04	0.15 ± 0.03	↓ 0.12 ± 0.06	↓ 0.03 ± 0.03
	10 days	0.11 ± 0.03	0.09 ± 0.05	↓ 0.03 ± 0.03	↑ 0.28 ± 0.03	↑ 0.22 ± 0.03	↑ 0.12 ± 0.06
hippocampus	pre	0.05 ± 0.02	0.04 ± 0.02	0.01 ± 0.01	0.05 ± 0.02	0.03 ± 0.02	0.02 ± 0.02
	3 days	↑ 0.07 ± 0.02	0.06 ± 0.02	↑ 0.04 ± 0.01	0.06 ± 0.02	0.05 ± 0.02	0.02 ± 0.01
	10 days	↓ 0.05 ± 0.02	0.06 ± 0.03	0.03 ± 0.01	↑ 0.11 ± 0.02	↑ 0.09 ± 0.02	0.01 ± 0.02
subiculum	pre	0.08 ± 0.02	0.04 ± 0.03	0.00 ± 0.02	0.07 ± 0.04	0.08 ± 0.02	0.07 ± 0.03
	3 days	↑ 0.12 ± 0.03	↑ 0.09 ± 0.04	0.01 ± 0.04	0.09 ± 0.02	0.07 ± 0.02	↓ 0.03 ± 0.02
	10 days	↓ 0.06 ± 0.03	0.07 ± 0.04	↑ 0.06 ± 0.02	↑ 0.16 ± 0.03	↑ 0.15 ± 0.04	↑ 0.06 ± 0.03
retrohippo- campal areas	pre	0.19 ± 0.03	0.10 ± 0.04	0.18 ± 0.05	0.13 ± 0.04	0.10 ± 0.02	0.07 ± 0.02
	3 days	↑ 0.30 ± 0.07	↑ 0.23 ± 0.07	↓ 0.10 ± 0.05	0.11 ± 0.04	↓ 0.07 ± 0.03	0.07 ± 0.02
	10 days	↓ 0.15 ± 0.02	↓ 0.07 ± 0.05	↓ 0.03 ± 0.02	↑ 0.22 ± 0.04	↑ 0.16 ± 0.04	↑ 0.14 ± 0.06
amygdala	pre	0.07 ± 0.08	0.07 ± 0.04	0.02 ± 0.03	0.01 ± 0.07	0.01 ± 0.08	0.15 ± 0.04
	3 days	↑ 0.28 ± 0.11	↑ 0.23 ± 0.07	0.05 ± 0.04	0.04 ± 0.06	↑ 0.11 ± 0.09	↓ -0.01 ± 0.08
	10 days	↓ 0.03 ± 0.07	↓ 0.05 ± 0.05	↓ -0.01 ± 0.07	↑ 0.11 ± 0.03	0.15 ± 0.04	↑ 0.07 ± 0.08
septal nuclei	pre	0.04 ± 0.03	0.06 ± 0.04	0.01 ± 0.02	0.07 ± 0.02	0.05 ± 0.02	0.02 ± 0.02
	3 days	↑ 0.13 ± 0.04	↑ 0.10 ± 0.03	↑ 0.04 ± 0.03	0.08 ± 0.02	0.06 ± 0.02	↓ -0.01 ± 0.02
	10 days	↓ 0.06 ± 0.03	↓ 0.05 ± 0.05	0.05 ± 0.02	↑ 0.14 ± 0.04	↑ 0.14 ± 0.03	↑ 0.05 ± 0.03
metathalamus	pre	0.15 ± 0.03	0.13 ± 0.02	0.12 ± 0.02	0.20 ± 0.04	0.15 ± 0.04	0.16 ± 0.02
	3 days	↑ 0.19 ± 0.04	↑ 0.19 ± 0.04	0.13 ± 0.02	0.21 ± 0.03	0.15 ± 0.03	0.15 ± 0.04
	10 days	↓ 0.13 ± 0.04	0.15 ± 0.05	0.12 ± 0.03	↑ 0.29 ± 0.05	↑ 0.32 ± 0.05	↑ 0.19 ± 0.03

--- Table 7 continued on following page ---

--- Table 7 continued from previous page ---

epithalamus	pre		0.15 ± 0.04	0.18 ± 0.04	0.05 ± 0.02	0.19 ± 0.04	0.13 ± 0.04	0.12 ± 0.03
	3 days	↑	0.25 ± 0.06	0.23 ± 0.06	0.13 ± 0.02	0.23 ± 0.03	0.20 ± 0.02	0.10 ± 0.03
	10 days	↓	0.14 ± 0.04	0.16 ± 0.07	0.13 ± 0.03	0.38 ± 0.06	0.37 ± 0.06	0.17 ± 0.03
subthalamus	pre		0.15 ± 0.05	0.09 ± 0.03	0.09 ± 0.03	0.12 ± 0.05	0.14 ± 0.04	0.11 ± 0.06
	3 days		0.16 ± 0.04	0.18 ± 0.04	0.03 ± 0.05	0.09 ± 0.05	0.15 ± 0.03	0.08 ± 0.04
	10 days	↓	0.08 ± 0.04	0.10 ± 0.03	0.05 ± 0.03	0.23 ± 0.05	0.24 ± 0.05	0.12 ± 0.03
tectum mesencephalon	pre		0.09 ± 0.02	0.09 ± 0.02	0.08 ± 0.01	0.14 ± 0.03	0.12 ± 0.04	0.15 ± 0.03
	3 days	↑	0.14 ± 0.07	0.12 ± 0.07	0.12 ± 0.02	0.18 ± 0.03	0.14 ± 0.03	0.17 ± 0.03
	10 days		0.10 ± 0.03	0.15 ± 0.06	0.12 ± 0.03	0.29 ± 0.03	0.29 ± 0.03	0.22 ± 0.03



← **Figure S 5: Other brain areas showing differences between good and bad learners during discrimination training with aP**

*In the comparison of BETA values, significant differences between good and bad learners are mostly showing after 10 sessions of training (Mixed-model ANOVAs with Bonferroni multiple comparisons correction; N=8 per group; *p < 0.05; **p < 0.01)*

i: Exclusion of one bad learner from 10-days-training measurement analysis due to motion artefacts

Table 8: BETA values at time of reinforcement for good and bad learners trained with aP

Brain areas that show additional changes at time of reinforcement. Changes to the previous measurement that are bigger than the previous SEM are marked with ↓ for decrease and with ↑ for increase in BETA values. All values are given as mean and SEM in % (N=7; i: Exclusion of one good learner from 10-days-training measurement analysis due to motion artefacts).

		BETA values (%) of <i>good learners</i>			BETA values (%) of <i>bad learners</i>		
training		GO	nGo	control	GO	noGo	control
		mean ± SEM	mean ± SEM	mean ± SEM	mean ± SEM	mean ± SEM	mean ± SEM
AC	pre	-0.01 ± 0.02	-0.02 ± 0.02	0.01 ± 0.02	0.07 ± 0.03	0.06 ± 0.02	0.04 ± 0.05
	3 days	↑ 0.13 ± 0.07	↑ 0.05 ± 0.05	↑ 0.08 ± 0.03	↑ 0.16 ± 0.04	0.06 ± 0.05	0.03 ± 0.03
	10 days	0.09 ± 0.04	0.05 ± 0.05	0.05 ± 0.03	↑ 0.27 ± 0.03	↑ 0.19 ± 0.05	↑ 0.12 ± 0.04
rAC	pre	0.00 ± 0.03	-0.02 ± 0.02	0.01 ± 0.03	0.06 ± 0.05	0.08 ± 0.03	0.04 ± 0.05
	3 days	↑ 0.11 ± 0.05	↑ 0.07 ± 0.04	↑ 0.12 ± 0.05	↑ 0.12 ± 0.03	↓ 0.02 ± 0.02	0.06 ± 0.03
	10 days	↓ 0.05 ± 0.05	0.03 ± 0.05	↓ 0.03 ± 0.02	↑ 0.28 ± 0.04	↑ 0.20 ± 0.05	↑ 0.13 ± 0.04
lAC	pre	-0.02 ± 0.02	-0.02 ± 0.03	0.00 ± 0.04	0.08 ± 0.03	0.02 ± 0.02	0.03 ± 0.06
	3 days	↑ 0.15 ± 0.10	↑ 0.01 ± 0.06	0.02 ± 0.03	↑ 0.20 ± 0.05	↑ 0.07 ± 0.08	0.00 ± 0.03
	10 days	0.14 ± 0.04	↑ 0.07 ± 0.05	↑ 0.07 ± 0.05	0.25 ± 0.04	↑ 0.17 ± 0.05	↑ 0.11 ± 0.07
somatosensory cortex	pre	0.00 ± 0.02	-0.01 ± 0.01	0.00 ± 0.02	0.02 ± 0.01	0.03 ± 0.00	0.04 ± 0.02
	3 days	↓ -0.02 ± 0.06	↑ 0.01 ± 0.03	↑ 0.04 ± 0.02	↑ 0.04 ± 0.01	0.03 ± 0.02	0.02 ± 0.01
	10 days	-0.01 ± 0.01	0.01 ± 0.02	0.02 ± 0.02	↑ 0.09 ± 0.02	↑ 0.09 ± 0.02	↑ 0.05 ± 0.01
motor cortex	pre	0.01 ± 0.01	0.02 ± 0.01	0.00 ± 0.02	0.00 ± 0.02	0.01 ± 0.02	-0.01 ± 0.02
	3 days	↓ 0.00 ± 0.03	0.02 ± 0.02	↑ 0.02 ± 0.01	↑ 0.04 ± 0.01	↑ 0.04 ± 0.01	0.00 ± 0.02
	10 days	-0.01 ± 0.01	0.03 ± 0.01	0.02 ± 0.01	↑ 0.08 ± 0.03	↑ 0.08 ± 0.04	↑ 0.02 ± 0.02
visual cortex	pre	0.05 ± 0.02	0.06 ± 0.03	0.03 ± 0.03	0.10 ± 0.01	0.10 ± 0.03	0.08 ± 0.03
	3 days	0.07 ± 0.04	0.07 ± 0.05	↑ 0.08 ± 0.04	↑ 0.12 ± 0.02	↓ 0.05 ± 0.03	↓ 0.03 ± 0.02
	10 days	↓ 0.00 ± 0.02	0.05 ± 0.02	0.06 ± 0.02	↑ 0.17 ± 0.04	↑ 0.14 ± 0.03	↑ 0.08 ± 0.02
posterior parietal cortex	pre	0.03 ± 0.02	0.01 ± 0.02	-0.01 ± 0.02	0.08 ± 0.02	0.08 ± 0.03	0.04 ± 0.03
	3 days	↑ 0.09 ± 0.03	↑ 0.05 ± 0.02	↑ 0.08 ± 0.02	↑ 0.10 ± 0.03	0.07 ± 0.02	0.04 ± 0.01
	10 days	↓ 0.04 ± 0.03	0.08 ± 0.03	↓ 0.05 ± 0.02	↑ 0.18 ± 0.03	↑ 0.16 ± 0.04	↑ 0.09 ± 0.02
striatum	pre	0.01 ± 0.01	0.01 ± 0.01	0.00 ± 0.02	0.03 ± 0.01	0.03 ± 0.02	0.03 ± 0.02
	3 days	0.01 ± 0.03	0.00 ± 0.01	↑ 0.02 ± 0.02	0.03 ± 0.01	↓ 0.01 ± 0.01	↓ 0.00 ± 0.01
	10 days	0.02 ± 0.01	↑ 0.04 ± 0.03	0.01 ± 0.02	↑ 0.09 ± 0.01	↑ 0.08 ± 0.02	↑ 0.03 ± 0.02

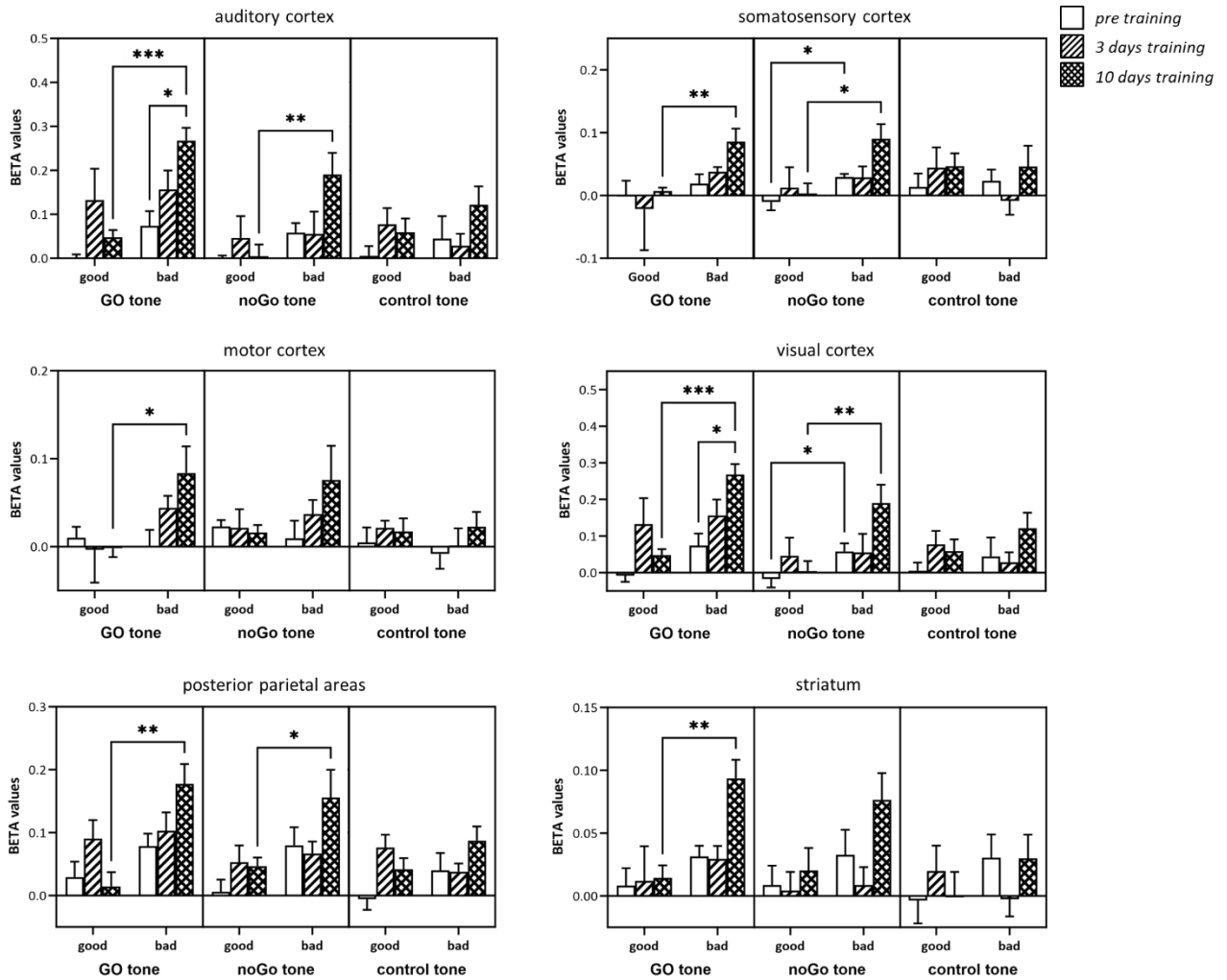


Figure S 6: Brain areas showing additional statistically significant differences due to discrimination training with aP at time of reinforcement

*Good and bad learners show significant activation differences in several brain areas at time of reinforcement after 10 days of discrimination training, more pronounced for GO tone stimulation. (Mixed-model ANOVAs with Bonferroni multiple comparisons correction; N=8 per group; * $p < 0.05$; ** $p < 0.01$; *** $p < 0.001$)*

i: Exclusion of one bad learner from 3-days-training measurement analysis due to motion artefacts

Table 9: Exemplary BETA values for brain structures showing activation changes due to the direction discrimination training with aP

For the comparison of BETA values presented for the whole group of gerbils trained without aP. Activation changes to the previous measurement that are larger than the SEM are marked by ↑ for BETA increase and ↓ for BETA decrease. All values are given as mean and SEM in %. (N=14; i: Exclusion of one animal from 10-days-training measurement analysis due to motion artefacts)

	training	GO		noGo		control	
			mean ± SEM		mean ± SEM		mean ± SEM
AC	pre		0.53 ± 0.036		0.50 ± 0.029		0.36 ± 0.018
	3 days		0.55 ± 0.041	↓	0.46 ± 0.046	↓	0.30 ± 0.030
	10 days		0.53 ± 0.039		0.45 ± 0.040	↑	0.38 ± 0.039
rAC	pre		0.46 ± 0.038		0.45 ± 0.034		0.31 ± 0.028
	3 days		0.43 ± 0.059	↓	0.39 ± 0.052	↓	0.26 ± 0.047
	10 days		0.43 ± 0.044		0.35 ± 0.041		0.27 ± 0.040
lAC	pre		0.61 ± 0.069		0.56 ± 0.055		0.41 ± 0.032
	3 days		0.66 ± 0.074		0.53 ± 0.066	↓	0.34 ± 0.039
	10 days		0.67 ± 0.073		0.59 ± 0.065	↑	0.53 ± 0.072
MGB	pre		0.28 ± 0.038		0.25 ± 0.032		0.25 ± 0.026
	3 days		0.31 ± 0.038		0.26 ± 0.037	↓	0.22 ± 0.032
	10 days		0.32 ± 0.063	↑	0.34 ± 0.058	↑	0.27 ± 0.030
IC	pre		0.15 ± 0.035		0.12 ± 0.031		0.25 ± 0.033
	3 days	↑	0.18 ± 0.055	↑	0.16 ± 0.042		0.25 ± 0.042
	10 days		0.24 ± 0.036	↑	0.21 ± 0.031		0.28 ± 0.043
PFC	pre		0.03 ± 0.020		0.01 ± 0.022		0.01 ± 0.024
	3 days	↑	0.17 ± 0.048	↑	0.11 ± 0.034		0.02 ± 0.014
	10 days		0.14 ± 0.036		0.11 ± 0.046	↑	0.04 ± 0.021
RSC	pre		0.11 ± 0.031		0.13 ± 0.032		0.05 ± 0.022
	3 days	↑	0.22 ± 0.060	↑	0.19 ± 0.050	↑	0.10 ± 0.018
	10 days		0.19 ± 0.045		0.19 ± 0.048	↓	0.08 ± 0.026
Th	pre		0.12 ± 0.020		0.10 ± 0.017		0.06 ± 0.017
	3 days	↑	0.15 ± 0.025	↑	0.14 ± 0.025		0.05 ± 0.018
	10 days		0.15 ± 0.034		0.16 ± 0.041	↑	0.07 ± 0.012

(i) Information on the additional surgical interventions

Photolytic lesions of interhemispheric projection neurons

The elimination of projection neurons connecting the auditory cortices was pursued with a targeted laser-induced apoptosis approach established in the Mongolian gerbil by Saldeitis et al., 2022 (Saldeitis et al., 2022). Aim of the experiment was to investigate the importance of cortical interaction during auditory learning with auditory fMRI by studying effects of disturbance and compensation.

Accordingly, red retrobeads™ IX (Lumafluor Inc, USA, *excitation 530 nm, emission 590 nm*) were conjugated with the photolytic chromophore chlorine e6(-monoethylene-diamineamide) (*Phytochlorine*, Frontier Scientific, USA). A 1 mM solution of chlorine e6 was created with 3 mL 0.01 M phosphate buffer (PB, pH of 7.4) and activated with 5 mg N-Cyclohexyl-N'-(2-morpholinoethyl)carbodiimide metho-p-toluenesulfonate (Sigma-Aldrich, Switzerland) at 4 °C on a rocker table (70 rpm) for 30 min. To this, retrobeads diluted in PB (50 µL in 300 µL buffer) were added and incubated for the coating process at 4 °C on the rocker table. After 60 min, the reaction was stopped with 335 µL 0.1 M glycine buffer (pH of 8.0). For clean-up, the mixture was repeatedly centrifuged at 140000 g/45000 rpm for 60 min (Optima MAX Ultracentrifuge with MLA-80 rotor, Beckman Coulter, USA), the liquid over the retrobead pellet replaced with 3 mL PB for resuspension after each round. When there was no visible discoloration of the supernatant left, the pellet was resuspended in 50 µL PB and stored at 4 °C. The e6 chlorine conjugated retrobeads were used within 14 days and put into an ultrasound bath (Sonorex Super10P, Bandelin, Germany) immediately before usage to prevent clotting.

The conjugated retrobeads were introduced into either the left or the right primary auditory cortex (A1) of Mongolian gerbils by stereotactic pressure injections. The animals were anaesthetized by an initial *i.p.* injection of a combination of ketamine (*Ketabel*, 1.5 mg/kg, bela-pharm GmbH & Co. KG, Germany) and xylazine (0.033 mg/kg, Serumwerk Bernburg AG, Germany) diluted in isotonic saline solution. Throughout the surgery, the animals' body temperature was maintained with a heating blanket, depth of anaesthesia was periodically examined by their pedal withdrawal reflexes and adjusted by additional anaesthetics if necessary. The hair of the animals was removed on surgical site and Gingicain applied as additional local anaesthetic. Then a vertical incision of approximately 1 cm length was cut into the skin between eye and external ear. Parts of the temporal muscle were carefully detached from the bone and pushed down to expose the bone plate covering the auditory areas of the cerebral cortex. Guided by bone and vascular landmarks (Budinger et al., 2000a), 2 or 4 holes were drilled unilaterally into the bone in region of either the left or the right A1 with a dental drill (AEU-17B, Aseptico Inc., USA). The retrobeads were injected through a fine glass micropipette (3.5", World Precision Instruments Inc., USA). In preparation this pipette was previously pulled (Micropipette Puller Model P-87, Sutter Instruments, USA), broken off at the tip to an outer diameter of approximately 20 µm, filled with silicone oil from its non-pulled end with a MicroFil needle (World Precision Instruments Inc., USA), and mounted on an oil hydraulic nanoliter injector (Nanoliter2000, World Precision Instruments Inc., USA). After drawing up the retrobead solution, the micropipette was vertically inserted into the brain, lowered to a depth of approximately 0.8 mm measured from the brain surface. The coated retrobeads were injected over a period of two minutes per hole either in steps of 5 x 18.4 nL for the animals with 2 holes (exclusively animals of the discrimination training group without aP), or 3 x 13.8 nL for the animals with 4 holes (exclusively animals of the aP group). After the

injection, the drilled holes were sealed with bone wax (W30, Ethicon, Germany), the wound rinsed off with isotonic saline solution, the temporal muscle loosely pushed back to its original location and the incision closed with self-absorbing sutures (V32H, Ethicon Vicryl rapide, Germany). For pain management, the gerbils received 0.2 mg/kg meloxicam (*Metakam*, Boehringer Ingelheim, Germany) as *s.c.* injection at the end of the surgeries and every 24 h for the following 4 days.

After 10 days, a second surgery was performed on the contralateral AC of the animals to induce photolytic apoptosis of the retrogradely labelled projection neurons with a laser of 670 nm wavelength. The animals were again anaesthetized (1.5 mg/kg ketamine + 0.033 mg/kg xylazine), and the bone plate covering the contralateral AC exposed in the same manner. The AC was irradiated transcranially with a 670 nm diode laser (Flatbeam-Laser 670, Schäfter + Kirchhoff GmbH, Germany), positioned directly on the bone and tuned to 50 mW for 2 x 5 min, with a 2 min break to prevent tissue damage through overheating. Sham animals were treated accordingly without switching on the power to the laser. After the irradiation, the animals were taken care of in the same manner as for the injection surgery described above.

Immunohistochemistry and histological analysis

After completion of the FM direction discrimination training and last auditory fMRI measurement, the gerbils were sacrificed and perfused transcardially with PBS, followed by 4% paraformaldehyde (PFA). Brains were extracted, fixated in 4% PFA overnight, cryoprotected through immersion in 30% sucrose for 2 days before freezing in isopentane at -50 °C. Horizontal sections of 50 µm thickness were cut with a cryostat (Leica CM 1950, Leica Biosystems, Germany). Every 4th section in the area of the injection site in AC was immuno-stained for estimation of the efficacy of photolytic lesioning for neurons with a mouse anti-NeuN antibody (1:1000, overnight, Millipore Europe, catalogue# MAB377, lot# 3519281). This NeuN antibody was fluorescently labelled by a secondary anti-mouse Alexa 488 (1:200, 2 h, Invitrogen by Thermo Fisher Scientific, catalogue# A11017, lot# 2274781). The sections were mounted on slides and sealed with a coverslip.

The NeuN immuno-labelled sections of 10 animals were scanned at a fluorescent slide scanner (20 x magnification, 5 confocal planes; Nanozoomer S60, Hamamatsu Photonics Deutschland GmbH, Germany) for visual inspection and documentation of the injection site (Figure S 7).

Precise neuronal density per cortical layer in the AC contralateral to the injection site was inspected of randomly selected animals containing 3 lesioned L<R, 3 lesioned R<L, and 3 control animals, that received injections but no laser irradiation. The AC region of 6 NeuN-stained slices of each animal was imaged with a confocal microscope (Leica TCS SP8, Leica Microsystems, Germany) with 10 x magnification in 15 to 20 confocal planes with channels at 500-530 nm for the NeuN-staining and 580-620 nm for retrograde labelling. A maximum intensity projection of the images was manually separated into the cortical Layer I, II&III, IV, V and VI with ImageJ/Fiji ([Schindelin et al., 2012](#)). The number of stained cells within each individual layer was counted automatically with Cellpose v2.0 ([Stringer et al., 2021](#)). The neuronal densities for each cortical layer was calculated by division through the measured area. Additionally the relative cell density in comparison to the overall neuronal densities throughout the entire AC of each slice was calculated by division through that value. After normal distribution of the values was tested with the Shapiro-Wilk test and the Kolmogorov-Smirnov test, ANOVAs were performed on both values, which did not lead to any significant differences between groups for either value: with N=3 per group; cells densities yielded p = 0.4,

and ratio cell densities $p = 0.2$. The cell counting process and results are visualized in Figure S 8. Neuronal cell loss would be predominantly expected in Layer V and Layer III of the lesioned animals (Saldeitis et al., 2022). As these layers in particular did not show any trends of lower neuronal density in the lesioned animals, the photolytic lesioning was considered not successful.

The stained sections of the remaining animals were visually inspected for noticeable changes in neuronal density and retrograde labelling with an epifluorescence microscope. Here, no changes in neuronal density were noted.

Lack of photolytic lesions

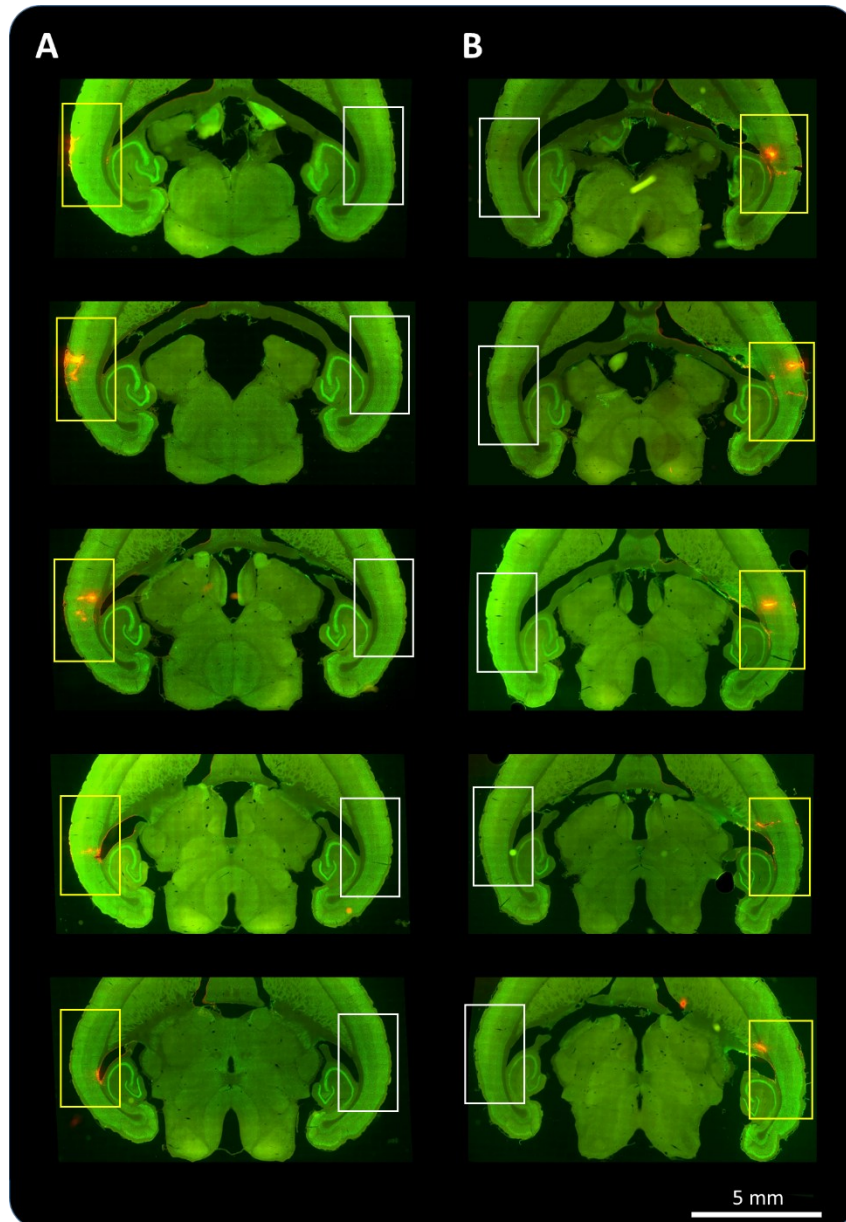


Figure S 7: There is no impact of injection of e6-chlorine-conjugated retrobeads as shown here in exemplary animals of the FM direction discrimination training group with aP
Horizontal NeuN-stained (green) sections in region of AC show the injection site (yellow box) of the red-fluorescent retrobeads and of contralateral side (white box) in exemplary animals in left (A) and right (B) AC. There is neither gross damage of neuronal tissue at injection sites nor at the lasered contralateral side visible. Scale bar: 5 mm.

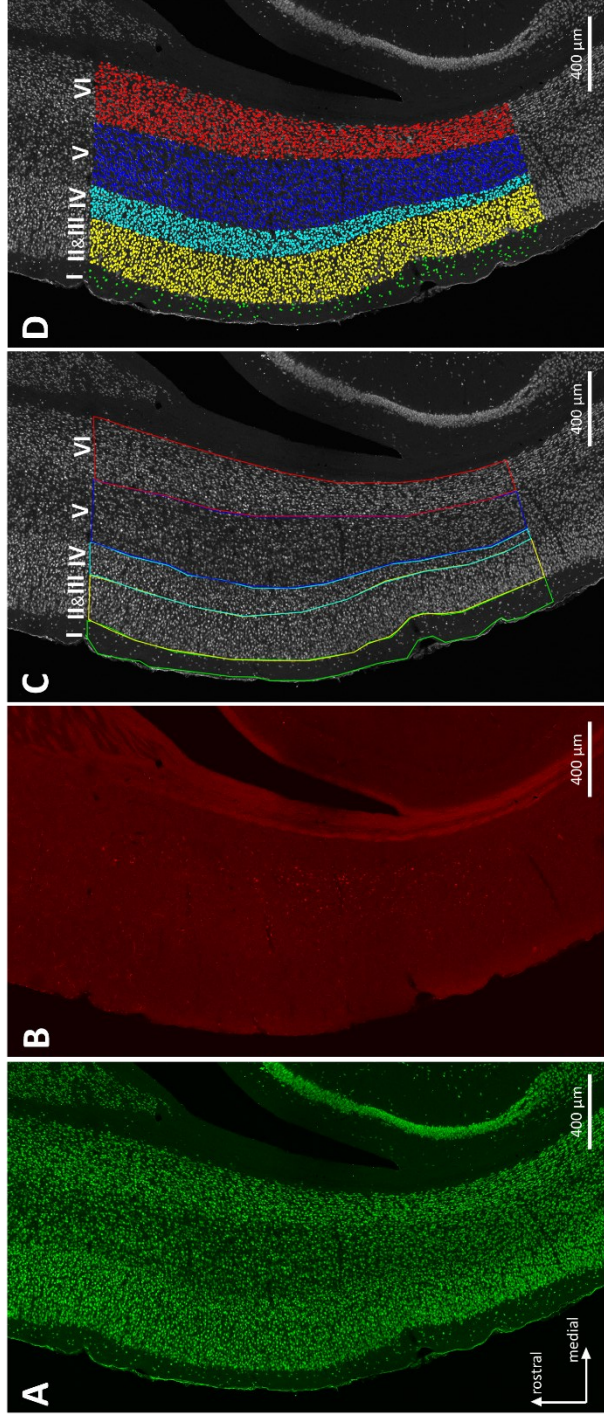
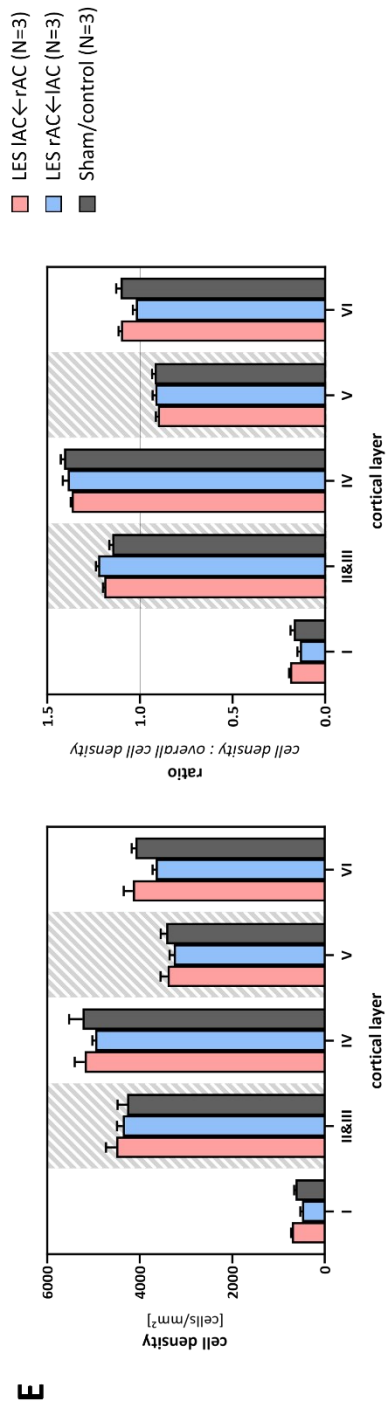


Figure 8: There is no impact of photolytic lesioning on neuronal density (NeuN staining)

A&B. Representative confocal images (maximum intensity projection) of AC contralateral to injection site with the red-fluorescent retrobeads, showing NeuN staining in green (**A**). Notably, the retrograde labelling through the retrobeads (red, **B**) is sparse in comparison to previously published images (Saldeitis et al., 2022). Scale bar: 400 μm . **C.** Same image (NeuN channel in grey) with delineated cortical layer boundaries (Layer I in green, II&III in yellow, IV in cyan, V in blue and VI in red) within the AC region and (**D**) automatically detected and counted cells via Cellpose (Stringer et al., 2021).

E. Resulting average neuronal density within each layer, calculated through cell count divided by measured area (left), and ratio of layer-wise neuronal density to overall cell density within AC of each tissue section (right). Gerbils lesioned L \leftarrow R in light red, gerbils lesioned R \leftarrow L in blue and gerbils injected but not laser irradiated in grey serving as control (mean \pm SEM). ANOVA testing of neither value did lead to any significant differences between groups (N=3 per group).



Lack of behavioural impact

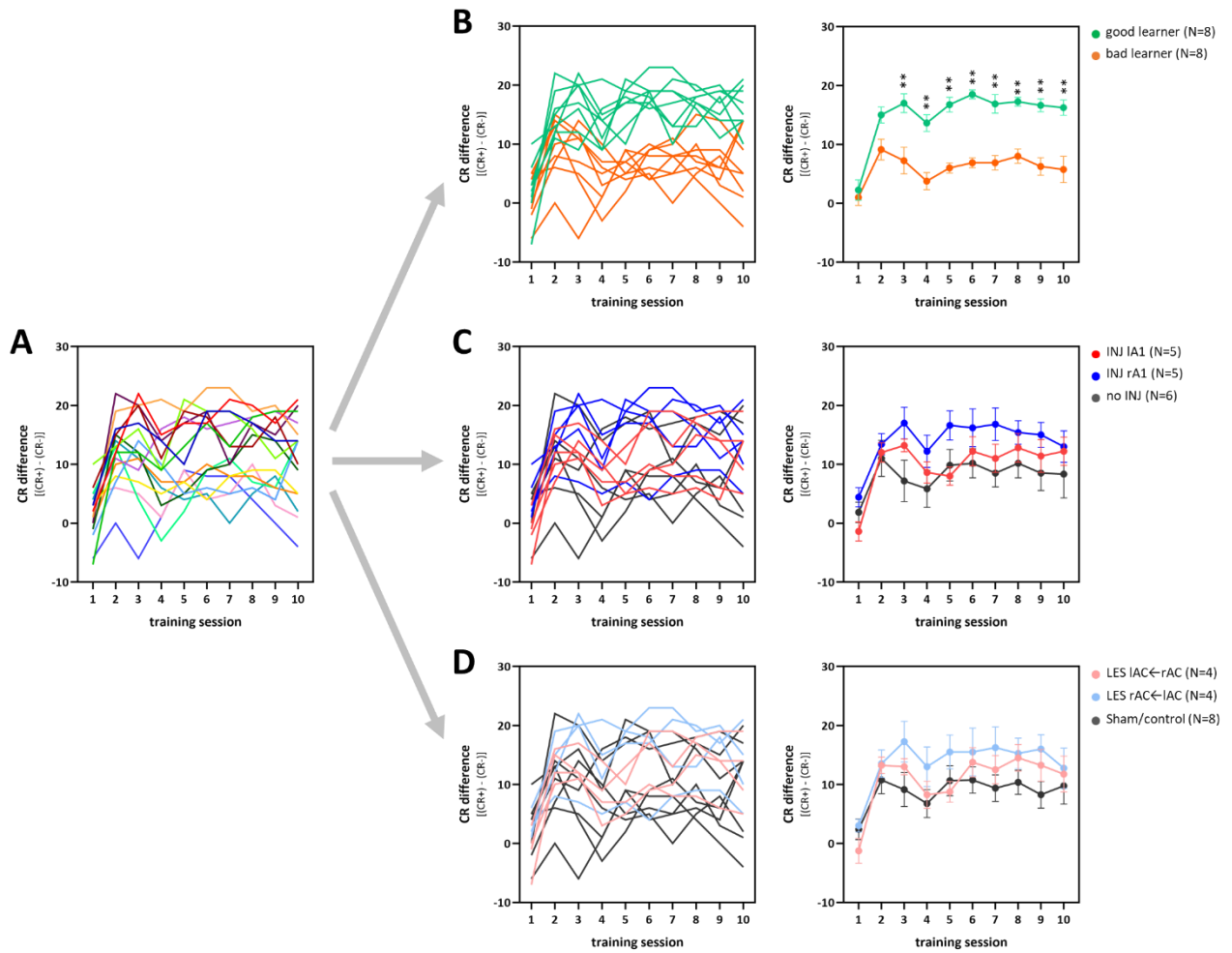


Figure S 9: There is no impact of surgical interventions on animals' behaviour in the direction discrimination training without aP

A. Individual range of CR differences, separated into groups by **B.** performance, **C.** injection side (INJ), and **D:** direction of projection neurons targeted with laser induced apoptosis (LES). Only performance based division lead to any statistically significant differences between the groups. Neither tracer injection, nor laser apoptosis surgeries led to any decrease in performance. Statistical comparison between groups performed with Mann-Whitney tests with Holm-Šidák multiple comparison correction, withholding the correction did not result in significant differences caused by the surgical interventions either. (Adjusted p -values indicated by * $p < 0.05$; ** $p < 0.01$)

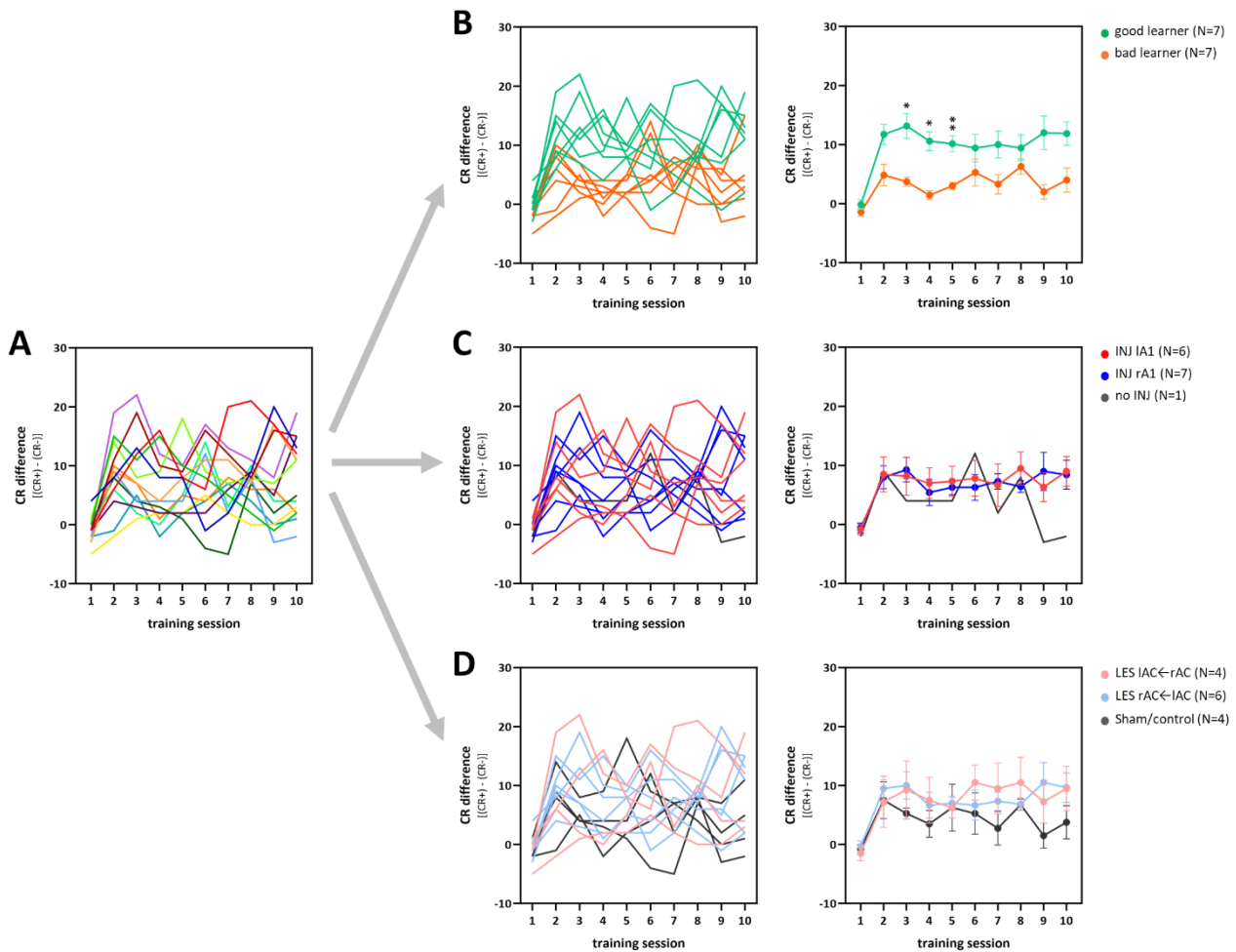


Figure S 10: There is no impact of surgical interventions on animals' behaviour in the direction discrimination training of the animals with aP

A. Individual range of CR differences, separated into groups by **B.** performance, **C.** injection side (INJ), and **D.** direction of projection neurons targeted with laser induced apoptosis (LES). Only performance based division lead to any statistically significant differences between the groups. Neither tracer injection, nor laser apoptosis surgeries led to any decrease in performance. Statistical comparison between groups performed with Mann-Whitney tests with Holm-Šidák multiple comparison correction, withholding the correction did not result in significant differences caused by the surgical interventions either. (Adjusted p -values indicated by * $p < 0.05$; ** $p < 0.01$)

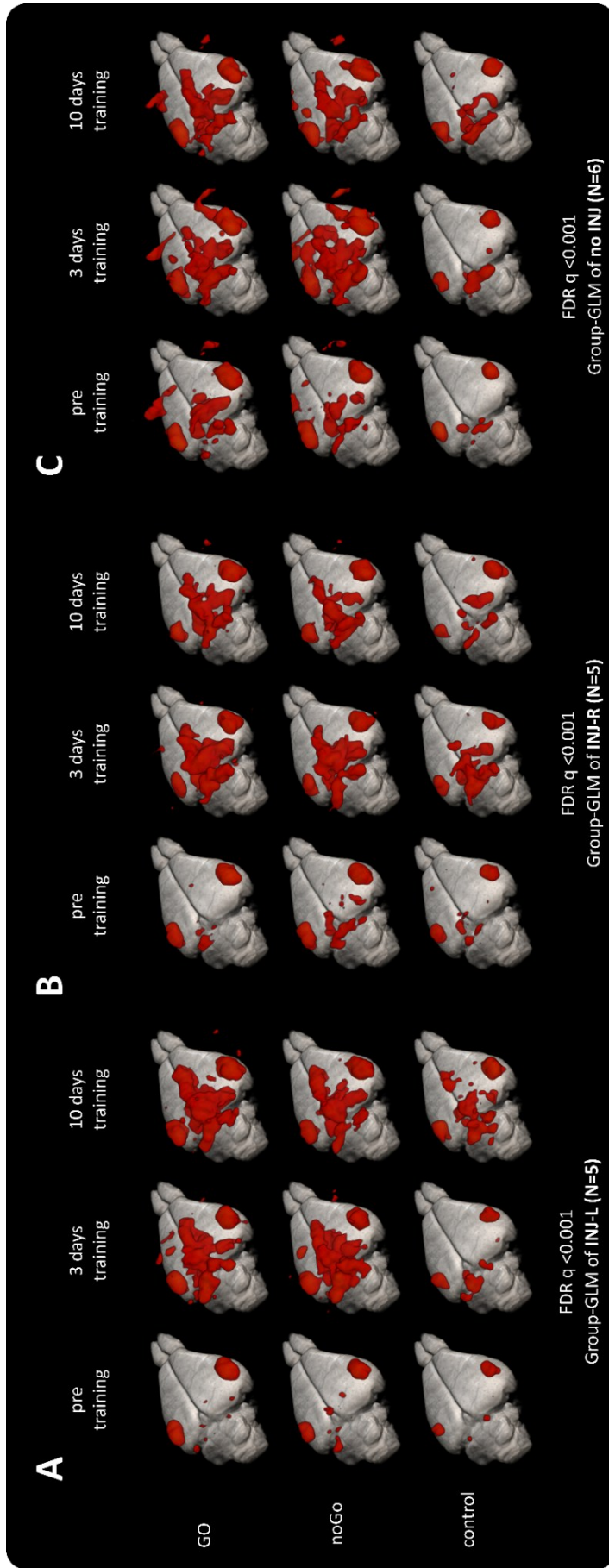


Figure S 11: There is no impact of the tracer injections on the brain activation pattern recorded with auditory fMRI of animals trained without aP
 Comparison of brain activation patterns between animals injected into **A: left A1**, **B: right A1** and **C: control animals** without any surgeries showed no gross activation differences between those groups. The control group shows slightly higher activation in subcortical brain areas in the pre training measurement, but this activation can be attributed to a single animal. Group-GLMs performed with BrainVoyager, FDR correction with $q < 0.001$